

Inter-hemispheric temperature variability over the past millennium

Raphael Neukom^{1,2*}, Joëlle Gergis³, David J. Karoly^{3,4}, Heinz Wanner¹, Mark Curran^{5,6}, Julie Elbert¹, Fidel González-Rouco⁷, Braddock K. Linsley⁸, Andrew D. Moy^{5,6}, Ignacio Mundo^{9,10}, Christoph C. Raible^{1,11}, Eric J. Steig¹², Tas van Ommen^{5,6}, Tessa Vance⁶, Ricardo Villalba⁹, Jens Zinke^{13,14} and David Frank^{1,2}

The Earth's climate system is driven by a complex interplay of internal chaotic dynamics and natural and anthropogenic external forcing. Recent instrumental data have shown a remarkable degree of asynchronicity between Northern Hemisphere and Southern Hemisphere temperature fluctuations, thereby questioning the relative importance of internal versus external drivers of past as well as future climate variability^{1–3}. However, large-scale temperature reconstructions for the past millennium have focused on the Northern Hemisphere^{4,5}, limiting empirical assessments of inter-hemispheric variability on multi-decadal to centennial timescales. Here, we introduce a new millennial ensemble reconstruction of annually resolved temperature variations for the Southern Hemisphere based on an unprecedented network of terrestrial and oceanic palaeoclimate proxy records. In conjunction with an independent Northern Hemisphere temperature reconstruction ensemble⁵, this record reveals an extended cold period (1594–1677) in both hemispheres but no globally coherent warm phase during the pre-industrial (1000–1850) era. The current (post-1974) warm phase is the only period of the past millennium where both hemispheres are likely to have experienced contemporaneous warm extremes. Our analysis of inter-hemispheric temperature variability in an ensemble of climate model simulations for the past millennium suggests that models tend to overemphasize Northern Hemisphere–Southern Hemisphere synchronicity by underestimating the role of internal ocean-atmosphere dynamics, particularly in the ocean-dominated Southern Hemisphere. Our results imply that climate system predictability on decadal to century timescales may be lower than expected based on assessments of external climate forcing and Northern Hemisphere temperature variations^{5,6} alone.

From over 25 hemispheric-scale temperature reconstructions published in recent decades, only three cover the ocean-dominated

Southern Hemisphere⁷. These Southern Hemisphere temperature reconstructions include only seven⁸ or fewer⁹ proxy datasets for the entire Southern Hemisphere, or were provided as peripheral components of Northern Hemisphere and global reconstruction efforts⁴ with the caveat that 'more confident statements about long-term temperature variations in the Southern Hemisphere and globe on the whole must await additional proxy data collection'⁴. Consequently, attribution of temperature changes to external forcings^{10,11} and investigations of the coupling between temperature and greenhouse gas concentrations^{5,6} have focused on the Northern Hemisphere.

Data spanning inter-annual to multi-millennial timescales suggest limited temperature coherence between the two hemispheres. The degree of independence in Northern Hemisphere and Southern Hemisphere temperature trends over the past 150 years² indicates that responses to external forcing may be modulated by ocean–atmosphere variability, reducing predictability of the climate system in twenty-first century model projections^{1,3}. Patterns of late Quaternary deglaciation have also demonstrated high inter-hemispheric variability, attributed to a coupling of orbital forcing, ice-albedo feedbacks and the Atlantic Meridional Overturning Circulation^{12,13}. Finally, a recent evaluation of multi-centennial reconstructions from seven continents also suggests stronger regional temperature coherence within the hemispheres than between them¹⁴. Yet, the preliminary nature of existing annually resolved Southern Hemisphere temperature reconstructions has hindered knowledge of the existence and driving mechanisms of inter-hemispheric climate variability on the societally relevant multi-decadal to centennial timescales.

Here, we introduce a Southern Hemisphere temperature reconstruction ensemble and assess inter-hemispheric temperature variability over the past millennium in both empirical reconstructions and state-of-the-art climate model simulations. We use an extensive Southern Hemisphere palaeoclimate data network from more than 300 individual sites¹⁵ yielding 111 temperature

¹Oeschger Centre for Climate Change Research, University of Bern, CH-3012 Bern, Switzerland, ²Swiss Federal Institute WSL, Zürcherstrasse 111, CH-8903 Birmensdorf, Switzerland, ³School of Earth Sciences, University of Melbourne, Victoria 3010, Australia, ⁴ARC Centre of Excellence for Climate System Science, University of Melbourne, Victoria 3010, Australia, ⁵Department of the Environment, Australian Antarctic Division, Kingston, Tasmania 7050, Australia, ⁶Antarctic Climate and Ecosystems Cooperative Research Centre, University of Tasmania, Hobart, Tasmania 7000, Australia, ⁷Departamento Astrofísica y CC de la Atmósfera, Instituto de Geociencias (CSIC-UCM) Universidad Complutense de Madrid, Madrid, 28040, Spain, ⁸Lamont-Doherty Earth Observatory, Columbia University, Palisades, New York 10964, USA, ⁹Instituto Argentino de Nivología, Glaciología y Ciencias Ambientales (IANIGLA), CCT CONICET-Mendoza, Mendoza, 5500, Argentina, ¹⁰LISEA, Facultad de Ciencias Agrarias y Forestales, Universidad Nacional de La Plata, B1900 La Plata, Argentina, ¹¹Climate and Environmental Physics, University of Bern, CH-3012 Bern, Switzerland, ¹²Quaternary Research Center and Department of Earth and Space Sciences, University of Washington, Seattle, Washington 98195, USA, ¹³School of Earth and Environment, University of Western Australia Oceans Institute, 35 Stirling Highway, Crawley WA 6009, Australia, ¹⁴Australian Institute of Marine Science, Nedlands WA 6009, Australia. [†]Present address: University of Zürich, Physical Geography Division, Department of Geography, Winterthurerstrasse 190, CH-8057 Zürich, Switzerland. *e-mail: neukom@giub.unibe.ch

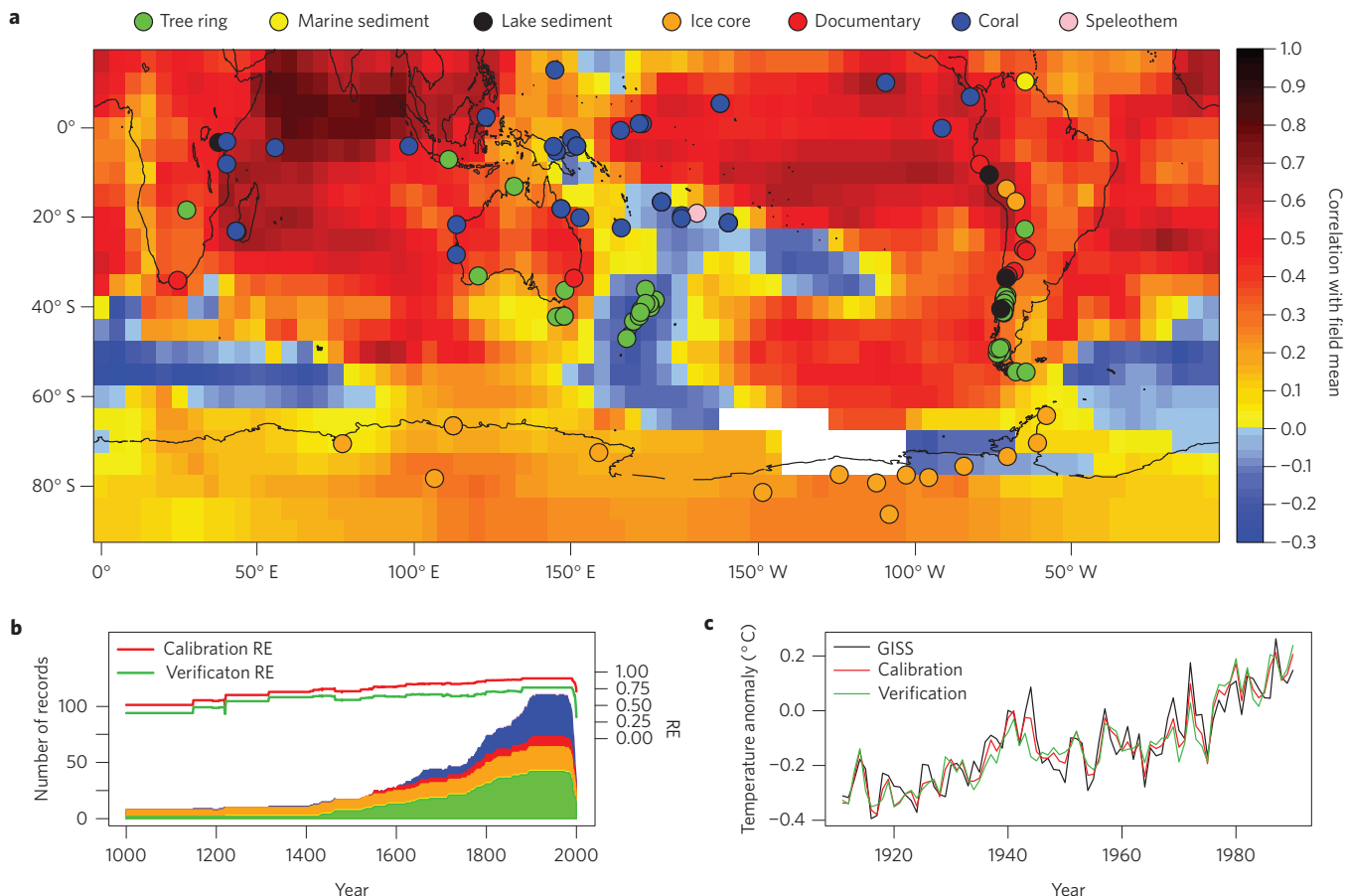


Figure 1 | Proxy data and calibration performance. **a**, Southern Hemisphere temperature reconstruction proxies. Shading represents GISS instrumental grid-cell temperature²⁸ correlations in the period 1911–1990, with the Southern Hemisphere field mean used as reconstruction target (all data linearly detrended). Cells with less than 30 years of data are blank. **b**, Temporal evolution of the number of proxy time series used in the reconstruction, with colours indicating the relative contribution of each archive and calibration (red) and verification (green) RE skill metric for the period 1000–2000. **c**, Instrumental target temperatures (with respect to 1961–1990) over the 1911–1990 calibration/verification period (black) and reconstruction ensemble means of the years used for calibration (red) and verification (green) for the most replicated proxy nest. Details in Methods and Supplementary Section 3.1.3.

predictors (Supplementary Section 1). This proxy collection nearly doubles the number of records considered in the most advanced previous reconstruction attempt⁴, now allowing the development of an annually resolved and well-verified Southern Hemisphere temperature reconstruction for the past millennium (Fig. 1 and Supplementary Section 2) which is insensitive to moderate changes in reconstruction methodology or proxy network composition (Supplementary Section 3).

Although our database is weighted towards the Pacific sector of the Southern Hemisphere (Fig. 1a), the proxy network captures the inter-annual to long-term variability in Southern Hemisphere mean temperatures recorded by instrumental data (calibration: $r = 0.73\text{--}0.95$, RE = 0.50–0.91; verification: $r = 0.57\text{--}0.88$, RE = 0.32–0.77; all $p \ll 0.01$; Fig. 1b,c). The Southern Hemisphere reconstruction ensemble shows temperatures in the period 1000 to 1200 CE (all years hereafter Common Era) that are close to the long term (1000–2000) average. This is followed by an approximately 150-year warm phase (1200–1350) containing the warmest pre-industrial temperatures of the past millennium (Fig. 2a). The subsequent long-term cooling trend reaches a minimum around 1600, with negative decadal-scale ensemble-mean temperature anomalies prevailing until the early twentieth century. 99.7% of the Southern Hemisphere reconstruction ensemble members indicate that the late twentieth century contained the warmest decade of the past millennium. This

finding complements well-established evidence for the anomalous characteristics of Northern Hemisphere industrial-era warming⁵. Besides the positive twentieth century temperature anomalies, simultaneous cold anomalies in both hemispheres are identified between 1571 and 1722 (based on the 1000–2000 long term mean; Fig. 2a). During the rest of the millennium, the Northern Hemisphere and Southern Hemisphere are more prominently characterized by differences in the occurrence, timing and phase of warm and cold episodes. In medieval times, Southern Hemisphere temperature anomalies are notably colder than the Northern Hemisphere both before 1100 and around 1400, and warmer between 1280 and 1350. Expression of the industrial-era warming trend in the Southern Hemisphere also lags by approximately 25 years behind the Northern Hemisphere. Moreover, Southern Hemisphere temperatures tend to show a weaker cooling response to strong volcanic eruptions, for example, during the early nineteenth century.

To determine the extent to which reconstructed temperature patterns are independently identified by climate models, we investigate inter-hemispheric temperature coherence from a 24-member multi-model ensemble (simulation details in Supplementary Table 9). Very similar temperature evolutions are modelled for the two hemispheres (Fig. 2b). The majority of model ensemble members show warmest pre-industrial temperatures sometime between 1050 and 1250 in the Northern Hemisphere

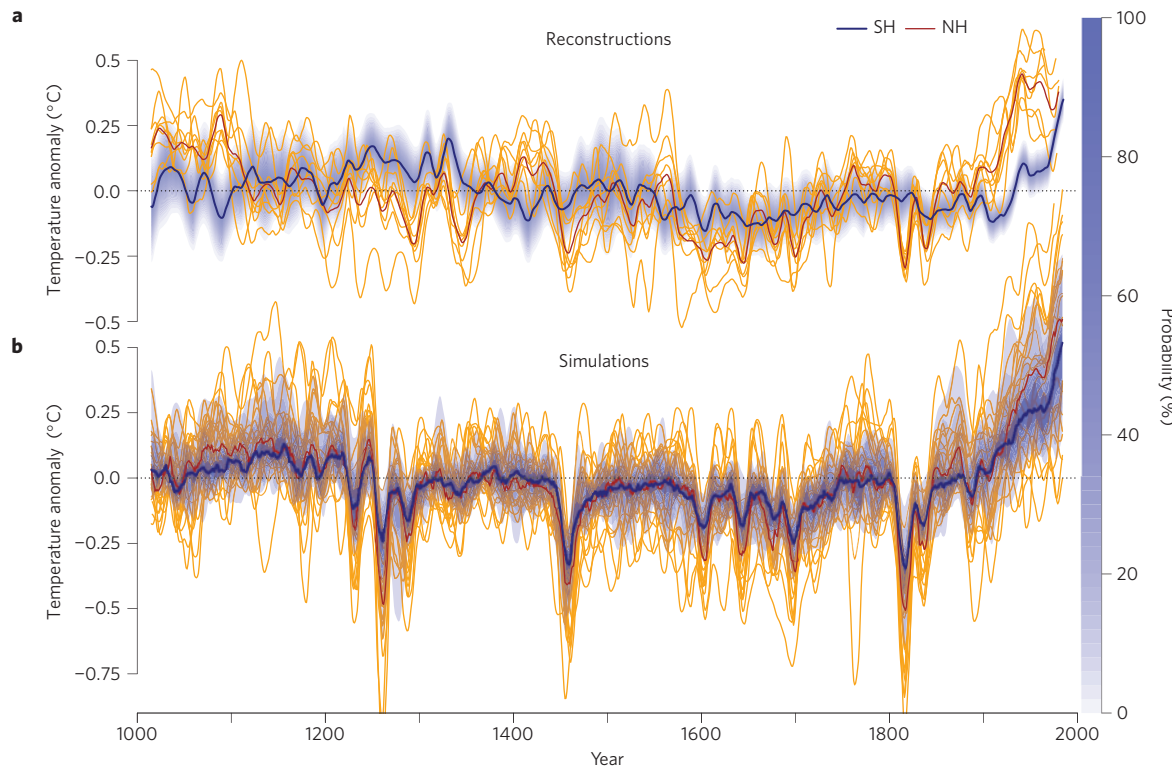


Figure 2 | Temperature variability over the past millennium. **a**, 30-year loess filtered ensemble mean temperature reconstruction for the Southern Hemisphere (SH; blue) and Northern Hemisphere (NH; red) relative to the millennium mean for the period 1000–2000. Blue shading based on Southern Hemisphere reconstruction uncertainties (Supplementary Section 2.4). Thin orange lines represent the ensemble means of the nine individual temperature reconstructions making up the Northern Hemisphere dataset⁵. **b**, as **a** but for the 24-member climate model ensemble. Note for consistency with reconstruction data, simulated temperatures are shown as individual simulations for the Northern Hemisphere and a probabilistic range based on ensemble percentiles for the Southern Hemisphere.

(79% of ensemble members), the Southern Hemisphere (75%), and simultaneously in both (67%) hemispheres. Interestingly, this simulated warm period is delayed compared to the reconstructed medieval warmth in the Northern Hemisphere and precedes the phase of maximum Southern Hemisphere pre-industrial warmth¹⁶. Between 1300 and 1900, simulated temperatures are close to the 1000–2000 average, periodically interrupted by shorter volcanically induced cold excursions. In contrast to the delay in industrial Southern Hemisphere warming in the reconstructions, the climate model simulations show a mostly synchronous temperature increase after 1850. Mean correlations between 30-year filtered reconstructions and simulations for all possible ensemble pairs are $r = 0.29 \pm 0.22$ (2σ ensemble spread) for the Southern Hemisphere and $r = 0.47 \pm 0.33$ for the Northern Hemisphere. These values increase to $r = 0.35$ and $r = 0.77$ for the ensemble means. As the model ensemble means are subjected less to internal variability than each individual simulation and better represent the temperature response to external forcing, these values suggest substantially weaker links between external forcing and Southern Hemisphere temperature variability compared to the Northern Hemisphere.

We quantify coherence between Northern Hemisphere and Southern Hemisphere temperature extremes by identifying the percentage of ensemble members showing decadal average temperatures more than one standard deviation above or below the 1000–2000 baseline (Fig. 3). Extended periods where at least 33% of the reconstruction ensemble members in both hemispheres simultaneously show extreme cold or warm temperatures are identified only between 1594 and 1677 and since 1967, respectively. Since 1974 more than 66%, and since 1979 more than 90%, of ensemble members show synchronous positive extremes

(corresponding to ‘likely’ and ‘very likely’ categories using IPCC AR5 calibrated uncertainty classification). This analysis provides evidence for a global cold phase coinciding with the peak of the Northern Hemisphere ‘Little Ice Age’ (LIA) and a late-twentieth century warm phase of unprecedented duration and magnitude within the past 1000 years. In contrast, we find no empirical support for a globally coherent ‘Medieval Climate Anomaly’ (MCA) at decadal timescales during the past millennium¹⁴. Our new temperature reconstruction from the Southern Hemisphere suggests that data from the Northern Hemisphere alone are insufficient to characterize global scale temperature anomalies, trends and extremes.

Simulated extreme conditions shown in Fig. 3 are a direct expression of external forcing (Fig. 3d). The notable reconstructed seventeenth-century peak LIA is less prominent in the model ensemble, which shows the clearest global cooling signal in response to volcanic eruptions around 1815 (Tambora), the 1450s (Kuwee) and 1258 (Samalas). External climate forcing as incorporated in the current climate model simulations does not account for key features of reconstructed temperature variation. This suggests that internal variability was a key driver for hemispheric and global decadal-scale extreme periods.

To further investigate inter-hemispheric temperature coherence, we calculate the ten-year running temperature differences between the standardized Northern Hemisphere and Southern Hemisphere reconstructions (Fig. 4a). The variability and amplitude of the Northern Hemisphere–Southern Hemisphere temperature difference fluctuates considerably over time, showing periods with large divergence (for example, around 1100 and 1575) and with more in-phase variability (for example, the thirteenth and eighteenth centuries). The distinct and internally driven

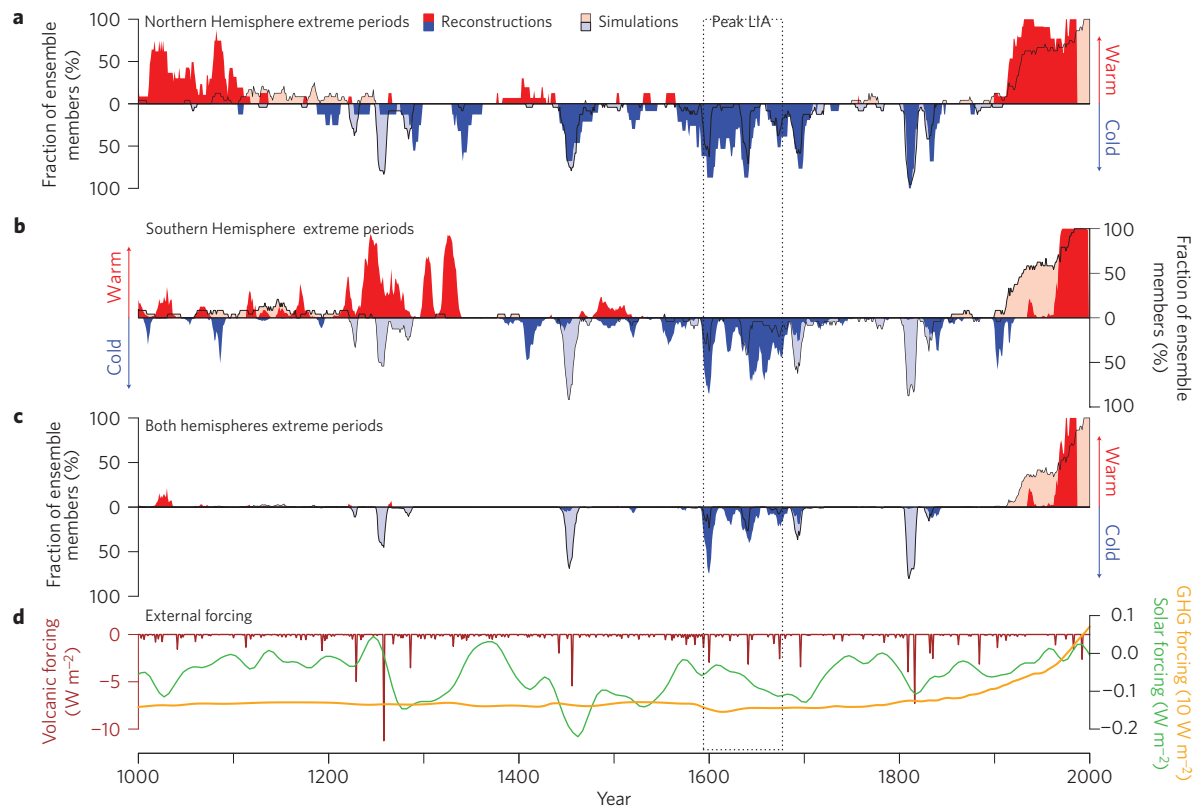


Figure 3 | Extreme periods. **a,b**, Fraction of ensemble members with extreme warm (red) or cold (blue) decadal temperatures in the Northern Hemisphere, (**a**) and Southern Hemisphere (**b**), respectively. Dark shading represents the reconstructions, light shading with black border the model simulations. **c**, Probabilities for simultaneous extreme periods in both hemispheres are calculated by multiplying the fractions in **a** and **b**. **d**, Volcanic²⁹ (brown), solar³⁰ (green) and greenhouse gas forcing¹⁹ (yellow) relative to 1961–1990. Dotted lines enclose the globally expressed peak Little Ice Age (LIA) 1594–1677.

drop in Northern Hemisphere temperatures around 1970² was preceded by several other analogous periods of contrasting hemispheric temperature trends. Internal ocean-atmosphere processes appear to be the main driver of the larger Northern Hemisphere–Southern Hemisphere differences; only two episodes of contrasting temperature regimes coincide with strong volcanic eruptions (Kuwae and Tambora). Model simulations also contain periods of contrasting inter-hemispheric temperature trends, but with notably smaller differences between the hemispheres (Supplementary Figs 36–59): median reconstructed Northern Hemisphere–Southern Hemisphere differences are outside the 10th–90th percentile range of model simulations 42% of the time (Fig. 4). The lower Northern Hemisphere–Southern Hemisphere temperature contrasts within the simulations are not only evident in the pre-instrumental period but also during the twentieth century³ (Fig. 4b,c), when both the reconstructions and instrumental data² show strong inter-hemispheric variability.

The Southern Hemisphere reconstruction presented here allows new insights into the characteristics of the global climate system. For example, it has been proposed that the Southern Hemisphere response to external forcing may be delayed and buffered by the large heat capacity of the oceans^{17,18}. The greater amplitude of pre-industrial temperature variation in the Northern Hemisphere ($0.67^{\circ}\text{C} \pm 0.46^{\circ}\text{C}$ (2σ ensemble spread) versus $0.37^{\circ}\text{C} \pm 0.11^{\circ}\text{C}$ in the Southern Hemisphere), the approximately two-century Northern Hemisphere lead during medieval times and the approximately 25 year lead during the era of industrial warming are in line with this hypothesis. However, we find no evidence for a consistent lag between Northern Hemisphere and Southern Hemisphere temperatures (Supplementary Section 8). The coherent and extreme cool conditions in both hemispheres

around 1600 are unique within the past millennium and now offer perhaps the most viable explanation for the drop in global CO₂ (difference of 8.37 ppm or 0.19 W m^{-2} between 1540–1580 and 1600–1640^{5,19,20}; Fig. 3d), which may not be sufficiently explained by land use change²¹ or Northern Hemisphere-temperature–CO₂ feedbacks⁵.

Our results suggest that large, internally driven temperature contrasts between the hemispheres, such as identified in the twentieth century² have repeatedly occurred on the policy-relevant multi-decadal to centennial timescales. This finding is strengthened by evidence from annually resolved regional temperature reconstructions^{14,22,23} and the timing of glacial fluctuations in New Zealand and the Northern Hemisphere²⁴. Our data support hypotheses that global and hemispheric temperature extremes and transitions may be initiated^{11,16,25} and prolonged²⁶ by internal variability and feedbacks. Analyses targeting periods where climate models and reconstructions differ will be necessary to identify weaknesses in both proxy- and model-based representations of the Earth's climate system. However, the strong inter-hemispheric coupling in the simulations assessed herein suggests that models overestimate the strength of externally forced relative to internal climate system variability, therefore implying more limited predictability not only on regional^{1,27} but also hemispheric scales. The stronger coherence between the Northern Hemisphere temperature reconstructions and external forcings similarly implies that detection and attribution studies¹⁰ and climate sensitivity estimates^{5,6} based on Northern Hemisphere data alone may not be representative of the global climate system. Future consideration of Southern Hemisphere temperature evolution should reduce uncertainties in estimating and attributing natural and anthropogenically forced climate variations.

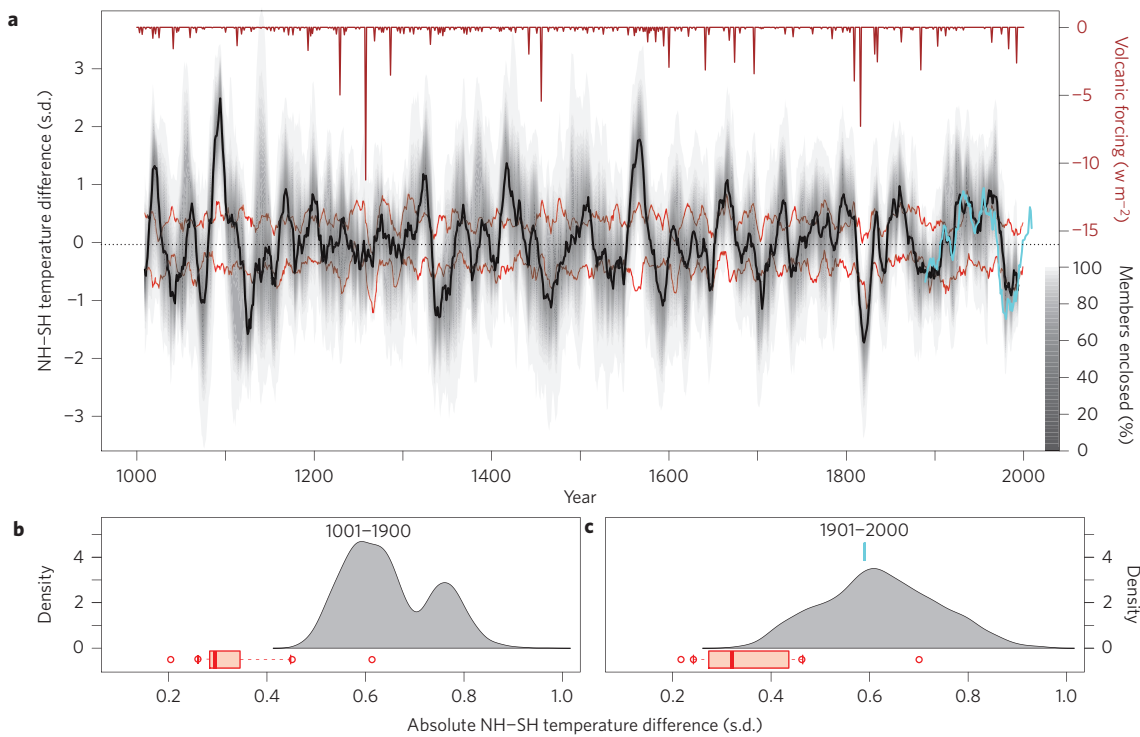


Figure 4 | Inter-hemispheric temperature difference. **a**, Difference between 10-year filtered Northern Hemisphere–Southern Hemisphere temperatures in the ensemble reconstructions after detrending and standardizing (black). The solid line represents the ensemble median, grey shading the percentiles. Cyan shows the instrumental data 1880–2010²⁸. Red lines are the 10th and 90th percentiles from the ensemble of model simulations. Volcanic forcing²⁹ shown at the top in brown. **b**, Ensemble distribution of the reconstructed absolute Northern Hemisphere–Southern Hemisphere temperature difference averaged over the 1000–1900 period. Red boxplot represents model simulations. **c** as **b** but for the twentieth century, cyan represents instrumental data.

Methods

Southern Hemisphere reconstruction ensemble. We use the Southern Hemisphere spatial mean of the Goddard Institute for Space Studies (GISS) Surface Temperature Analysis (GISTEMP) temperature grid²⁸ as the instrumental predictand for the reconstruction. The palaeoclimate data network¹⁵ consists of 48 marine (46 coral and 2 sediment time series) and 277 terrestrial (206 tree-ring sites, 42 ice core, 19 documentary, 8 lake sediment and 2 speleothem) records (details in Supplementary Section 1). Although proxy records are preferentially located towards land areas, the network represents a considerable improvement of both geographical coverage and proxy quantity and quality (for example, resolution, length) since the last Southern Hemisphere reconstruction effort⁴. Proxies are screened with local grid-cell temperatures²⁸ yielding 111 temperature predictors (Fig. 1) for the nested multivariate principal component regression procedure²³. A 3,000-member ensemble reconstruction of annual Southern Hemisphere temperatures over the period 1000–2000 was generated with the spread of ensemble members considered a measure of uncertainty.

For each ensemble member we use different reconstruction parameters by randomly selecting a subset of proxies, as well as varying the calibration/verification intervals within 1911–1990, and other reconstruction parameters (details in Supplementary Section 2.2). The perturbation of calibration/verification periods allows a ‘verification ensemble mean’ to be calculated over the 1911–1990 period by averaging all members where a given year was used for verification (and not for calibration). Analogously, a ‘calibration ensemble mean’ was calculated. These time series and their corresponding Reduction of Error (RE) skills are shown in Fig. 1c,b, respectively. These statistics along with additional verification based on the sparse early Southern Hemisphere instrumental data (RE = 0.41–0.90; Supplementary Fig. 10) point to reconstructive skill over the past millennium. In addition to traditional reconstruction uncertainty estimates based on regression residuals, we assess the influence of the ensemble perturbations on the reconstruction outcome. Uncertainty envelopes in Fig. 2a represent combined calibration and ensemble uncertainties (details in Supplementary Section 2.4).

Although we have taken steps to provide robust results considering the challenges of proxy-based reconstructions (for example, potential underestimation of past climate amplitudes) discussed in the literature, we note that all reconstruction approaches contain uncertainties. The fact that our reconstruction verifies well and captures interannual and decadal-scale temperature fluctuations during the instrumental period (Fig. 1 and

Supplementary Section 3) indicates reduced probability of such artefacts. An extensive assessment of reconstruction robustness is provided in Supplementary Section 3.2 and Supplementary Figs 13–26, with tests demonstrating that the potential bias introduced by the proxy-screening and reconstruction methods or by single dominant records or proxy archives is small.

Northern Hemisphere reconstruction ensemble. Details concerning the Northern Hemisphere reconstructions are provided in ref. 5 and Supplementary Section 5. The most important difference from our Southern Hemisphere reconstruction is that it is not based on a single predictor matrix but uses nine published Northern Hemisphere reconstructions based on different (but not independent) proxy sets and various reconstruction methodologies. In ref. 5, the individual single-member reconstructions were recalibrated to instrumental temperature data using different calibration periods as ensemble parameters, resulting in a total of 521 ensemble members. The Northern Hemisphere ensemble spread is larger than in the Southern Hemisphere owing to the relatively large differences between some of the original sub-reconstructions and the composite-plus-scaling approach over a range of time windows in ref. 5. To best illustrate these two approaches, the ensemble means of the nine sub-reconstructions are shown for the Northern Hemisphere in Fig. 2a. As a consequence of these methodological differences and the larger ensemble spread in the Northern Hemisphere, one would expect generally reduced probabilities for extreme periods in the Northern Hemisphere. However, Fig. 3a,b shows similar fractions of periods with high probabilities for extremes, indicating a similar consistency between ensemble members in the timing of extreme periods in both hemispheres.

Extreme periods (Fig. 3). To quantify extreme periods, we calculate 10-year running averages relative to the 1000–2000 mean. All years exceeding the ± 1 standard deviation range (calculated over the unfiltered 1000–2000 period) are considered extreme. We quantify the probability of extreme periods as the fraction of ensemble members exceeding this threshold for each year (Fig. 3a,b). Probabilities for simultaneous extreme periods are calculated by multiplying the probabilities of each hemisphere (Fig. 3c).

Northern Hemisphere–Southern Hemisphere difference (Fig. 4). To evaluate the decadal to centennial coherence, reconstruction and climate model data are detrended using a 200-year loess-filter before the analysis. Instrumental data are

linearly detrended. Ten-year running averages are then calculated and divided by the standard deviation over 1000–2000 to allow relative comparison of hemispheric fluctuations. Each of the standardized filtered Southern Hemisphere reconstructions is subtracted from a randomly selected Northern Hemisphere reconstruction, with shaded probabilities in Fig. 4a indicating the fraction of ensemble members enclosed. Modelled Northern Hemisphere–Southern Hemisphere differences are calculated individually for each simulation (alternative calculations in Supplementary Section 10). The distributions in Fig. 4b,c are calculated from the average absolute Northern Hemisphere–Southern Hemisphere difference over the respective time interval for each ensemble member. Boxes, whiskers and circles of the boxplots in Fig. 4b,c represent interquartile range, 5th/95th percentiles and extremes, respectively; bold line indicates the median.

Received 18 November 2013; accepted 25 February 2014;
published online 30 March 2014

References

- Deser, C., Knutti, R., Solomon, S. & Phillips, A. S. Communication of the role of natural variability in future North American climate. *Nature Clim. Change* **2**, 775–779 (2012).
- Thompson, D. W. J., Wallace, J. M., Kennedy, J. J. & Jones, P. D. An abrupt drop in Northern Hemisphere sea surface temperature around 1970. *Nature* **467**, 444–447 (2010).
- Friedmann, A., Hwang, Y., Chiang, J. & Frierson, D. Interhemispheric temperature asymmetry over the 20th century and in future projections. *J. Clim.* **26**, 5419–5433 (2013).
- Mann, M. *et al.* Proxy-based reconstructions of hemispheric and global surface temperature variations over the past two millennia. *Proc. Natl Acad. Sci. USA* **105**, 13252–13257 (2008).
- Frank, D. C. *et al.* Ensemble reconstruction constraints on the global carbon cycle sensitivity to climate. *Nature* **463**, 527–532 (2010).
- Hegerl, G. C., Crowley, T. J., Hyde, W. T. & Frame, D. J. Climate sensitivity constrained by temperature reconstructions over the past seven centuries. *Nature* **440**, 1029–1032 (2006).
- Frank, D., Esper, J., Zorita, E. & Wilson, R. A noodle, hockey stick, and spaghetti plate: A perspective on high-resolution paleoclimatology. *WIREs Clim. Change* **1**, 507–516 (2010).
- Jones, P. D., Briffa, K. R., Barnett, T. P. & Tett, S. F. B. High-resolution palaeoclimatic records for the last millennium: Interpretation, integration and comparison with General Circulation Model control-run temperatures. *Holocene* **8**, 455–471 (1998).
- Mann, M. E. & Jones, P. D. Global surface temperatures over the past two millennia. *Geophys. Res. Lett.* **30**, 1820 (2003).
- Hegerl, G. *et al.* Detection of human influence on a new, validated 1500-year temperature reconstruction. *J. Clim.* **20**, 650–666 (2007).
- Gosse, H. *et al.* The role of forcing and internal dynamics in explaining the “Medieval Climate Anomaly”. *Clim. Dynam.* **39**, 2847–2866 (2012).
- WAIS Divide Project Members. Onset of deglacial warming in West Antarctica driven by local orbital forcing. *Nature* **500**, 440–444 (2013).
- Shakun, J. D. *et al.* Global warming preceded by increasing carbon dioxide concentrations during the last deglaciation. *Nature* **484**, 49–54 (2012).
- PAGES 2k Consortium. Continental-scale temperature variability during the past two millennia. *Nature Geosci.* **6**, 339–346 (2013).
- Neukom, R. & Gergis, J. Southern Hemisphere high-resolution palaeoclimate records of the last 2000 years. *Holocene* **22**, 501–524 (2012).
- Fernández-Donado, L. *et al.* Large-scale temperature response to external forcing in simulations and reconstructions of the last millennium. *Clim. Past* **9**, 393–421 (2013).
- Stouffer, R. J., Manabe, S. & Bryan, K. Interhemispheric asymmetry in climate response to a gradual increase of atmospheric CO₂. *Nature* **342**, 660–662 (1989).
- Gosse, H. *et al.* A late medieval warm period in the Southern Ocean as a delayed response to external forcing? *Geophys. Res. Lett.* **31**, L06203 (2004).
- MacFarling-Meure, C. *et al.* Law Dome CO₂, CH₄ and N₂O ice core records extended to 2000 years BP. *Geophys. Res. Lett.* **33**, L14810 (2006).
- Jungclaus, J. H. *et al.* Climate and carbon-cycle variability over the last millennium. *Clim. Past* **6**, 723–737 (2010).
- Pongratz, J., Caldeira, K., Reick, C. H. & Claussen, M. Coupled climate-carbon simulations indicate minor global effects of wars and epidemics on atmospheric CO₂ between AD 800 and 1850. *Holocene* **21**, 843–851 (2011).
- Wahl, E. R. & Smerdon, J. E. Comparative performance of paleoclimate field and index reconstructions derived from climate proxies and noise-only predictors. *Geophys. Res. Lett.* **39**, L06703 (2012).
- Neukom, R. *et al.* Multiproxy summer and winter surface air temperature field reconstructions for southern South America covering the past centuries. *Clim. Dynam.* **37**, 35–51 (2011).
- Schaefer, J. M. *et al.* High-frequency holocene glacier fluctuations in New Zealand differ from the northern signature. *Science* **324**, 622–625 (2009).
- González-Rouco, F. J. *et al.* Medieval Climate Anomaly to Little Ice Age transition as simulated by current climate models. *PAGES News* **19**, 7–8 (2011).
- Miller, G. H. *et al.* Abrupt onset of the Little Ice Age triggered by volcanism and sustained by sea-ice/ocean feedbacks. *Geophys. Res. Lett.* **39**, L02708 (2012).
- Braconnot, P. *et al.* Evaluation of climate models using palaeoclimatic data. *Nature Clim. Change* **2**, 417–424 (2012).
- Hansen, J., Ruedy, R., Sato, M. & Lo, K. Global surface temperature change. *Rev. Geophys.* **48**, RG4004 (2010).
- Crowley, T. J. *et al.* Volcanism and the Little Ice Age. *PAGES News* **16**, 22–23 (2008).
- Steinliber, F., Beer, J. & Fröhlich, C. Total solar irradiance during the Holocene. *Geophys. Res. Lett.* **36**, L19704 (2009).

Acknowledgements

This work has been possible thanks to the collaboration of many members of the Australasian, South American, African and Antarctic working groups of the PAGES Regional 2K initiative. Researchers from these working groups are warmly thanked for providing metadata inventories and access to data. S. J. Phipps is acknowledged for support with model data. We acknowledge funding from the Swiss National Science Foundation and funding from the Australian Research Council (Projects LP0990151 and DE130100668) and the Australian Department of Climate Change and Energy Efficiency.

Author contributions

R.N. performed data analyses and developed the figures and tables. R.N., D.F. and J.G. led the writing of the paper. R.N., J.G., D.J.K., H.W. and D.F. designed the study. M.C., J.E., B.K.L., A.D.M., I.M., E.J.S., T.V., R.V., T.v.O. and J.Z. assisted with proxy data and F.G. and C.C.R. with climate model data. All authors discussed the results and commented jointly on the manuscript.

Additional information

Supplementary information is available in the [online version of the paper](#). Reprints and permissions information is available online at [www.nature.com/reprints](#). Correspondence and requests for materials should be addressed to R.N.

Competing financial interests

The authors declare no competing financial interests.

Inter-hemispheric temperature variability over the past millennium

Raphael Neukom^{1,2*}, Joëlle Gergis³, David J. Karoly^{3,4}, Heinz Wanner¹, Mark Curran^{5,6}, Julie Elbert¹, Fidel González-Rouco⁷, Braddock K. Linsley⁸, Andrew D. Moy^{5,6}, Ignacio Mundo^{9,10}, Christoph C. Raible^{1,11}, Eric J. Steig¹², Tas van Ommen^{5,6}, Tessa Vance⁶, Ricardo Villalba⁹, Jens Zinke^{13,14} and David Frank^{1,2}

¹ *Oeschger Centre for Climate Change Research, University of Bern, 3012 Bern, Switzerland*

² *Swiss Federal Research Institute WSL, Zürcherstrasse 111, CH-8903 Birmensdorf, Switzerland*

³ *School of Earth Sciences, University of Melbourne, VIC 3010, Australia*

⁴ *ARC Centre of Excellence for Climate System Science, University of Melbourne, VIC 3010, Australia*

⁵ *Department of the Environment, Australian Antarctic Division, Kingston, Tasmania 7050, Australia*

⁶ *Antarctic Climate & Ecosystems Cooperative Research Centre, University of Tasmania, Hobart, Tasmania, 7000, Australia*

⁷ *Departamento Astrofísica y CC de la Atmósfera, Instituto de Geociencias (CSIC-UCM) Universidad Complutense de Madrid, Madrid, 28040, Spain*

⁸ *Lamont-Doherty Earth Observatory, Columbia University, Palisades, NY 10964, USA*

⁹ *Instituto Argentino de Nivología, Glaciología y Ciencias Ambientales (IANIGLA), CCT CONICET-Mendoza, 5500, Argentina*

¹⁰ *LISEA, Facultad de Ciencias Agrarias y Forestales, Universidad Nacional de La Plata, B1900 La Plata, Argentina*

¹¹ *Climate and Environmental Physics, University of Bern, 3012 Bern, Switzerland*

¹² *Quaternary Research Center and Department of Earth and Space Sciences, University of Washington, Seattle, WA 98195, USA*

¹³ *School of Earth and Environment, University of Western Australia Oceans Institute, 35 Stirling Highway, Crawley WA 6009, Australia*

¹⁴ *Australian Institute of Marine Science, Nedlands WA 6009, Australia*

*Corresponding author

Raphael Neukom

Now at institute of Geography, University of Zurich, Switzerland

Email: neukom@giub.unibe.ch

Contents

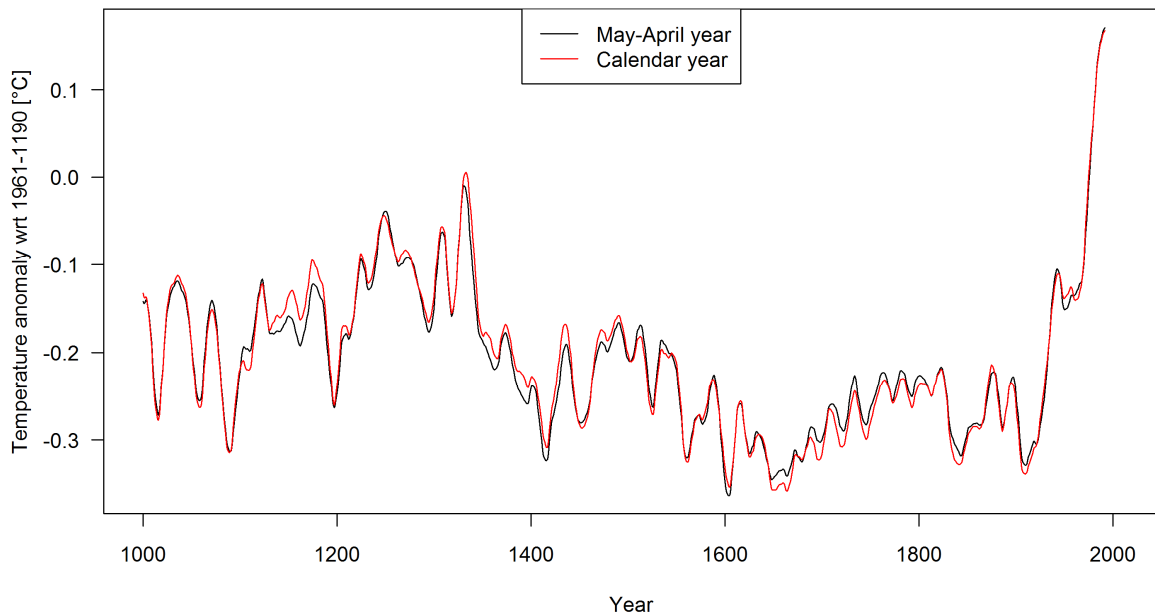
1.	Data processing and predictor selection.....	3
1.1.	Instrumental Data.....	3
1.2.	Proxy database	4
1.2.1.	Tree-ring records.....	5
1.2.2.	Subannually resolved coral records.....	5
1.2.3.	Documentary records	5
1.3.	Predictor selection.....	10
1.4.	Missing values 1911-1990	12
2.	Ensemble reconstruction.....	17
2.1.	Reconstruction methodology	17
2.2.	Ensemble parameters	17
2.3.	Required number of ensemble members	21
2.4.	Reconstruction uncertainties	23
2.5.	Unfiltered SH mean reconstruction.....	24
3.	Reconstruction reliability.....	26
3.1.	Reconstruction skill	26
3.1.1.	Ensemble validation	27
3.1.2.	Ensemble mean early verification	27
3.1.3.	Ensemble mean verification and calibration years	28
3.1.4.	Ensemble mean RMSE.....	28
3.1.5.	Noise predictors.....	28
3.1.6.	Ensemble vs. single reconstruction	30
3.2.	Reconstruction robustness.....	32
3.2.1.	Alternative reconstruction methods: CPS.....	32
3.2.2.	Alternative reconstruction methods: LNA.....	34
3.2.3.	Influence of changes in proxy replication.....	37
3.2.4.	Influence of different proxy screening approaches.....	41
3.2.5.	Influence of different proxy archives	42
3.2.6.	Influence of individual proxy records.....	44
3.2.7.	Ensemble median vs. mean	46
3.3.	Conclusions.....	47
4.	Sensitivity to instrumental target data.....	48
5.	NH reconstruction ensemble.....	49
6.	Simultaneous extreme periods	50
7.	Details on climate model simulations	51
8.	Lag between the hemispheres	54
9.	Alternative reference period and comparison with earlier SH and regional reconstructions.....	55
10.	Alternative illustrations of inter-hemispheric differences	59
10.1.	Inter-model comparisons.....	59
10.2.	Raw vs. detrended data.....	61
10.3.	Bimodal distribution in Figure 4b	62
10.4.	Outlier in the model simulations (Figures 4b and 4c)	63
11.	NH-SH differences in the individual model simulations.....	64
12.	References	88

1. Data processing and predictor selection

1.1. Instrumental Data

We use the Goddard Institute for Space Studies surface temperature analysis (GISTEMP) combined land and ocean temperature grid (Hansen *et al.*, 2010) as target data for our reconstructions. The version allowing for a search radius of 1200 km for the temperature station measurements of each grid cell is used (details see Hansen *et al.*, 2010). We use the latitude weighted spatial average of all grid cells south of the equator as the reconstruction target.

We choose the May to April year as the target seasonal window, because phase changes in ENSO, typically occur in austral autumn (Karoly, 1989; Trenberth and Hurrell, 1994; Karoly *et al.*, 1996; Karoly and Vincent, 1998). Also, calendar years are not an optimal window for Southern Hemisphere (SH) reconstructions because the tree-ring growing season in the SH extends over two calendar years during austral summer. Supplementary Figure 1 compares our final reconstruction using a May-April target seasonal window to a reconstruction using a calendar year mean target. The two reconstructions are very similar, and so the choice of the target seasonal window does not affect our conclusions.



Supplementary Figure 1 | Reconstruction based on different target seasons. Comparison of our reconstruction using May-April averages for the instrumental target data (black) and a calendar year average (red).

1.2. Proxy database

As a basis for our proxy selection we use the SH proxy network presented by Neukom and Gergis (2012). Additionally, new records are added to the network (details and references see Supplementary Tables 1-4): Laguna Pumacocha and Lake Challa Sediments, the high resolution sections (<5 years) of El Junco Lake, Lake Edward and Lake Masoko, a new documentary record from New South Wales and sea salt from an ice core at Law Dome, Antarctica.

Some tree-ring records from South America that were used in Neukom and Gergis (2012) had to be excluded because of lack of permission from the original authors to make the chronologies publicly available (Supplementary Table 1). Correlations of all proxies with the dominant climate modes of the SH in the May to April window are provided by Neukom and Gergis (2012).

The most important details of proxy data preparation are summarized in the following paragraphs. For further details we refer to Neukom & Gergis (2012).

1.2.1. Tree-ring records

Tree-ring records from individual sites are grouped into regional composites where possible. This grouping strengthens the common signal, reduces the number of records from more than 200 to 84 and improves the balance of records from different climate archives. All composite records are listed in Supplementary Table 1, and the individual sub-chronologies that were aggregated into the composites are listed in Table S1 in Neukom & Gergis (2012). All tree-ring chronologies are established using either signal free detrending (Melvin *et al.*, 2007; Melvin and Briffa, 2008) or negative exponential curves. In order to avoid reconstruction biases based on the detrending method, we randomly choose between one of the two methods for each tree-ring record and ensemble member (see below, section 2.2). Years where less than five samples are available or where the expressed population signal (EPS; Briffa and Jones, 1990) is <0.85 are excluded.

1.2.2. Subannually resolved coral records

All coral records with higher than annual resolution are averaged over the May to April window. All coral records are listed in Supplementary Table 2.

1.2.3. Documentary records

Some documentary records did not originally cover the 20th century (Supplementary Table 4). In order to be able to calibrate them, we extend them to present using the “pseudo documentary” approach described by Neukom *et al.* (2009; 2013). In this approach, the representative instrumental data for each record are degraded with white noise and then classified into the index categories of the documentary record in order to realistically mimic its statistical properties and not overweight the record in the multiproxy calibration process. The amount of noise to be added is determined based on the overlap correlations with the instrumental data. In order to avoid potential biases by using only one iteration of noise-

degrading, we create 1,000 “pseudo documentaries” for each record and randomly sample one realization for each ensemble member (see below, Section 2.2). All documentary records are listed in Supplementary Table 4.

Supplementary Table 1 (next page) | Metadata of the available tree-ring records (before the proxy screening). Site name, longitude ($^{\circ}$ E), latitude ($^{\circ}$ N), altitude (m.a.s.l.), start year (Common Era CE), end year (CE), species code, sample depth, number of sub-sites for composite records, reference(s). Updated from Neukom & Gergis (2012). The red shaded records are excluded from the reconstructions because of lack of permission to publish the final chronology.

SiteName	Lon	Lat	Alt	Start	End	Species	n	Subs	Reference(s)
Africa									
Zimbabwe	27.33	-18.5	1000	1875	1996	PTAN	36		Therrell et al. (2006)
Die Bos, South Africa	19.2	-32.4		1763	1976	WICE	55		Dunwiddie and LaMarche (1980)
Australasia									
Teak Indonesia	111	-7		1780	2005	TEGR	239		D'Arrigo et al. (2006)
Northern Territory Callitris	132	-13		1896	2006	CAIN	54		Baker et al. (2008)
Western Australia Callitris	120.8	-33.03	300	1758	2005	CACO	37		Cullen et al. (2009)
Kauri NZ	174	-36	200	1577	2002	AGAU	527		Cook et al. (2006), Fowler et al. (2008)
Baw Baw Victoria	148.3	-36.42	2000	1818	2002	EUPA	223		Brookhouse et al. (2008)
Urewera NZ	177.2	-38.68	930	1462	1987	LIBI	68		Xiong and Palmer (2000)
North Island LIBI Composite 2	174.1	-39.27	1000	1651	1990	LIBI	129	2	Xiong and Palmer (2000)
Mangawhero NZ	175.5	-39.35	1000	1551	1994	LGCO	56		D'Arrigo et al. (2000)
North Island LIBI Composite 1	175.5	-39.5	1100	1526	1992	LIBI	235	5	Xiong and Palmer (2000)
Takapari NZ	176	-40.07	960	1533	1992	LIBI	63		Xiong and Palmer (2000)
Moa Park NZ	172.9	-40.93	1036	1623	1991	LIBI	49		Xiong and Palmer (2000)
Flanagans Hut NZ	172.6	-41.27	950	1776	1991	LIBI	33		Xiong and Palmer (2000)
CTP East Tasmania	148	-42	600	1430	1994	PHAS	165	2	Allen et al. (2001)
CTP West Tasmania	146	-42	600	1547	1998	PHAS	301	8	Allen et al. (2001), Allen (2002), LaMarche et al. (1979c)
Mount Read Tasmania	147	-42	600	494	1999	LGFR	317		Cook et al. (2000), Cook et al. (2006)
Pink Pine NZ	172	-42		1457	1999	HABI	356	7	Duncan et al. (2010)
Buckley's Chance Tasmania	145.9	-42.26	900	1463	1991	LGFR	84		Buckley et al. (1997)
Oroko Temperature recon	170.3	-43.23	110	1	2003	LGCO	330		Cook et al. (2006)
Stewart Island NZ	168	-47	450	1758	1993	HABI	106	3	D'Arrigo et al. (1995), D'Arrigo et al. (2000)
South America									
ALT Composite 1	-69	-17.5	4300	1872	2002	POTA	77	3	Soliz et al. (2009)
ALT Composite 2	-69.08	-18.45	4730	1542	2002	POTA	78	2	Soliz et al. (2009), Christie et al. (2009b)
ALT Composite 3	-67.5	-21.5	4500	1630	2003	POTA	214	6	Argollo et al. (2004), Soliz et al. (2009), Morales et al. (2004)
La Meseda	-65.02	-23	1600	1822	1999	CELI	23		unpublished (R. Villalba pers. comm. 2007)
NWA Composite 1	-65	-23	1200	1899	1998	JGAU	35	2	Villalba et al. (1992)
NWA Composite 4	-65	-24	1750	1858	1981	CEAN	50	2	Villalba et al. (1992)
NWA Composite 2	-65	-24	2200	1858	1995	ALAC, CELI, JGAU	126	4	Villalba et al. (1992), Morales et al. (2004)
Rio Sala and Popayan	-64.6	-24.6	700	1879	2002	JGAU	39		Villalba et al. (1992)
NWA Composite 5	-65.5	-25	2000	1874	2001	JGAU	92	3	Villalba et al. (1992)
Dique Escaba	-65.78	-27.7	900	1877	1985	JGAU	24		Villalba et al. (1992)
EI Asiento	-70.82	-32.48	1800	1515	1972	AUCH	65		La Marche et al. (1979b)
Le Quesne precip recon	-70.5	-34	1700	1200	2000	AUCH	525	7	Le Quesne et al. (2006)
CAN Composite 1	-70.5	-34.5	1200	1520	1975	AUCH	165	3	La Marche et al. (1979b)
Vilches	-71.03	-35.6	1530	1873	1996	NOPU	49		Lara et al. (2001)
Christie AUCH Composite	-71.3	-37	1135	1346	2004	AUCH	511	5	Christie et al. (2009a)
Huinganco	-70.6	-37.75	1400	1673	2000	AUCH	101		La Marche et al. (1979a)
CAN Composite 2	-71	-37.83	1530	1714	2006	ARAR	83	3	La Marche et al. (1979a), Mundo et al. (2012)
CAN Composite 3	-71.25	-38	1570	1868	1975	ARAR	41	2	La Marche et al. (1979a)
Volcan Lonquimay	-71.57	-38.38	1510	1700	1975	ARAR	47		La Marche et al. (1979b)
CAN Composite 6	-71.5	-38.5	1400	1435	2006	ARAR	357	8	La Marche et al. (1979a), Villalba (1990a), Mundo et al. (2012)
CAN Composite 5	-71.58	-38.62	1640	1843	1996	NOPU	76	2	Lara et al. (2001)
Pino Hachado	-70.75	-38.63	1400	1767	1974	ARAR	31		La Marche et al. (1979a)
Conguillio (Lenga abajo)	-71.6	-38.63	1490	1788	1996	NOPU	55		Lara et al. (2001)
CAN Composite 4	-71.5	-39	1500	1807	1994	NOPU	120	4	Lara et al. (2001), Schmelter (2000)
CAN Composite 8	-71.17	-39.17	1125	1773	1989	AUCH	69	2	Villalba and Veblen (1997)
CAN Composite 31	-71.3	-39.2	1168	1731	2006	ARAR	83	2	Mundo et al. (2012)
Lago Rucachoroi	-71.17	-39.22	1330	1721	1976	AUCH	26		La Marche et al. (1979a)
CAN Composite 9	-71.25	-39.33	1100	1636	2006	ARAR	283	6	La Marche et al. (1979a), Mundo et al. (2012)
CAN Composite 10	-70.83	-39.5	1320	1784	1989	ARAR, AUCH	44	2	La Marche et al. (1979a), Villalba and Veblen (1997)
CAN Composite 12	-71	-40	800	1645	1992	AUCH	175	5	La Marche et al. (1979b), Villalba and Veblen (1997)
Chapelco	-71.23	-40.33	1700	1814	1985	NOPU	29		ITRDB series arge029
CAN Composite 11	-72.32	-40.62	805	1567	2002	PLUV	146	3	Lara et al. (2008)
Paso Cordova	-71.25	-40.67	1890	1811	1986	NOPU	37		ITRDB series arge050
CAN Composite 13	-71.25	-41	1000	1532	2003	AUCH	360	11	Villalba and Veblen (1997), Lara et al. (2008)
CAN Composite 16	-71.8	-41.13	1500	1857	1991	NOPU	43	2	Villalba et al. (1997b)
CAN Composite 14	-71.8	-41.13	1500	1859	1994	NOPU	79	3	Villalba et al. (1997b), Schmelter (2000)
CAN Composite 17	-71.83	-41.17	1700	1892	1994	NOPU	55	3	Villalba et al. (1997b), Schmelter (2000)
CAN Composite 15	-71.92	-41.17	1300	1582	1991	NOPU	102	4	Villalba et al. (1997b)
CAN Composite 19	-72.27	-41.17	1225	1858	1998	NOPU	130	2	Lara et al. (2005)
CAN Composite 18	-71.5	-41.25	1550	1639	1994	NOPU	113	3	Schmelter (2000)
CAN Composite 20	-71.83	-41.33	900	1117	1995	FICU	184	4	Villalba (1990b), Lara et al. (2000)
CAN Composite 21	-71.5	-41.5	670	1790	1991	AUCH	38	2	Villalba and Veblen (1997)
CAN Composite 22	-71.75	-41.75	1300	1720	1994	NOPU	71	3	Villalba et al. (1998), Schmelter (2000)
CAN Composite 23	-71.83	-42	1220	1204	1993	FICU	60	2	Lara et al. (2000)
CAN Composite 24	-71.33	-42.5	765	1749	2002	AUCH	33	2	La Marche et al. (1979a), Lara et al. (2008)
CAN Composite 26	-73.83	-42.5	750	1794	1987	FICU, PLUV	60	2	Villalba (1990a), Roig (1991)
CAN Composite 25	-71.83	-42.5	550	769	1990	FICU	137	3	Lara et al. (2000)
Santa Lucia	-72.5	-43	540	1680	1986	PLUV	60		Szeicz et al. (2000)
Cisnes	-71.7	-44.65	1100	1834	1997	NOPU	54		Lara et al. (2005)
Puesto Miraflores	-72.15	-48.45	1039	1755	1998	NOPU	23		Unpublished (R. Villalba pers. comm. 2010)
CAN Composite 32	-72.25	-48.45	945	1730	2007	NOPU	88	2	Villalba et al. (2003)
O Higgins	-72.5	-48.5	1200	1886	1999	NOPU	24		Lara et al. (2005)
CAN Composite 27	-72	-49	800	1715	2002	NOPU	199	3	Boninsegna et al. (1989), Sru et al. (2008)
El Chalten bajo	-72.9	-49.37	760	1826	2003	NOPU	100		Sru et al. (2008)
CAN Composite 33	-73.33	-49.45	775	1726	2007	NOPU	125	3	Villalba et al. (2003), unpublished (R. Villalba pers. comm. 2010)
Torre Morena 4	-73.5	-49.5	658	1798	2007	NOPU	42		Unpublished (R. Villalba pers. comm. 2010)
Valle Ameghino	-72.17	-50.42	700	1766	1997	NOPU	41		Masiokas and Villalba (2004)
CAN Composite 34	-73.7	-50.6	461	1795	2007	NOPU	67	2	Unpublished (R. Villalba pers. comm. 2010)
Heim Morena Este	-73.7	-50.6	650	1806	2007	NOPU	33		Unpublished (R. Villalba pers. comm. 2010)
CAN Composite 30	-70	-53	220	1851	1986	NOPU	128	2	Aravena et al. (2002)
SAN Composite 5	-67.67	-54.75	600	1718	1984	NOBE	131	4	Boninsegna et al. (1989)
Puerto Parryn	-64.37	-54.83	20	1893	1986	NOBE	25		Boninsegna et al. (1989)
SAN Composite 6	-64.33	-54.83	40	1781	1986	NOBE	49	2	Boninsegna et al. (1989)

Supplementary Table 2 | Metadata of the available coral records (before the proxy screening). Site name, longitude ($^{\circ}$ E), latitude ($^{\circ}$ N), start year (CE), end year (CE), species, temporal resolution, proxy variable(s), reference(s). Updated from Neukom & Gergis (2012).

SiteName	Longitude	Latitude	Start	End	Species	Resolution	Proxy	Reference(s)
<i>Indian Ocean</i>								
Malindi	40.00	-3.00	1801	1994	Porites lutea	Annual	d18O	Cole et al. (2000)
Mafia, Tanzania	40.00	-8.00	1622	1998	Diplastrea heliopora	Monthly	d18O	Damassa et al. (2006)
Ifaty, Madagascar 1	43.00	-23.00	1882	1994	Porites lutea	Annual	d18O, Sr/Ca	Unpublished (J. Zinke pers. comm.)
Ifaty, Madagascar 4	43.58	-23.15	1858	2007	Porites lutea	Bim., ann.	d18O, Sr/Ca	Zinke et al. (2004), unpublished (J. Zinke pers. comm.)
Mayotte	45.10	-12.65	1865	1993	Porites solida	Bimonthly	d18O	Zinke et al. (2009)
La Reunion	55.25	-21.03	1832	1995	Porites	Bimonthly	d18O	Pfeiffer et al. (2004)
Seychelles	55.80	-4.62	1846	1995	Porites lutea	Monthly	d18O	Charles et al. (1997), Abram et al. (2008)
Rodrigues	63.00	-19.00	1789	2005	Porites	Ann., mon.	d18O, Sr/Ca	Unpublished (J. Zinke pers. comm.)
Mentawai West Sumatra	98.50	-4.00	1858	1997	Porites	Monthly	d18O	Abram et al. (2008)
Abrolhos	113.77	-28.45	1794	1993	Porites lutea	Bimonthly	d18O	Kuhnert et al. (1999)
Ningaloo	113.97	-21.90	1878	1995	Porites lutea	Seasonal	d18O	Kuhnert et al. (2000)
Bali	115.00	-8.00	1783	1990	Porites	Monthly	d18O	Charles et al. (2003)
Bunaken	123.00	2.80	1863	1990	Porites	Monthly	d18O	Charles et al. (2003)
<i>Pacific Ocean</i>								
Laing	144.88	-4.15	1884	1993	Porites	Seasonal	d18O	Tudhope et al. (2001)
Guam	145.00	13.00	1790	2000	Porites lobata	Monthly	d18O	Asami et al. (2005)
Madang Lagoon	145.82	-5.22	1880	1993	Porites	Seasonal	d18O	Tudhope et al. (2001)
Great Barrier Reef precip recon	147.00	-18.00	1630	1981	Porites	Annual	Luminescence	Lough (2011)
Kavieng, Papua New Guinea	150.50	-2.50	1823	1997	Porites	Monthly	Sr/Ca, Ba/Ca	Alibert and Kinsley (2008a,b)
Rabaul	152.00	-4.00	1867	1997	Porites	Monthly	d18O, Sr/Ca	Quinn et al. (2006)
Abraham	153.00	-20.00	1638	1983	Porites	Annual	d18O	Druffel and Griffin (1999)
Nauru	166.00	-0.83	1897	1995	Porites lutea	Seasonal	d18O	Guilderson et al. (1999)
Amedee New Caledonia	166.45	-22.48	1657	1992	Porites lutea	Seasonal	d18O	Quinn et al. (1998)
Vanuatu	167.00	-15.00	1806	1979	Platygya	Annual	d18O	Quinn et al. (1993)
Tarawa	172.00	1.00	1893	1989	Hydropora microconos	Monthly	d18O	Cole et al. (1993)
Maiana	173.00	1.00	1840	1994	Porites spp.	Bimonthly	d18O	Urban et al. (2000)
Fiji 1F	179.23	-16.82	1780	1997	Porites lutea	Monthly	d18O, Sr/Ca	Linsley et al. (2004)
Fiji AB	179.23	-16.82	1617	2001	Porites lutea	8/year	d18O	Linsley et al. (2006)
Savusau, Fiji	179.23	-16.82	1776	2001	Diplastrea heliopora	Annual	d18O	Bagnato et al. (2005)
Tonga TNI2	-174.82	-20.27	1849	2004	Porites lutea	8/year	d18O	unpublished
Tonga TH1	-174.72	-19.93	1794	2004	Porites lutea	Annual	d18O	unpublished
Palmyra Island	-162.13	5.87	1886 ^a	1998	Porites	Monthly	d18O, Sr/Ca	Cobb et al. (2003), Nurhati et al. (2011)
Rarotonga 3R	-159.83	-21.23	1874	2000	Porites	Seasonal	d18O	Linsley et al. (2006), Linsley et al. (2008)
Rarotonga	-159.83	-21.23	1761	1996	Porites	Seas., mon.	d18O, Sr/Ca	Linsley et al. (2006), Linsley et al. (2008)
Moorea	-149.83	-17.50	1852	1990	Porites lutea	Annual	d18O	Boiseau et al. (1999)
Clipperton Atoll	-109.22	10.30	1893	1994	Porites lobata	Monthly	d18O	Linsley et al. (2000a)
Urvina, Galapagos Islands	-91.23	-0.03	1607	1981	Pavona clavus	Annual	d18O	Dunbar et al. (1994)
Secas	-82.05	7.00	1707	1983	Porites	Seasonal	d18O	Linsley et al. (1994)

^a Non-continuous fossil d18O sequences extend back to AD 928

Supplementary Table 3 | Metadata of the available ice records (before the proxy screening). Site name, longitude (°E), latitude (°N), altitude (m.a.s.l.), start year (CE), end year (CE), proxy variable(s), reference(s). Updated from Neukom & Gergis (2012).

SiteName	Longitude	Latitude	Altitude	Start	End	Proxy	Reference(s)
<i>South America</i>							
Quelccaya	-70.83	-13.93	5670	488	2003	d18O, accumulation	Thompson et al. (1984, 2006)
Illimani	-67.78	-16.65	6300	1750	1998	dD, NH ₃	Hoffmann et al.(2003), Ramirez et al. (2003), Kellerhals et al. (2010)
<i>Antarctica</i>							
James Ross Island	-58.13	-64.37	1640	1791	2000	dD	Aristarain et al. (2004)
Law Dome	112.80	-66.77	1370	179 ^a	2005	d18O, accumulation, Na, sss, chem. species. PC1	VanOmmen & Morgan. (2010), Unpublished (M. Curran, T. Vance, A. Moy & T. van Ommen pers. comm.)
Dyer Plateau	-54.50	-70.66	2002	1505	1988	d18O	Thompson et al. (1994)
Princess Elizabeth Land	77.1	-70.85	1850	1745	1996	d18O, accumulation, chem. species. PC1	Xiao et al. (2004)
Dollman	-61.55	-70.97	398	1652	1992	d18O, chem. species. PC1	Russell et al. (2006)
Talos	159.10	-72.80	2316	1217	1996	dD	Stenni et al. (2002)
Gomez	-70.35	-73.60	1400	1854	2006	d18O, accumulation	Thomas et al. (2008, 2009)
Dronning Maud Land	0.00	-75.00	2900	1025	1997	d18O, accumulation, Na	Graf et al. (2002), Taufetter et al. (2004)
Siple Station	-84.15	-75.92	1054	1417	1983	d18O	Moseley-Thompson et al. (1990)
ITASE 2001 5	-89.14	-77.06	1239	1779	2000	d18O	Schneider et al. (2005)
ITASE 2000 5	-124.00	-77.67	1828	1800	1999	d18O	Schneider et al. (2005)
ITASE 2001 2	-102.91	-77.84	1336	1891	2001	d18O	Steig et al. (2005)
ITASE 2000 4	-120.08	-78.08	2595	1794	1999	d18O	Steig et al. (2005)
ITASE 2001 3	-95.65	-78.12	1620	1858	2000	d18O	Steig et al. (2005)
Vostok Pits	106.83	-78.45	3500	1774	1999	d18O, accumulation	Eckaykin et al. (2004)
WDC05A	-112.13	-79.46	1759	1775	2004	Accumulation	Banta et al. (2008)
WDC05Q	-112.09	-79.47	1759	1521	2004	Accumulation	Banta et al. (2008)
Berkner Island	-45.72	-79.61	886	1000	1994	d18O, accumulation	Mulvaney et al. (2002)
ITASE 2000 1	-111.38	-79.63	1791	1800	1999	d18O, accumulation	Schneider et al. (2005), Banta et al. (2008)
ITASE 1999 1	-122.63	-80.62	1350	1723	1999	d18O	Steig et al. (2005)
Siple Dome A	-148.81	-81.65	615	1000	1993	dD	Steig et al. (2013)
Siple Dome B	-148.81	-81.65	615	1654	1994	d18O	Steig et al. (2013)
Siple Dome Na	-148.81	-81.65	615	0	1980	Na	Mayewski et al. (2004)
ITASE 2002 2	-104.99	-83.50	1957	1894	2001	d18O	Jacobel et al. (2005)
ITASE 2002 4	-107.99	-86.50	2586	1593	1997	d18O	Jacobel et al. (2005)

^a Only d18O goes back to AD 179, the other proxies are available back to the 11th or 13th century

Supplementary Table 4 | Metadata of the available documentary, sediment and speleothem records (before the proxy screening). Site name, longitude ($^{\circ}$ E), latitude ($^{\circ}$ N), start year (CE), end year (CE), proxy variable, reference(s). Updated from Neukom & Gergis (2012).

SiteName	Longitude	Latitude	Start	End	Proxy	Reference(s)
<i>Documentary - Africa</i>						
Southem Kalahari precipitaiton ^a	26.00	-25.00	1815	2002	Historical documents	Nash & Endfield (2008), Neukom et al. (2013)
Namaqualand precipitaiton ^a	17.00	-29.00	1817	1997	Historical documents	Kelso & Vogel (2007), Neukom et al. (2013)
Lesotho precipitaiton ^a	27.50	-29.50	1824	1994	Historical documents	Nash & Grab (2010), Neukom et al. (2013)
Eastern Cape South Africa precipitaiton ^a	24.50	-34.00	1821	2007	Historical documents	Vogel (1989), Neukom et al. (2013)
Southem Cape South Africa precipitaiton ^a	20.00	-34.00	1821	1996	Historical documents	Vogel (1989), Neukom et al. (2013)
<i>Documentary - South America</i>						
Peru ENSO index	-79.02	-8.10	1550	1990	Historical documents	Garcia-Herrera et al. (2008), Quinn & Neal (1992)
Potosi precipitation ^a	-65.75	-19.58	1585	2005	Historical documents	Gioda & Prieto (1999)
Rio Sali / Rio Dulce streamflow ^a	-65.00	-27.00	1750	1977	Historical documents	Herrera et al. (2003)
Tucuman precipitaiton ^a	-65.00	-27.03	1548	2005	Historical documents	Prieto et al. (2000)
Santiago del Estero precipitaiton ^a	-64.27	-27.77	1750	2005	Historical documents	Herrera et al. (2003)
Santa Fe and Corrientes precipitation ^a	-60.00	-30.00	1590	2006	Historical documents	Prieto (2007)
Rio Parana streamflow ^a	-60.00	-30.00	1590	1994	Historical documents	Prieto (2007)
Cordoba precipitaiton ^a	-64.00	-31.00	1700	2005	Historical documents	Prieto & Herrera (2001)
Mendoza precipitaiton	-68.00	-32.00	1600	1985	Historical documents	Prieto et al. (2000)
Rio Mendoza streamflow ^a	-68.00	-32.00	1601	2000	Historical documents	Prieto et al. (1999)
Central Andes snow depth	-70.00	-33.00	1760	1996	Historical documents	Neukom et al. (2009)
Central Andes snow occurrence	-70.00	-33.00	1885	1996	Historical documents	Prieto et al. (2001)
Santiago de Chile precipitaiton ^a	-70.78	-33.38	1540	2006	Historical documents	Taulis (1934)
<i>Documentary - Australia</i>						
NSW precipitation	115.20	-33.90	1788	2008	Historical documents	Fenby & Gergis (2013)
<i>Lake Sediment</i>						
Lake Edward	29.75	-0.4	920 ^b	1974	Mg/Ca ratio	Russell & Johnson (2007)
El Junco Lake	-89.5	-0.9	1791 ^b	2004	Diatoms	Conroy et al. (2009)
Lake Challa	37.75	-3.3	-1050	2005	Varve thickness	Wolff et al. (2011)
Lake Masoko	33.75	-9.35	1779 ^b	2002	Magnetic susceptibility	Garcin et al. (2007)
Laguna Pumacocha	-76.1	-10.75	-277	2007	d18O	Bird et al. (2011)
Laguna Aculeo	-70.90	-33.83	856	1997	Pigment reflection	von Gunten et al. (2009)
Lago Puyehue	-72.45	-40.65	1408	1997	Varve thickness	Boes & Fagel (2008)
Lago Plomo	-72.87	-46.98	1530	2000	Mass accumulation rate	Elbert et al. (2011)
<i>Marine Sediment</i>						
106KL off Peruvian Coast	-77.67	-12.05	-13550	2000	Lithics concentration	Rein (2007)
Cariaco Basin	-64.77	10.75	1222	1990	Mg/Ca	Black et al. (2007)
<i>Speleothem</i>						
Avaiki Cave, Niue	-169.83	-19.00	1829	2001	Lamina thickness	Rasbury & Aharon (2006)
Cascayunga Cave, Peru	-77.20	-6.05	1089	2005	d18O	Reuter et al. (2009)

^a The documentary record ends in the 19th or early 20th century and was extended to present using "pseudo documentaries" (see Neukom et al. 2009 and Neukom et al. 2013)

^b Only the high resolution section (<5 years) is used

1.3. Predictor selection

The predictors for the reconstructions are selected based on their local correlations with the target grid. We use the domain covering 55° S- 10° N and all longitudes for the proxy screening. High latitude regions of the grid are excluded from the correlation analysis because south of 55° S, the instrumental data are not reliable at the grid-point level over large parts of the 20th century due to very sparse data coverage (Hansen *et al.*, 2010). We include the regions between 0° N and 10° N because the equatorial regions have a strong influence on SH

temperature variability. Proxy records from these areas with a significant local temperature correlation are expected to be strongly correlated to SH climate. The spatial mean of the domain 55°S-10°N is very similar to the full SH mean, which is used as the reconstruction target (Supplementary Figure 2).

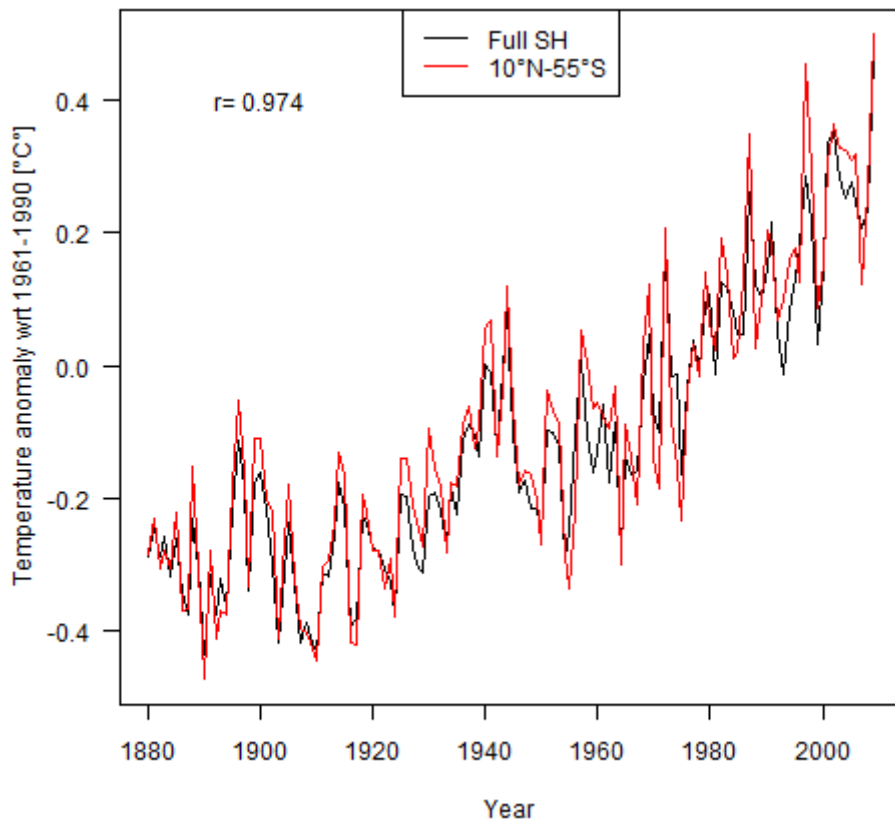
Both the proxy and instrumental data are linearly detrended over the 1911-1990 overlap period prior to the correlation analyses. Correlations of each proxy record with all grid cells are then calculated for the period 1911-1990. The calculations are repeated after lagging the proxy data for one year in both directions. This lagging allows dating uncertainties and the different seasonal windows represented by the proxy data to be accounted for. For example, ice core, documentary and coral records often represent annual averages based on calendar year or rain-year (e.g. July-June) definitions in contrast to our May-April target seasonal window. Significance levels (5% threshold) are calculated taking AR1 autocorrelation into account (Bretherton et al., 1999). We consider the “local” correlation of each record as the highest absolute correlation of a proxy with all grid cells within a radius of 1000 km and for all the three lags (0, 1 or -1 years). A proxy record is included in the predictor set if this local correlation is significant ($p < 0.05$). Reconstruction results using an alternative search radius of 500 km, leading to a smaller predictor set (85 instead of 111 records) are similar (Supplementary Figure 20, see section 3.2.2). Proxies from Antarctica, which are outside the domain used for proxy screening, are included, if they correlate significantly with at least 10% of the grid-area used for screening (latitude weighted). An alternative reconstruction using the full un-screened proxy network yields very similar results (Supplementary Figure 20, see section 3.2.2), demonstrating that the screening procedure has only a limited effect on the reconstruction outcome. The spatial and temporal distribution of the 111 proxy records that passed the screening is shown in Figure 1 in the main text and their properties are listed in Supplementary Table 5. Supplementary Table 6 shows the local correlations of all selected proxies as well as their correlations with the SH mean reconstruction target.

More than 99% of the SH proxies are independent from the records used in the NH reconstruction (see section 5). The one exception in the 111 records is the Quelccaya d₁₈O dataset, which was one out of thirteen proxies in one (Juckes *et al.*, 2007) of the nine reconstructions in the NH ensemble. Juckes *et al.* (2007) furthermore note that this record is only of very minor importance in their NH reconstruction, as it is only weakly correlated with the composite of their remaining proxies ($r=0.15$) and omitting the record does not change the maximum pre-industrial temperature in their NH reconstruction ($\Delta T=0.000K$).

Nine out of the 111 selected records are from sites located slightly north of the equator (Supplementary Table 5). None of these time series has been used in one of the NH reconstructions that we use for comparison. With two exceptions, all of the nine low-latitude NH-proxies in our dataset have stronger correlations with SH spatial mean temperatures than with the NH. The exceptions are Guam, which has very similar correlations with both hemispheres (SH: $r=-0.49$, $p<0.01$ over 1911-1990; NH: $r=-0.51$, $p<0.01$) and Bunaken which shows a strong relation to local temperatures ($r=-0.56$, $P<0.01$) and NINO3.4 ($r=0.52$, $p<0.01$) but non-significant correlations with both hemispheric means (SH: $r=-0.08$, $p=0.56$; NH: $r=-0.18$, $p=0.15$). Eight out of the nine low latitude NH proxies are corals, one is a marine sediment. Supplementary Figure 21 (below, page 43) shows that our reconstruction is robust to the removal of corals and marine sediments indicating that our results are not biased by the NH proxy records.

1.4. Missing values 1911-1990

Missing values in the predictor matrix (1.28%) during the 1911-1990 calibration/verification period are infilled using RegEM (Mann *et al.*, 2008).



Supplementary Figure 2 | Reconstruction vs. screening target. Comparison of the field mean of the GISStemp target grid using the full SH average (black; 90°S-0°S) and the domain 55°S-10°N (red) respectively. The first was used as reconstruction target, the latter for the calculation of the local correlations between proxies and instrumental data. Annual averages are shown for the May-April window.

Supplementary Table 5 | Proxies selected for the SH temperature reconstruction.

Name	Archive	Proxy	Start	End	Lat (°S)	Lon (°E)	Reference
Lake Challa Kenya	Lake Sediments	Varve thickness	-1050	2005	3.32	37.7	Wolff et al. (2011)
Mt. Read Tasmania	Tree Rings	Tree ring width	-494	1999	42	147	Cook et al. (2000), Cook et al. (2006)
Laguna Pumacocha	Lake Sediments	d18O	-277	2007	10.7	-76.07	Bird et al. (2011)
Oroko	Tree Rings	Tree ring width	1	2003	43.23	170.28	Cook et al. (2006)
Law Dome d18O	Ice Cores	d18O	179	2007	66.83	112.83	Unpublished
Quelccaya	Ice Cores	d18O	488	2002	13.93	-70.83	Thompson et al. (1984, 2006)
Laguna Aculeo	Lake Sediments	Pigment reflection	856	1997	33.83	-70.9	von Gunten et al. (2009)
Palmyra Island d18O	Corals	d18O	928	1998	-5.87	-162.13	Cobb et al. (2003)
Law Dome sea salt	Ice Cores	Summer sea salt	1000	2009	13	112.83	Unpublished
Talos	Ice Cores	dD	1217	1996	72.8	159.1	Stenni et al. (2002)
Cariaco Basin	Marine Sediments	Mg/Ca	1222	1990	-10.75	-64.77	Black et al. (2007)
Lago Puyehue	Lake Sediments	Lamina thickness	1408	1997	40.65	-72.45	Boes & Fagel (2008)
Siple Station	Ice Cores	d18O	1417	1983	75.92	-84.15	Graf et al. (2002), Taufetter et al. (2004)
CTP East Tasmania	Tree Rings	Tree ring width	1430	1994	42	148	Allen et al. (2001)
CAN Composite 6	Tree Rings	Tree ring width	1435	2006	38.5	-71.5	La Marche et al. (1979a), Villalba (1990a), Mundo et al. (2012)
Pink Pine NZ	Tree Rings	Tree ring width	1457	1999	42	172	Duncan et al. (2010)
Urewera	Tree Rings	Tree ring width	1462	1987	38.68	177.2	Xiong and Palmer (2000)
Buckles Chance	Tree Rings	Tree ring width	1463	1991	42.27	145.87	Buckley et al. (1997)
WDC05Q Accumulation	Ice Cores	Accumulation	1521	2004	79.45	-112.08	Banta et al. (2008)
NI LIBI Composite 1	Tree Rings	Tree ring width	1526	1992	39.5	175.5	Xiong and Palmer (2000)
Takapari	Tree Rings	Tree ring width	1533	1992	40.07	175.98	Xiong and Palmer (2000)
Santiago de Chile	Documentary	Documentary	1540	2006	33.38	-70.78	Taulis (1934), Neukom et al. (2009)
CTP West Tasmania	Tree Rings	Tree ring width	1547	1998	42	146	Allen et al. (2001), Allen (2002), LaMarche et al. (1979c)
Tucuman	Documentary	Documentary	1548	2005	27.03	-65	Prieto et al. (2000), Neukom et al. (2009)
Peru ENSO index	Documentary	Documentary	1550	1990	8.1	-79.02	Garcia-Herrera et al. (2008), Quinn & Neal (1992)
Mangawhero	Tree Rings	Tree ring width	1551	1994	39.35	175.48	D'Arrigo et al. (2000)
Kauri NZ	Tree Rings	Tree ring width	1577	2002	36	174	Cook et al. (2006), Fowler et al. (2008)
CAN Composite 15	Tree Rings	Tree ring width	1582	1991	41.17	-71.92	Villalba et al. (1997b)
ITASE 2002 4	Ice Cores	d18O	1593	1997	86.5	-108	Jacobel et al. (2005)
Rio Mendoza	Documentary	Documentary	1601	2000	32	-68	Prieto et al. (1999), Neukom et al. (2009)
Urina, Galapagos	Corals	d18O	1607	1981	0.03	-91.23	Dunbar et al. (1994)
Fiji AB	Corals	d18O	1617	2001	16.82	179.23	Linsley et al. (2006)
Mafia, Tanzania	Corals	d18O	1622	1998	8	40	Damassa et al. (2006)
Moa Park	Tree Rings	Tree ring width	1623	1991	40.93	172.93	Xiong and Palmer (2000)
CAN Composite 9	Tree Rings	Tree ring width	1636	2006	39.33	-71.25	La Marche et al. (1979a), Mundo et al. (2012)
Abraham	Corals	d18O	1638	1983	20	153	Druffel and Griffin (1999)
CAN Composite 12	Tree Rings	Tree ring width	1645	1992	40	-71	La Marche et al. (1979b), Villalba and Veblen (1997)
NI LIBI Composite 2	Tree Rings	Tree ring width	1651	1990	39.27	174.1	Xiong and Palmer (2000)
Dolleman	Ice Cores	Chem. species PC1	1652	1991	70.57	-60.93	Russell et al. (2006)
Siple Dome B	Ice Cores	d18O	1654	1994	81.65	-148.8	Steig et al. (2013)
Amedee New Caledonia	Corals	d18O	1657	1992	22.48	166.45	Quinn et al. (1998)
Ifaty 4	Corals	d18O	1660	1994	23	43	Unpublished
Ifaty, Madagascar	Corals	d18O	1660	1995	23.15	43.58	Zinke et al. (2004)
Huinganco	Tree Rings	Tree ring width	1673	2000	37.75	-70.6	La Marche et al. (1979a)
Secas	Corals	d18O	1707	1983	-7	-82.05	Linsley et al. (1994)
CAN Composite 2	Tree Rings	Tree ring width	1714	2006	37.83	-71	La Marche et al. (1979a), Mundo et al. (2012)
CAN Composite 27	Tree Rings	Tree ring width	1715	2002	49	-72	Boninsegna et al. (1989), Srur et al. (2008)
SAN Composite 5	Tree Rings	Tree ring width	1718	1984	54.75	-67.67	Boninsegna et al. (1989)
Princess Elizabeth Land	Ice Cores	Chem. species PC1	1745	1996	70.83	77.07	Xiao et al. (2004)
Santiago del Estero	Documentary	Documentary	1750	2005	27.77	-64.27	Herrera et al. (2003), Neukom et al. (2009)
Stewart Island	Tree Rings	Tree ring width	1758	1993	47	168	D'Arrigo et al. (1995), D'Arrigo et al. (2000)

Supplementary Table 5 (continued)

WA Callitris	Tree Rings	Tree ring width	1758	2005	33.03	120.77	Cullen et al. (2009)
Central Andes snow dept	Documentary	Documentary	1760	1996	33	-70	Neukom et al. (2009)
Rarotonga d18O	Corals	d18O	1761	1996	21.23	-159.83	Linsley et al. (2006), Linsley et al. (2008)
Rarotonga SrCa	Corals	Sr/Ca	1761	1996	21.23	-159.83	Linsley et al. (2006), Linsley et al. (2008)
Valle Ameghino	Tree Rings	Tree ring width	1766	1997	50.42	-72.17	Masiokas and Villalba (2004)
Pino Hachado	Tree Rings	Tree ring width	1767	1974	38.63	-70.75	La Marche et al. (1979a)
CAN Composite 8	Tree Rings	Tree ring width	1773	1989	39.17	-71.17	Villalba and Veblen (1997)
Vostok Pits	Ice Cores	d18O	1774	1999	78.45	106.83	Eckaykin et al. (2004)
Flanagans Hut	Tree Rings	Tree ring width	1776	1991	41.27	172.6	Xiong and Palmer (2000)
Savusavu, Fiji	Corals	d18O	1776	2001	16.82	179.23	Bagnato et al. (2005)
Fiji 1F SrCa	Corals	Sr/Ca	1780	1997	16.82	179.23	Linsley et al. (2004)
Teak Indonesia	Tree Rings	Tree ring width	1780	2005	7	111	D'Arrigo et al. (2006)
Fiji 1F d18O	Corals	d18O	1781	1997	16.82	179.23	Linsley et al. (2004)
GBR precip recon rec4	Corals	Luminescence	1783	1981	18	147	Lough (2011)
Eastern NSW	Documentary	Documentary	1788	2008	33.9	115.2	Fenby & Gergis (2013)
CAN Composite 21	Tree Rings	Tree ring width	1790	1991	41.5	-71.5	Villalba and Veblen (1997)
Guam	Corals	d18O	1790	2000	-13	145	Asami et al. (2005)
James Ross Island	Ice Cores	dD	1791	2000	64.37	-58.13	Aristarain et al. (2004)
Abrolhos	Corals	d18O	1794	1993	28.45	113.77	Kuhnert et al. (1999)
Tonga TH1	Corals	d18O	1794	2004	19.93	-174.72	Unpublished
CAN Composite 34	Tree Rings	Tree ring width	1795	2007	50.6	-73.67	Unpublished
Torre Morena 4	Tree Rings	Tree ring width	1798	2007	49.5	-73.5	Unpublished
Illimani	Ice Cores	NH4	1800	1998	16.65	-67.78	Kellerhals et al. (2010)
ITASE 2000 5	Ice Cores	d18O	1800	1999	77.67	-124	Schneider et al. (2005)
Malindi	Corals	d18O	1801	1994	3	40	Cole et al. (2000)
Paso Cordova	Tree Rings	Tree ring width	1811	1986	40.67	-71.25	ITRDB series arge050
Chapelco	Tree Rings	Tree ring width	1814	1985	40.33	-71.23	ITRDB series arge029
Baw Baw	Tree Rings	Tree ring width	1818	2002	36.42	148.33	Brookhouse et al. (2008)
Eastern Cape	Documentary	Documentary	1821	2007	34	24.5	Vogel (1989), Neukom et al. (in review)
La Meseda	Tree Rings	Tree ring width	1822	1999	23	-65.02	Unpublished
Kavieng	Corals	Sr/Ca	1823	1997	2.5	150.5	Alibert and Kinsley (2008a,b)
El Chalten bajo	Tree Rings	Tree ring width	1826	2003	49.37	-72.9	Srur et al. (2008)
Avaiki	Speleothems	Lamina thickness	1829	2001	19	-169.83	Rasbury & Aharon (2006)
Maiana	Corals	d18O	1840	1994	-1	173	Urban et al. (2000)
Seychelles	Corals	d18O	1846	1995	4.62	55.8	Charles et al. (1997), Abram et al. (2008)
Tonga TNI2	Corals	d18O	1849	2004	20.27	-174.82	unpublished
CAN Composite 16	Tree Rings	Tree ring width	1857	1991	41.13	-71.8	Villalba et al. (1997b)
Gomez	Ice Cores	d18O	1857	2005	73.6	-70.35	Thomas et al. (2008, 2009)
ITASE 2001 3	Ice Cores	d18O	1858	2000	78.12	-95.65	Steig et al. (2005)
Mentawai West Sumatra	Corals	d18O	1858	1997	4	98.5	Abram et al. (2008)
CAN Composite 14	Tree Rings	Tree ring width	1859	1994	41.13	-71.8	Villalba et al. (1997b), Schmelter (2000)
Bunaken	Corals	d18O	1863	1990	-2.8	123	Charles et al. (2003)
Rabaul d18O	Corals	d18O	1867	1997	4	152	Quinn et al. (2006)
Rabaul Sr/Ca	Corals	Sr/Ca	1867	1997	4	152	Quinn et al. (2006)
Rarotonga 3R	Corals	d18O	1874	2000	21.23	-159.83	Linsley et al. (2006), Linsley et al. (2008)
Zimbabwe	Tree Rings	Tree ring width	1875	1996	18.5	27.33	Therrell et al. (2006)
Ningaloo	Corals	d18O	1878	1995	21.9	113.97	Kuhnert et al. (2000)
Madang Lagoon	Corals	d18O	1880	1993	5.22	145.82	Tudhope et al. (2001)
Ifaty 1	Corals	d18O	1882	1994	23	43	Unpublished
Laing	Corals	d18O	1884	1993	4.15	144.88	Tudhope et al. (2001)
Central Andes snow occurrence	Documentary	Documentary	1885	1996	33	-70	Prieto et al. (2001), Neukom et al. (2009)
Palmyra Island SrCa	Corals	Sr/Ca	1886	1998	-5.87	-162.13	Nurhati et al. (2011)
GBR precip recon rec17	Corals	Luminescence	1891	1981	18	147	Lough (2011)
ITASE 2001 2	Ice Cores	d18O	1891	2001	77.83	-102.92	Steig et al. (2005)
CAN Composite 17	Tree Rings	Tree ring width	1892	1994	41.17	-71.83	Villalba et al. (1997b), Schmelter (2000)
Clipperton	Corals	d18O	1893	1994	-10.3	-109.22	Linsley et al. (2000a)
Puerto Parryn	Tree Rings	Tree ring width	1893	1986	54.83	-64.37	Boninsegna et al. (1989)
Tarawa	Corals	d18O	1893	1989	-1	172	Cole et al. (1993)
NT Callitris	Tree Rings	Tree ring width	1896	2006	13	132	Baker et al. (2008)
Nauru	Corals	d18O	1897	1995	0.83	166	Guilderson et al. (1999)

Supplementary Table 6 | Temperature correlations of proxies. Local correlations (r_{local}) and correlations with the SH mean reconstruction target (r_{SH}) for the selected predictors. Proxies from outside the screening area have no local correlation (NA).

Name	r_{local}	r_{SH}	Name	r_{local}	r_{SH}
Lake Challa Kenya	-0.38	-0.17	Pino Hachado	-0.25	0.31
Mt. Read Tasmania	0.43	0.65	CAN Composite 8	0.23	0.35
Laguna Pumacocha	-0.34	0.28	Vostok Pits	NA	0.31
Oroko	0.36	0.22	Flanagans Hut	0.36	0.13
Law Dome d18O	NA	-0.05	Savusavu, Fiji	-0.53	-0.26
Quelccaya	0.32	0.17	Fiji 1F SrCa	-0.49	-0.14
Laguna Aculeo	0.36	0.46	Teak Indonesia	0.29	0.16
Palmyra Island d18O	-0.82	-0.61	Fiji 1F d18O	-0.47	-0.24
Law Dome sea salt	NA	-0.21	GBR precip recon rec4	0.30	-0.04
Talos	NA	-0.12	Eastern NSW	-0.39	-0.03
Cariaco Basin	NA	0.76	CAN Composite 21	-0.31	-0.10
Lago Puyehue	0.34	-0.05	Guam	-0.47	-0.49
Siple Station	NA	0.20	James Ross Island	NA	-0.58
CTP East Tasmania	-0.31	0.37	Abrolhos	-0.53	-0.24
CAN Composite 6	-0.31	0.00	Tonga TH1	-0.37	0.07
Pink Pine NZ	0.49	0.24	CAN Composite 34	0.30	0.31
Urewera	-0.45	-0.11	Torre Morena 4	-0.27	-0.12
Buckleys Chance	0.41	-0.03	Illimani	0.45	0.38
WDC05Q Accumulation	NA	0.09	ITASE 2000 5	NA	0.13
NI LIBI Composite 1	-0.30	0.24	Malindi	-0.46	-0.55
Takapari	-0.33	0.59	Paso Cordova	-0.28	-0.27
Santiago de Chile	0.26	0.17	Chapelco	-0.30	-0.06
CTP West Tasmania	0.29	0.57	Baw Baw	-0.41	0.04
Tucuman	0.43	0.37	Eastern Cape	0.31	-0.07
Peru ENSO index	0.67	0.14	La Meseda	-0.29	-0.02
Mangawhero	0.36	0.51	Kavieng	-0.38	-0.02
Kauri NZ	-0.52	0.36	El Chalten bajo	-0.32	0.13
CAN Composite 15	0.28	0.23	Avaiki	-0.31	-0.06
ITASE 2002 4	NA	0.06	Maiana	-0.70	-0.58
Rio Mendoza	0.39	0.12	Seychelles	-0.42	-0.55
Urvina, Galapagos	-0.49	-0.14	Tonga TNI2	-0.45	0.14
Fiji AB	-0.59	-0.09	Gomez	NA	0.14
Mafia, Tanzania	-0.24	-0.50	CAN Composite 16	0.31	0.01
Moa Park	-0.34	0.08	Mentawai West Sumatra	-0.30	-0.41
CAN Composite 9	-0.30	-0.08	ITASE 2001 3	NA	0.00
Abraham	0.27	-0.16	CAN Composite 14	0.38	0.49
CAN Composite 12	-0.41	-0.17	Bunaken	-0.65	-0.08
NI LIBI Composite 2	-0.29	0.38	Rabaul d18O	-0.41	-0.03
Dolleman	NA	0.11	Rabaul Sr/Ca	-0.46	0.01
Siple Dome B	NA	-0.09	Rarotonga 3R	0.41	-0.33
Amedee New Caledonia	-0.44	-0.37	Zimbabwe	-0.33	-0.01
Ifaty, Madagascar	-0.30	-0.20	Ningaloo	-0.35	-0.58
Ifaty 4	-0.27	-0.21	Madang Lagoon	-0.36	-0.08
Huinganco	-0.33	-0.16	Ifaty 1	-0.32	-0.52
Secas	-0.26	-0.31	Laing	-0.54	-0.36
CAN Composite 2	0.28	-0.36	Central Andes snow occurrence	0.28	0.25
CAN Composite 27	0.34	0.19	Palmyra Island SrCa	-0.59	-0.33
SAN Composite 5	-0.37	0.24	GBR precip recon rec17	0.35	0.02
Princess Elizabeth Land	NA	0.43	ITASE 2001 2	NA	0.07
Santiago del Estero	0.27	0.23	CAN Composite 17	0.57	0.64
Stewart Island	0.40	0.25	Tarawa	-0.62	-0.44
WA Callitris	-0.29	-0.03	Clipperton	-0.49	-0.63
Central Andes snow depth	0.24	0.31	Puerto Parryn	-0.29	-0.52
Rarotonga d18O	0.49	-0.22	NT Callitris	0.24	0.19
Rarotonga SrCa	-0.50	0.02	Nauru	-0.46	-0.70
Valle Ameghino	0.32	0.24			

2. Ensemble reconstruction

2.1. Reconstruction methodology

Temperature reconstructions are based on nested multivariate principal component regression (PCR; Luterbacher *et al.*, 2002; Luterbacher *et al.*, 2004; Neukom *et al.*, 2010; Neukom *et al.*, 2011; Neukom *et al.*, 2013). Detailed description of the PCR method is provided in Luterbacher *et al.*(2002), Luterbacher *et al.* (2004) and Wahl and Smerdon (2012).

2.2. Ensemble parameters

The ensemble approach (see also Frank *et al.*, 2010; Neukom *et al.*, 2010; Neukom *et al.*, 2013) allows for the provision of additional uncertainty estimates, complementing the traditional error estimates which quantify the unexplained variance in the calibration period (cf. Wahl and Smerdon, 2012, for an alternative probabilistic ensemble approach using PCR). The outcome of a climate reconstruction depends on the methodological choices that have to be made during the reconstruction process. For most of these choices, objective “best” solutions are largely missing in literature. The main limitation is that the real-world performance of different approaches and parameters can only be verified over the instrumental period, which is short and contains a strong trend, complicating quality assessments. We assess the influence of these methodological choices by varying methodological parameters in the ensemble and quantifying their effect on the reconstruction results. Obviously, the range within which these parameters are varied in the ensemble is also subjective, but we argue that the ranges chosen herein are within reasonable thresholds, based our own experience and the literature. Given the limited possibilities to identify the “best” ensemble members, we treat all reconstruction results equally and consider the ensemble mean our best estimate. Because our ensemble members can be approximated by a normal

distribution (Supplementary Figure 3, see also Supplementary Figure 26 below), the ensemble mean also represents the most probable value in the ensemble distribution function.

We perform an ensemble of 3,000 reconstructions. For each ensemble member we use different settings by randomly:

1. Selecting 10% of the temperature proxies (i.e. 11 records) that are removed from the proxy matrix. In the early parts of the reconstruction (CE 1000–1222) between nine and eleven proxies are available, the number of predictors used for each ensemble member varies between one and eleven.

Rationale: We introduce this ensemble parameter because the proxy matrix in a multi-proxy reconstruction is always dependent on some pre-reconstruction choices such as proxy screening procedures based on statistical calculations, literature review or the effort invested in the data compilation. This perturbation allows us to assess the robustness of the reconstruction against changes in the predictor network and to assess the potential dominance of individual records (see section 3.2.6). This perturbation contributes to approximately 11% of the total ensemble spread (calculated during the 1911-1990 period; this fraction increases back in time due to the decreasing number of proxies available).

2. Sampling the years for calibration (between 40 and 55 years within the 1911-1990 overlap period). The remaining 25-40 years are used for verification.

Rationale: Given the limited number of years available in the instrumental-proxy overlap period, the outcome of a reconstruction strongly depends on the choice of calibration and verification periods (Frank *et al.*, 2010; Gergis *et al.*, 2011). This perturbation contributes to approximately 43% of the total ensemble spread.

3. Sampling the number of PCs to be used. We use the first n PCs that explain between 50%-90% of the total variance of the predictor matrix.

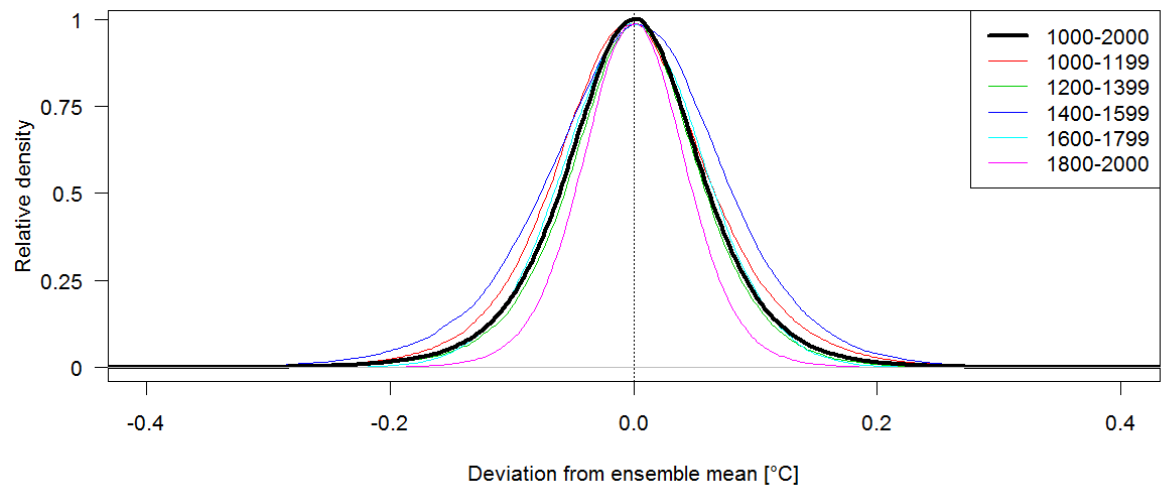
Rationale: There are various approaches described in literature to identify the best PC truncation (North *et al.*, 1982; Smerdon *et al.*, 2010) with currently no widely accepted “best” approach. Furthermore, the eigenvalues of the proxy PCs are strongly depending on the period chosen over which to calculate the PCs. This perturbation contributes to approximately 17% of the total ensemble spread.

4. Sampling the weight that each proxy gets in the PC analysis by increasing its variance by a factor of 0.67-1.5 (after scaling all proxies to mean zero and unit standard deviation over their common period).

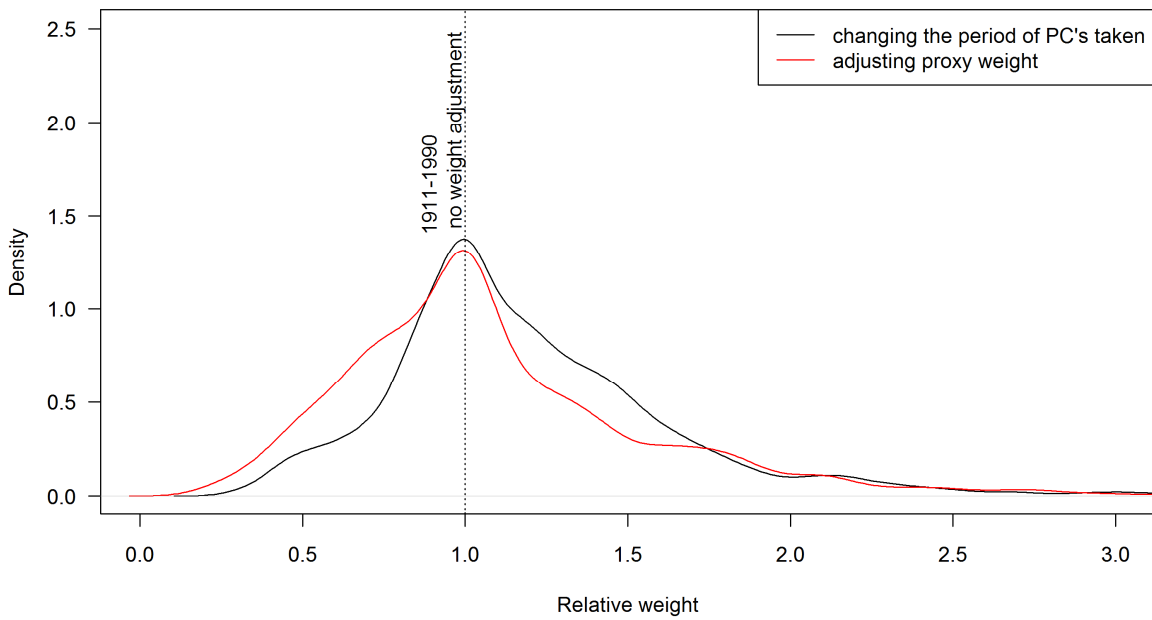
Rationale: The weight that each proxy record gets in the PC analysis is strongly dependent on the time period chosen (Supplementary Figure 4). Given the short period available for calibration, there is a high probability that the resulting proxy weights may not reflect the “true” weight of each proxy in the data matrix. This perturbation contributes to approximately 20% of the total ensemble spread.

5. Selecting one chronology for proxies where multiple time series based on different methods are available (tree-rings and documentaries, sections 1.2.1 and 1.2.3)

Rationale: The pre-processing of some records also involves some subjective choices. To overcome this limitation to a certain extent, we allow multiple versions of the same record to be used in different ensemble members. This perturbation contributes to approximately 8% of the total ensemble spread.



Supplementary Figure 3 | Ensemble distribution. Distribution of the difference between the individual ensemble members and the reconstruction ensemble mean. Distribution over all years within 1000-2000 (bold black) and within 200-year blocks (coloured lines) are shown.

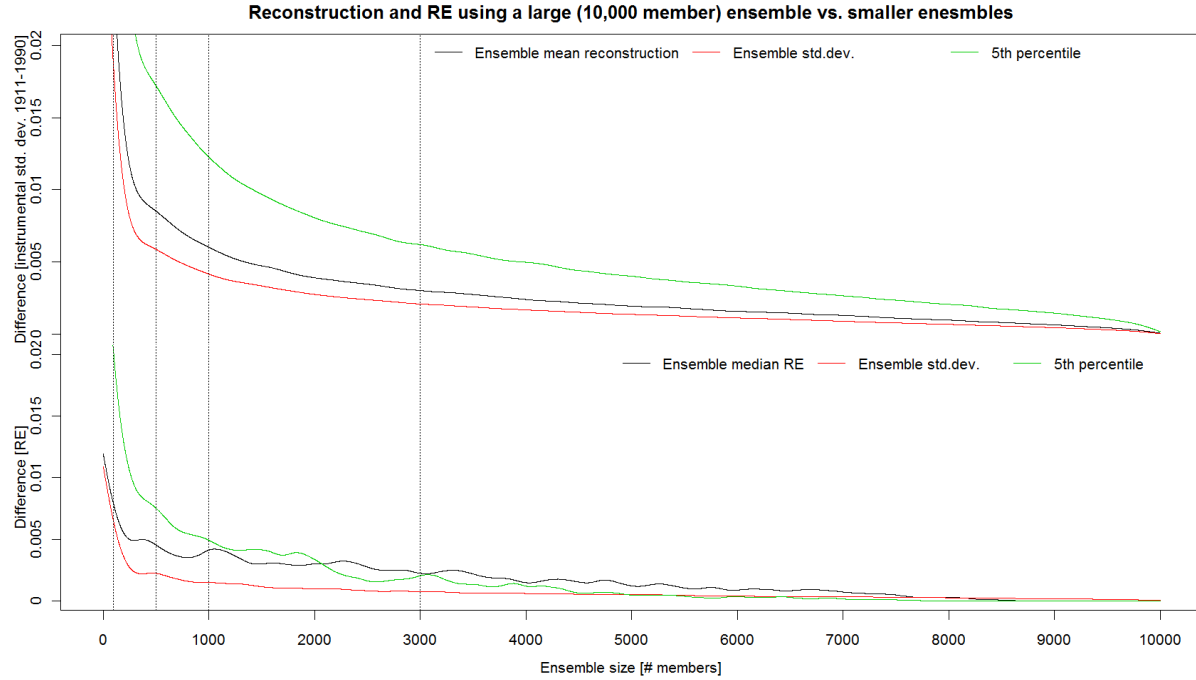


Supplementary Figure 4 | Sensitivity of proxy weight in the PC-routine. PCs of the proxy matrix are calculated over different time windows (black line) and using artificial variance inflation as in the ensemble perturbation #4 (red line). Weights of each proxy record are calculated as the average absolute loading to the first five PCs and expressed relative to the value of the unweighted proxy matrix over 1911-1990. For the temporal dependence (black line) PCs are calculated over 80-year periods starting between 1850 and 1910. Prior to 1850, the number of proxy records available strongly decreases and the change in the composition of the proxy matrix becomes more important, masking the effect of the choice of period. For the red line, variance inflation with random factors between 0.67 and 1.5 was applied to each proxy. The figure illustrates that this variance inflation mimics the temporal sensitivity of the PC calculation.

2.3. Required number of ensemble members

Supplementary Figure 5 shows the variability of different measures as a function of the number of ensemble members. The black line shows the difference between the ensemble mean using n members and the ensemble mean using 10,000 members. For an ensemble of 3,000 members, all measures are sufficiently close to a very large ensemble (e.g. the difference for the ensemble mean reconstruction is less than 0.001°C over the 1911-1990 period) but allow a significant reduction in the computational time and disk space required. For the AR-noise reconstructions (see below section 3.1.5), the use of 1000 member ensembles is sufficient because we only work with the RE skill values of these

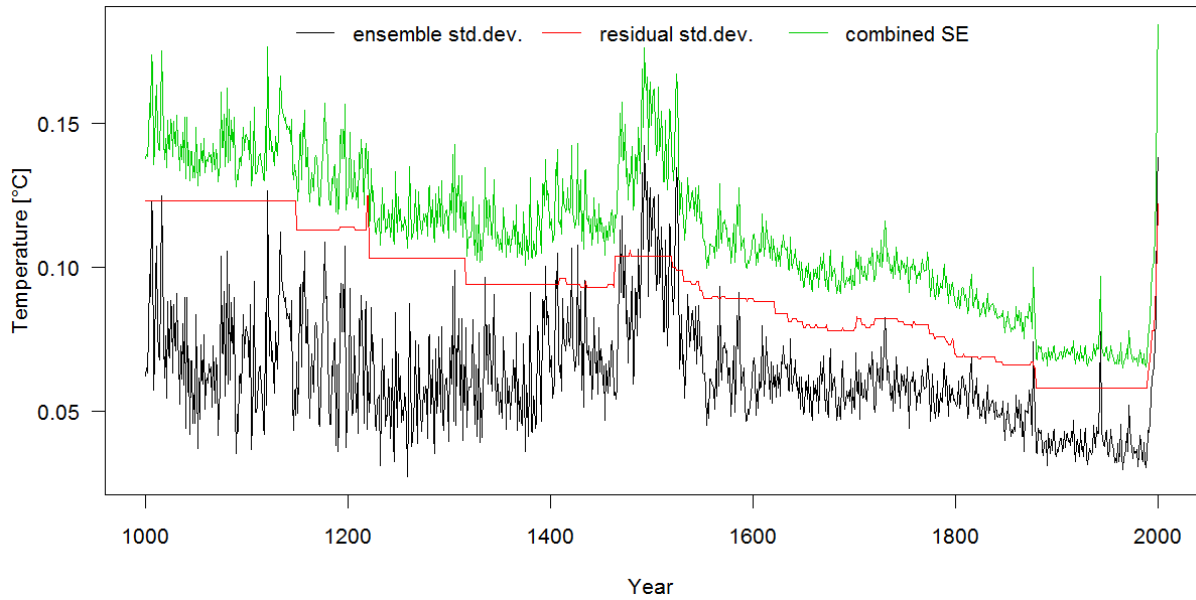
reconstructions, which are still very close to the values of the large 10,000 member ensemble (Supplementary Figure 5, bottom).



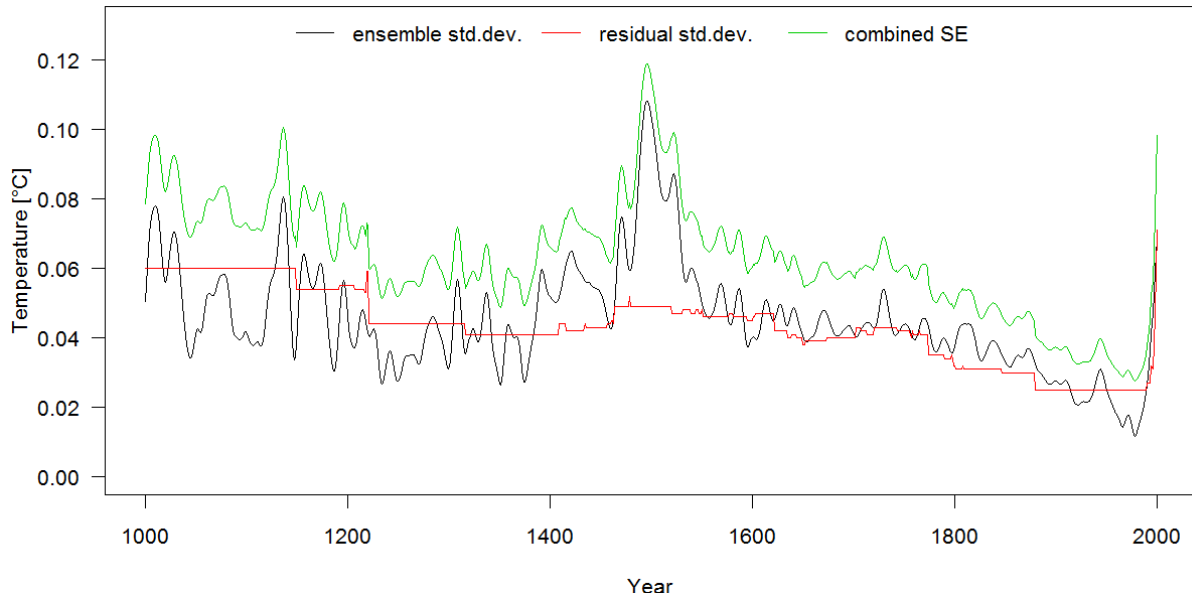
Supplementary Figure 5 | Reconstruction statistics for different ensemble sizes. The absolute differences between an ensemble of n members and an ensemble of 10,000 members is shown. We use the statistics for the period 1911–1990 of the most replicated nest (111 proxies). Top: Ensemble mean reconstruction (black), standard deviation between ensemble members (red) and 5th percentile of ensemble members (green). All values are shown relative to the instrumental standard deviation 1911–1990 (0.15°C). Bottom: Ensemble median RE (black), standard deviation between RE of ensemble members (red) and 5th percentile of RE of ensemble members (green). The dotted vertical lines represent the ensemble sizes used for the SH-mean reconstruction (3,000 members), the AR noise reconstructions (1,000 members, see below) and 500 and 100 members, respectively.

2.4. Reconstruction uncertainties

The combined calibration and ensemble uncertainties (SE) are calculated where $SE = \sqrt{\sigma_{res}^2 + \sigma_{ens}^2}$ with σ_{res} denoting the standard deviation of the regression residuals and σ_{ens} the standard deviation of the ensemble members. σ_{res} remains constant for all years with the same predictor availability, whereas σ_{ens} is different for each year. Blue shaded probabilities in Figure 2 in the main text represent the quantiles of a normal distribution around the ensemble mean with a standard deviation of SE . Temporal evolution of the interannual and 30-year filtered reconstruction uncertainties are shown in Supplementary Figure 6 and Supplementary Figure 7, respectively. The increasing ensemble uncertainties back in time are caused by the decrease of available proxy records further back in time



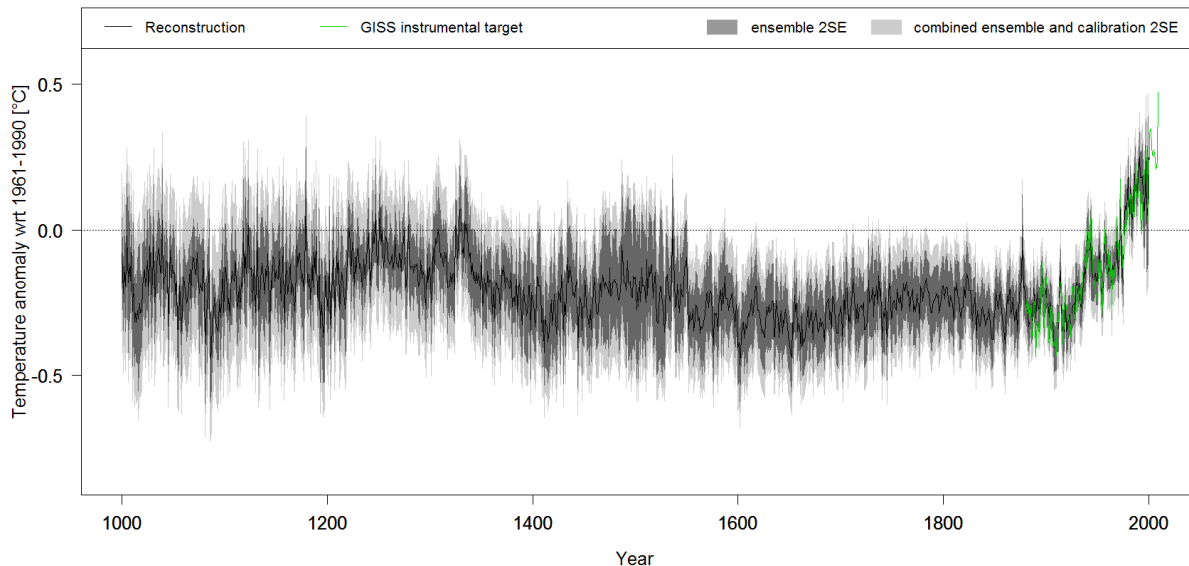
Supplementary Figure 6 | Reconstruction uncertainties. Ensemble standard deviation σ_{ens} (black), residual standard deviation σ_{res} (red) and combined SE uncertainties (green) of the unfiltered reconstruction.



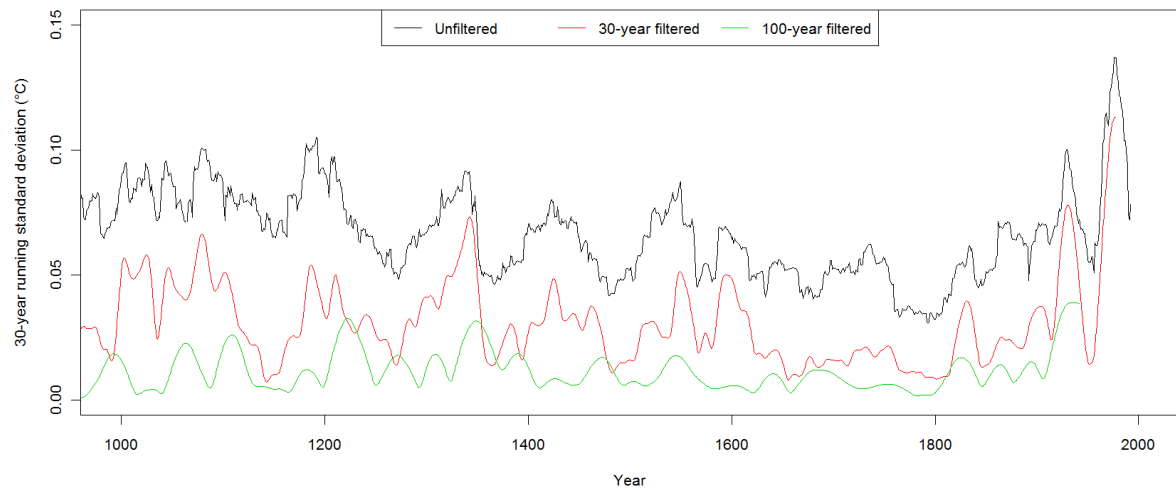
Supplementary Figure 7 | Filtered reconstruction uncertainties. Same as Supplementary Figure 6 but for the 30-year filtered reconstruction.

2.5. Unfiltered SH mean reconstruction

Supplementary Figure 8 shows the unfiltered reconstruction ensemble mean and associated uncertainties. The unfiltered data shows some long-term changes in the variance structure (Supplementary Figure 9) that may be an artifact of changes in proxy replication over time. The long-term changes in variance are not so evident at decadal to centennial time-scales (Supplementary Figure 9). Because our interpretations and conclusions focus on the decadal and lower resolution, these potential variance artifacts do not influence or findings or conclusions. We note that long-term trends in climate variability, e.g., related to ENSO, have been advocated in literature (e.g., McGregor *et al.*, 2013, who also find a reduction of temperature variance in their ENSO record over 1590–1880), so we do not wish to exclude a priori the possibility that long-term changes in climate variability exist, but rather to draw attention to possible uncertainties in the variance structure of our new record.



Supplementary Figure 8 | Unfiltered SH reconstruction. Black: reconstruction ensemble mean; dark grey shading: ensemble 2σ bounds, light grey shading: combined 2SE uncertainties. Green: Instrumental target data.



Supplementary Figure 9 | Running standard deviations. 30-year running standard deviations of the unfiltered SH reconstruction ensemble mean (black) and of the 30-year (red) and 100-year (green) loess filtered ensemble mean.

3. Reconstruction reliability

To assess the ‘reliability’ of the reconstruction we consider a range of reconstruction ‘skill’ and ‘robustness’ measures. Reconstruction skill assesses the ability of our proxies to reconstruct instrumental temperatures over verification periods that are independent from the calibration years. Robustness is assessed by investigating the effect of different reconstruction methods, proxy archives and individual records on the outcome of the reconstruction.

3.1. Reconstruction skill

The aim of reconstruction skill assessments is to verify the ability to capture temperature fluctuations during a verification period, which is independent from the time window used for calibration. Traditionally, a time slice of the overlap-period between proxy and instrumental data is used for this verification exercise. This time slice can be at the beginning, at the end or within the calibration period. The ensemble approach with individual calibration/verification windows for each member allows us to further elaborate this concept to ensemble-based verification metrics. We adapt the traditional RE (reduction of error) and RMSE (root mean square error) statistics (Cook *et al.*, 1994) to quantify the reconstruction skill over the ensemble members as well as for the ensemble mean. The RE measure is defined as

$$RE = 1 - \frac{\sum_{i=1}^n (x_{inst_i} - x_{recon_i})^2}{\sum_{i=1}^n (x_{inst_i} - x_{calib})^2},$$

with x_{inst} denoting instrumental values and x_{recon} the reconstructed values for each year i of the verification period. x_{calib} is the calibration period mean of the instrumental data. The RE tests whether the reconstruction has more predictive skill than the climatology of the calibration period (x_{calib}). RE values between 0 and 1 (a hypothetically perfect reconstruction) indicate a skillful reconstruction, while RE values <0 indicate no predictive skill.

The RMSE is defined as

$$RMSE = \sqrt{\frac{1}{n} \sum_{i=1}^n (x_{inst_i} - x_{recon_i})^2}$$

We calculate the verification values for each existing proxy combination (proxy nest) during the reconstruction period. The value of the calibration/verification exercise using only the proxies available in the year 1000 is assigned to the year 1000 etc. This yields a time series of validation values covering the full reconstruction period (Figure 1b in the main text and Supplementary Figure 10). The ensemble-based validation metrics are described in the following sections.

3.1.1. Ensemble validation

For each reconstruction ensemble member, we calculate the RE statistic from years withheld for verification within the 1911–1990 calibration/verification period. The number of years available for verification varies between 25 and 40 years. The ensemble median RE time series is derived by calculating the median of the RE values of all ensemble members for each year. We use the median here, because the distribution of the RE values is strongly skewed and a small number of very large negative RE values can bias the ensemble distribution and lead to an artificially low ensemble mean RE. The ensemble median RE of our reconstruction is consistently positive over the 1000-2000 period, except for the year 2000 which has a negative value (Supplementary Figure 10).

3.1.2. Ensemble mean early verification

The ensemble mean reconstruction is verified against the instrumental data in the 1880–1910 period, which is independent from the 1911–1990 calibration/verification interval and does not exhibit a significant temperature trend. Note, however, that the quality of the instrumental record is very limited in the SH during this early period. The early verification RE of our reconstruction is positive over the full 1000-2000 period.

3.1.3. Ensemble mean verification and calibration years

For each year over the 1911–1990 calibration/verification period, the ensemble mean reconstruction is calculated for all members where the year was used for verification (and not for calibration). This returns a time series covering 1911–1990 and representing the ensemble mean based only on verification years. This ‘verification ensemble mean’ is then used as x_{recon} and tested against the instrumental target over the full 1911–1990 period. This RE value is slightly different from the traditional RE statistic because the verification years (covered by x_{inst} and x_{recon}) and the calibration years (represented by x_{calib}) are both drawn from the same 1911–1990 period. Similarly we also calculate the calibration years RE using the ensemble mean of all years that are used for calibration as x_{recon} . The calibration and verification years RE are shown in Figure 1b in the main text. They are positive over the full 1000-2000 period.

3.1.4. Ensemble mean RMSE

The RMSE between the ensemble mean reconstruction and the instrumental data is calculated over the 1911-1990 calibration/verification window.

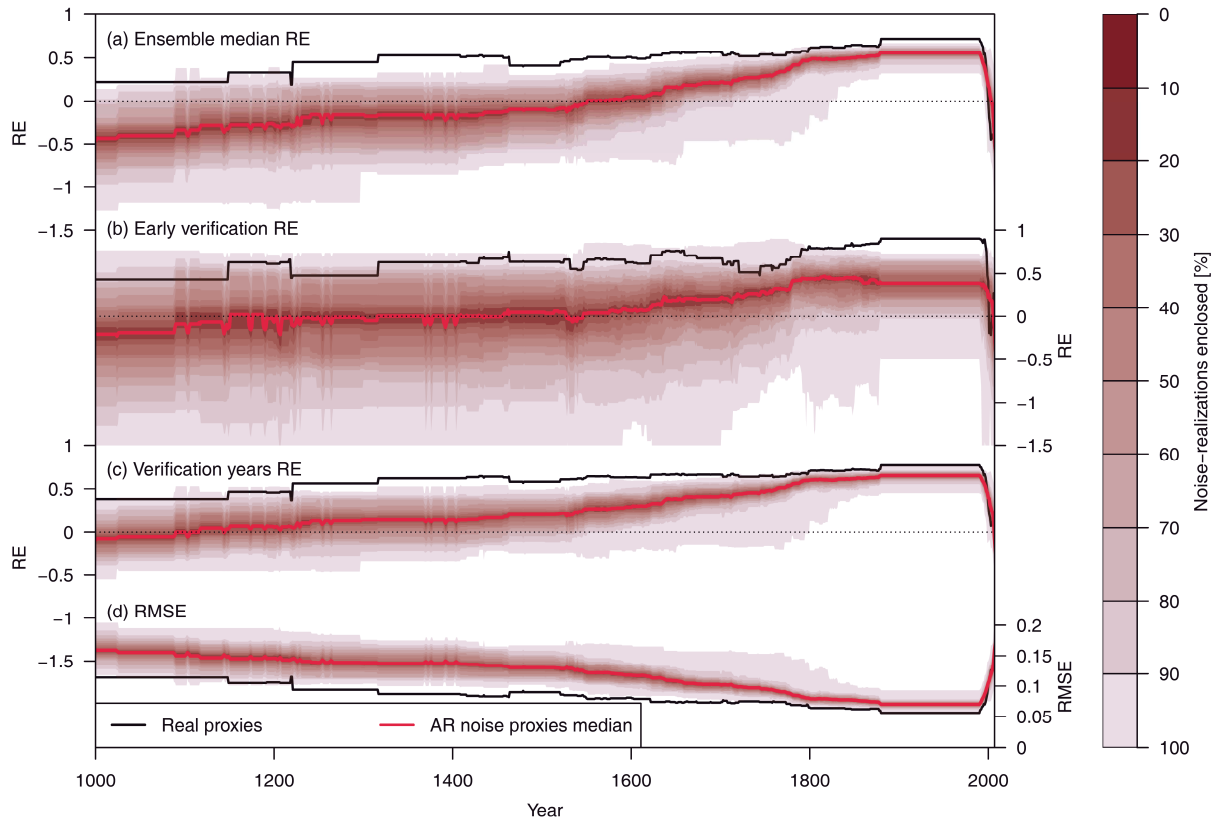
3.1.5. Noise predictors

To test if our reconstruction has more predictive skill than noise predictors, we compare the above RE values against the REs of reconstructions based on AR noise proxies. The ‘AR noise proxies’ are noise time series of the same length and autoregressive properties as our real proxy data (reflecting the full temporal autoregressive structure of the proxies; Wahl and Smerdon, 2012). For this exercise, AR noise proxy generation, screening and reconstructions are repeated 100 times using 1000-member ensembles.

Supplementary Figure 10 shows the temporal evolution of the reconstruction skill measures using real and AR noise proxies. The results demonstrate that RE values using real proxies are consistently positive (except for the negative ensemble median RE in the year 2000) and all

RE and RMSE measures clearly outperform the noise reconstructions, indicating a skillful temperature reconstruction is possible over the full 1000-2000 period. Less than 0.24% of noise reconstructions outperform our real temperature reconstruction over the entire reconstruction period using the ensemble median RE. The corresponding numbers for the early verification RE and verification years RE are 2.88% and 0.50%. Note that the fraction of predictors selected in the proxy-screening procedure (see section 1.3) is much smaller in the case of noise-proxies (74.6 ± 12 out of 191 proxies reflecting a fraction of $39.1\% \pm 6.3\%$) than for the real proxies (111 out of 191 proxies reflecting 58.1%).

Our results demonstrate that even though our conservative approach to derive noise-predictors can yield noise-based reconstructions with positive skill, it is very unlikely that noise predictors can reproduce the levels of predictive skill observed in the real proxy based reconstructions (cf. Wahl and Smerdon, 2012, section 4 and Fig. 2, for a parallel result). As a result, we have increased confidence that the skill we see in the reconstruction is evidence of a realistic estimation of past temperature variations.

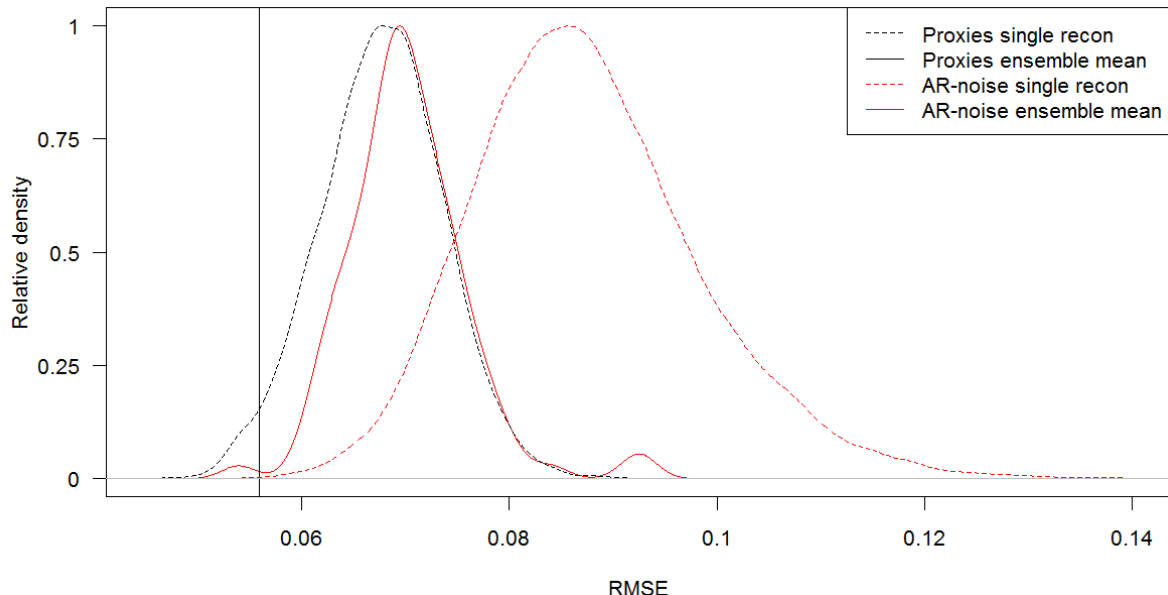


Supplementary Figure 10 | Reconstruction skill: RE and RMSE skill measures of our PCR reconstruction using real proxies (black lines) and median of 100 reconstructions using AR noise proxies (red lines). **a** Ensemble median RE, **b** early verification RE **c** verification years RE and **d** RMSE. The shaded areas represent the relative probability distribution of the results from 100 AR noise proxy reconstructions, expressed as percentiles: the lightest shading encloses the area between the minimum and maximum value, the next darker shading the area between the 5th and 95th percentile and so on. The darkest shading represents the area between the 45th and the 55th percentile. Values below -1.5 are not shown.

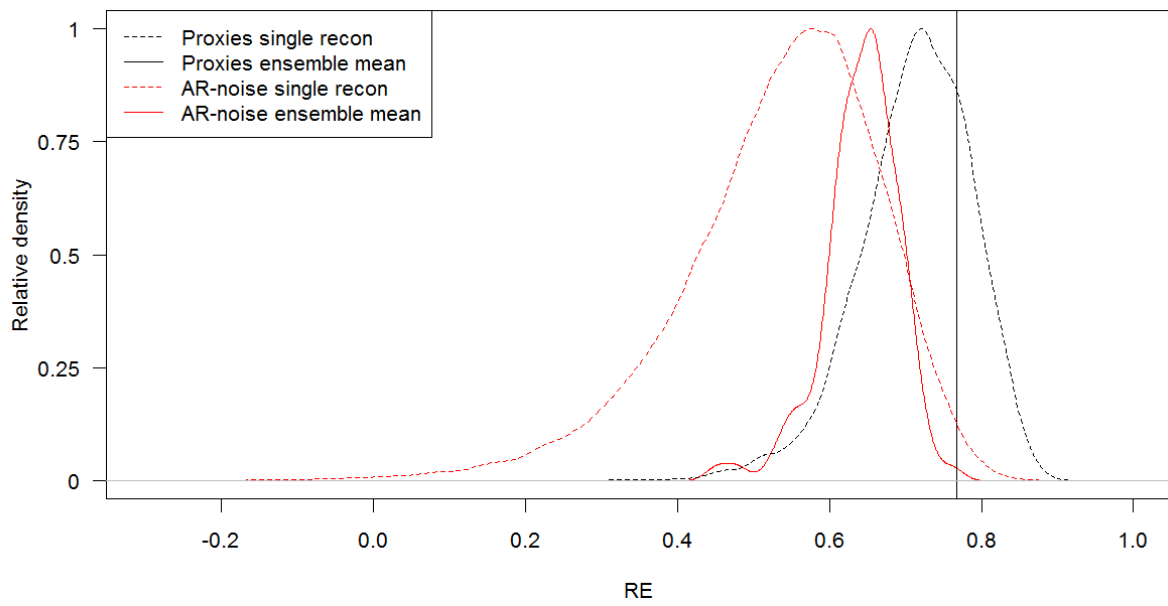
3.1.6. Ensemble vs. single reconstruction

Supplementary Figure 11 and Supplementary Figure 12 illustrate the RMSE and RE values of the individual ensemble members and the ensemble mean, respectively. They show that the skill of the ensemble mean is clearly higher than the average skill of the individual ensemble members, indicating that using ensemble reconstructions not only allows us to better address reconstruction uncertainties but also leads to more accurate results compared to single-member approaches. Supplementary Figure 11 and Supplementary Figure 12 also show that in

the most replicated nest during the 20th century, where AR noise reconstructions also have positive RE values, the real proxies clearly outperform the artificial data.



Supplementary Figure 11 | Ensemble vs. single-reconstruction RMSE: Dashed lines: Ensemble distribution of verification RMSE values of the most replicated proxy nest in the reconstruction using real proxies (black) and AR-noise proxies (red). Solid lines represent the RMSE of the ensemble mean reconstruction using real proxies (black) and distribution of 100 AR-noise based ensemble reconstructions (red).



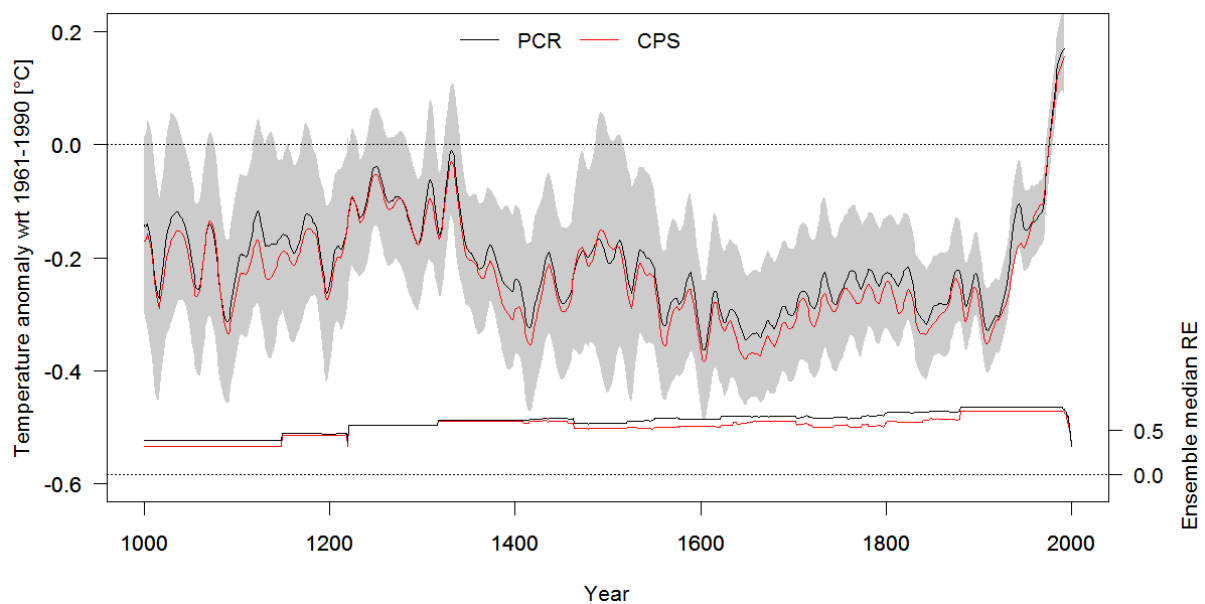
Supplementary Figure 12 | Ensemble vs. single-reconstruction RE. Same as Supplementary Figure 11 but for the RE. Solid lines represent the Verification years RE (see section 3.1.3).

3.2. Reconstruction robustness

Ideally, the reconstructed signal in multi-proxy reconstructions is inherent in multiple predictors and not dominated by a single proxy. Hence, the final reconstruction should not be too sensitive to changes in the proxy network. Similarly, individual archives (such as tree-rings or corals) should not dominate the reconstruction. Also, the choice of the reconstruction method should not influence the conclusions. Our ensemble reconstruction approach allows these questions to be addressed and allows the robustness of our reconstruction to be evaluated.

3.2.1. Alternative reconstruction methods: CPS

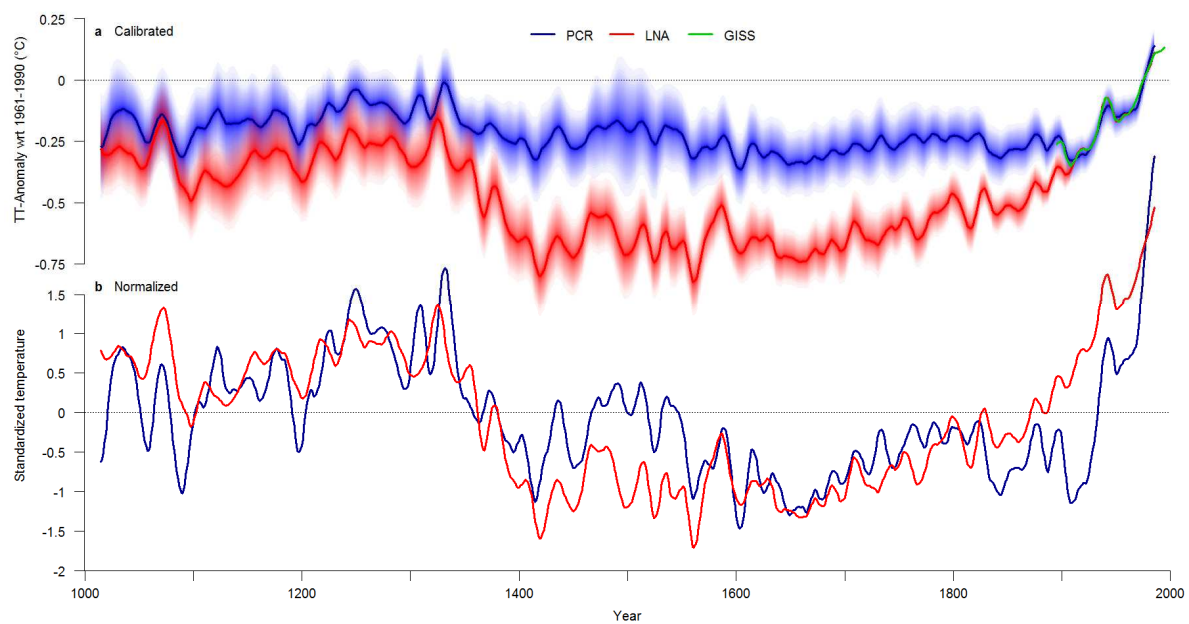
To address the influence of the reconstruction method on our results, we perform an additional 3000-member reconstruction using the Composite Plus Scale method (CPS; Mann *et al.*, 2008; Neukom *et al.*, 2011). We use the CPS approach of Neukom *et al.* (2011), which calculates the predictor composite by weighting each record with its correlation coefficient with the target over the calibration period. Supplementary Figure 13 compares the PCR and CPS reconstructions. They are generally very similar, indicating robustness of the results with regards to the reconstruction methodology. The low frequency amplitude is slightly larger in the CPS reconstruction resulting in colder reconstructed pre-industrial temperatures as compared to PCR. In terms of reconstruction skill, PCR performs slightly better. Therefore PCR is used for the analysis in the main manuscript.



Supplementary Figure 13 | PCR vs. CPS reconstruction. Top: 30-year filtered ensemble mean PCR (black, with grey shaded 2SE uncertainties) and CPS (red) reconstructions. Bottom: Verification years RE values of the PCR (black) and CPS (red) reconstructions.

3.2.2. Alternative reconstruction methods: LNA

We compare our results to an independent reconstruction using Bayesian hierarchical models developed by Li *et al.* (2010) , referred to as “LNA” in Hanhijärvi *et al.* (2013) and PAGES (2013). We used the same parameters as in PAGES (2013). The resulting reconstruction is compared to our PCR reconstruction in Supplementary Figure 14. We use the 2σ ensemble standard deviation of the LNA reconstruction as uncertainties to compare with our combined 2SE (see section 2.4). While the two methods yield a qualitatively similar temperature evolution, the LNA reconstruction shows a much larger amplitude between pre-industrial and present day temperatures. This amplitude is smaller (larger) in the PCR (LNA) reconstruction than in the NH reconstruction and most simulations of both hemispheres. Correlation between the two ensemble mean reconstructions is 0.71 ($p<<0.01$) and 0.74 ($p=0.01$) on interannual and 30-year filtered timescales, respectively. Supplementary Table 7 provides further comparison between the two reconstruction approaches. Notably we find that the early verification statistics of the LNA method are substantially weaker (e.g., RE values of 0.52 versus 0.9 for LNA and PCR, respectively). Yet, interestingly, most of the quantification provided in the main text related to NH-SH coherence and extreme periods (with the exception of the temperature amplitude) is similar for these two reconstruction approaches. The two methods also show very similar results in terms of extreme periods and interhemispheric differences. Given that our conclusions are based on decadal to centennial time-scale analyses, uncertainties in the overall amplitude (e.g., plausibly larger amplitude in the LNA reconstruction despite weaker early verification statistics) do not affect our main findings.



Supplementary Figure 14 | PCR vs. LNA reconstruction. **a** Comparison of 30-year filtered PCR (blue) and LNA (red) reconstruction ensemble means with shaded uncertainties and instrumental data (green). **b** Comparison of 30-year filtered PCR (blue) and LNA (red) reconstruction ensemble means after standardization to a mean of zero and unit standard deviation over the period 1000–2000.

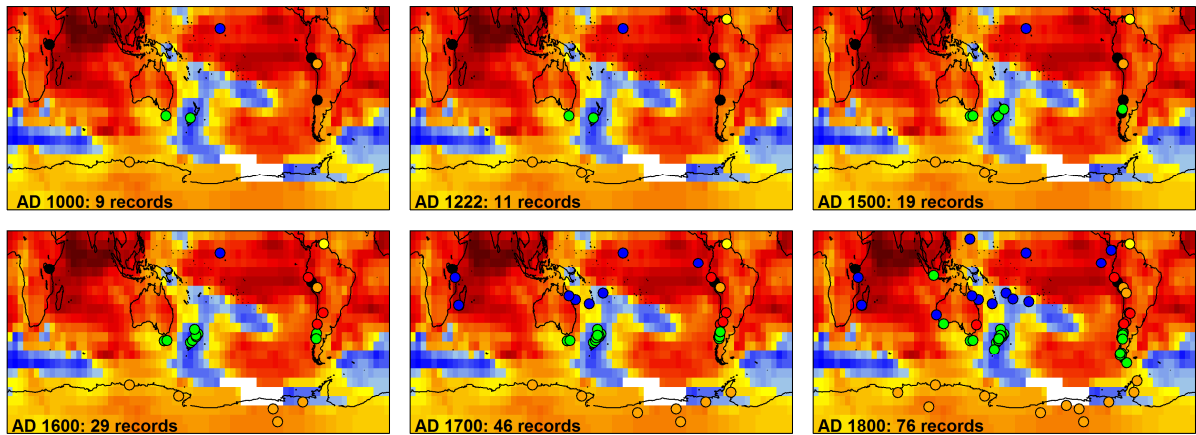
Supplementary Table 7 | Comparison of PCR and LNA reconstructions. Comparison of early verification statistics, uncertainties and the statistics and properties mentioned in the main text.

	PCR	LNA
<i>Early verification statistics (1880-1910; full proxy replication)</i>		
r ²	0.57	0.02
RE	0.9	0.52
Percentage of members with decade of highest temperature after 1970 (main text, line 93)	99.7	98.8
<i>Reconstruction-model correlations (line 114)</i>		
ensemble mean correlations	0.29	0.46
ensemble 2*std. dev.	0.22	0.24
correlation of ensemble means	0.35	0.58
<i>Periods with decades showing a certain fraction of ensemble members with extreme temperatures synchronously in both hemispheres (lines 120ff)</i>		
>= 33% members with cold extremes	within 1594-1677	within 1449-1452 and 1597-1695
>66% members with positive extremes	since 1974	since 1974
>90% members with positive extremes	since 1979	since 1979
Fraction of years (%) with ensemble mean NH-SH difference outside the 10th-90th percentile range of model simulations (line 148)	41.6	43.1
<i>Pre-industrial temperature amplitude (°C; line 155)</i>		
Ensemble mean	0.37	0.75
Ensemble 2*std. dev.	0.11	0.13
<i>Uncertainties (°C; temporal average)</i>		
Interannual data	0.22	0.27
30-year filtered data	0.13	0.11

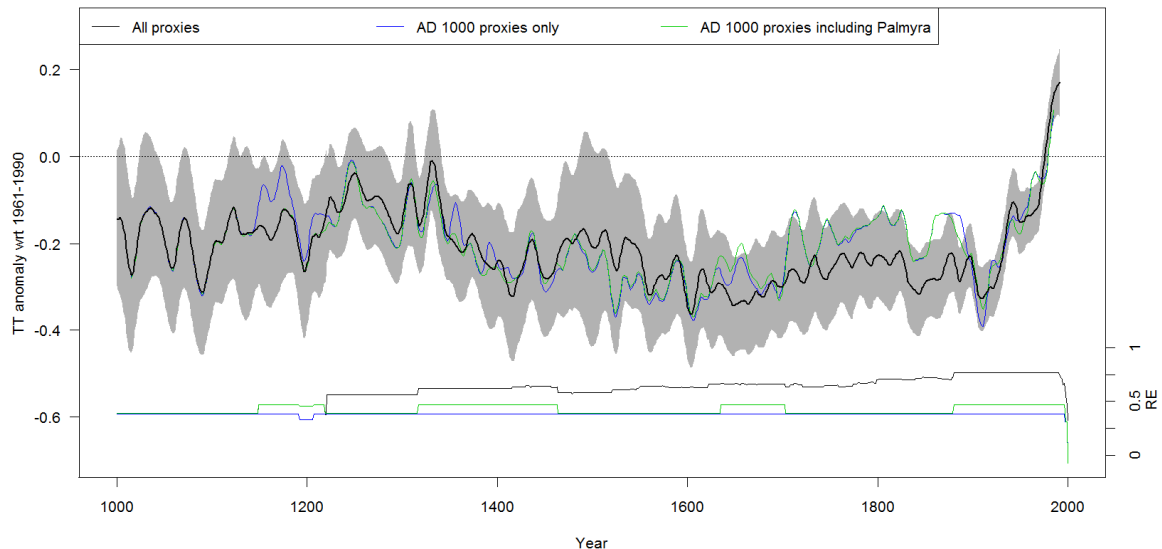
3.2.3. Influence of changes in proxy replication

A potential uncertainty of nested climate reconstructions is that the changes in proxy replication may bias the temporal representativity of the reconstruction. The proxy databases available throughout the reconstruction period may have different properties such as spatial distribution, land/ocean signal, seasonal response and spectral properties. If these differences are substantial, the reconstructions of different proxy combinations (nests) may not be comparable and splicing them together can lead to misinterpretations. To test this, we performed an additional reconstruction using only the records that extend back to the year 1000 or beyond (henceforth R8 reconstruction), resulting in a reconstruction with constant proxy replication over time.

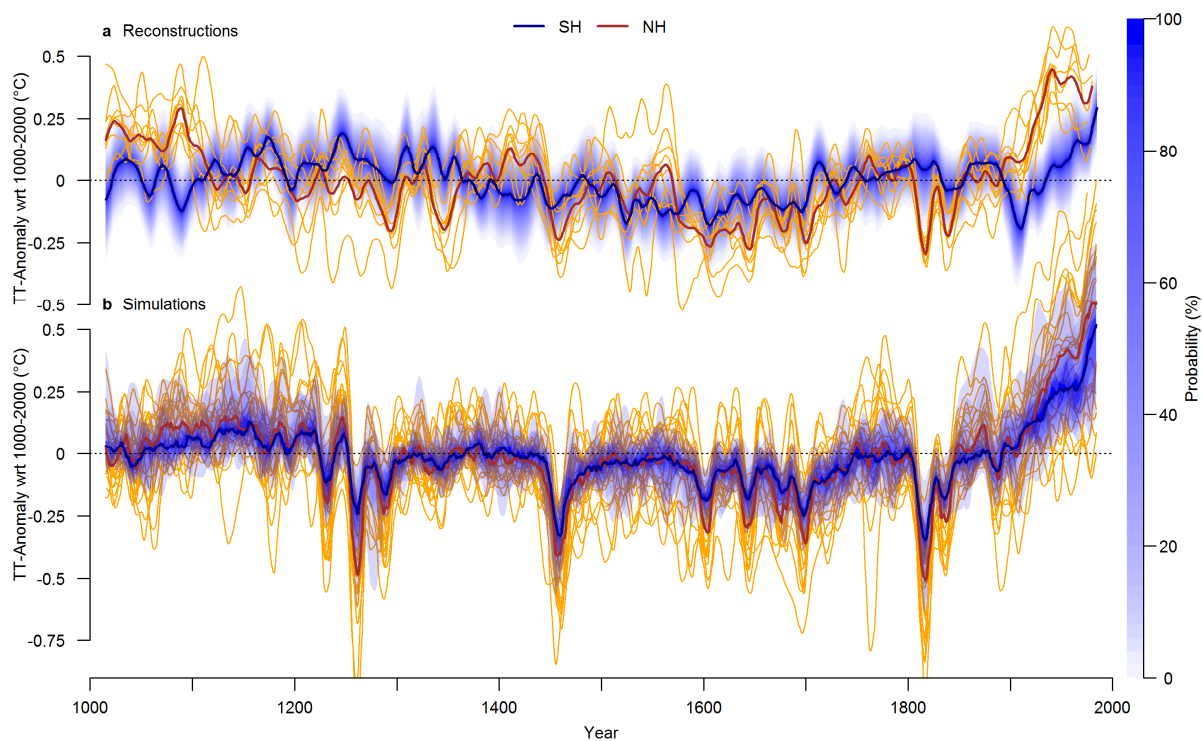
Supplementary Figure 15 shows the spatial distribution of proxy data over time. Supplementary Figure 16 compares the R8 reconstruction to the full spliced reconstruction using all 111 records. The figure shows that the two reconstructions generally have a very similar temperature evolution. The greatest differences occur between 1700 and 1900, where the R8 reconstruction shows warmer temperatures but the fluctuations are mostly in phase with the full reconstruction. Inclusion of the floating Palmyra coral record does not substantially change the R8 reconstruction except that it yields colder conditions in the late 11th century. Supplementary Figure 17-Supplementary Figure 19 show the analogues of Figures 2-4 in the main text for the R8 network. The figures are very similar to the results using the full network, indicating that our conclusions are not affected by the changing proxy replication over time.



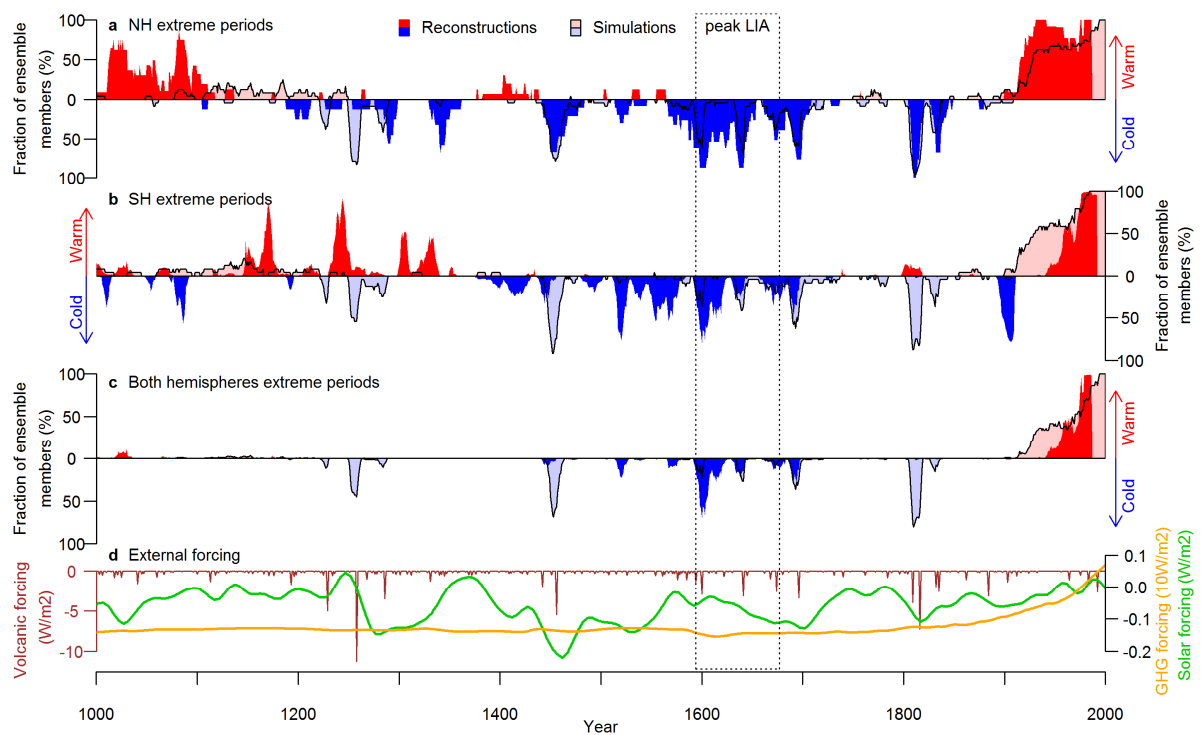
Supplementary Figure 15 | Spatial distribution of proxy data over time. Same as Figure 1a in the main text but showing proxy data availability for different years within the last millennium. The R8 network is shown in the top left panel (where the discontinuous Palmyra coral record is shown additionally as blue circle).



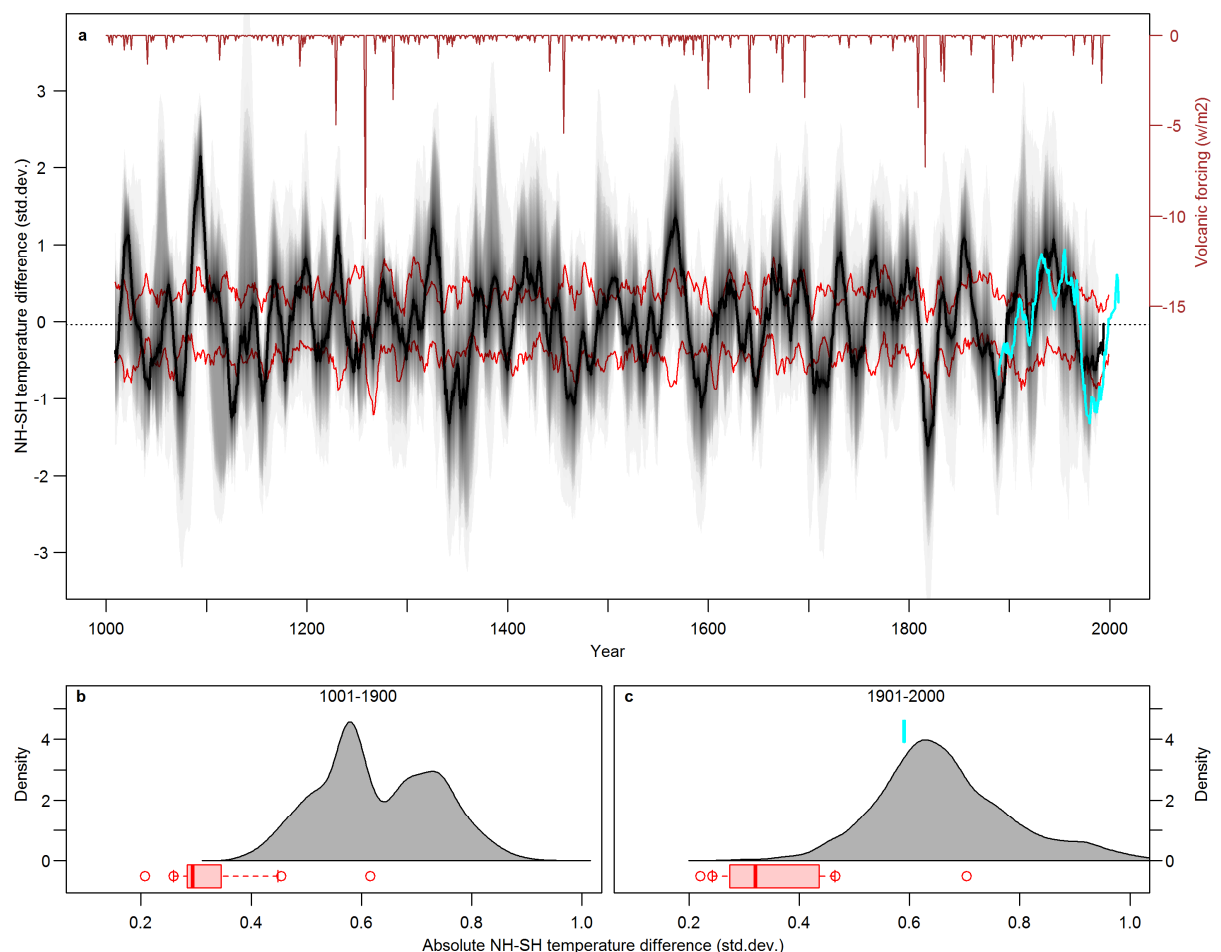
Supplementary Figure 16 | R8 reconstruction. Comparison of our SH reconstruction (black) with alternative reconstructions using only the proxies covering the full AD1000-2000 period (R8, blue) and additionally the floating and interrupted Palmyra coral record (green). Top: 30-year filtered reconstruction ensemble means. Grey shading represents the 2SE uncertainty bounds of the fully replicated reconstruction. Bottom: Corresponding verification years RE values.



Supplementary Figure 17 | Temperature variability over the last millennium using long proxies only. Same as Figure 2 in the main text but using the SH reconstruction that includes only the proxies extending to the year 1000.



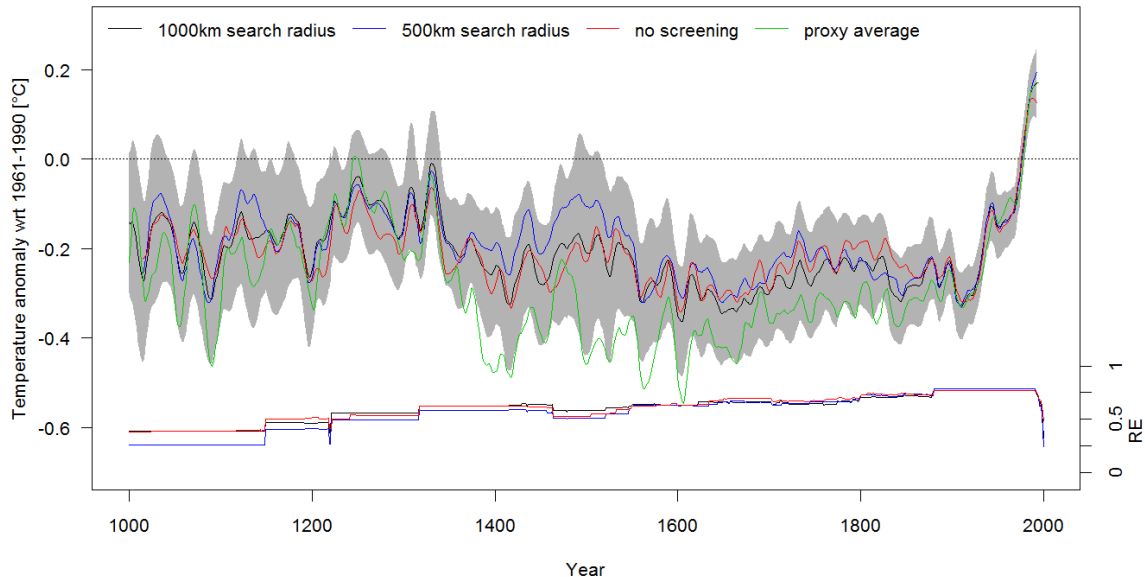
Supplementary Figure 18 | Extreme periods using long proxies only. Same as Figure 3 in the main text but using the SH reconstruction that includes only the proxies extending to the year 1000.



Supplementary Figure 19 | Inter-hemispheric temperature difference using long proxies only. Same as Figure 4 in the main text but using the SH reconstruction that includes only the proxies extending to the year 1000.

3.2.4. Influence of different proxy screening approaches

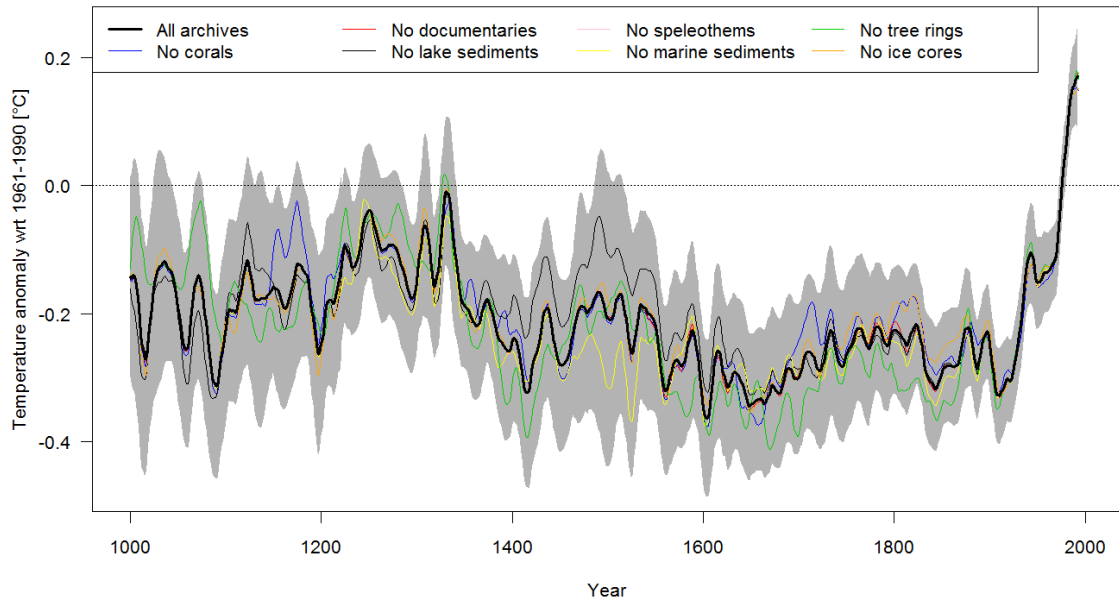
Supplementary Figure 20 compares our 30-year filtered reconstruction with alternative reconstructions using the same method but different proxy matrices: a pre-screened network using a search radius of 500 km (instead of 1000 km) and the full, unscreened network. The resulting reconstructions are very similar to the results presented in the main text and always remain within the 2SE uncertainty bands. Additionally a simple unweighted average of all 111 proxies used in the final reconstruction is shown by the green line in Supplementary Figure 20. This composite shows a similar temperature history, but with stronger cooling during the period 1400-1900. We interpret this difference as meaning that some regions with a high density of proxy data may have experienced colder conditions than the hemispheric average.



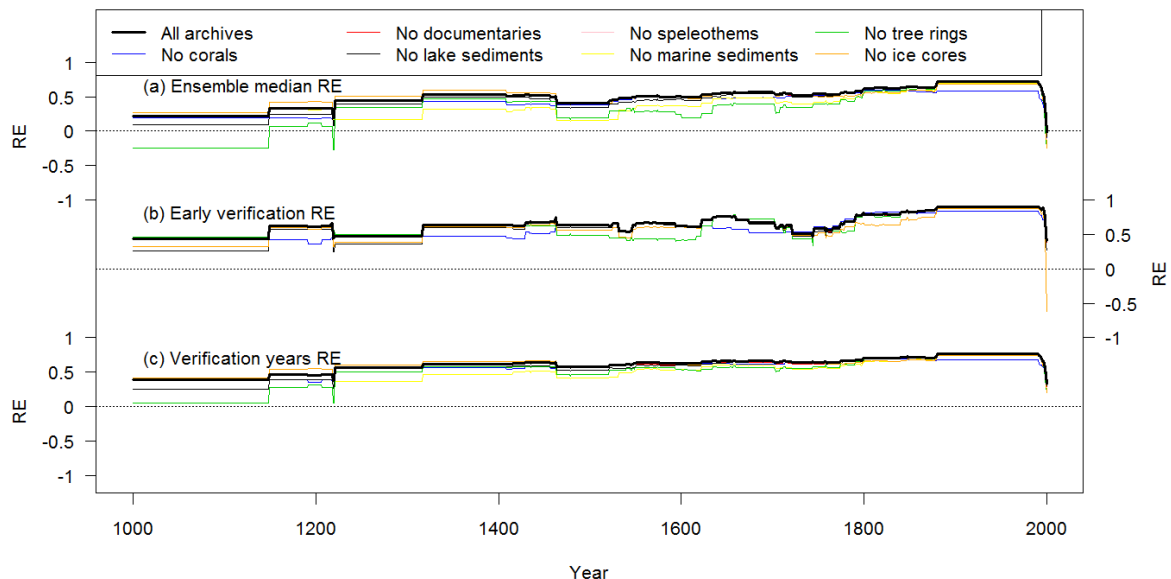
Supplementary Figure 20 | Influence of proxy screening. Comparison of 30-year filtered ensemble mean temperature reconstruction (top) and verification years RE (bottom) based on different predictor sets. Black: final predictor selection based on a search radius of 1,000 km (111 proxies). Blue: Predictor selection based on a search radius of 500 km (85 proxies). Red: No pre-screening of the proxies, all records are used (205 proxies). The green line represents a simple average of the 111 proxies used in the reconstruction (after adjusting them to a mean of zero and unit variance over the 1911-1990 period).

3.2.5. Influence of different proxy archives

Our proxy records are not evenly distributed over the different paleoclimate archives. Figure 1b in the main text shows that tree-rings and corals are the archives with the largest fraction of proxies used. This bias towards tree-rings and corals is very strong in the more recent past, but less distinct in the early period of the reconstruction. In the year 1000, our predictor set consists of three lake sediment and ice core chronologies, two tree-ring and one coral record. To assess whether one archive dominates the reconstruction and biases the results, we recalculated the reconstruction omitting all records from each archive separately. The resulting reconstructions and RE measures are shown in Supplementary Figure 21 and Supplementary Figure 22, respectively. The reconstructions with the individual archives removed always remain within the 2SE uncertainties of the final reconstruction (Supplementary Figure 21). Comparison of the RE values (Supplementary Figure 22) shows that in the first 200 years of the reconstruction, tree-ring data are required to obtain positive ensemble median RE values. For the other archives and skill measures, removing individual archives only marginally changes the reconstruction skill.



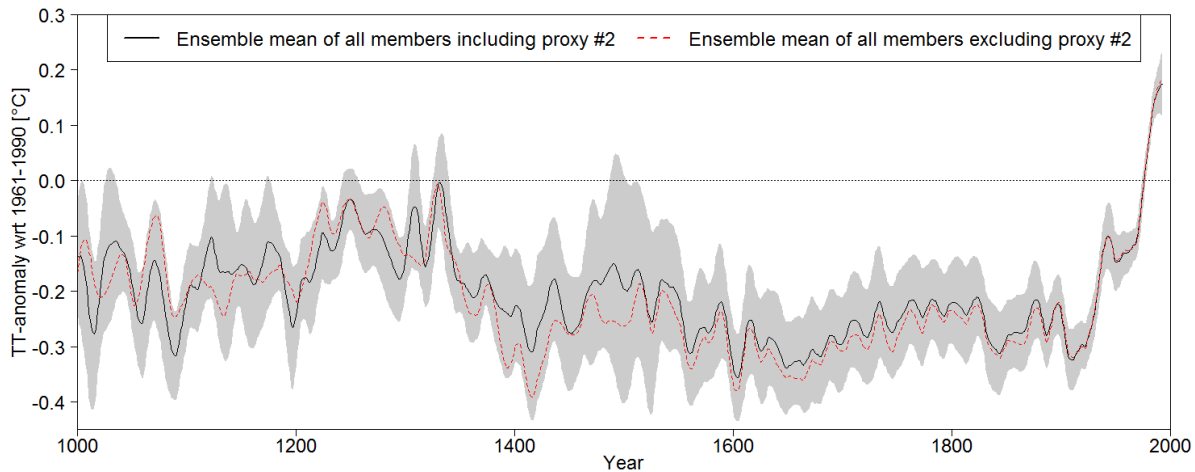
Supplementary Figure 21 | Influence of proxy archives. 30-year filtered ensemble mean reconstructions based on different combinations of proxy archives. Bold black is the final reconstruction using all archives with 2SE uncertainty bands shaded in grey. Blue is the reconstruction after removing all coral records; similarly for documentaries (red), lake sediments (thin black), speleothems (pink), marine sediments (yellow), tree-rings (green) and ice cores (orange).



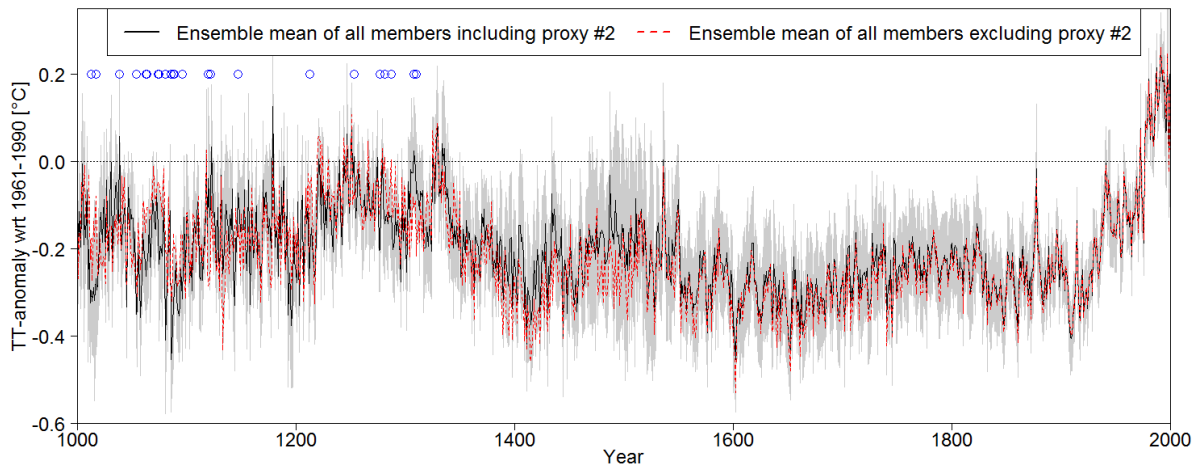
Supplementary Figure 22 | Influence of proxy archives on reconstruction skill. Same as Supplementary Figure 21 but for the RE measures of the reconstructions.

3.2.6. Influence of individual proxy records

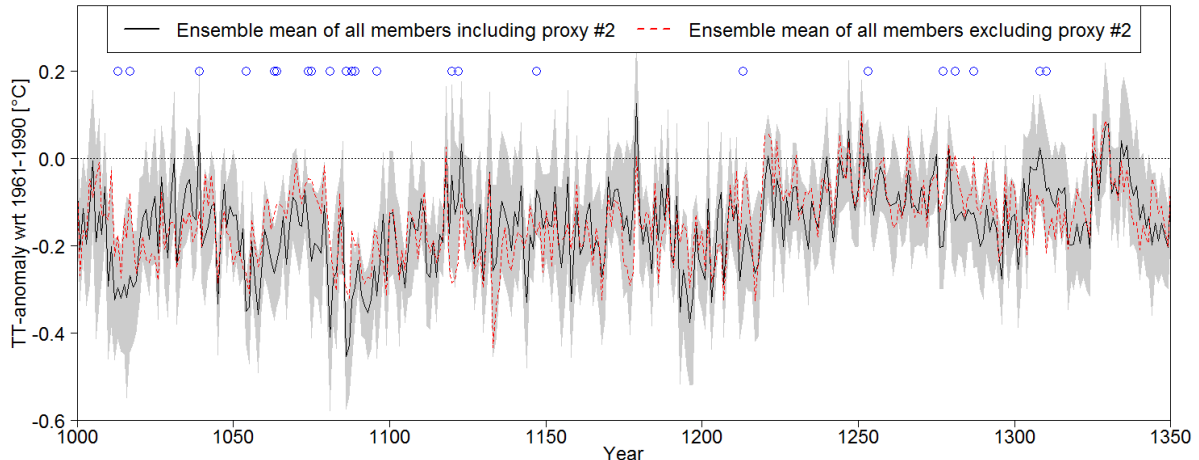
To assess whether our reconstruction is dominated by individual proxy records, we compare the ensemble members where a proxy was included and excluded, respectively. For each proxy we repeat the following calculations. The ensemble mean of all members where the proxy was included in the reconstruction ($mean_{inc}$) and excluded from the reconstruction ($mean_{exc}$) are calculated, respectively. The ensemble standard deviation of all members where the proxy was included (σ_{inc}) was also calculated. If the $mean_{exc}$ fell outside the $mean_{inc} \pm 2\sigma_{inc}$ range in one or more years, these periods are considered less robust. Note that this $\pm 2\sigma_{inc}$ range is different from the total combined uncertainties as it represents only the spread of a sub-sample of the full ensemble and does not include calibration uncertainties. This analysis was repeated using the 30-year filtered data. Supplementary Figure 23 illustrates the results using the example of proxy #2 (Mt. Read Tasmania) and the 30-year filtered data. Supplementary Figure 24 and Supplementary Figure 25 show the results of the interannual analysis for the same proxy. Note that out of all 111 proxies, the effect of removing a record is largest for the proxy #2 shown in these Figures. Over all proxies, this robustness criterion is not fulfilled during 25 (0) years of our unfiltered (30-year filtered) reconstruction. The 25 years where the criterion is not fulfilled on interannual timescales are all between 1000 and 1360. The proxies affected are #2 (Mt. Read; 23 years) and #8 (Palmyra, 2 years). Given this small fraction of years and proxies affected, we conclude that our reconstruction is robust with regard to changes in the predictor network, particularly during the post-1360 period and on decadal timescales.



Supplementary Figure 23 | Example for the influence of single proxies. Effect of removing proxy #2 (Mt. Read) from the predictor set on the 30-year filtered reconstructions. Black: mean of all ensemble members where this proxy was included into the reconstruction ($mean_{inc}$). Grey shading: 2 standard deviation bounds of these ensemble members ($mean_{inc} \pm 2\sigma_{inc}$). Red dashed: mean of all members where this proxy was withheld from the reconstruction ($mean_{exc}$).



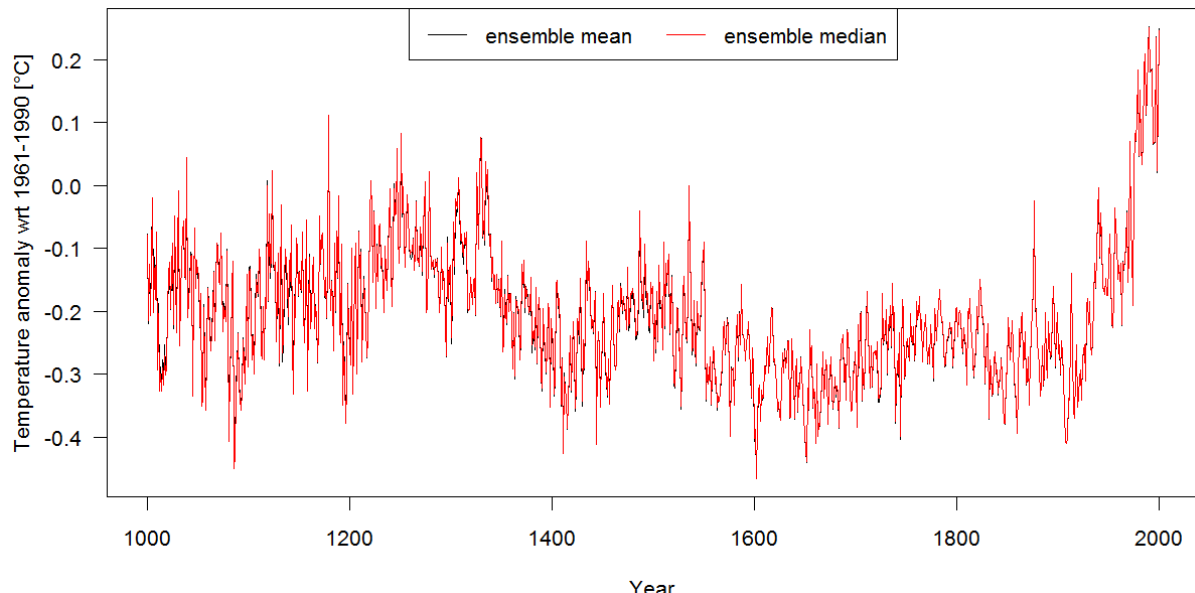
Supplementary Figure 24 | Example for the influence of single proxies on interannual scale. Same as Supplementary Figure 23 but for the unfiltered data. Blue circles indicate less robust years where the red dashed line falls outside the grey 2 standard deviation bounds.



Supplementary Figure 25 | Example for the influence of single proxies on interannual scale between 1000-1350. Same as Supplementary Figure 24 but over the period 1000-1350.

3.2.7. Ensemble median vs. mean

Supplementary Figure 5 shows the reconstruction ensemble median and mean, which are very similar (see also Supplementary Figure 4). The largest (average) absolute difference between the mean and the median over the period 1001-2000 is 0.15 (0.02) standard deviations of instrumental temperatures 1901-1999. For computational reasons we therefore use the ensemble mean to estimate the most probable reconstructed value. However, for the RE measures we use the ensemble median, as the mean is often biased by a small number of ensemble members with extremely large negative REs.



Supplementary Figure 26 | Ensemble mean vs. median. SH mean reconstruction ensemble mean (black) and median (red). See also Supplementary Figure 3

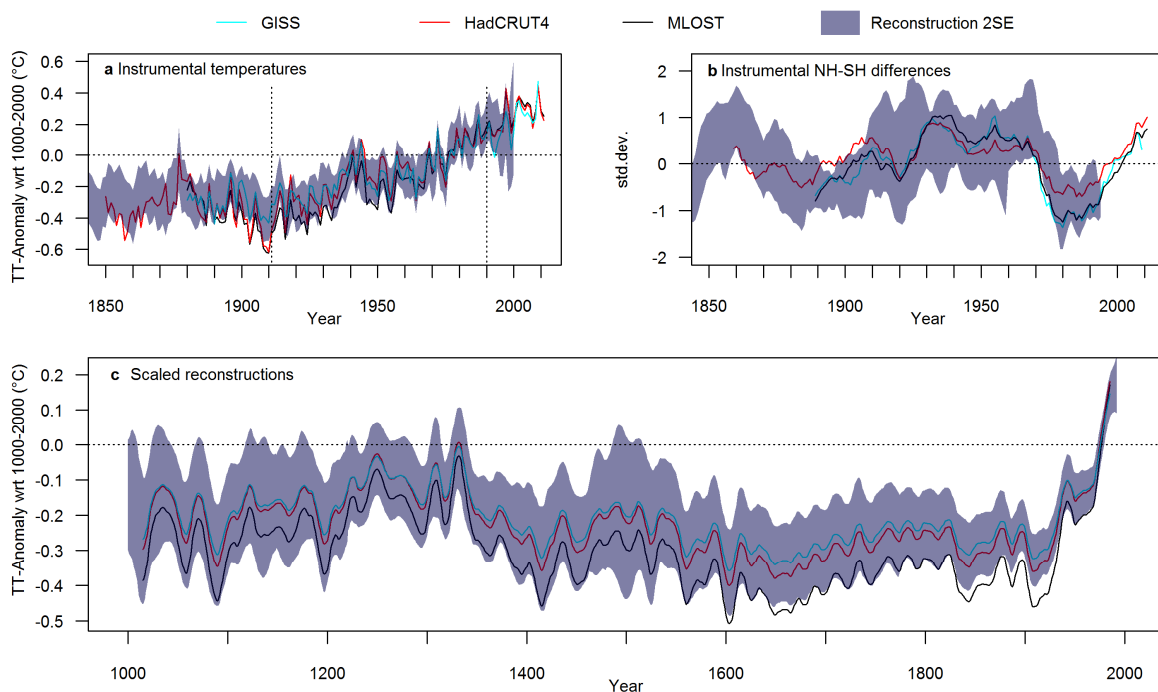
3.3. Conclusions

In summary, our reliability assessments indicate a skilful and robust reconstruction over the last millennium. More high resolution proxy records are required to allow a robust SH temperature reconstruction prior the year 1000.

4. Sensitivity to instrumental target data

Supplementary Figure 27 shows the sensitivity of our reconstruction to the choice of the instrumental dataset used for calibration. While the SH means of the three instrumental grids GISS (Hansen et al., 2010), HadCRUT4 (Morice et al., 2012) and MLOST (Smith et al., 2008) are highly correlated over the 1911-1990 calibration period (all $r>0.94$, $p<<0.01$), they exhibit some differences in amplitude and trend (GISS: $0.50^{\circ}\text{C}/\text{century}$; HadCRUT4: $0.58^{\circ}\text{C}/\text{century}$; MLOST: $0.74^{\circ}\text{C}/\text{century}$). The NH-SH differences, however, are similar and do not affect our conclusions (see also Drost and Karoly, 2012; Drost *et al.*, 2012).

To assess the influence of the instrumental dataset on our reconstruction, we re-scaled our ensemble mean reconstruction to the mean and variance of the three instrumental data (Supplementary Figure 27c). While the results from GISS and HadCRUT4 are very similar, the reconstruction rescaled to MLOST reveals lower pre-industrial temperatures (average offset of 0.1°C between GISS and MLOST over 1000-1850). This suggests that our estimates of the unusual nature of late 20th century temperatures are rather conservative given our choice of the instrumental calibration dataset.



Supplementary Figure 27 | Comparison of different instrumental temperature datasets. Comparison of the GISS dataset (cyan; Hansen et al., 2010) used for our reconstruction with the other gridded instrumental temperature records HadCRUT4 (red; Morice et al., 2012) and NOAA MLOST (black; Smith et al., 2008). Instrumental 2SE envelopes are blue shaded. **a** Instrumental SH mean temperatures (cf. Figure 1c in the main text). Start and end dates of the calibration/verification period of our reconstruction (1911-1990) are indicated by vertical dotted lines. **b** NH-SH differences 1850-2010 (cf. Figure 4a in the main text). **c** 30-year filtered SH reconstruction ensemble means re-scaled to the mean and variance of each instrumental target over the 1911-1990 period.

5. NH reconstruction ensemble

Details concerning the NH reconstructions are provided in Frank *et al.* (2010). The most important difference from our SH reconstruction is that it is not based on a single predictor matrix but uses nine published NH reconstructions, based on different (but not independent) proxy sets and various reconstruction methodologies (Jones *et al.*, 1998; Briffa, 2000; Mann and Jones, 2003; Moberg *et al.*, 2005; D'Arrigo *et al.*, 2006a; Frank *et al.*, 2007; Hegerl *et al.*, 2007; Juckes *et al.*, 2007; Mann *et al.*, 2008). In Frank *et al.* (2010), the individual single-member reconstructions were recalibrated to instrumental temperature data using different calibration periods as ensemble parameters, resulting in a total of 521 ensemble members. Although the approach is different, the NH reconstruction ensemble also represents a combination of calibration, proxy data and methodological perturbations. The latter two are introduced through the nine different original reconstructions in the NH, whereas for the SH they are sampled for each ensemble member. In the NH approach, the variable calibration window resulted in a quantification of amplitude uncertainty only, whereas in our SH approach changing the calibration period also influences the shape of the reconstructed temperature history. The NH ensemble spread is larger than in the SH due to the relatively large differences between some of the original sub-reconstructions and the composite-plus-scaling approach over a range of time-windows in ref. (Frank *et al.*, 2010). Note that the increase in ensemble uncertainties back in time is much larger in the SH (the ratio of uncertainties 11th century/20th century is 2.34 for the SH and 1.2 for the NH). To best illustrate these two approaches, the ensemble means of the nine sub-reconstructions are shown for the NH in Figure 2a. As a consequence of these methodological differences and the larger ensemble spread in the NH, one would expect generally reduced probabilities for extreme periods in the NH. However, Figures 3a-b show similar fractions of periods with high probabilities for extremes, indicating a similar consistency between ensemble members in the timing of extreme periods in both hemispheres. The relatively small ensemble spread in the NH-SH differences (Figure 4a), particularly during extreme phases, where in most cases all ensemble members are of the same sign, also indicates consistency among the NH reconstructions in identifying decadal-scale temperature trends.

6. Simultaneous extreme periods

Supplementary Table 8 | Synchronous extreme periods. Periods where both hemispheres exhibit extreme periods in at least 33% of their reconstruction ensemble members. The years indicated are the start years of 10-year running temperature averages as used to generate Figure 3 in the main text. Extremes are defined as 10-year averages exceeding one standard deviation above or below the 1000-2000 CE baseline. Note that 1986 is the last year of this analysis (representing the average of 1986-1995), because the NH reconstruction ends in 1995.

Negative extremes	1594, 1595, 1596, 1597, 1598, 1599, 1600, 1601, 1602, 1603, 1619, 1620, 1621, 1622, 1623, 1635, 1636, 1639, 1640, 1641, 1642, 1643, 1644, 1645, 1646, 1671, 1672, 1673, 1674, 1675, 1676, 1677
Positive extremes	1030, 1965, 1967, 1968, 1969, 1970, 1971, 1972, 1973, 1974, 1975, 1976, 1977, 1978, 1979, 1980, 1981, 1982, 1983, 1984, 1985, 1986

7. Details on climate model simulations

Supplementary Table 9 provides an overview over the 24 model simulations used in this study. Ten of the simulations belong to the latest coordinated PMIP3-CMIP5 simulation effort (Taylor *et al.*, 2012) using recommendations for forcings from Schmidt et al. (2011; 2012). For further details we refer to the references provided in the table. We use hemispheric averages and May-April years for the SH and calendar years for the NH, as represented by the reconstructions.

Supplementary Table 9 | Details of the model simulations used in this study. Name, time period covered and forcing datasets used. Weak/Strong in the column for solar forcing is a qualitative remark for the strength of solar variability over the last millennium (see e.g. Jungclaus *et al.*, 2010). For further details we refer to the references provided in the table. Note that for some simulations, references for the simulation of the last millennium are not yet available. In these cases, general references to the model are provided. The last column indicates whether the simulation belongs to the latest PMIP3/CMIP5 dataset (Taylor *et al.*, 2012) using recommendations for forcings from Schmidt *et al.* (2011; 2012).

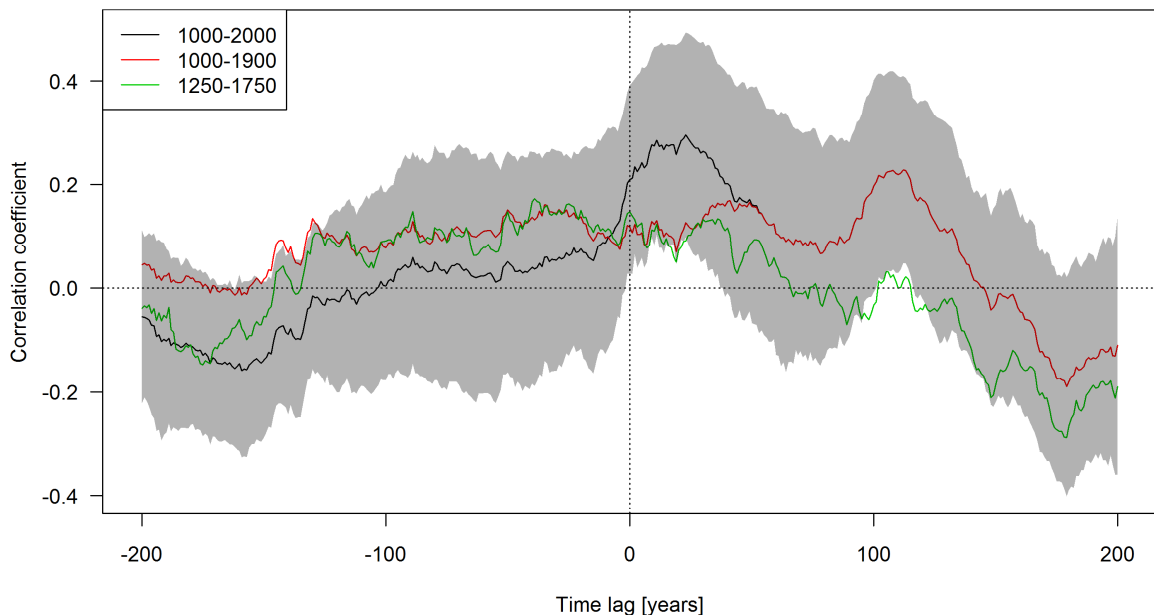
Model	Simulation	Time span	Volcanic forcing	Solar forcing	GHG forcing	Orbital forcing	Land-use-land-cover forcing	Aerosol forcing	Reference(s)	PMIP3/CMIP5
BCC-CSM		0850-2000	(Gao <i>et al.</i> , 2008)	Weak (Vieira and Solanki, 2010) spliced to (Wang <i>et al.</i> , 2005)	(MacFarling-Meure <i>et al.</i> , 2006); (Schmidt <i>et al.</i> , 2011 and references therein)	(Berger, 1978)		(Lamarque <i>et al.</i> , 2010)	(Xin <i>et al.</i> , 2013)	X
CCSM3		1000-2000	(Ammann <i>et al.</i> , 2003)	Strong (Bard <i>et al.</i> , 2000), spliced to (Lean <i>et al.</i> , 1995)	CO ₂ : (Etheridge <i>et al.</i> , 1996), CH ₄ : Blunier <i>et al.</i> (1995), (Blunier <i>et al.</i> , 1995), N ₂ O: (Flückiger <i>et al.</i> , 1999; Flückiger <i>et al.</i> , 2002)				(Hofer <i>et al.</i> , 2011)	
CCSM4		850-2005	(Gao <i>et al.</i> , 2008)	Weak (Vieira and Solanki, 2010) spliced to (Wang <i>et al.</i> , 2005)	(Schmidt <i>et al.</i> , 2011 and references therein)	(Berger, 1978)	(Pongratz <i>et al.</i> , 2009) spliced to (Hurtl <i>et al.</i> , 2006)	(Lamarque <i>et al.</i> , 2010)	(Laundrum <i>et al.</i> , 2013)	X
CSIRO Mk3L-1-2	1-3	1000-2000	(Gao <i>et al.</i> , 2008)	Weak (Steinhilber <i>et al.</i> , 2009) spliced to (Wang <i>et al.</i> , 2005)	(MacFarling-Meure <i>et al.</i> , 2006)	(Berger, 1978)			(Phipps <i>et al.</i> , 2011; Phipps <i>et al.</i> , 2012; Phipps <i>et al.</i> , 2013)	
CSIRO-Mk3L-1-2		0850-2000	(Crowley and Unterman, 2013)	Weak (Steinhilber <i>et al.</i> , 2009) spliced to (Wang <i>et al.</i> , 2005)	(MacFarling-Meure <i>et al.</i> , 2006); (Schmidt <i>et al.</i> , 2011 and references therein)	(Berger, 1978)			(Phipps <i>et al.</i> , 2011; Phipps <i>et al.</i> , 2012)	X
ECHO-G	Erik 1 & 2	1000-1990	(Crowley, 2000)	Strong (Bard <i>et al.</i> , 2000), spliced to (Lean <i>et al.</i> , 1995)	CO ₂ : (Etheridge <i>et al.</i> , 1996), CH ₄ : (Etheridge <i>et al.</i> , 1998), N ₂ O: (Battle <i>et al.</i> , 1996)				(González-Rouco <i>et al.</i> , 2006)	
FGOALS-g1		1000-1999	(Crowley, 2000)	Strong (Bard <i>et al.</i> , 2000), spliced to (Lean <i>et al.</i> , 1995)	CO ₂ : (Etheridge <i>et al.</i> , 1996), CH ₄ : Blunier <i>et al.</i> (1995), (Blunier <i>et al.</i> , 1995), N ₂ O: (Flückiger <i>et al.</i> , 1999; Flückiger <i>et al.</i> , 2002)				(Yongqiang <i>et al.</i> , 2002; Yongqiang <i>et al.</i> , 2004)	X ^a

Model	Simulation	Time span	Volcanic forcing	Solar forcing	GHG forcing	Orbital forcing	Land-use-land-cover forcing	Aerosol forcing	Reference(s)	PMIP3/CMIP5
GISS-E2-R	p121	850-2005	(Crowley and Unterman, 2013)	Weak (Steinhilber et al., 2009) spliced to (Wang et al., 2005)	(MacFarling-Meure et al., 2006); (Schmidt et al., 2011 and references therein)	(Berger, 1978)	(Pongratz et al., 2009) spliced to (Hurtt et al., 2006)	(Lamarque et al., 2010)	(Schmidt et al., 2006)	X
GISS-E2-R	p124	850-2005	(Crowley and Unterman, 2013)	Weak (Vieira and Solanki, 2010) spliced to (Wang et al., 2005)	(MacFarling-Meure et al., 2006); (Schmidt et al., 2011 and references therein)	(Berger, 1978)	(Pongratz et al., 2009) spliced to (Hurtt et al., 2006)	(Lamarque et al., 2010)	(Schmidt et al., 2006)	X
GISS-E2-R	p127	850-2005	(Crowley and Unterman, 2013)	Weak (Vieira and Solanki, 2010) spliced to (Wang et al., 2005)	(MacFarling-Meure et al., 2006); (Schmidt et al., 2011 and references therein)	(Berger, 1978)	(Kaplan et al., 2011)	(Lamarque et al., 2010)	(Schmidt et al., 2006)	X
HadCM3		800-2000	(Crowley and Unterman, 2013)	Weak (Steinhilber et al., 2009) spliced to (Wang et al., 2005)	(MacFarling-Meure et al., 2006); (Schmidt et al., 2011 and references therein)	(Berger, 1978)	(Pongratz et al., 2009) spliced to (Hurtt et al., 2006)	(Johns et al., 2003)	(Schurer et al., 2013)	X
IPSL-CM5A-LR		0850-2005	(Ammann et al., 2007)	Weak (Vieira and Solanki, 2010) spliced to (Wang et al., 2005)	(MacFarling-Meure et al., 2006); (Schmidt et al., 2011 and references therein)	(Berger, 1978)			(Dufresne et al., 2012)	X
MPI-ESM E1	1-5	800-2005	(Crowley and Unterman, 2013)	Weak (Krivova et al., 2007)	CO ₂ : diagnosed (Marland et al., 2003) CH ₄ and N ₂ O: (MacFarling-Meure et al., 2006)	(Bretagnon and Francou, 1988)	(Pongratz et al., 2008)	(Lefohn et al., 1999)	(Jungclaus et al., 2010)	
MPI-ESM E2	1-3	800-2005	(Crowley and Unterman, 2013)	Strong (Bard et al., 2000)	CO ₂ : diagnosed (Marland et al., 2003) CH ₄ and N ₂ O: (MacFarling-Meure et al., 2006)	(Bretagnon and Francou, 1988)	(Pongratz et al., 2008)	(Lefohn et al., 1999)	(Jungclaus et al., 2010)	
MPI-ESM-P		850-2005	(Crowley and Unterman, 2013)	Weak (Vieira and Solanki, 2010) spliced to (Wang et al., 2005)	(MacFarling-Meure et al., 2006); (Schmidt et al., 2011 and references therein)	(Berger, 1978)	(Pongratz et al., 2009) spliced to (Hurtt et al., 2006)	(Lamarque et al., 2010)	(Jungclaus et al., 2012; Jungclaus et al., 2013)	X

^a Does not follow the Schmidt et al. (2011; 2012) guidelines for PMIP3/CMIP5 forcing.

8. Lag between the hemispheres

The statement in the main text that we find no evidence for a consistent lag between NH and SH temperatures is supported by a correlation analysis. We correlate each NH reconstruction ensemble members with a randomly chosen SH reconstruction member which is temporally lagged by -200 to 200 years (Supplementary Figure 28). The maximum correlation ($r=0.30\pm0.19$) is identified at a lag of +23 years, being slightly higher than the correlation at lag 0 ($r=0.21\pm0.18$). However, this peak around lags of 10-30 years is dominated by the industrial period, where the SH temperature rise is ~ 25 years delayed compared to the NH. This peak disappears if the analysis is only calculated over the 1000-1900 period (red line in Supplementary Figure 28). The second peak around a lag of +110 years is not evident if the analysis is reduced to the 1250-1750 period (green line in Supplementary Figure 28), indicating that these peaks are not stable over time but influenced by individual periods.



Supplementary Figure 28 | Lagged inter-hemispheric temperature correlations. Correlation between reconstructed NH and SH temperatures lagging the SH data for -200 to 200 years. Black: Ensemble mean correlations using the full 1000-2000 period. Grey shading represents the 2σ ensemble range. Red (green): Same as black but using only the 1000-1900 (1250-1750) period.

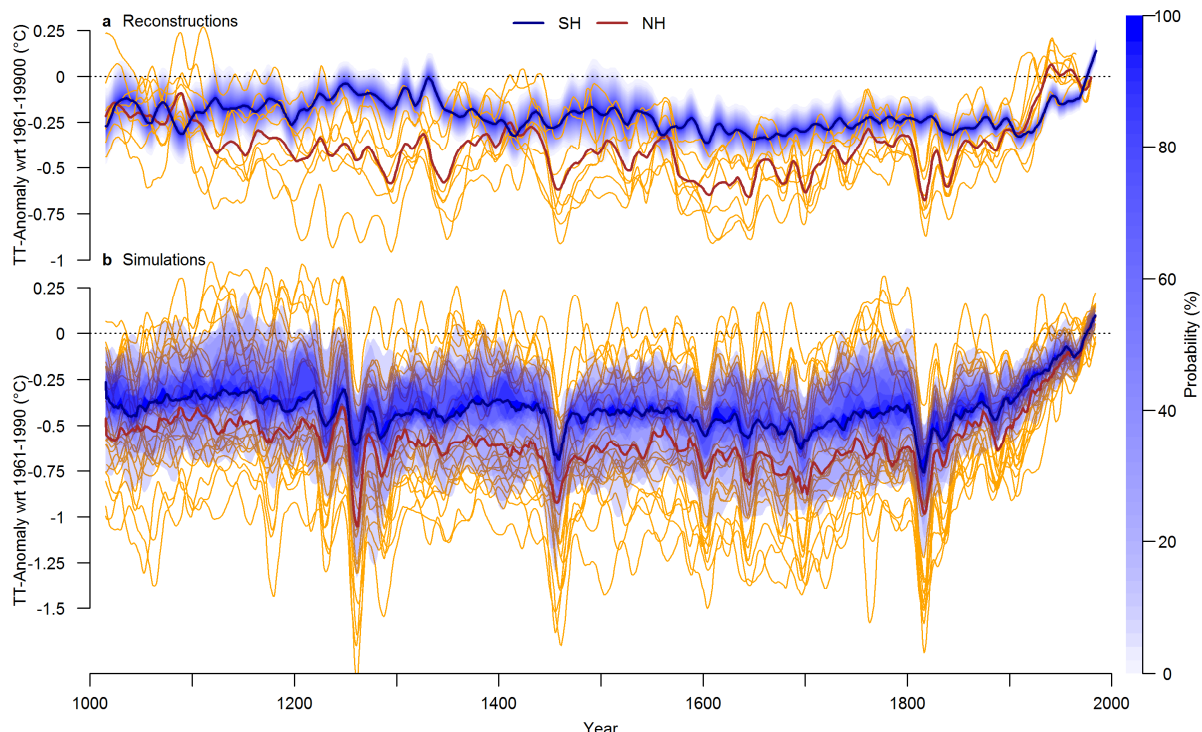
9. Alternative reference period and comparison with earlier SH and regional reconstructions

Supplementary Figure 29 shows an alternative illustration of Figure 2, using 1961-1990 as the reference period. It illustrates the reduced pre-industrial cooling in the SH seen in the reconstructions and simulations (compared to the stronger 20th century warming in the NH, expressed by the 1000-2000 baseline in Figure 2 in the main text).

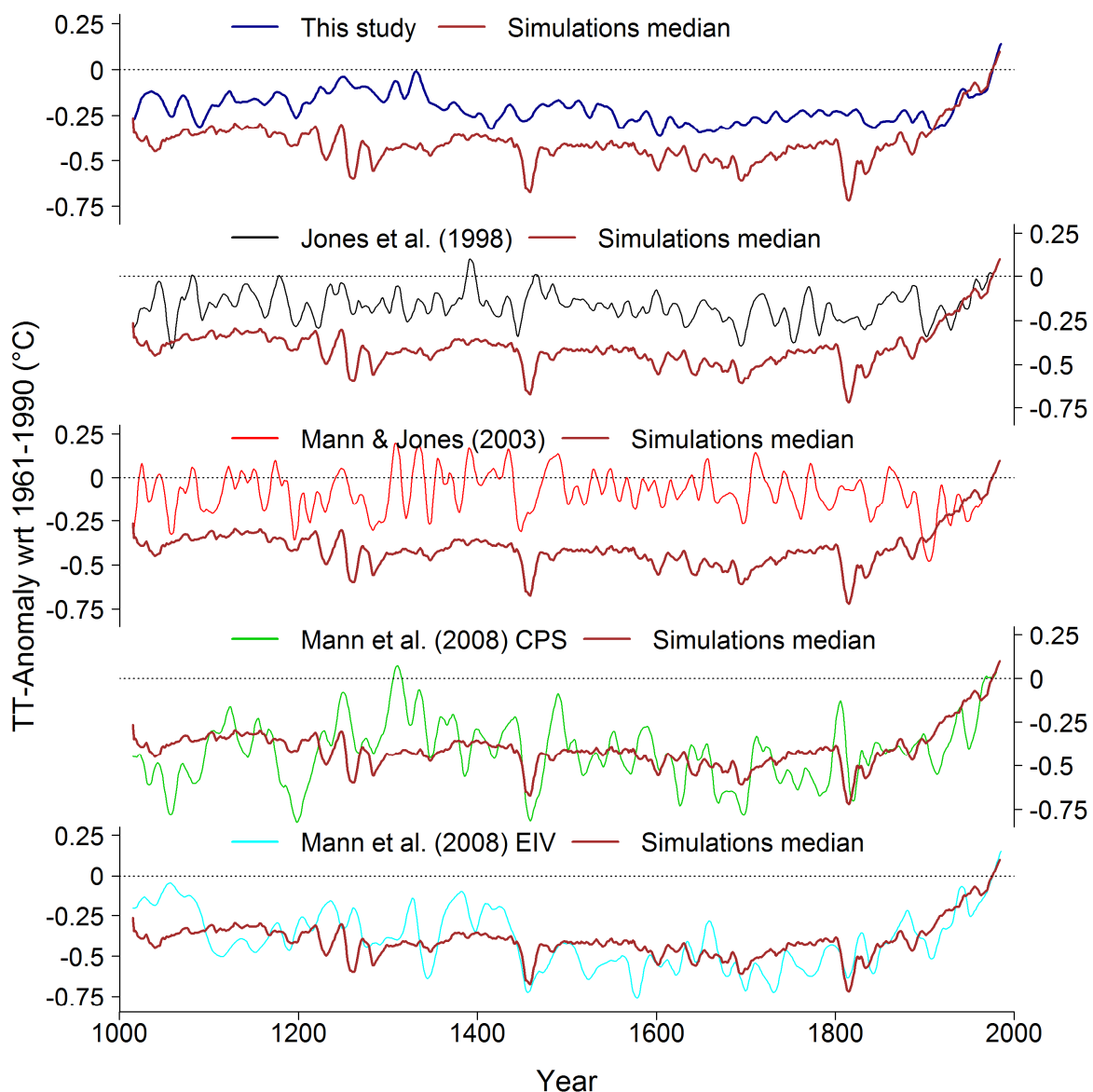
Supplementary Figure 30 compares our SH reconstruction with the model ensemble median and provides comparison with earlier SH temperature reconstructions (Jones *et al.*, 1998; Mann and Jones, 2003; Mann *et al.*, 2008). The number of proxy records available for these earlier reconstructions is seven (Jones *et al.*, 1998), five (Mann and Jones, 2003) and 165 (Mann *et al.*, 2008; 173 records if decadally resolved data are counted as well), respectively, compared to our network of 325 sites (Supplementary Table 1-4; to allow comparison, all tree-ring sites that were aggregated to composites herein need to be counted individually). The overlap of our proxy network with the Mann *et al.* (2008) records is small: Out of the nine long proxies extending to the year 1000, three have also been used by Mann et al. (2008): Mt. Read, Oroko and Quelccaya (Law Dome $\delta^{18}\text{O}$ is in the Mann *et al.* (2008) dataset as well, but they used an older record that covers only the period 1761-1970). For the records extending back to the year 1500 and beyond, 5 out of 18 records overlap (28%) plus one tree-ring composite with partial overlap.

Supplementary Figure 31 compares our SH reconstruction with regional reconstructions from Antarctica, Australasia and South America (PAGES 2013). Note that the regional reconstructions have different targets in terms of seasons and coverage (Antarctica and South America are land only, whereas Australasia is also a combined land-ocean reconstruction). This may explain the large differences in variance among the reconstructions. The SH reconstruction is strongly correlated with the Australasian ($r=0.46$, $p<<0.01$ over 1000-2000) and South American reconstructions ($r=0.33$, $p<<0.01$) and only weakly but significantly with

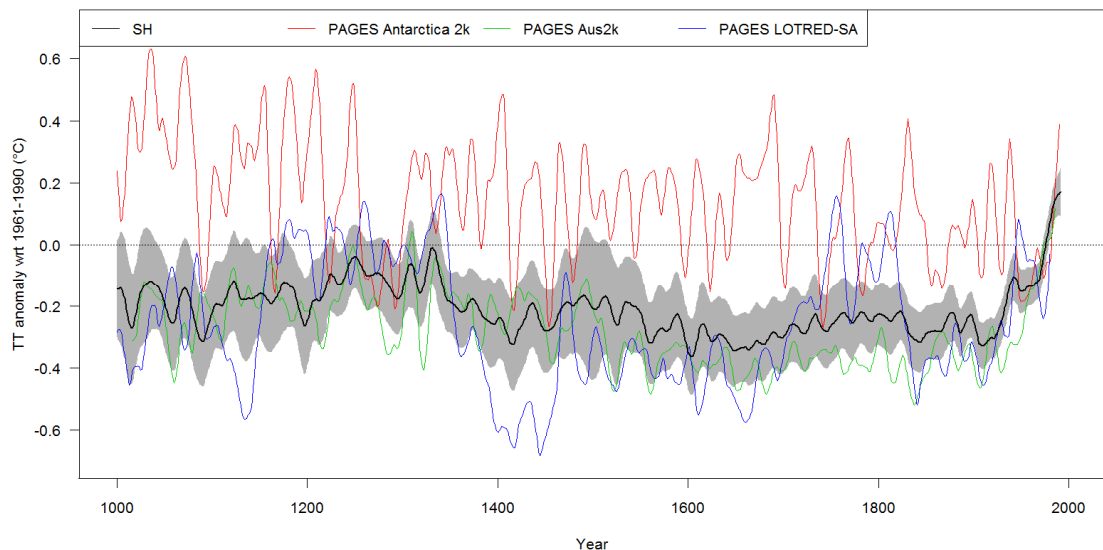
Antarctica ($r=0.15$, $p<<0.01$). These numbers are qualitatively comparable, albeit with lower values, to the corresponding instrumental data (Antarctica: $r=0.33$, $p=0.10$ over 1957-1990; Australasia: $r=0.63$, $p<<0.01$, over 1911-1990; South America: $r=0.42$, $p<0.01$ over 1911-1990). The SH relative warm period between ca. 1250-1350 and the cold periods in the 17th and 19th centuries are also inherent in the Australasian and South American reconstructions. These three datasets also show similar average pre-industrial temperatures relative to the 1961-1990 mean. The 14th-century cooling as well as the relatively warm 18th century are much stronger in the South American data. The Antarctic reconstruction shows a clearly different temperature history with reduced low-frequency variability. Given the small influence of Antarctica on the SH mean temperatures (Supplementary Figure 2), these differences are not surprising. Note that the regional reconstructions are not independent from our SH data due to considerable overlaps in the proxy data.



Supplementary Figure 29 | Temperature variability over the last millennium with alternative reference period. Same as Figure 2 in the main text but using a 1961-1990 reference period.



Supplementary Figure 30 | Direct comparison with simulations and earlier SH reconstructions. Top: Comparison of our SH reconstruction ensemble mean (blue) with the ensemble median of the simulations (brown) relative to the 1961-1990 baseline. Lower panels: Comparisons of earlier SH temperature reconstructions (Jones *et al.*, 1998; Mann and Jones, 2003; Mann *et al.*, 2008) with the model ensemble median.

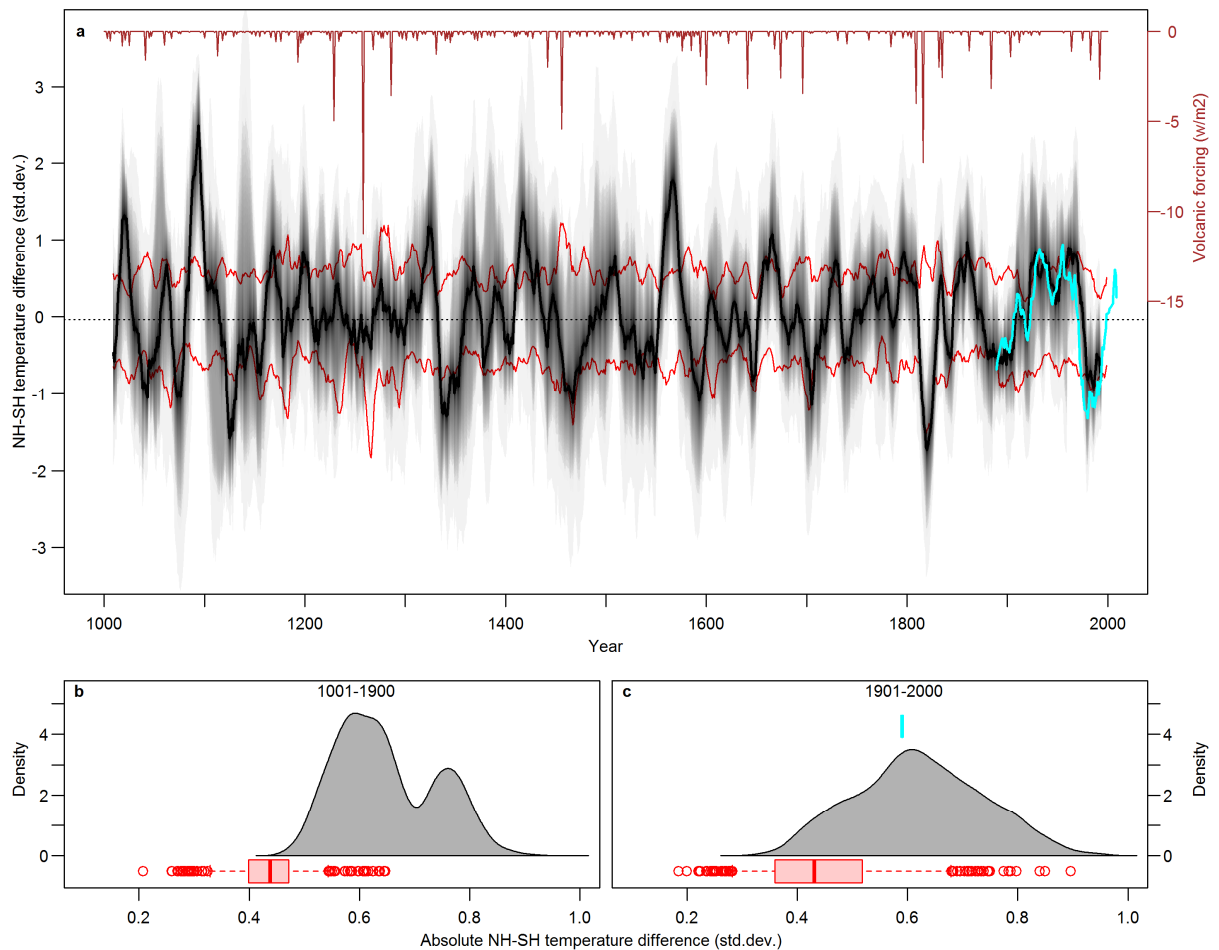


Supplementary Figure 31 | Comparison with regional SH reconstructions. Comparison of our SH reconstruction ensemble mean (black with shaded 2SE bounds), with regional reconstructions from Antarctica (red), Australasia (green) and South America (blue) published in a global synthesis of regional reconstructions (PAGES 2013).

10. Alternative illustrations of inter-hemispheric differences

10.1. Inter-model comparisons

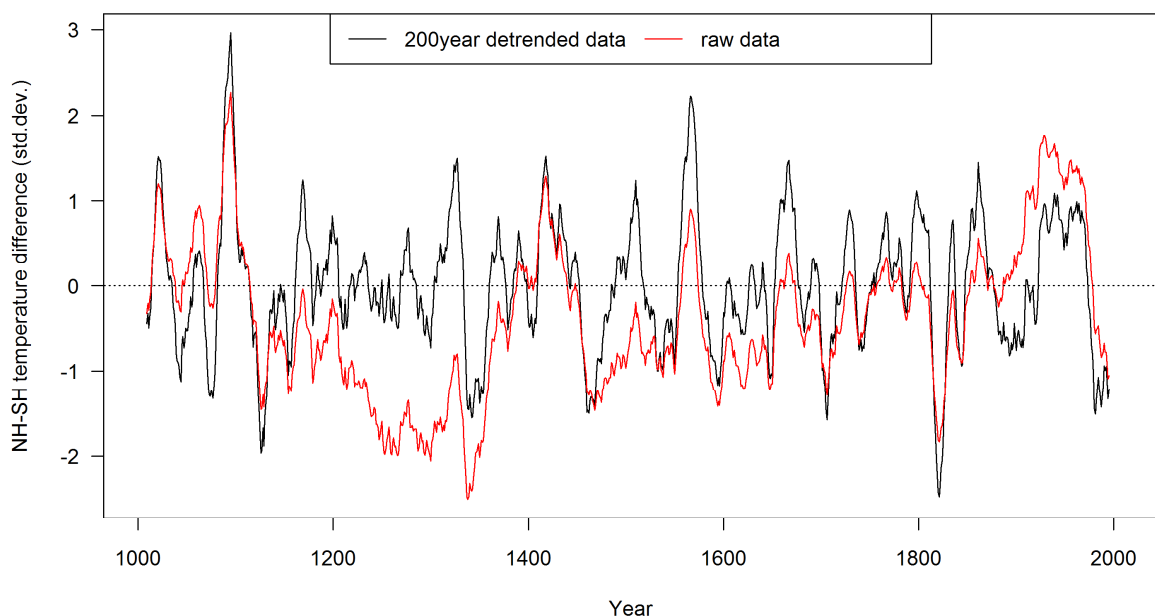
A potential caveat in our data-model comparisons is the fact that the reconstructions are noisy estimates of temperature variability with different and largely independent noise in the reconstructions of the two hemispheres. In contrast, within each model simulation there is no such noise between the hemispheres. Although the simulations do not reflect the true temperature history, the hemispheric extractions reflect a direct picture of temperatures in the model world. Inter-hemispheric differences are potentially inflated in the reconstructions relative to the simulations because of the noisy nature of the reconstructions. This may partially explain the larger values in reconstructed NH-SH differences shown in Figure 4 in the main text. To test this hypothesis, we repeat the analysis calculating the NH-SH differences not only within each simulation but also across the 24 different model simulations, to mimic the noisy behavior of the reconstructions. Results are shown in Supplementary Figure 32. Although the simulated NH-SH differences have increased with the inter-model calculations, they are still clearly smaller than in the reconstructions. We therefore argue that our conclusions are not biased by the different noise structure in reconstructions and simulations but reflect true differences between reconstructed and simulated temperatures.



Supplementary Figure 32 | NH-SH differences using inter-model calculations. Same as Figure 4 in the main text but after calculating the NH-SH differences across all model simulations. Boxes and whiskers of the boxplots in c and d represent the interquartile range and 5th/95th percentiles, respectively; circles represent results outside the 5th and 95th percentiles.

10.2. Raw vs. detrended data

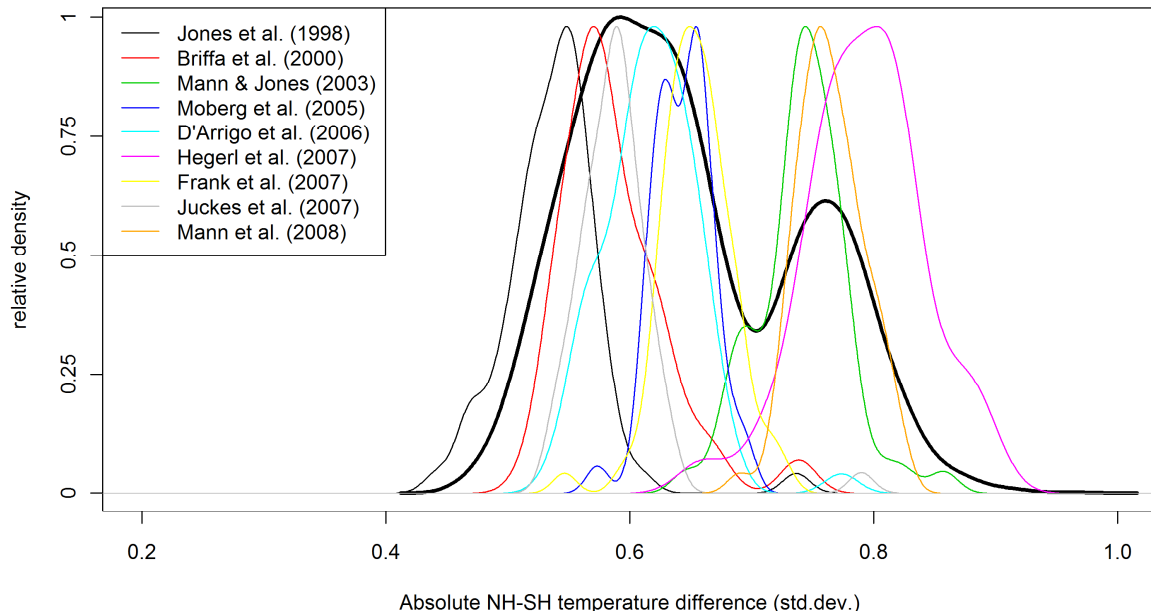
Given that we focus on decadal to multi-decadal timescales in our analyses, we show the NH-SH differences in Figure 4 after detrending reconstructed and simulated temperatures with a 200-year filter. An alternative illustration for the reconstructions using non-detrended data is provided in Supplementary Figure 33. The NH-SH differences based on raw data show larger absolute values before 1400 and in the 20th century (see also Figure 2a), but the general pattern remains similar and the differences do not affect our conclusions. We show the detrended data in the main text, as this illustration is less dependent on the reference period chosen.



Supplementary Figure 33 | Raw vs. detrended NH-SH differences. NH-SH temperature difference using 200-year detrended data (black; as in Figure 4a in the main text) and raw data (red).

10.3. Bimodal distribution in Figure 4b

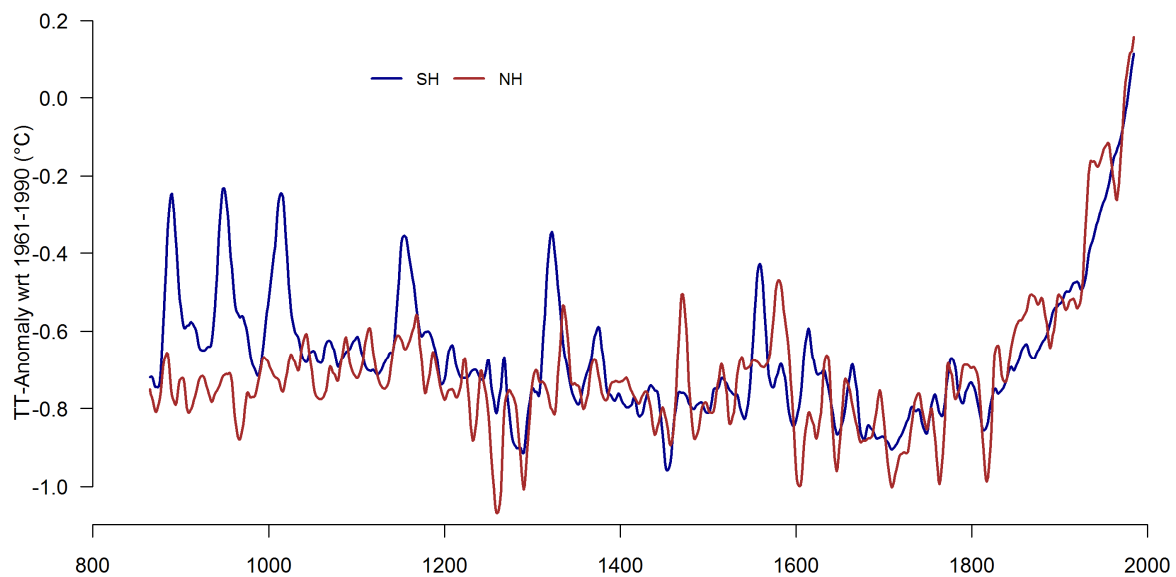
Figure 4b in the main text shows a bimodal distribution for the reconstruction data with two peaks around 0.6 and 0.75. This is caused by the fact that the NH reconstruction ensemble consists of nine sub-ensembles generated from different published reconstructions (see Methods). The distributions for these sub-ensembles are shown in Supplementary Figure 34. Three of these reconstructions (Mann and Jones, 2003; Hegerl et al., 2007; Mann et al., 2008) are only available at decadal resolution, leading to higher values in the NH-SH differences.



Supplementary Figure 34 | NH-SH differences for the NH sub-ensembles. Distribution of absolute NH-SH differences in the reconstructions during the pre-1900 period. Black solid: Full ensemble (as in Figure 4b in the main text); coloured lines: Individual sub-ensembles from the NH reconstruction.

10.4. Outlier in the model simulations (Figures 4b and 4c)

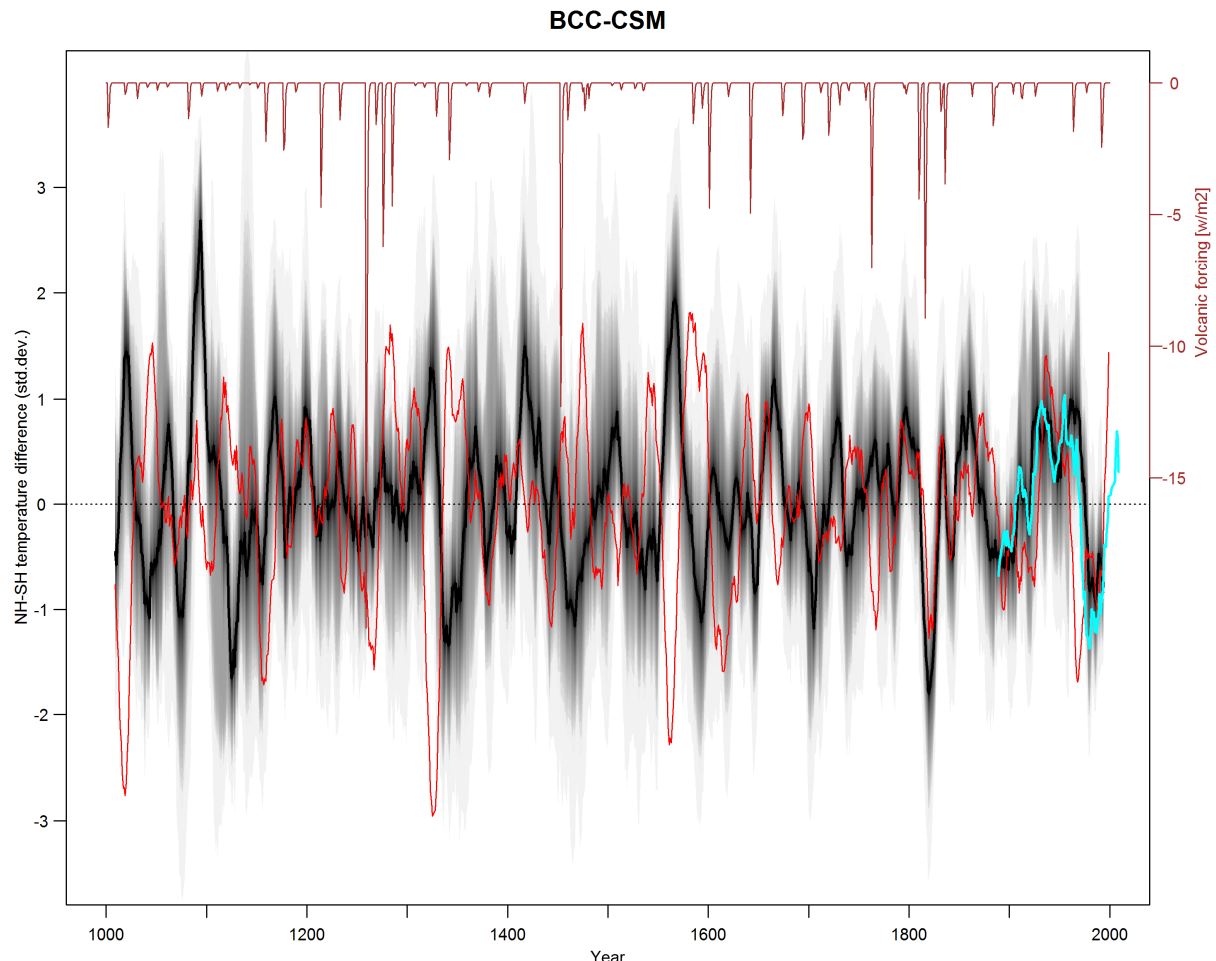
Figure 4b and 4c in the main text show an outlier in the model simulations, which has similar magnitudes in the NH-SH differences as the reconstructions. This outlier represents the model BCC-CSM. The SH temperatures of this model show repeated warming peaks that last about three decades in both the last millennium run (Supplementary Figure 35) as well as the pre-industrial control simulation (not shown). These warm peaks are mostly not reflected in the NH, which leads to very large NH-SH differences during these periods (see Supplementary Figure 36), explaining the larger values compared to the other simulations. The positive excursions in the SH are mostly limited to a very strong warming in the Southern Ocean off Antarctica in the Weddell Sea area (not shown). Given the temporal and spatial nature of these anomalies, we regard these as model-specific features that are unrealistically simulated by the BCC-CSM model.



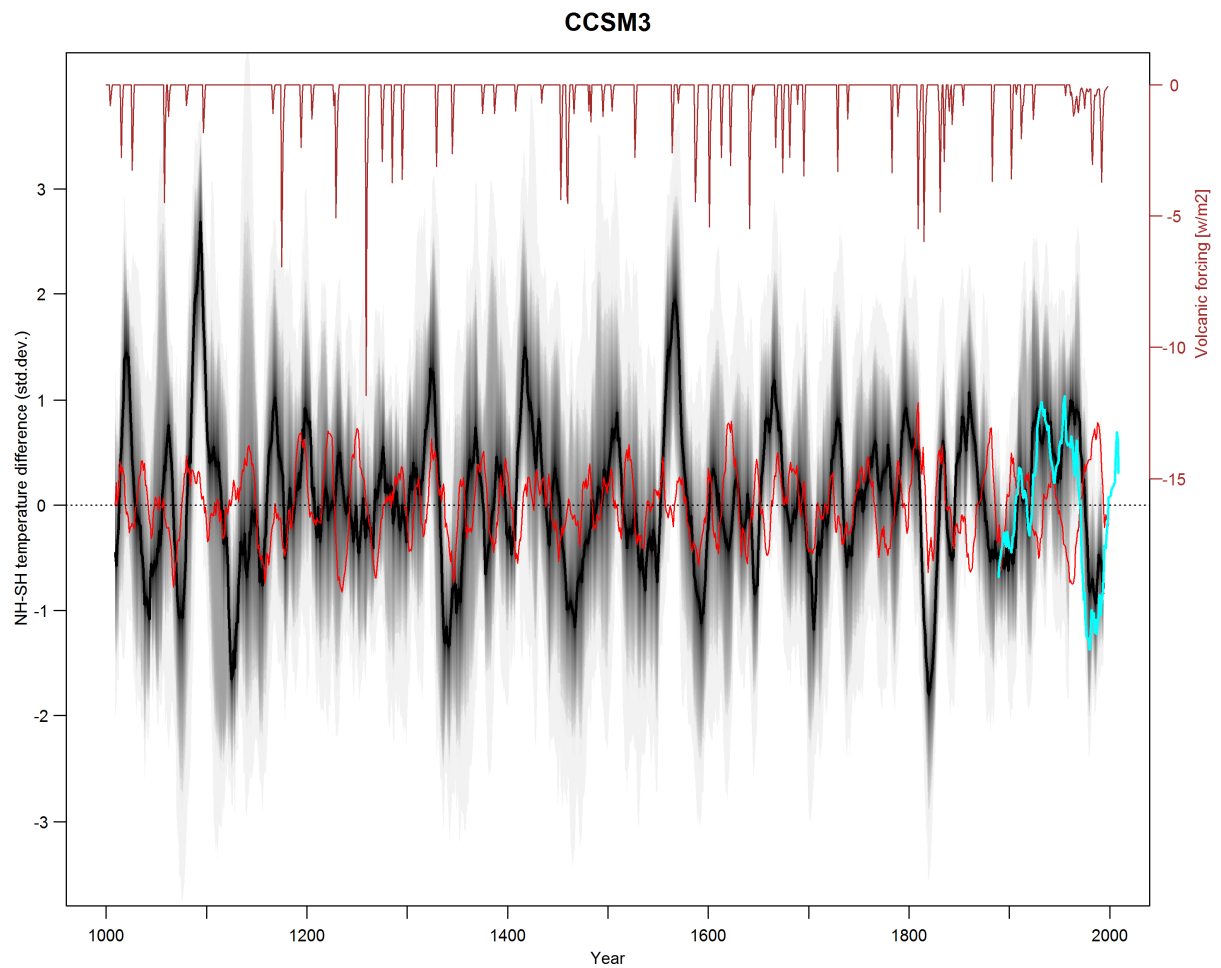
Supplementary Figure 35 | Hemispheric temeperatures in the BCC-CSM model. 30-year filtered SH (blue) and NH (red) temperatures over the period 850-2000 for the BCC-CSM model.

11.NH-SH differences in the individual model simulations

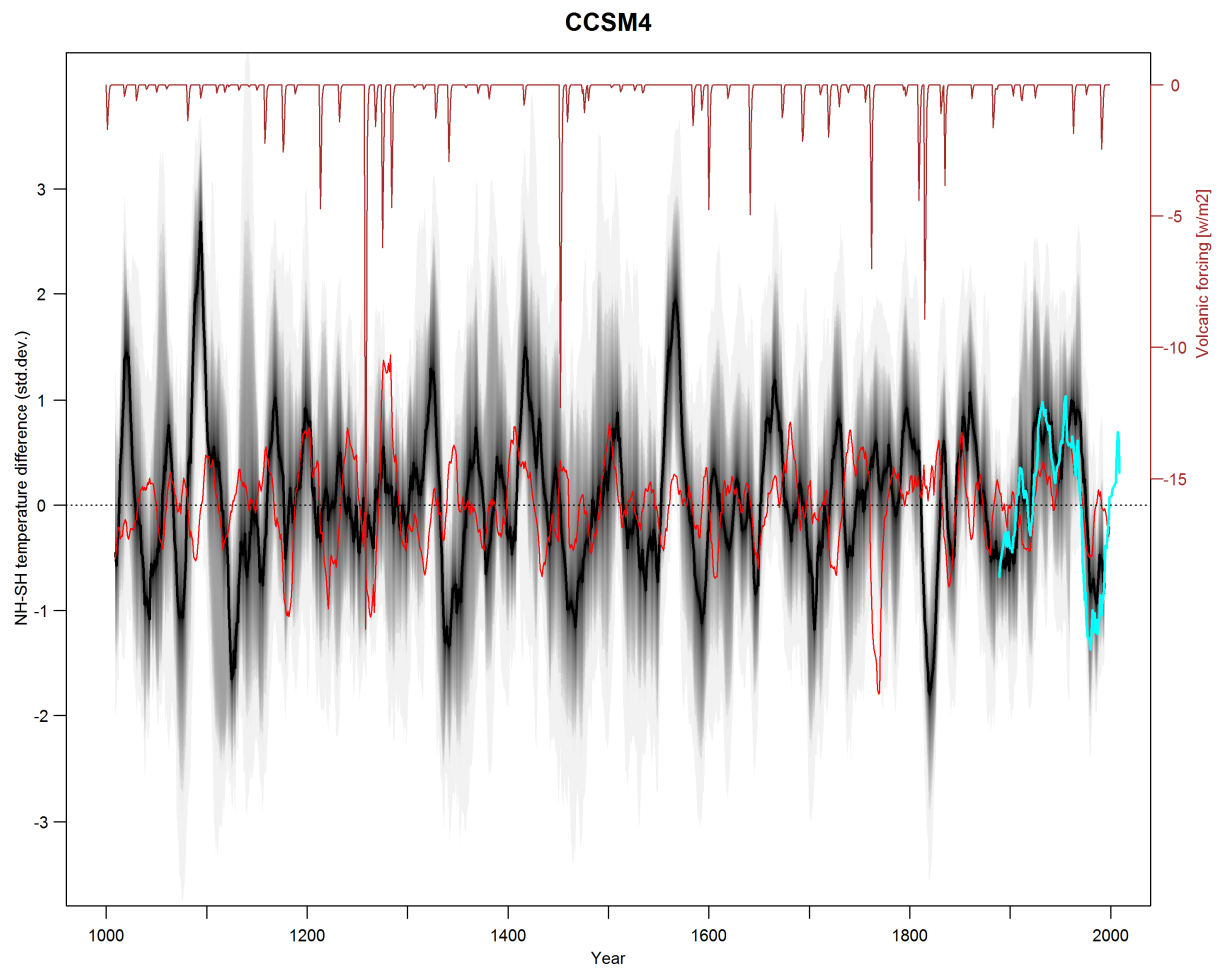
Supplementary Figure 39 - Supplementary Figure 59 show the NH-SH differences over the last millennium for the individual climate model simulations and compare them to the reconstructions (see also Figure 4 in the main text).



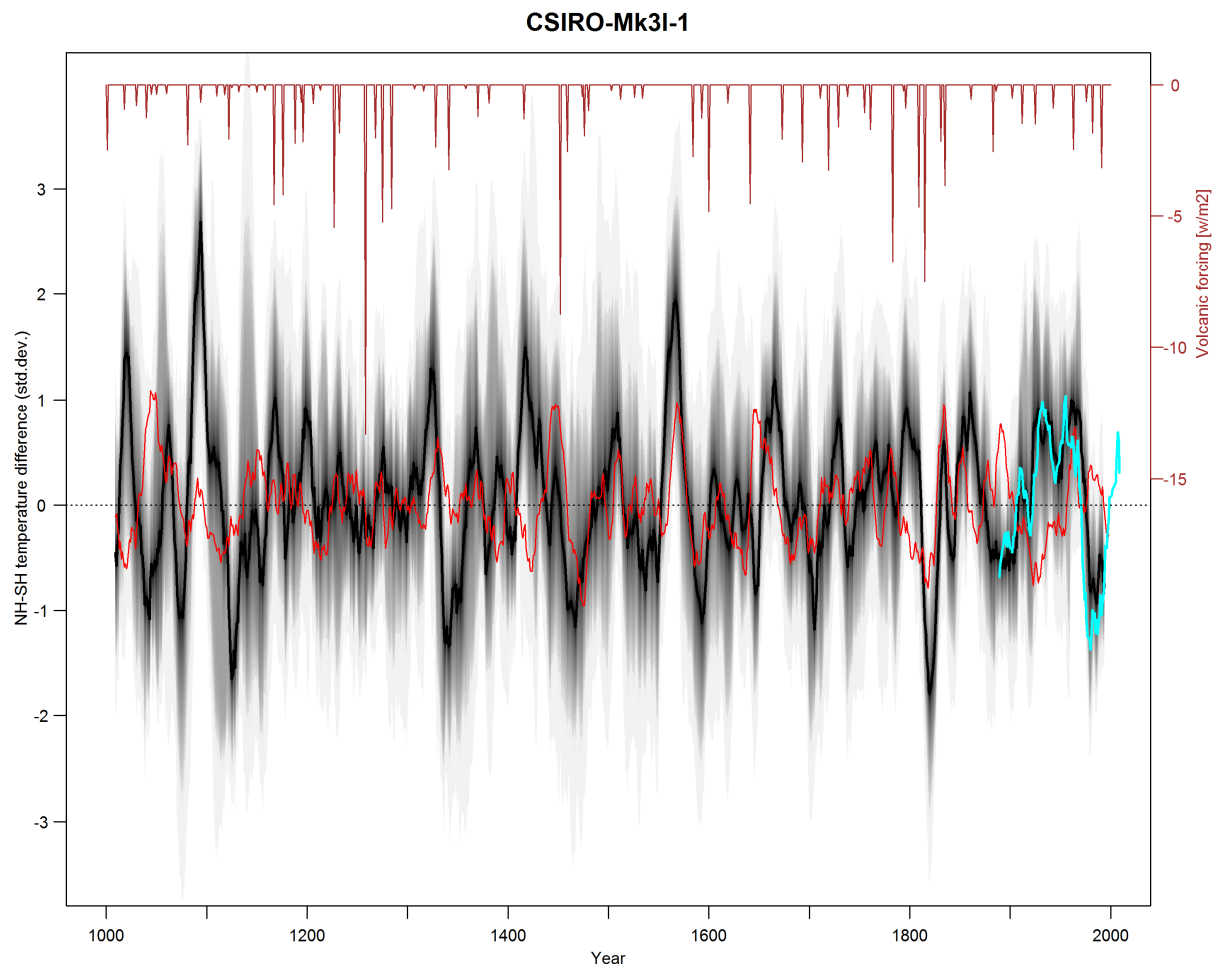
Supplementary Figure 36 | NH-SH differences for individual model simulations: BCC-CSM. Same as Figure 4a in the main text but showing the NH-SH difference for the climate model simulation BCC-CSM in red, instead of the 10th and 90th percentiles of all model simulations. Volcanic dataset (brown) is the forcing time series used for this simulation (Gao *et al.*, 2008). Instrumental data are cyan (Hansen *et al.*, 2010).



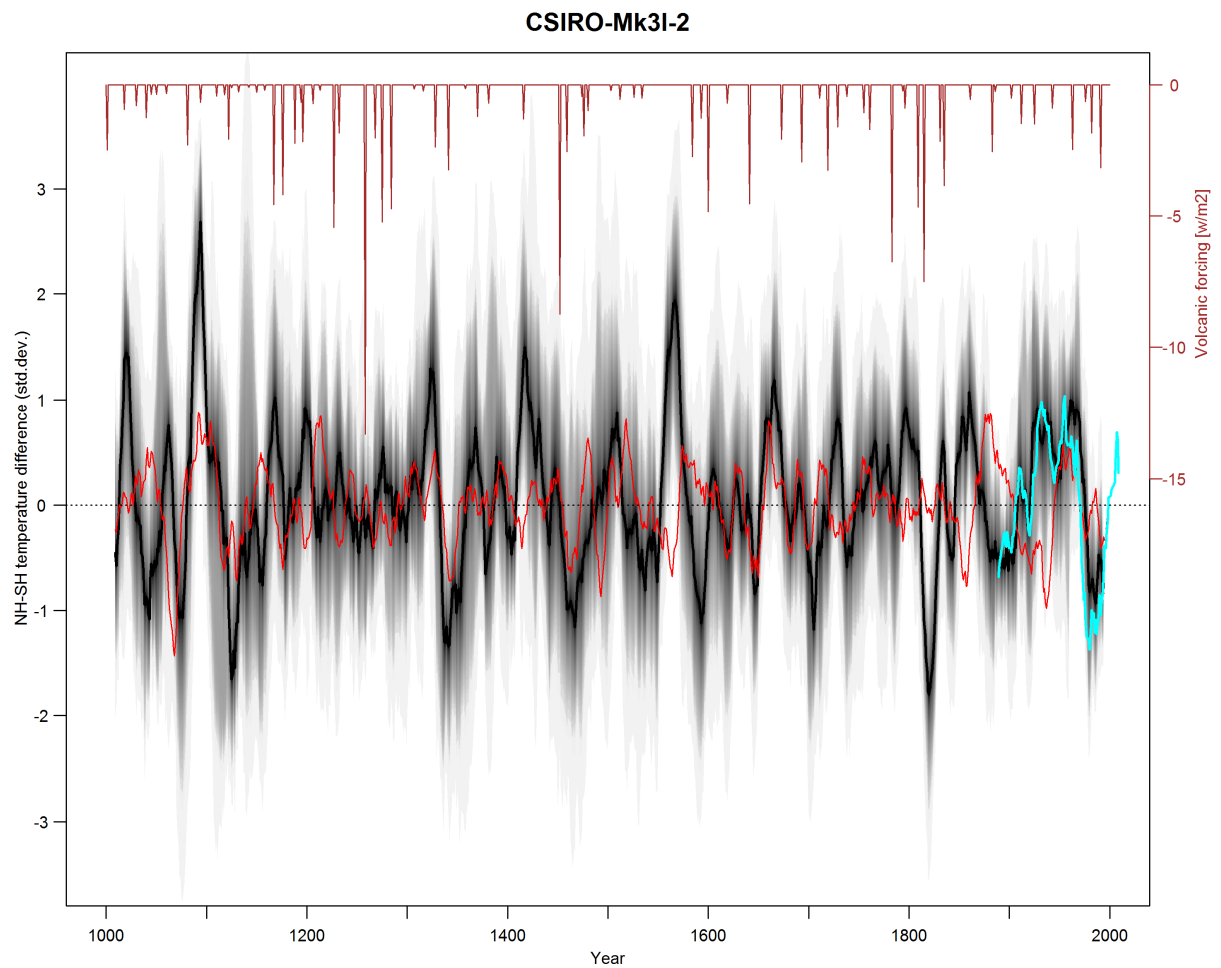
Supplementary Figure 37 | NH-SH differences CCSM3. Same as Supplementary Figure 36 but for the CCSM3 simulation and the corresponding volcanic forcing dataset (Crowley, 2000).



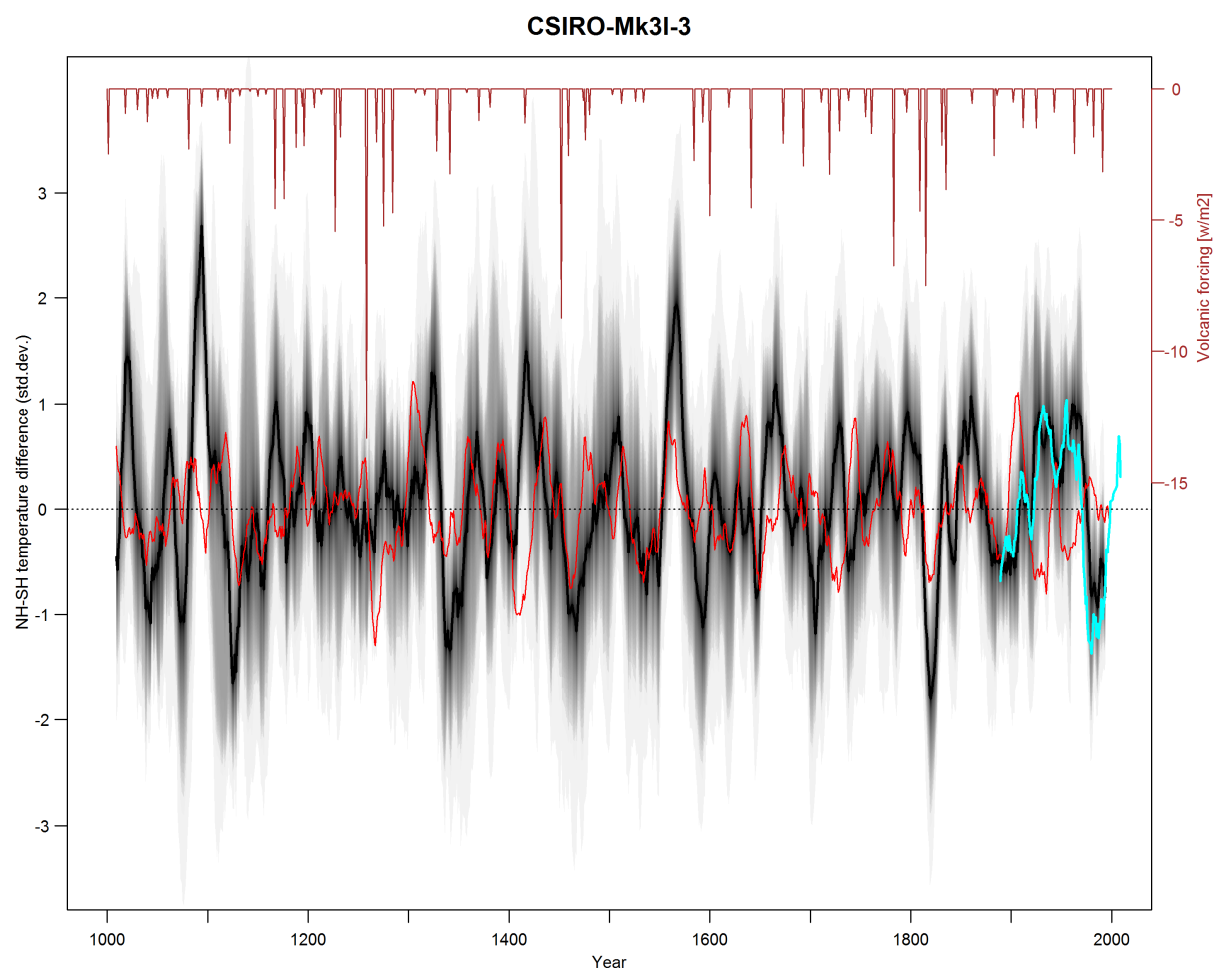
Supplementary Figure 38 | NH-SH differences CCSM4. Same as Supplementary Figure 36 but for the CCSM4 simulation and the corresponding volcanic forcing dataset (Gao *et al.*, 2008).



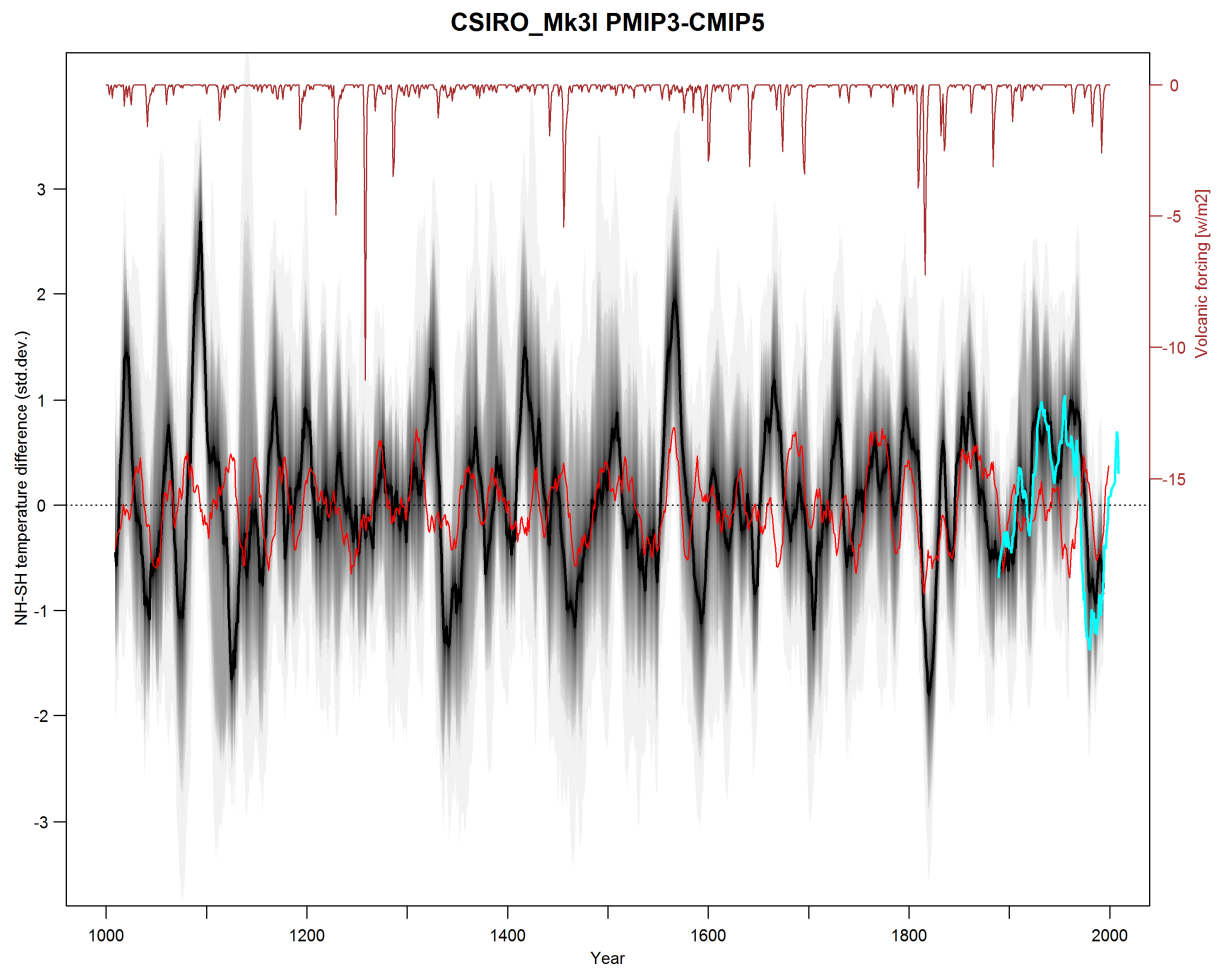
Supplementary Figure 39 | NH-SH differences for individual model simulations: CSIRO Mk3L-1. Same as Supplementary Figure 36 but for the CSIRO Mk3L, ensemble member 1 and the corresponding volcanic forcing dataset (Gao *et al.*, 2008).



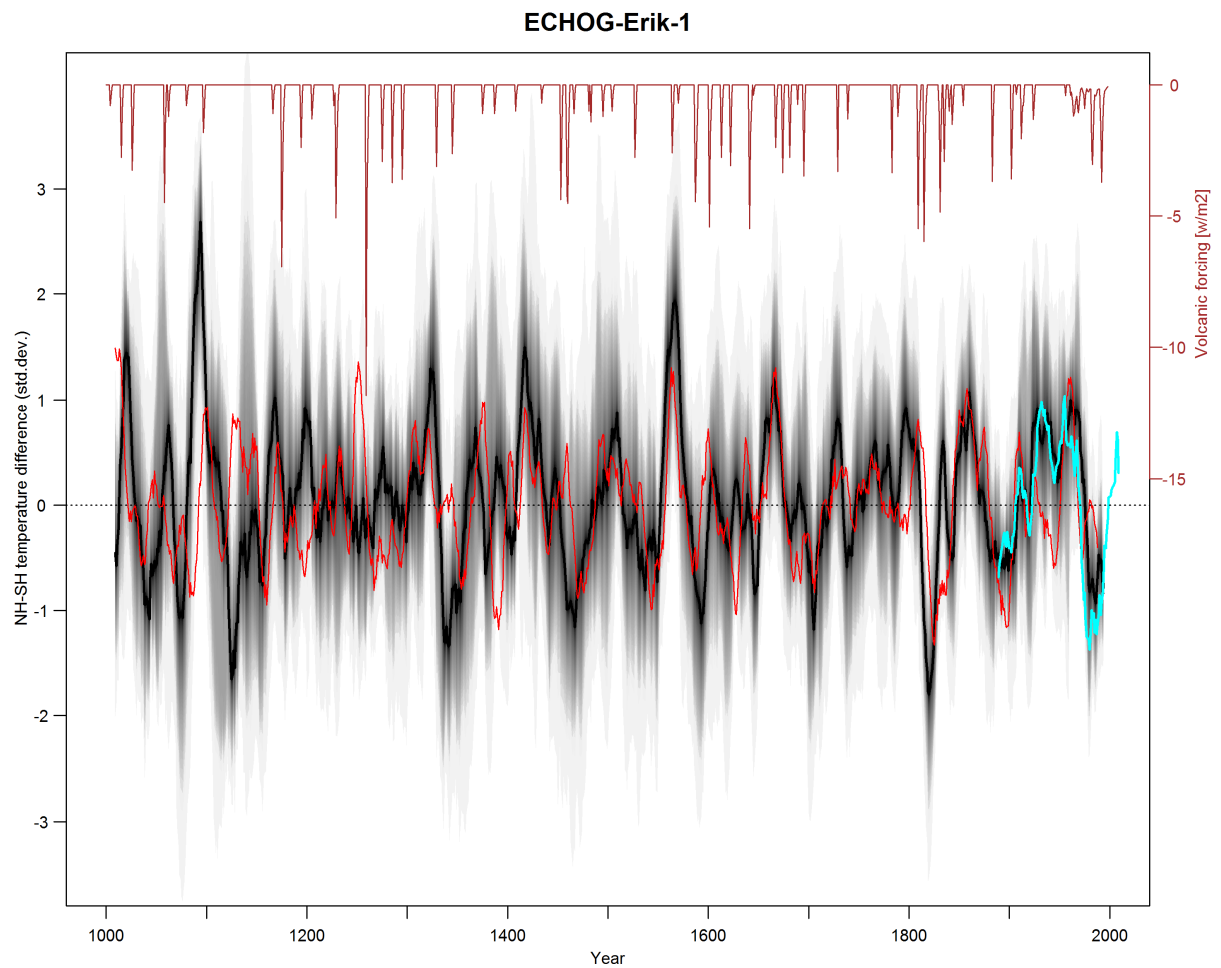
Supplementary Figure 40 | NH-SH differences CSIRO Mk3L-2. Same as Supplementary Figure 36 but for the CSIRO Mk3L simulation, ensemble member 2.



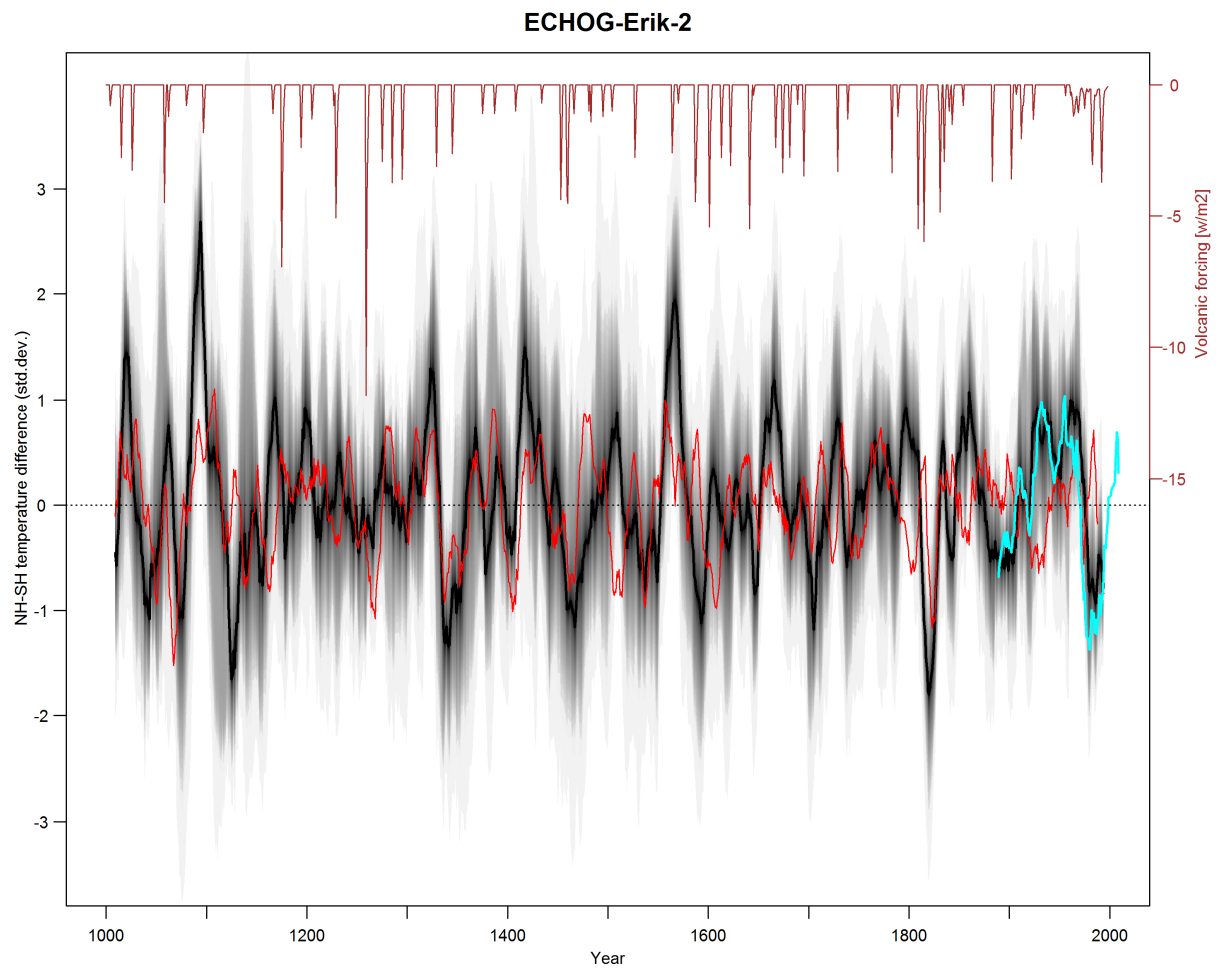
Supplementary Figure 41 | NH-SH differences CSIRO Mk3L-3. Same as Supplementary Figure 36 but for the CSIRO Mk3L simulation, ensemble member 3.



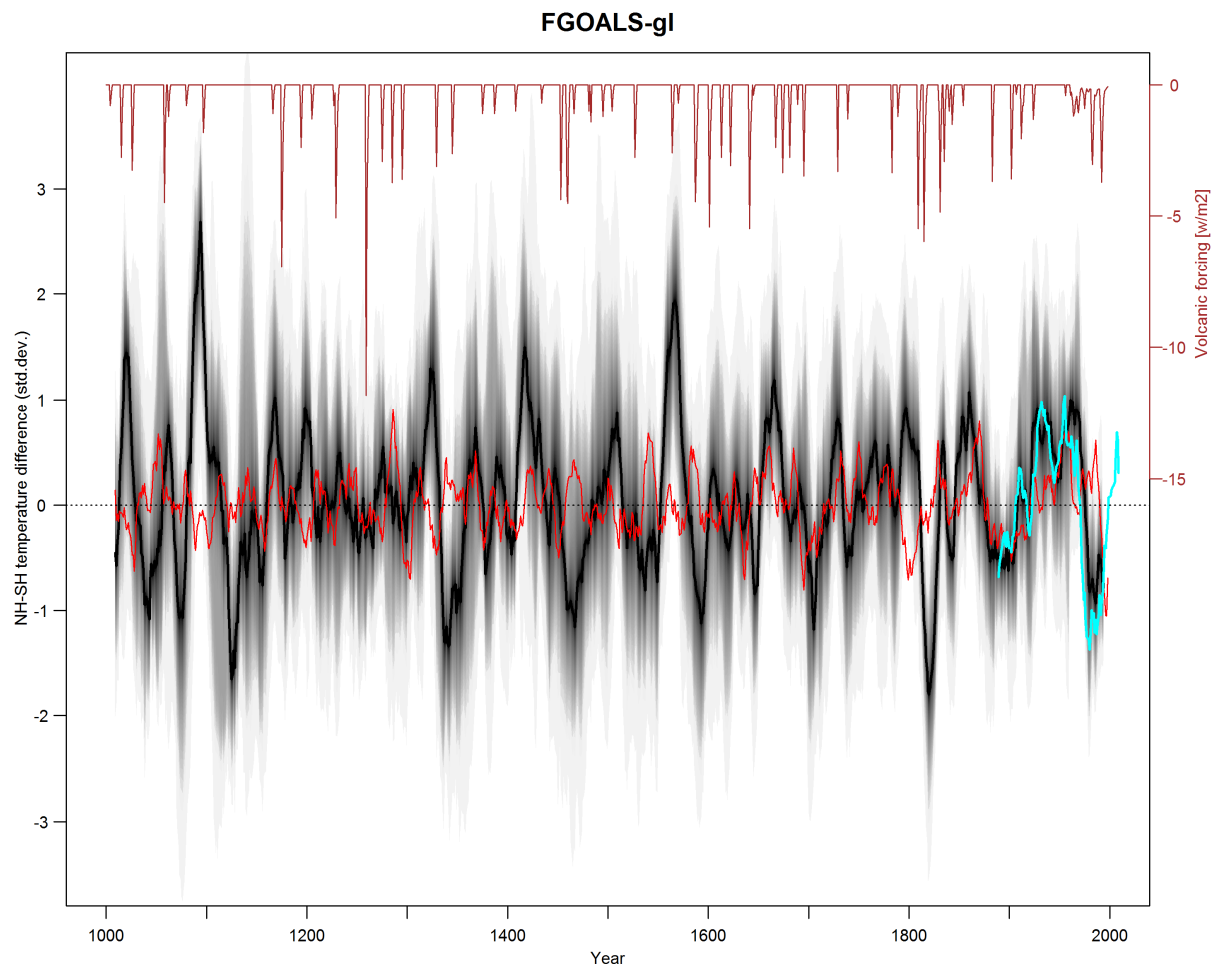
Supplementary Figure 42 | NH-SH differences CSIRO Mk3L PMIP3/CMIP5. Same as Supplementary Figure 36 but for the CSIRO Mk3L PMIP3/CMIP5 simulation and the corresponding volcanic forcing dataset (Crowley and Unterman, 2013).



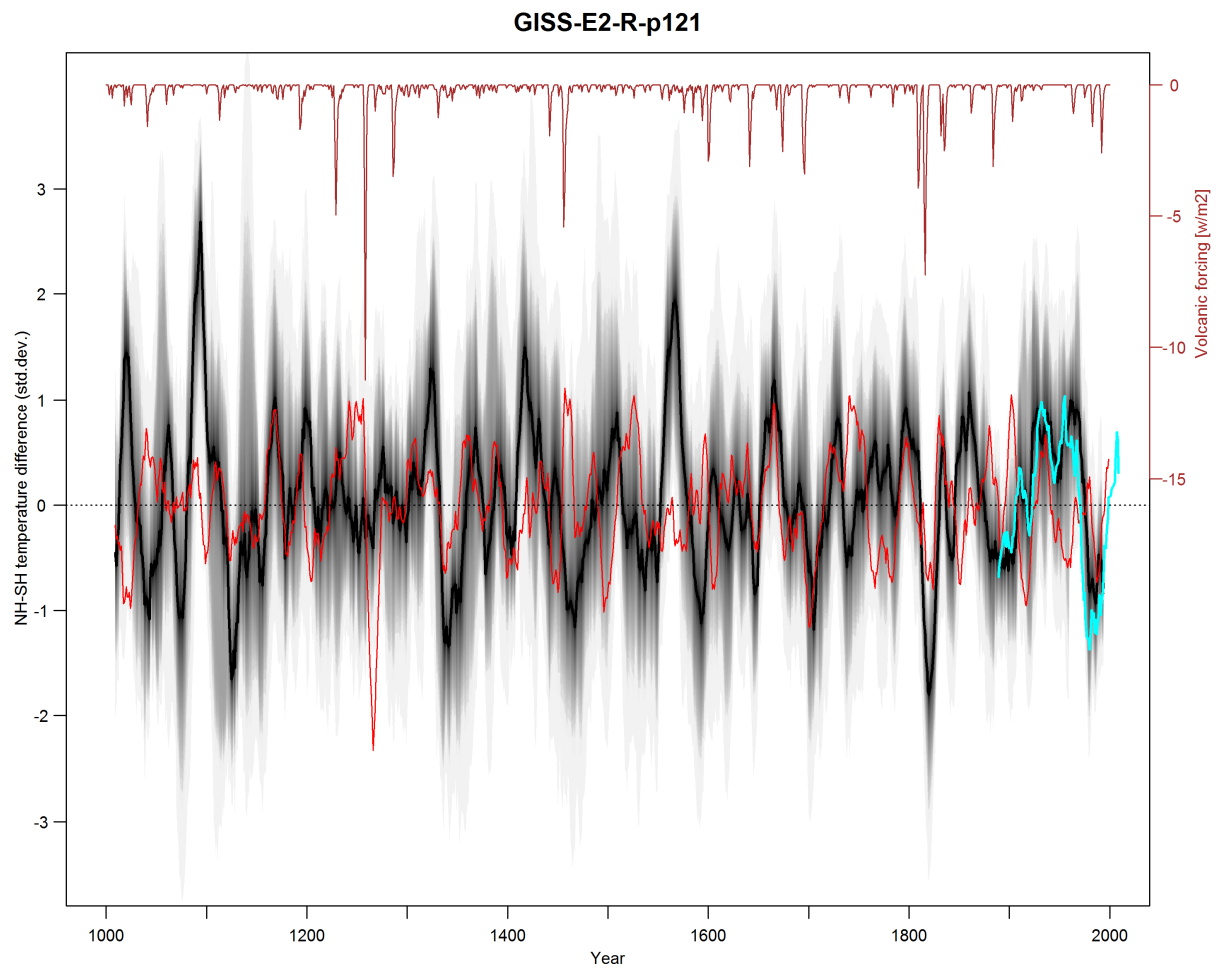
Supplementary Figure 43 | NH-SH differences ECHO-G Erik 1. Same as Supplementary Figure 36 but for the ECHO-G Erik 1 simulation and the corresponding volcanic forcing dataset (Crowley, 2000).



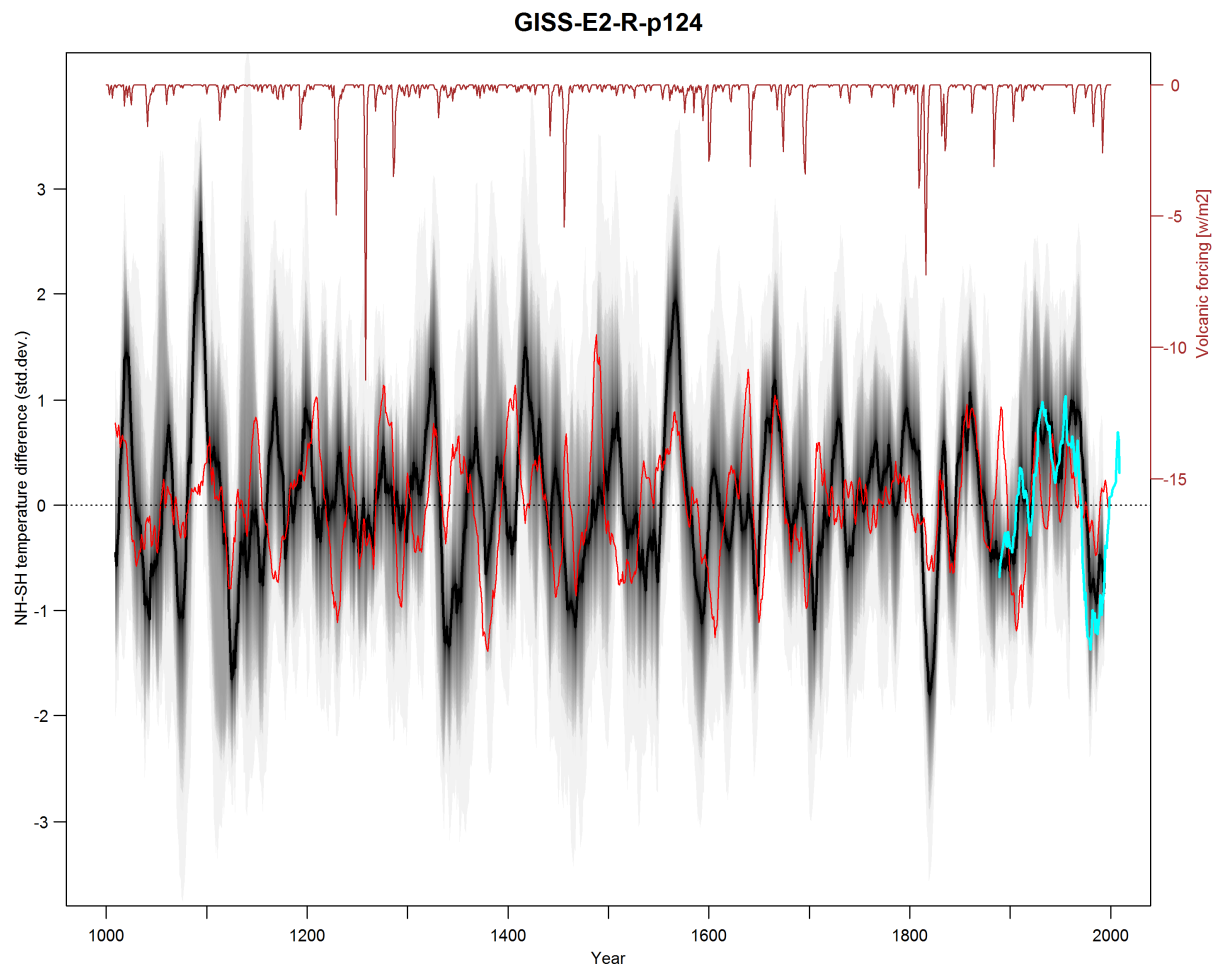
Supplementary Figure 44 | NH-SH differences ECHO-G Erik 2. Same as Supplementary Figure 36 but for the ECHO-G Erik 2 simulation and the corresponding volcanic forcing dataset (Crowley, 2000).



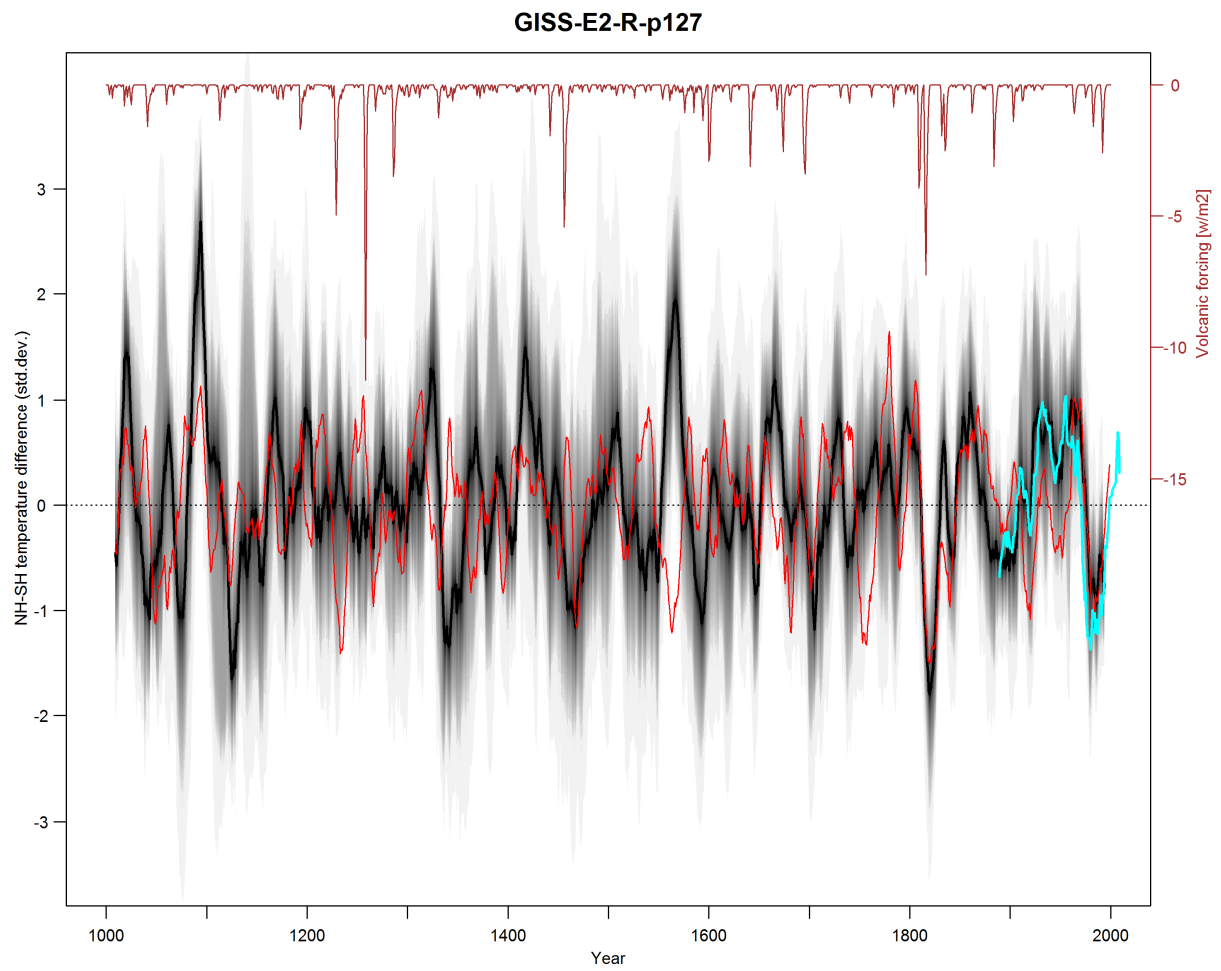
Supplementary Figure 45 | NH-SH differences FGOALS-g1. Same as Supplementary Figure 36 but for the FGOALS-g1 simulation and the corresponding volcanic forcing dataset (Crowley, 2000).



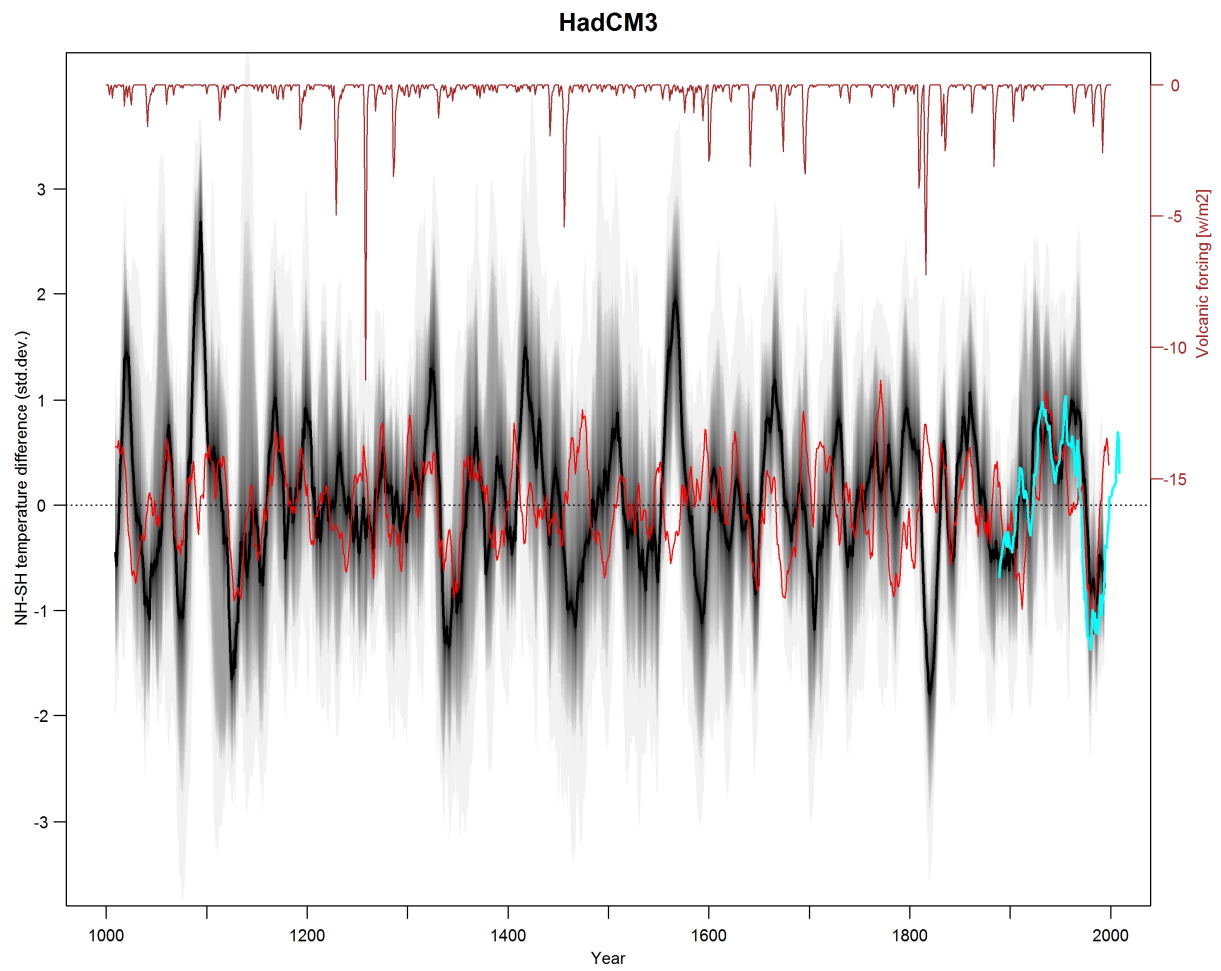
Supplementary Figure 46 | NH-SH differences GISS-E2-R p121. Same as Supplementary Figure 36 but for the GISS-E2-R p121 simulation and the corresponding volcanic forcing dataset (Crowley and Unterman, 2013).



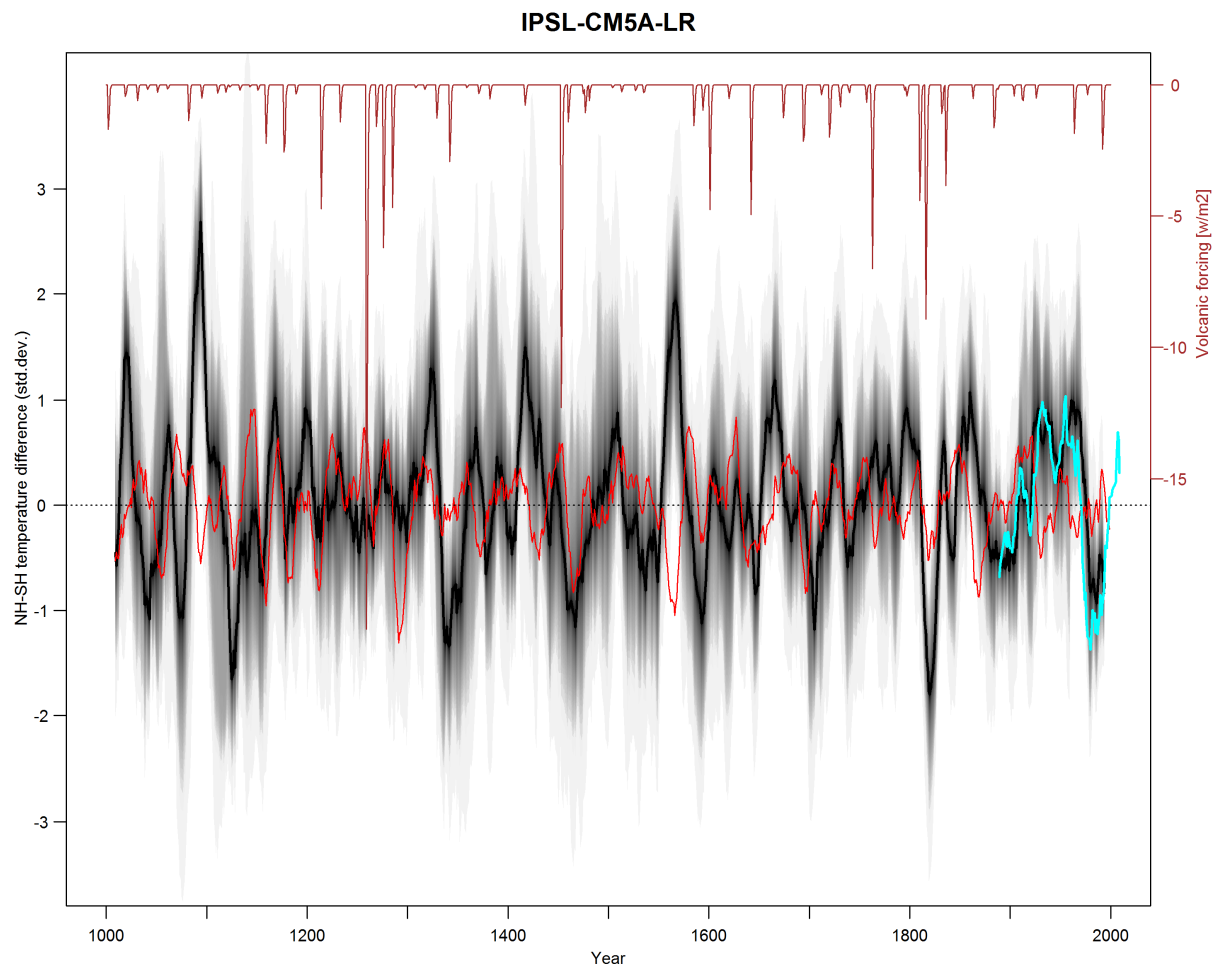
Supplementary Figure 47 | NH-SH differences GISS-E2-R p124. Same Supplementary Figure 36 but for the GISS-E2-R p124 simulation and the corresponding volcanic forcing dataset (Crowley and Unterman, 2013).



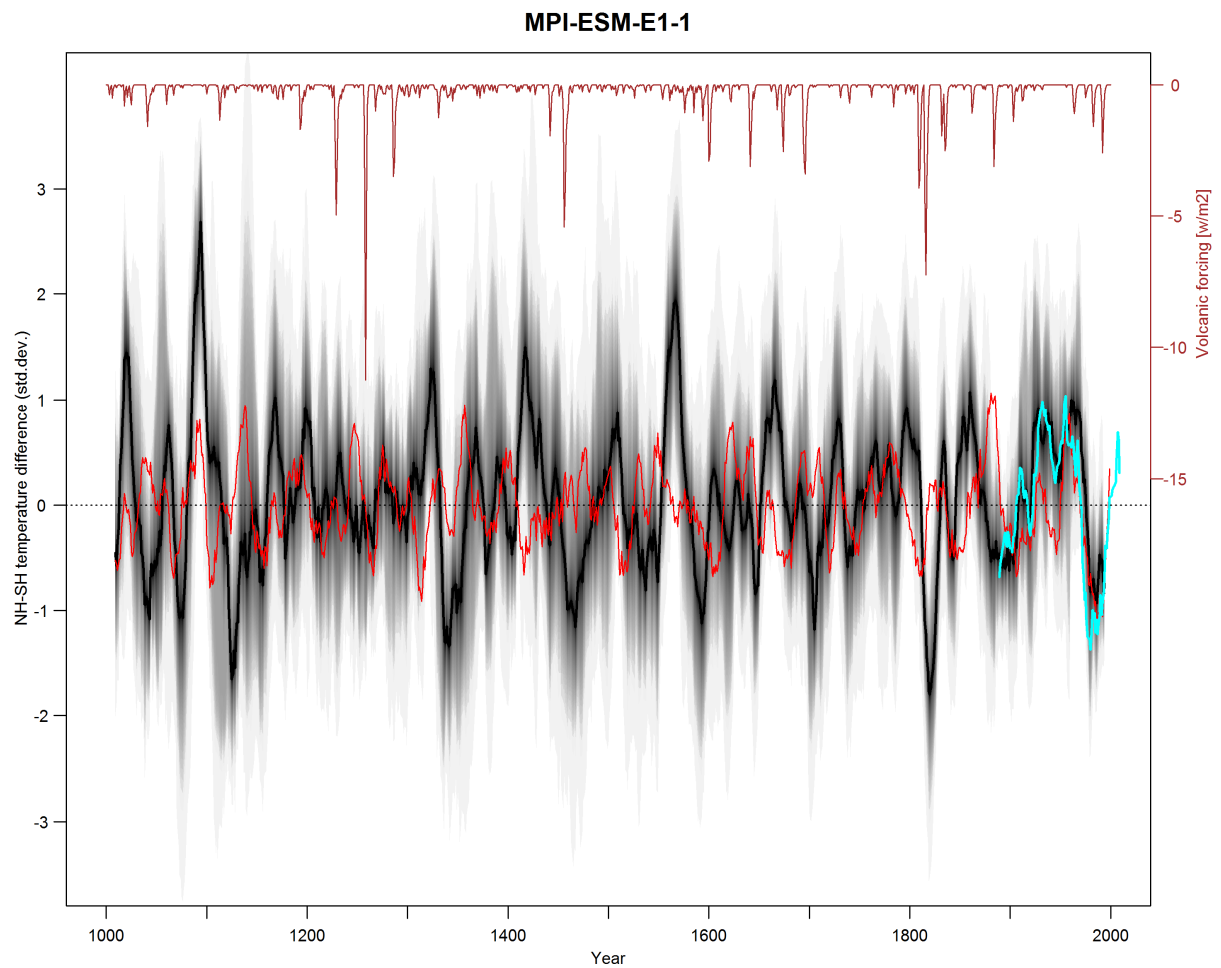
Supplementary Figure 48 | NH-SH differences GISS-E2-R p127. Same as Supplementary Figure 36 but for the GISS-E2-R p127 simulation and the corresponding volcanic forcing dataset (Crowley and Unterman, 2013).



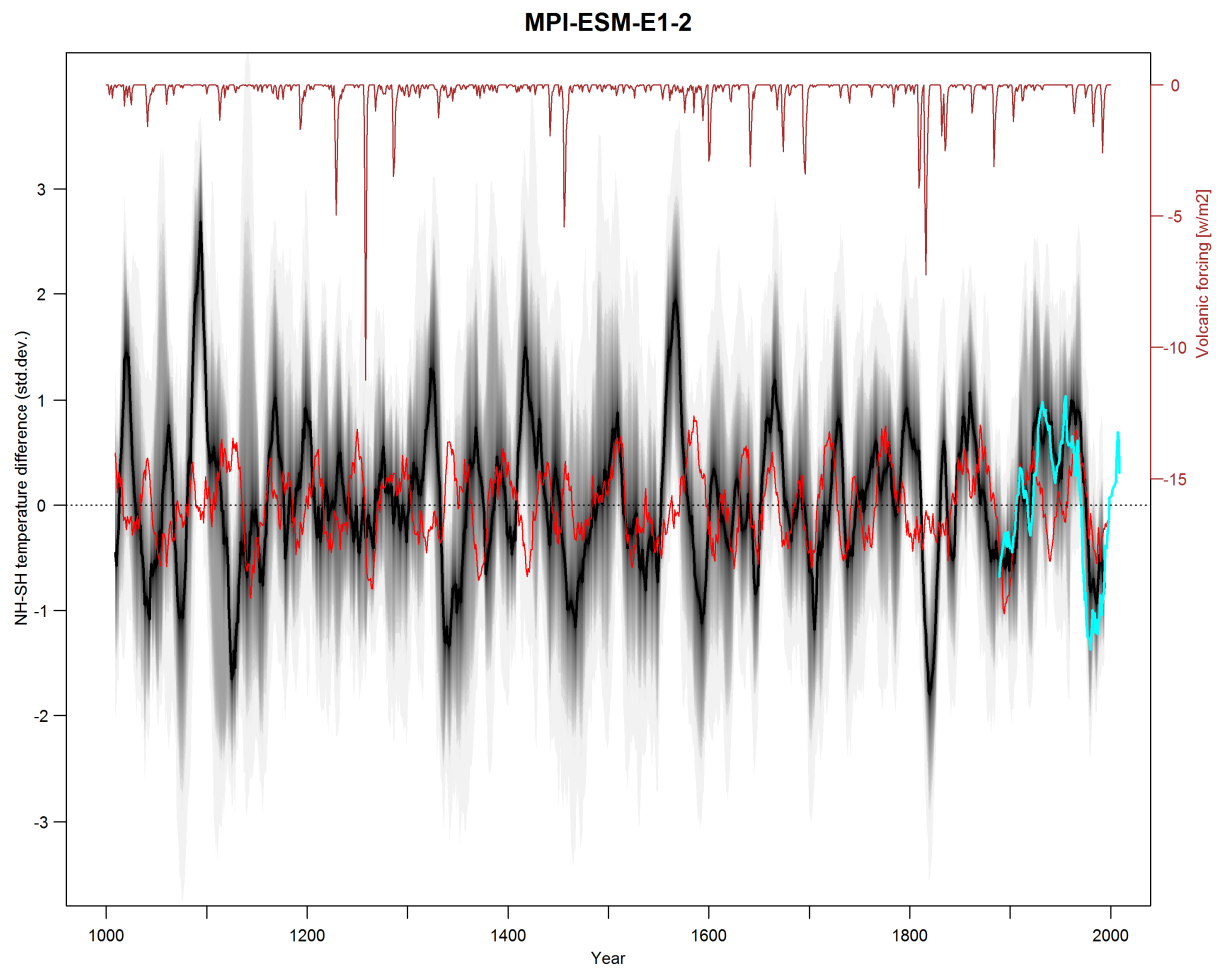
Supplementary Figure 49 | NH-SH differences HadCM3. Same as Supplementary Figure 36 but for HadCM3 simulation and the corresponding volcanic forcing dataset (Crowley and Unterman, 2013).



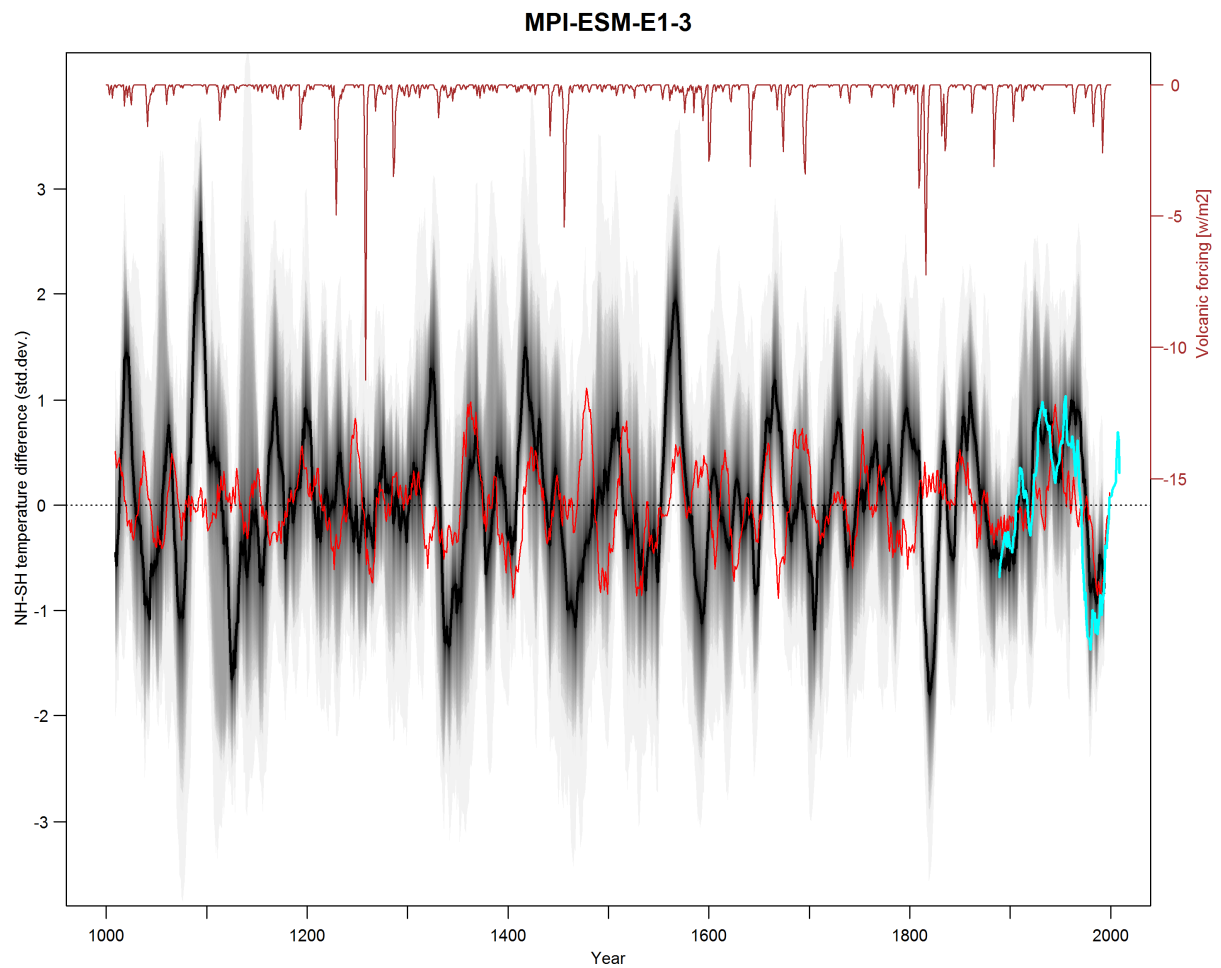
Supplementary Figure 50 | NH-SH differences IPSL-CM5A-LR. Same as Supplementary Figure 36 but for the IPSL-CM5A-LR simulation and the corresponding volcanic forcing dataset (Gao *et al.*, 2008).



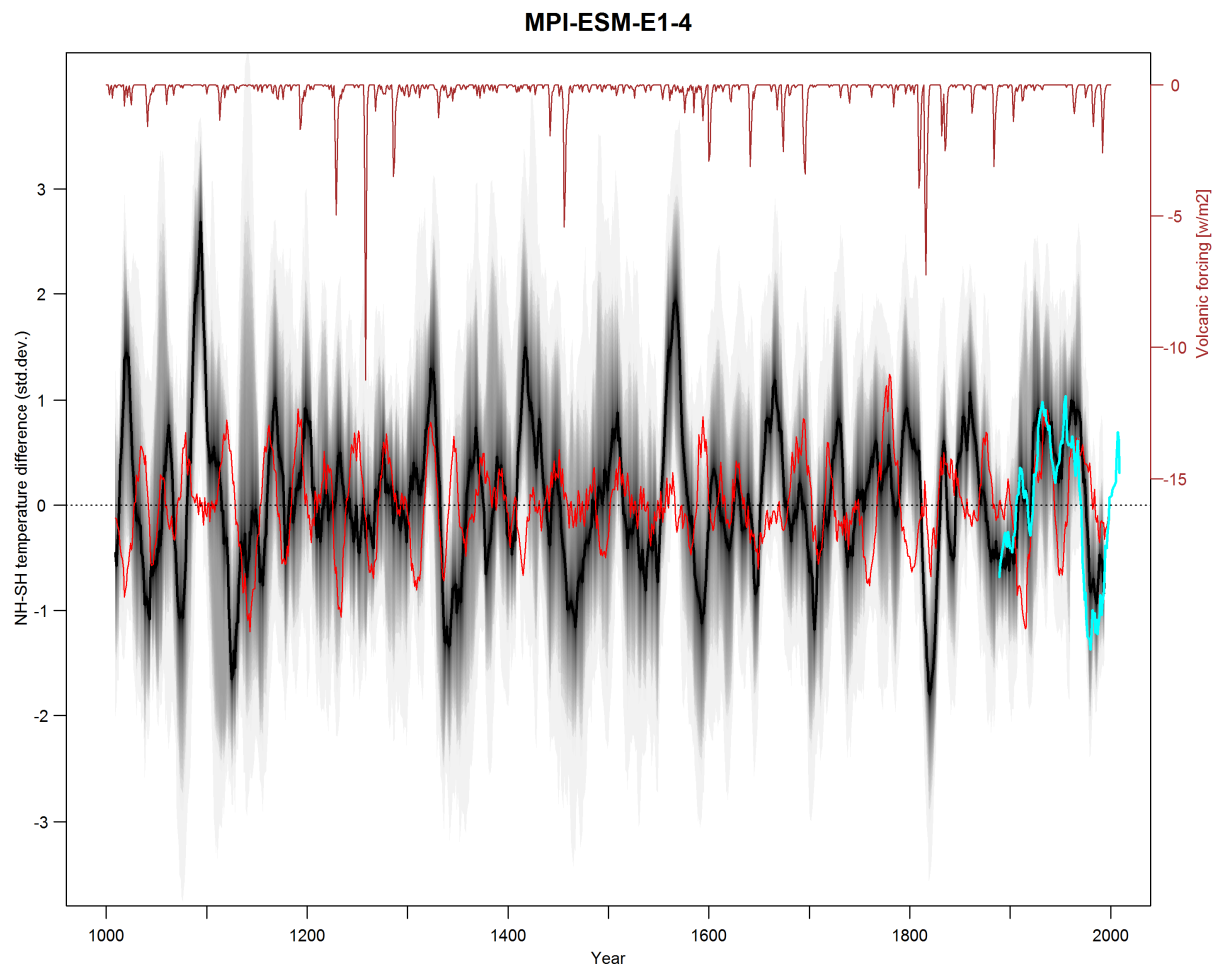
Supplementary Figure 51 | NH-SH differences MPI-ESM E1-1. Same as Supplementary Figure 36 but for the MPI ESM E1 simulation, ensemble member 1 and the corresponding volcanic forcing dataset (Crowley and Unterman, 2013).



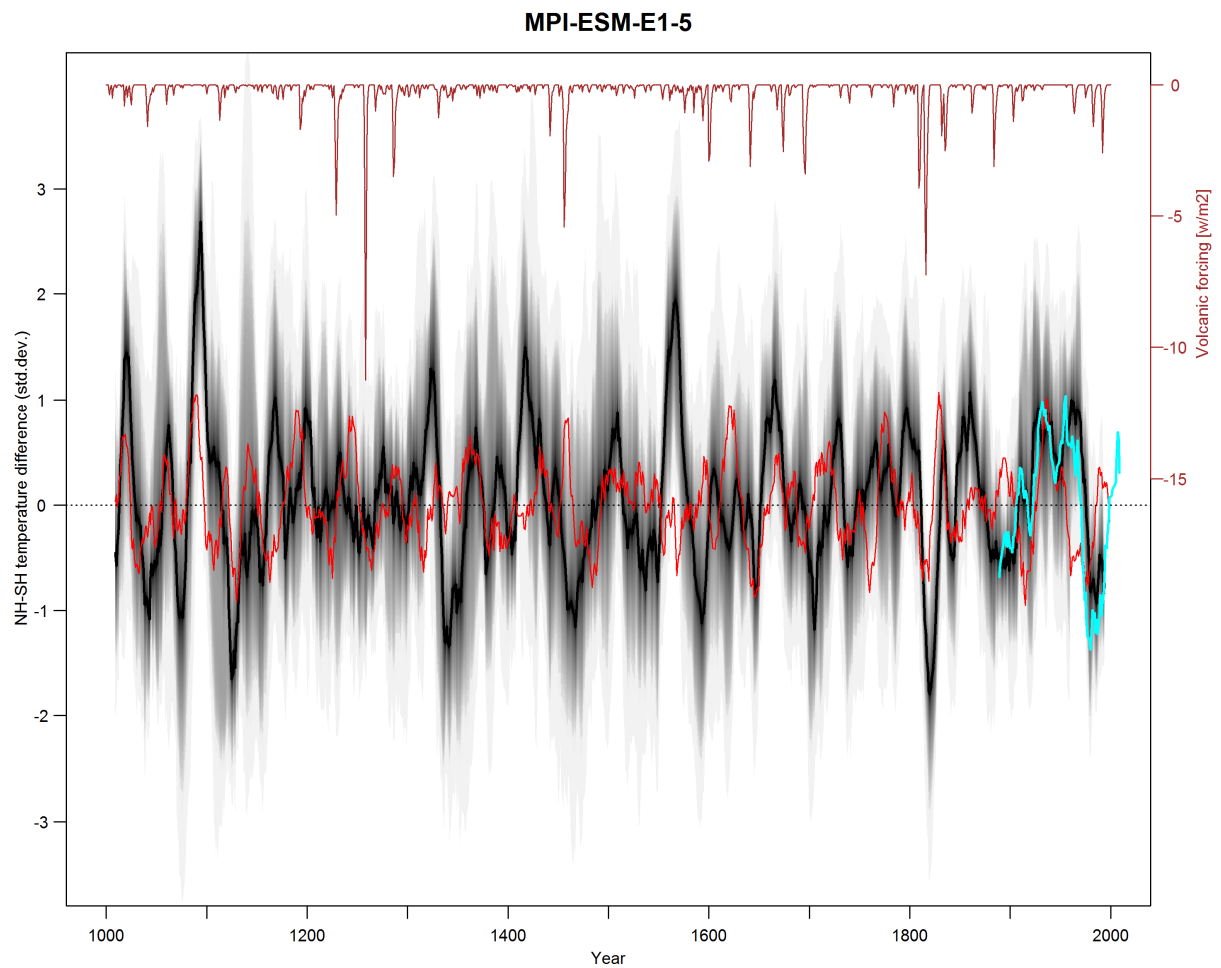
Supplementary Figure 52 | NH-SH differences MPI-ESM E1-2: Same as Supplementary Figure 51 but for the MPI-ESM E1 simulation, ensemble member 2.



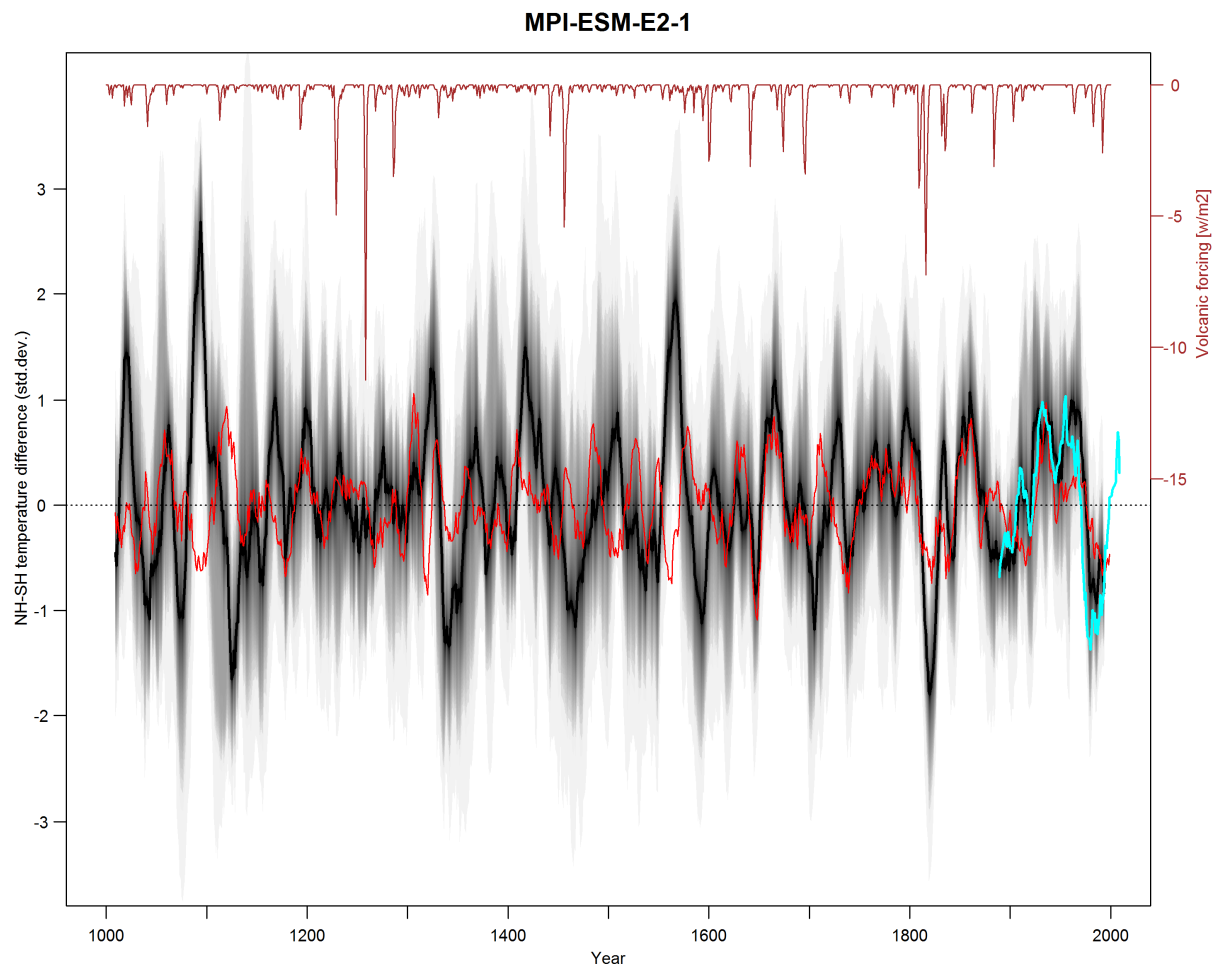
Supplementary Figure 53 | NH-SH differences MPI-ESM E1-3. Same as Supplementary Figure 51 but for the MPI-ESM E1 simulation, ensemble member 3.



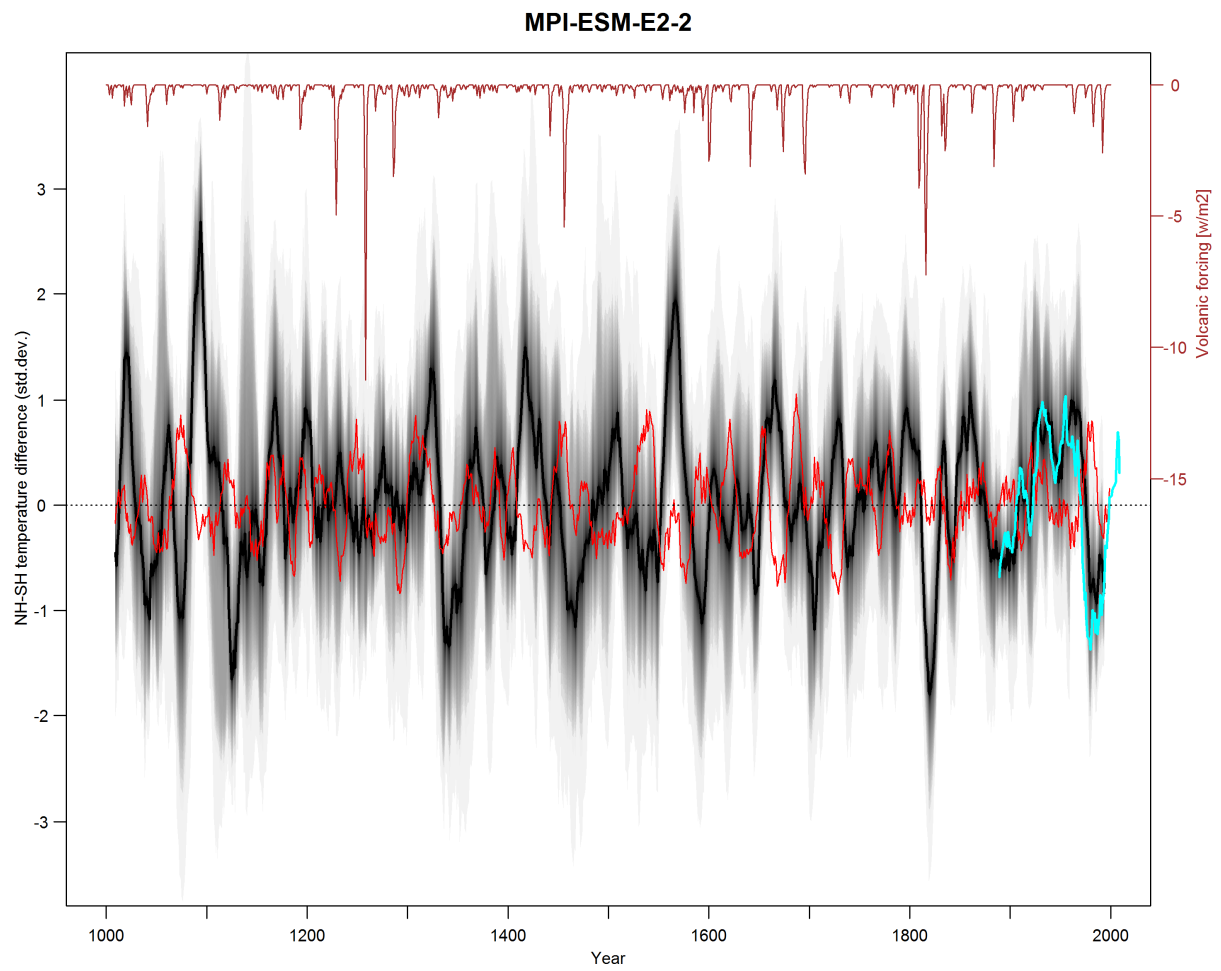
Supplementary Figure 54 | NH-SH differences MPI-ESM E1-4. Same as Supplementary Figure 51 but for the MPI-ESM E1 simulation, ensemble member 4.



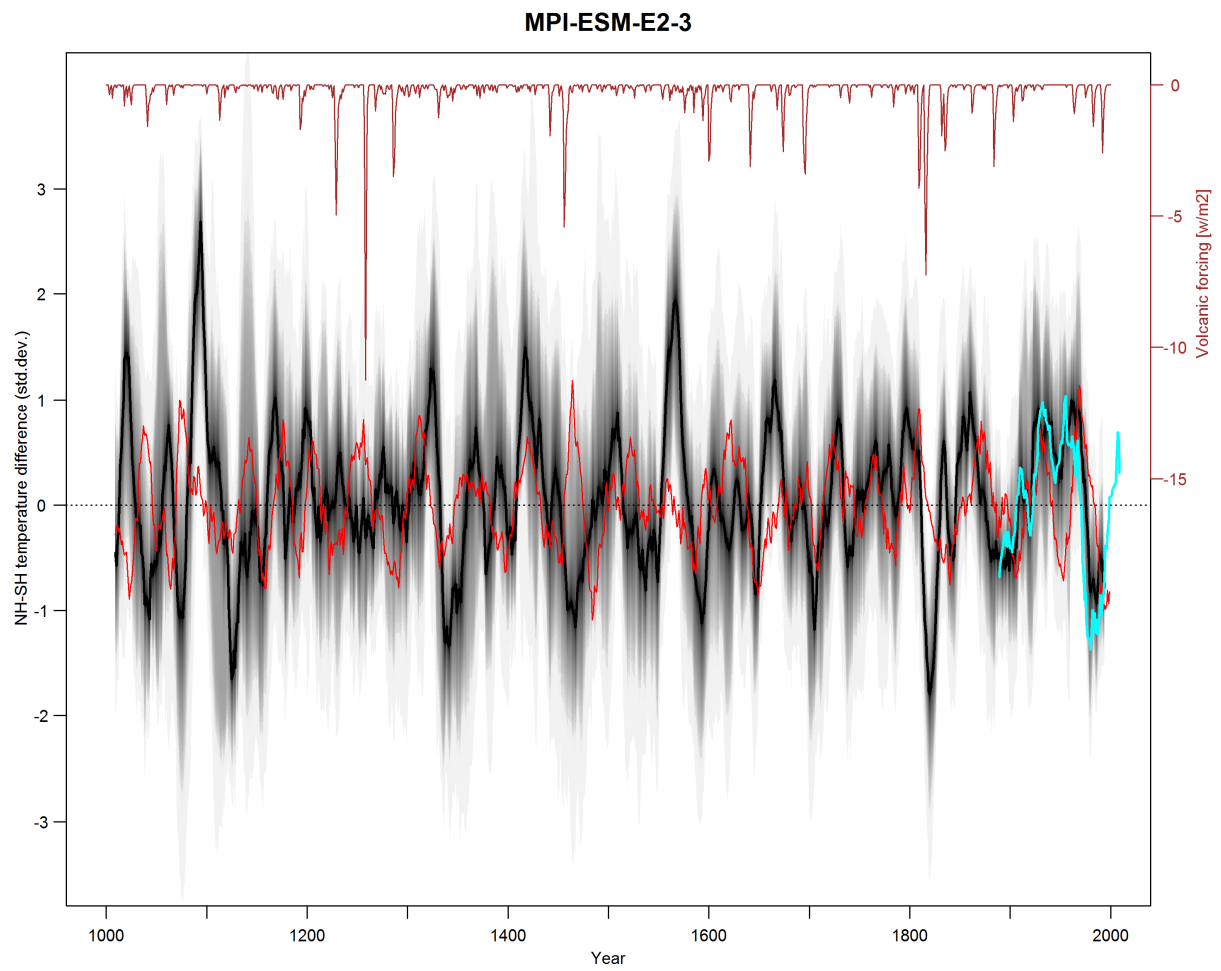
Supplementary Figure 55 | NH-SH differences MPI-ESM E1-5. Same as Supplementary Figure 51 but for the MPI-ESM E1 simulation, ensemble member 5.



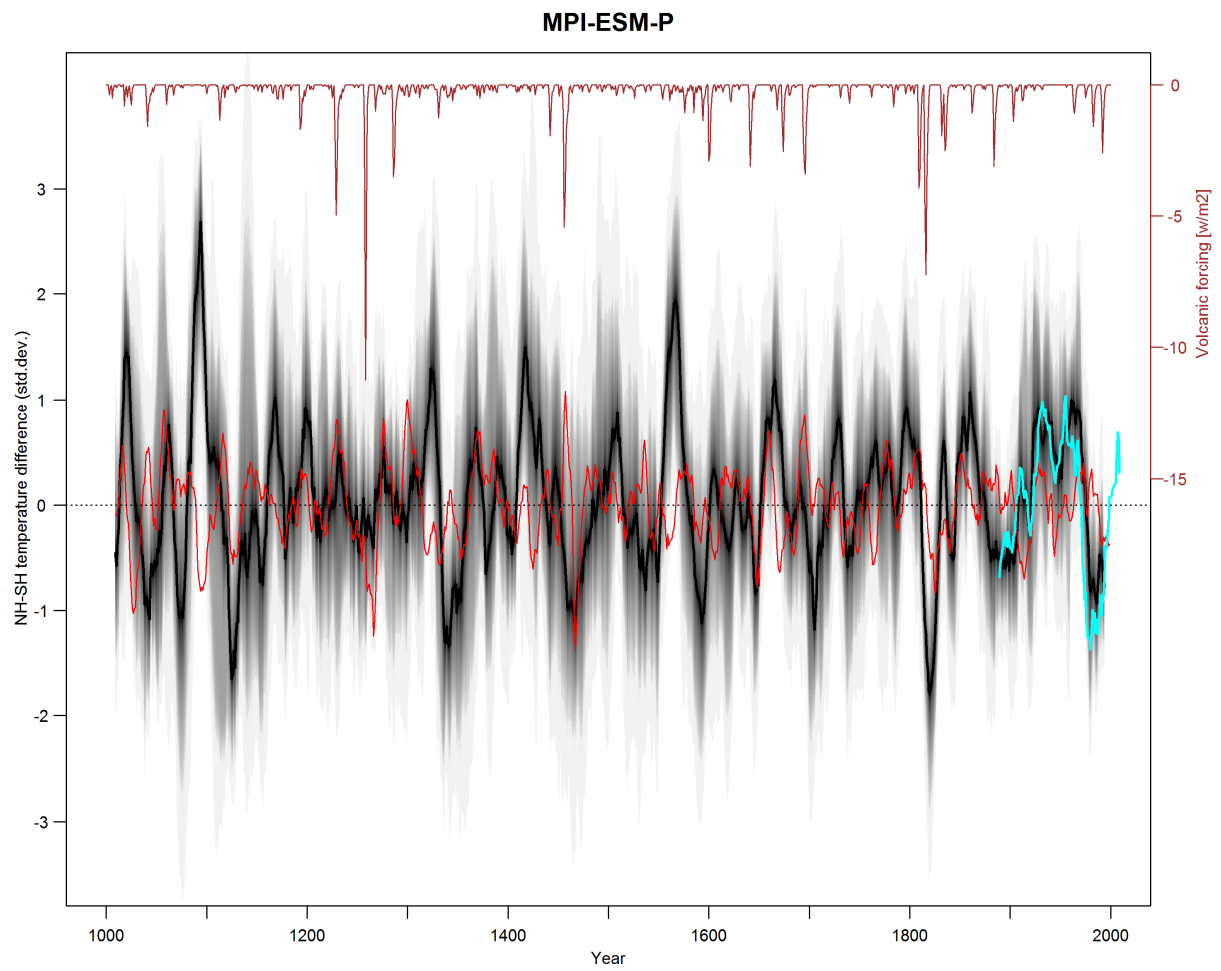
Supplementary Figure 56 | NH-SH differences MPI-ESM E2-1. Same as Supplementary Figure 51 but for the MPI -ESM E2 simulation, ensemble member 1.



Supplementary Figure 57 | NH-SH differences MPI-ESM E2-2. Same as Supplementary Figure 51 but for the MPI-ESM E2 simulation, ensemble member 2.



Supplementary Figure 58 | NH-SH differences MPI-ESM E2-3. Same as Supplementary Figure 51 but for the MPI -ESM E2 simulation, ensemble member 3.



Supplementary Figure 59 | NH-SH differences MPI-ESM-P. Same as Supplementary Figure 36 but for the MPI-ESM-P simulation and the corresponding volcanic forcing dataset (Crowley and Unterman, 2013).

12. References

- Abram, N., Gagan, M., Cole, J., Hantoro, W. and Mudelsee, M. (2008). Recent intensification of tropical climate variability in the Indian Ocean. *Nature Geoscience* **1**: 849-853.
- Alibert, C. and Kinsley, L. (2008a). A 170-year Sr/Ca and Ba/Ca coral record from the western Pacific warm pool: 1. What can we learn from an unusual coral record? *Journal of Geophysical Research* **113** (C4): C04008.
- Alibert, C. and Kinsley, L. (2008b). A 170-year Sr/Ca and Ba/Ca coral record from the western Pacific warm pool: 2. A window into variability of the New Ireland Coastal Undercurrent. *Journal of Geophysical Research* **113** (C6): C06006.
- Allen, K., Cook, E., Francey, R. and Michael, K. (2001). The climatic response of *Phyllocladus aspleniifolius* (Labill.) Hook. f in Tasmania. *Journal of Biogeography* **28**: 305-316.
- Allen, K. J. (2002). The Temperature Response in the Ring Widths of *Phyllocladus Aspleniifolius* (Celery-top Pine) Along an Altitudinal Gradient in the Warra LTER Area, Tasmania. *Australian Geographical Studies* **40** (3): 287-299.
- Ammann, C. M., Joos, F., Schimel, D. S., Otto-Bliesner, B. L. and Tomas, R. A. (2007). Solar influence on climate during the past millennium: results from transient simulations with the NCAR climate system model. *Proceedings of the National Academy of Sciences of the United States of America* **104**: 3713-3718.
- Ammann, C. M., Meehl, G. A., Washington, W. M. and Zender, C. S. (2003). A monthly and latitudinally varying volcanic forcing dataset in simulations of 20th century climate. *Geophysical Research Letters* **30** (12): 1657.
- Aravena, J. C., Lara, A., Wolodarsky-Franke, A., Villalba, R. and Cuq, E. (2002). Tree-ring growth patterns and temperature reconstruction from *Nothofagus pumilio* (Fagaceae) forests at the upper tree line of southern Chilean Patagonia. *Revista Chilena De Historia Natural* **75** (2): 361-376.
- Argollo, J., Soliz, C. and Villalba, R. (2004). Potencialidad dendrocronológica de *Polylepis tarapacana* en los Andes Centrales de Bolivia. *Ecología en Bolivia* **39** (1): 5-24.
- Aristarain, A. J., Delmas, R. J. and Stievenard, M. (2004). Ice-core study of the link between sea-salt aerosol, sea-ice cover and climate in the Antarctic Peninsula area. *Climatic Change* **67** (1): 63-86.
- Asami, R., Yamada, T. and Iryu, Y. (2005). Interannual and decadal variability of the western Pacific sea surface condition for the years 1787–2000: Reconstruction based on stable isotope record from a Guam coral. *Journal of Geophysical Research* **110**: 1-13.
- Bagnato, S., Linsley, B. K., Howe, S. S., Wellington, G. M. and Salinger, J. (2005). Coral oxygen isotope records of interdecadal climate variations in the South Pacific Convergence Zone region. *Geochemistry, Geophysics, Geosystems* **6** (6): Q06001.

- Baker, P., Palmer, J. and D'Arrigo, R. (2008). The dendrochronology of *Callitris intratropica* in Northern Australia: annual ring structure, chronology development and climate correlations. *Australian Journal of Botany* **56**: 311-320.
- Banta, J. R., McConnell, J. R., Frey, M. M., Bales, R. C. and Taylor, K. (2008). Spatial and temporal variability in snow accumulation at the West Antarctic Ice Sheet Divide over recent centuries. *J. Geophys. Res.* **113** (D23): D23102.
- Bard, E., G., R., Yiou, F. and J., J. (2000). Solar irradiance during the last 1200 years based on cosmogenic nuclides *Tellus* **52B**: 985-992.
- Battle, M., Bender, M., Sowers, T., Tans, P. P., Butler, J. H., Elkins, J. W., Ellis, J. T., Conway, T., Zhang, N., Lang, P. and Clarket, A. D. (1996). Atmospheric gas concentrations over the past century measured in air from firn at the South Pole. *Nature* **383**: 231-235.
- Berger, A. L. (1978). Long-Term Variations of Daily Insolation and Quaternary Climatic Changes. *Journal of the Atmospheric Sciences* **35** (12): 2362-2367.
- Bird, B. W., Abbott, M. B., Vuille, M., Rodbell, D. T., Stansell, N. D. and Rosenmeier, M. F. (2011). A 2,300-year-long annually resolved record of the South American summer monsoon from the Peruvian Andes. *Proceedings of the National Academy of Sciences* **108** (21): 8583-8588.
- Black, D. E., Abahazi, M. A., Thunell, R. C., Kaplan, A., Tappa, E. J. and Peterson, L. C. (2007). An 8-century tropical Atlantic SST record from the Cariaco Basin: Baseline variability, twentieth-century warming, and Atlantic hurricane frequency. *Paleoceanography* **22** (4): PA4204.
- Blunier, T., Chappellaz, J., Schwander, J., Stauffer, B. and Raynaud, D. (1995). Variations in atmospheric methane concentration during the Holocene epoch. *Nature* **374**: 46-49.
- Boës, X. and Fagel, N. (2008). Relationships between southern Chilean varved lake sediments, precipitation and ENSO for the last 600 years. *Journal of Paleolimnology* **39** (2): 237-252.
- Boiseau, M., Ghil, M. and Juillet-Leclerc, A. (1999). Climatic trends and interdecadal variability from south-central Pacific coral records. *Geophys. Res. Lett.* **26** (18): 2881-2884.
- Boninsegna, J. A., Keegan, J., Jacoby, G. C., D'Arrigo, R. and Holmes, R. L. (1989). Dendrochronological studies in Tierra del Fuego, Argentina. *Quaternary of South America and Antarctic Peninsula* **7**: 315-326.
- Bretagnon, P. and Francou, G. (1988). Planetary theories in rectangular and spherical variables - VSOP 87 solutions. *Astron. Astrophys.* **202**: 309-315.
- Bretherton, C. S., Widmann, M., Dymnikov, V. P., Wallace, J. M. and Bladé, I. (1999). The Effective Number of Spatial Degrees of Freedom of a Time-Varying Field. *Journal of Climate* **12** (7): 1990-2009.
- Briffa, K. and Jones, P. (1990). Basic chronology statistics and assessment. *Methods of Dendrochronology: applications in the environmental sciences*. E. Cook and L. Kairiukstis. Dordrecht, Kluwer Academic.

- Briffa, K. R. (2000). Annual climate variability in the Holocene: interpreting the message of ancient trees. *Quaternary Science Reviews* **19** (1-5): 87-105.
- Brookhouse, M., Lindesay, J. and Brack, C. (2008). The Potential of Tree Rings in Eucalyptus pauciflora for Climatological and Hydrological Reconstruction. *Geographical Research* **46** (4): 421-434.
- Buckley, B., Cook, E., Peterson, M. and Barbetti, M. (1997). A changing temperature response with elevation for Lagarostrobis franklinii in Tasmania, Australia. *Climatic Change* **36**: 477-498.
- Charles, C., Cobb, K., Moore, M. and Fairbanks, R. (2003). Monsoon–tropical ocean interaction in a network of coral records spanning the 20th century. *Marine Geology* **201** (1-3): 207-222.
- Christie, D. A., Boninsegna, J. A., Cleaveland, M., Lara, A., Le Quesne, C., Morales, M., Mudelsee, M., Stahle, D. and Villalba, R. (2011). Aridity changes in the Temperate-Mediterranean transition of the Andes since AD 1346 reconstructed from tree-rings. *Climate Dynamics* **36**: 1505-1521.
- Christie, D. A., Lara, A., Barichivich, J., Villalba, R., Morales, M. S. and Cuq, E. (2009). El Niño-Southern Oscillation signal in the world's highest-elevation tree-ring chronologies from the Altiplano, Central Andes. *Palaeogeography, Palaeoclimatology, Palaeoecology* **281** (3-4): 309-319.
- Cobb, K., Charles, C., Cheng, H. and Edwards, L. (2003). El Nino/Southern Oscillation and tropical Pacific climate during the last millenium. *Nature* **424**: 271-276.
- Cole, J., Dunbar, R., Mc Clanahan, T. and Muthiga, N. (2000). Tropical Pacific forcing of decadal SST variability in the Western Indian Ocean over the past two centuries. *Science* **287** (5453): 617-619.
- Cole, J., Fairbanks, R. and Shen, G. (1993). Recent variability in the Southern Oscillation; isotopic results from a Tarawa atoll coral. *Science* **260**: 1790-1793.
- Conroy, J. L., Restrepo, A., Overpeck, J. T., Steinitz-Kannan, M., Cole, J. E., Bush, M. B. and Colinvaux, P. A. (2009). Unprecedented recent warming of surface temperatures in the eastern tropical Pacific Ocean. *Nature Geoscience* **2** (1): 46-50.
- Cook, E. R., Briffa, K. R. and Jones, P. D. (1994). Spatial regression methods in dendroclimatology – a review and compariosn of two techniques. *International Journal of Climatology* **14** (4): 379-402.
- Cook, E. R., Buckley, B. M., D'Arrigo, R. D. and Peterson, M. J. (2000). Warm-season temperatures since 1600 BC reconstructed from Tasmanian tree rings and their relationship to large-scale sea surface temperature anomalies. *Climate Dynamics* **16** (2-3): 79-91.
- Cook, E. R., Buckley, B. M., Palmer, J. G., Fenwick, P., Peterson, M. J., Boswijk, G. and Fowler, A. (2006). Millennia-long tree-ring records from Tasmania and New Zealand: a basis for modelling climate variability and forcing, past, present and future. *Journal of Quaternary Science* **21** (7): 689-699.

Cook, E. R., Palmer, J. G., Cook, B. I., Hogg, A. and D'Arrigo, R. D. (2002). A multi-millennial palaeoclimatic resource from Lagarostrobos colensoi tree-rings at Oroko Swamp, New Zealand. *Global and Planetary Change* **33** (3-4): 209-220.

Crowley, T. (2000). Causes of Climate Change over the Past 1,000 years. *Science* **289**: 270-277.

Crowley, T. J. and Unterman, M. B. (2013). Technical details concerning development of a 1200 yr proxy index for global volcanism. *Earth Syst. Sci. Data* **5** (1): 187-197.

Cullen, L. and Grierson, P. (2009). Multi-decadal scale variability in autumn-winter rainfall in south-western Australia since 1655 AD as reconstructed from tree rings of *Callitris columellaris*. *Climate Dynamics* **33** (2-3): 433-444.

D'Arrigo, R., Cook, E., Villalba, R., Buckley, B., Salinger, M., Palmer, J. and Allen, K. (2000). Trans-Tasman Sea Climate Variability Since AD 1740 Inferred From Middle-High Latitude Tree-Ring Data. *Climate Dynamics* **16**: 603-610.

D'Arrigo, R., Wilson, R. and Jacoby, G. (2006a). On the long-term context for late twentieth century warming. *Journal of Geophysical Research-Atmospheres* **111**: D03103.

D'Arrigo, R., Wilson, R., Palmer, J., Krusic, P., Curtis, A., Sakulich, J., Bijaksana, S., Zulaikah, S. and Ngkoimani, L. O. (2006b). Monsoon drought over Java, Indonesia, during the past two centuries. *Geophysical Research Letters* **33** (4): L04709.

D'Arrigo, R. D., Buckley, B. M., Cook, E. R. and Wagner, W. S. (1995). Temperature-sensitive tree-ring width chronologies of pink pine (*Halocarpus biformis*) from Stewart Island, New Zealand. *Palaeogeography Palaeoclimatology Palaeoecology* **119** (3-4): 293-300.

Damassa, T., Cole, J., Barnett, H., Ault, T. and McClanahan (2006). Enhanced multidecadal climate variability in the seventeenth century from coral isotope records in the western Indian Ocean. *Paleoceanography* **21**: PA2016.

Drost, F. and Karoly, D. (2012). Evaluating global climate responses to different forcings using simple indices. *Geophysical Research Letters* **39** (16): L16701.

Drost, F., Karoly, D. and Braganza, K. (2012). Communicating global climate change using simple indices: an update. *Climate Dynamics* **39** (3-4): 989-999.

Druffel, E. R. M. and Griffin, S. (1999). Variability of surface ocean radiocarbon and stable isotopes in the southwestern Pacific. *J. Geophys. Res.* **104** (C10): 23607-23613.

Dufresne, J. L., Foujols, M. A., Denvil, S., Caubel, A., Marti, O., Aumont, O., Balkanski, Y., Bekki, S., Bellenger, H., Benshila, R., Bony, S., Bopp, L., Braconnot, P., Brockmann, P., Cadule, P., Cheruy, F., Codron, F., Cozic, A., Cugnet, D., Noblet, N., Duvel, J. P., Ethé, C., Fairhead, L., Fichefet, T., Flavoni, S., Friedlingstein, P., Grandpeix, J. Y., Guez, L., Guilyardi, E., Hauglustaine, D., Hourdin, F., Idelkadi, A., Ghattas, J., Joussaume, S., Kageyama, M., Krinner, G., Labeyrie, S., Lahellec, A., Lefebvre, M. P., Lefevre, F., Levy, C., Li, Z. X., Lloyd, J., Lott, F., Madec, G., Mancip, M., Marchand, M., Masson, S., Meurdésorff, Y., Mignot, J., Musat, I., Parouty, S., Polcher, J., Rio, C., Schulz, M., Swingedouw, D., Szopa, S., Talandier, C., Terray, P., Viovy, N. and Vuichard, N. (2012).

Climate change projections using the IPSL-CM5 Earth System Model: from CMIP3 to CMIP5. *Climate Dynamics* **40** (9-10): 2123-2165.

Dunbar, R. B., Wellington, G. M., Colgan, M. W. and Glynn, P. W. (1994). Eastern Pacific Sea-Surface Temperature since 1600-AD - the Delta-O-18 Record of Climate Variability in Galapagos Corals. *Paleoceanography* **9** (2): 291-315.

Duncan, R. P., Fenwick, P., Palmer, J. G., McGlone, M. S. and Turney, C. S. M. (2010). Non-uniform interhemispheric temperature trends over the past 550 years. *Climate Dynamics* **35** (7-8): 1429–1438.

Dunwiddie, P. W. and Lamarche, V. C. (1980). A Climatically Responsive Tree-Ring Record from Widdringtonia-Cedarbergensis, Cape-Province, South-Africa. *Nature* **286** (5775): 796-797.

Ekaykin, A. A., Lipenkov, V. Y., Kuzmina, I. N., Petit, J. R., Masson-Delmotte, V. and Johnsen, S. J. (2004). The changes in isotope composition and accumulation of snow at Vostok station, East Antarctica, over the past 200 years. *Annals of Glaciology* **39**: 569-575.

Elbert, J., Grosjean, M., von Gunten, L., Urrutia, R., Fischer, D., Wartenburger, R., Ariztegui, D. and Fujak, M. (2011). Quantitative high-resolution winter (JJA) precipitation reconstruction from varved sediments of Lago Plomo 47°S, Patagonian Andes, AD 1530 - 2001. *The Holocene*.

Etheridge, D., Steele, L., Francey, R. and Langenfelds, R. L. (1998). Atmospheric methane between 1000 A. D. and present: Evidence of anthropogenic emissions and climatic variability. *Journal of Geophysical Research* **103**: 15979-15993.

Etheridge, D. M., Steele, L. P., Langenfelds, R. L., Francey, R. J., Barnola, J. M. and Morgan, V. I. (1996). Natural and anthropogenic changes in atmospheric CO₂ over the last 1000 years from air in Antarctic ice and firn. *Journal of Geophysical Research-Atmospheres* **101**: 4115-4128.

Fenby, C. and Gergis, J. (2013). Rainfall variations in south-eastern Australia part 1: consolidating evidence from pre-instrumental documentary sources, 1788–1860. *International Journal of Climatology*: doi: 10.1002/joc.3640.

Flückiger, J., Dallenbach, A., Blunier, T., Stauffer, B., Stocker, T. F., Raynaud, D. and Barnola, J. M. (1999). Variations in atmospheric N₂O concentration during abrupt climatic changes. *Science* **285**: 227-230.

Flückiger, J., Monnin, E., Stauffer, B., Schwander, J., Stocker, T. F., Chappellaz, J., Raynaud, D. and Barnola, J. M. (2002). High-resolution Holocene N₂O ice core record and its relationship with CH₄ and CO₂. *Global Biogeochemical Cycles* **16**: 1010.

Fowler, A., Boswijk, G., Gergis, J. and Lorrey, A. (2008). ENSO history recorded in *Agathis australis* (Kauri) tree-rings Part A: Kauri's potential as an ENSO proxy. *International Journal of Climatology* **28** (1): 1-20.

Frank, D., Esper, J. and Cook, E. R. (2007). Adjustment for proxy number and coherence in a large-scale temperature reconstruction. *Geophysical Research Letters* **34** (16): L16709.

Frank, D. C., Esper, J., Raible, C. C., Buntgen, U., Trouet, V., Stocker, B. and Joos, F. (2010). Ensemble reconstruction constraints on the global carbon cycle sensitivity to climate. *Nature* **463** (7280): 527-532.

Gao, C., Robock, A. and Ammann, C. (2008). Volcanic forcing of climate over the past 1500 years: An improved ice core-based index for climate models. *J. Geophys. Res.* **113** (D23): D23111.

García-Herrera, R., Diaz, H. F., Garcia, R. R., Prieto, M. R., Barriopedro, D., Moyano, R., Hernández, E. (2008). A Chronology of El Niño Events from Primary Documentary Sources in Northern Peru. *Journal of Climate* **21** (9): 1948-1962.

Garcin, Y., Williamson, D., Bergonzini, L., Radakovitch, O., Vincens, A., Buchet, G., Guiot, J., Brewer, S., Mathé, P.-E. and Majule, A. (2007). Solar and anthropogenic imprints on Lake Masoko (southern Tanzania) during the last 500 years. *Journal of Paleolimnology* **37** (4): 475-490.

Gergis, J., Gallant, A., Braganza, K., Karoly, D., Allen, K., Cullen, L., D'Arrigo, R., Goodwin, I., Grierson, P. and McGregor, S. (2011). On the long-term context of the 1997–2009 ‘Big Dry’ in South-Eastern Australia: insights from a 206-year multi-proxy rainfall reconstruction. *Climatic Change*: 1-22.

Gioda, A. and Prieto, M. R. (1999). Histoire des sécheresses andines. Potosí, El Niño et le Petit Age Glaciaire. *Revue de la Société Météorologique de France. La Météorologie* **27**: 33-42.

González-Rouco, J. F., Beltrami, H., Zorita, E. and von Storch, H. (2006). Simulation and inversion of borehole temperature profiles in surrogate climates: Spatial distribution and surface coupling. *Geophysical Research Letters* **33**: L01703.

Graf, W., Oerter, H., Reinwarth, O., Stichler, W., Wilhelms, F., Miller, H. and Mulvaney, R. (2002). Stable-isotope records from Dronning Maud Land, Antarctica. *Annals of Glaciology* **35**: 195-201.

Guilderson, T. and Schrag, D. (1999). Reliability of coral isotope records from the western Pacific warm pool: A comparison using age-optimized records. *Paleoceanography* **14** (4): 457-464.

Hanhijärvi, S., Tingley, M. P. and Korhola, A. (2013). Pairwise comparisons to reconstruct mean temperature in the Arctic Atlantic Region over the last 2,000 years. *Climate Dynamics*.

Hansen, J., Ruedy, R., Sato, M. and Lo, K. (2010). Global surface temperature change. *Reviews of Geophysics* **48** (4): RG4004.

Hegerl, G., Crowley, T. J., Allen, M., Hyde, W. T., Pollack, H. N., Smerdon, J. and Zorita, E. (2007). Detection of human influence on a new, validated 1500-year temperature reconstruction. *Journal of Climate* **20** (4): 650-666.

Herrera, R., Prieto, M. R. and García-Herrera, R. (2003). Floods in the semiarid Argentinean Chaco during the 17th to 19th centuries. *Proceedings of Palaeofloods, Historical Data & Climatic Variability: Applications in Flood Risk Assessment*. V. R. Thorndycraft, G. Benito, M. Barriendos and M. Llasat. Madrid, CSIC-Centro de Ciencias Medioambientales: 107-112.

Hofer, D., Raible, C. C. and Stocker, T. F. (2011). Variations of the Atlantic meridional overturning circulation in control and transient simulations of the last millennium. *Climate of the Past* **7** (1): 133-150.

Hoffmann, G., Ramirez, E., Taupin, J. D., Francou, B., Ribstein, P., Delmas, R., Durr, H., Gallaire, R., Simoes, J., Schotterer, U., Stievenard, M. and Werner, M. (2003). Coherent isotope history of Andean ice cores over the last century. *Geophysical Research Letters* **30** (4).

Hurtt, G. C., Frolking, S., Fearon, M. G., Moore, B., Shevliakova, E., Malyshev, S., Pacala, S. W. and Houghton, R. A. (2006). The underpinnings of land-use history: three centuries of global gridded land-use transitions, wood-harvest activity, and resulting secondary lands. *Global Change Biology* **12** (7): 1208-1229.

Jacobel, R. W., Welch, B. C., Steig, E. J. and Schneider, D. P. (2005). Glaciological and climatic significance of Hercules Dome, Antarctica: An optimal site for deep ice core drilling. *Journal of Geophysical Research-Earth Surface* **110** (F1).

Johns, T. C., Gregory, J. M., Ingram, W. J., Johnson, C. E., Jones, A., Lowe, J. A., Mitchell, J. F. B., Roberts, D. L., Sexton, D. M. H., Stevenson, D. S., Tett, S. F. B. and Woodage, M. J. (2003). Anthropogenic climate change for 1860 to 2100 simulated with the HadCM3 model under updated emissions scenarios. *Climate Dynamics* **20** (6): 583-612.

Jones, P. D., Briffa, K. R., Barnett, T. P. and Tett, S. F. B. (1998). High-resolution palaeoclimatic records for the last millennium: interpretation, integration and comparison with General Circulation Model control-run temperatures. *The Holocene* **8** (4): 455-471.

Juckes, M., Allen, M., Briffa, K., Esper, J., Hegerl, G., Moberg, A., Osborn, T. and Weber, S. (2007). Millennial temperature reconstruction intercomparison and evaluation. *Climate of the Past* **3**: 591–609.

Jungclaus, J., Giorgetta, M., Reick, C., Legutke, S., Brovkin, V., Crueger, T., Esch, M., Fieg, K., Fischer, N., Glushak , K., Gayler, V., Haak, H., Hollweg, H.-D., Kinne, S., Kornblueh , L., Matei, D., Mauritzen, T., Mikolajewicz, U., Müller, W., Notz, D., Pohlmann, T., Raddatz, T., Rast, S., Roeckner, E., Salzmann, M., Schmidt, H., Schnur, R., Segschneider, J., Six, K., Stockhouse, M., Wegner, J., Widmann, H., Wieners, K.-H., Claussen, M., Marotzke, J. and Stevens, B. (2012). MIP5 simulations of the Max Planck Institute for Meteorology (MPI-M) based on the MPI-ESM-P model: The past1000 experiment, served by ESGF. World Data Center for Climate doi:10.1594/Wdcc/CMIP5.MXEPpk.

Jungclaus, J. H., Fischer, N., Haak, H., Lohmann, K., Marotzke, J., Matei, D., Mikolajewicz, U., Norz, D. and von Storch, J. S. (2013). Characteristics of the ocean simulations in MPIOM, the ocean component of the MPI-Earth System Model. *Journal of Advances in Modelling Earth Systems*: 10.1002/jame.20023.

Jungclaus, J. H., Lorenz, S. J., Timmreck, C., Reick, C. H., Brovkin, V., Six, K., Segschneider, J., Giorgetta, M. A., Crowley, T. J., Pongratz, J., Krivova, N. A., Vieira, L. E., Solanki, S. K., Klocke, D., Botzet, M., Esch, M., Gayler, V., Haak, H., Raddatz, T. J., Roeckner, E., Schnur, R., Widmann, H., Claussen, M., Stevens, B. and Marotzke, J. (2010). Climate and carbon-cycle variability over the last millennium. *Clim. Past* **6** (5): 723-737.

Kaplan, J. O., Krumhardt, K. M., Ellis, E. C., Ruddiman, W. F., Lemmen, C. and Goldewijk, K. K. (2011). Holocene carbon emissions as a result of anthropogenic land cover change. *The Holocene* **21** (5): 775-791.

Karoly, D. J. (1989). Southern-Hemisphere Circulation Features Associated with El Niño - Southern Oscillation Events. *Journal of Climate* **2** (11): 1239-1252.

Karoly, D. J., Hope, P. and Jones, P. D. (1996). Decadal variations of the Southern Hemisphere circulation. *International Journal of Climatology* **16** (7): 723-738.

Karoly, D. J. and Vincent, D. G. (1998). *Meteorology of the Southern Hemisphere*. Boston, USA, American Meteorological Association.

Kellerhals, T., Brutsch, S., Sigl, M., Knusel, S., Gaggeler, H. W. and Schwikowski, M. (2010). Ammonium concentration in ice cores: A new proxy for regional temperature reconstruction? *Journal of Geophysical Research-Atmospheres* **115**: D16123.

Kelso, C. and Vogel, C. H. (2007). The climate of Namaqualand in the nineteenth century. *Climatic Change* **83** (3): 357-380.

Krivova, N. A., Balmaceda, L. and Solanki, S. K. (2007). Reconstruction of solar total irradiance since 1700 from the surface magnetic flux. *Astronomy and Astrophysics* **467**: 335-346.

Kuhnert, H., Patzold, J., Hatcher, B., Wyrwoll, K. H., Eisenhauer, A., Collins, L. B., Zhu, Z. R. and Wefer, G. (1999). A 200-year coral stable oxygen isotope record from a high-latitude reef off western Australia. *Coral Reefs* **18** (1): 1-12.

Kuhnert, H., Pätzold, J., Wyrwoll, K. and Wefer, G. (2000). Monitoring climate variability over the past 116 years in coral oxygen isotopes from Ningaloo Reef, Western Australia. *International Journal of Earth Sciences* **88**: 725-732.

LaMarche, V. C., Holmes, R. L., Dunwiddie, P. W. and Drew, L. G. (1979a). *Tree-ring chronologies of the southern hemisphere: Vol. 1: Argentina. Chronology Series V*. Tucson, AZ, Laboratory of Tree-Ring Research, University of Arizona.

LaMarche, V. C., Holmes, R. L., Dunwiddie, P. W. and Drew, L. G. (1979b). *Tree-ring chronologies of the southern hemisphere: Vol. 2: Chile. Chronology Series V*. Tucson, AZ, Laboratory of Tree-Ring Research, University of Arizona, Tucson, USA.

LaMarche, V. C., Holmes, R. L., Dunwiddie, P. W. and Drew, L. G. (1979c). *Tree-ring chronologies of the Southern Hemisphere: Vol. 4: Australia.*, Laboratory of Tree-Ring Research, University of Arizona, Tucson, USA.

Lamarque, J. F., Bond, T. C., Eyring, V., Granier, C., Heil, A., Klimont, Z., Lee, D., Liousse, C., Mieville, A., Owen, B., Schultz, M. G., Shindell, D., Smith, S. J., Stehfest, E., Van Aardenne, J., Cooper, O. R., Kainuma, M., Mahowald, N., McConnell, J. R., Naik, V., Riahi, K. and van Vuuren, D. P. (2010). Historical (1850-2000) gridded anthropogenic and biomass burning emissions of reactive gases and aerosols: methodology and application. *Atmos. Chem. Phys.* **10** (15): 7017-7039.

Lara, A., Aravena, J. C., Villalba, R., Wolodarsky-Franke, A., Luckman, B. and Wilson, R. (2001). Dendroclimatology of high-elevation Nothofagus pumilio forests at their northern

distribution limit in the central Andes of Chile. *Canadian Journal of Forest Research-Revue Canadienne De Recherche Forestiere* **31** (6): 925-936.

Lara, A., Villalba, R., Aravena, J. C., Wolodarsky, A. and Neira, A. (2000). Desarollo de una red de cronologías de Fitzroya Cupressoides (Alerce) para Chile y Argentina. *Dendrochronología en América Latina*. F. Roig. Mendoza, Editorial Nacional de Cuyo: 193-215.

Lara, A., Villalba, R. and Urrutia, R. (2008). A 400-year tree-ring record of the Puelo River summer-fall streamflow in the Valdivian Rainforest eco-region, Chile. *Climatic Change* **86** (3-4): 331-356.

Lara, A., Villalba, R., Wolodarsky-Franke, A., Aravena, J. C., Luckman, B. H. and Cuq, E. (2005). Spatial and temporal variation in Nothofagus pumilio growth at tree line along its latitudinal range (35 degrees 40 '-55 degrees S) in the Chilean Andes. *Journal of Biogeography* **32** (5): 879-893.

Laundrum, L., Otto-Bliesner, B., Conley, P., Lawrence, P., Rosenbloom, N. and Teng, H. (2013). Last Millennium Climate and Its Variability in CCSM4. *Journal of Climate* **26** (1085): 1111.

Le Quesne, C., Stahle, D. W., Cleaveland, M. K., Therrell, M. D., Aravena, J. C. and Barichivich, J. (2006). Ancient Austrocedrus Tree-Ring Chronologies Used to Reconstruct Central Chile Precipitation Variability from a.d. 1200 to 2000. *Journal of Climate* **19** (22): 5731-5744.

Lean, J., Beer, J. and Bradley, R. (1995). Reconstruction of solar irradiance since 1610: Implications for climate change. *Geophysical Research Letters* **22** (23): 3195-3198.

Lefohn, A. S., Husar, J. D. and Husar, R. B. (1999). Estimating historical anthropogenic global sulfur emission patterns for the period 1850–1990. *Atmospheric Environment* **33** (21): 3435-3444.

Li, B., Nychka, D. and Ammann, C. (2010). The Value of Multiproxy Reconstruction of Past Climate. *Journal of the American Statistical Association* **105** (491): 883–895.

Linsley, B., Ren, L., Dunbar, R. and Howe, S. (2000a). El Niño Southern Oscillation (ENSO) and decadal-scale climate variability at 10N in the eastern Pacific from 1893 to 1994: A coral-based reconstruction from Clipperton Atoll. *Paleoceanography* **15** (3): 322-335.

Linsley, B., Wellington, G. and Schrag, D. (2000b). Decadal Sea Surface Temperature Variability in the Subtropical South Pacific from 1726 to 1997 AD. *Science* **290**: 1145-1149.

Linsley, B., Wellington, G., Schrag, D., Ren, L., Salinger, J. and Tudhope, A. (2004). Geochemical evidence from corals for changes in the amplitude and spatial pattern of South Pacific interdecadal climate variability over the last 300 years. *Climate Dynamics* **22**: 1-11.

Linsley, B. K., Dunbar, R. B., Wellington, G. M. and Mucciarone, D. A. (1994). A Coral-Based Reconstruction of Intertropical Convergence Zone Variability over Central-America since 1707. *Journal of Geophysical Research-Oceans* **99** (C5): 9977-9994.

Linsley, B. K., Kaplan, A., Gouriou, Y., Salinger, J., Demenocal, P. B., Wellington, G. M. and Howe, S. S. (2006). Tracking the extent of the South Pacific Convergence Zone since the early 1600s. *Geochemistry Geophysics Geosystems* **7**.

Linsley, B. K., Zhang, P. P., Kaplan, A., Howe, S. S. and Wellington, G. M. (2008). Interdecadal-decadal climate variability from multicoral oxygen isotope records in the South Pacific Convergence Zone region since 1650 A.D. *Paleoceanography* **23** (2): PA2219.

Lough, J. M. (2011). Great Barrier Reef coral luminescence reveals rainfall variability over northeastern Australia since the 17th century. *Paleoceanography* **26** (2): PA2201.

Luterbacher, J., Dietrich, D., Xoplaki, E., Grosjean, M. and Wanner, H. (2004). European seasonal and annual temperature variability, trends, and extremes since 1500. *Science* **303** (5663): 1499-1503.

Luterbacher, J., Xoplaki, E., Dietrich, D., Rickli, R., Jacobbeit, J., Beck, C., Gyalistras, D., Schmutz, C. and Wanner, H. (2002). Reconstruction of sea level pressure fields over the Eastern North Atlantic and Europe back to 1500. *Climate Dynamics* **18** (7): 545-561.

MacFarling-Meure, C., Etheridge, D., Trudinger, C., Steele, P., Langenfelds, R., van Ommen, T., Smith, A. and Elkins, J. (2006). Law Dome CO₂, CH₄ and N₂O ice core records extended to 2000 years BP. *Geophysical Research Letters* **33** (14): L14810.

Mann, M., Zhang, Z., Hughes, M., Bradley, R., Miller, S., Rutherford, S. and Ni, F. (2008). Proxy-based reconstructions of hemispheric and global surface temperature variations over the past two millennia. *Proceedings of the National Academy of Sciences* **105** (36): 13252–13257.

Mann, M. E. and Jones, P. D. (2003). Global surface temperatures over the past two millennia. *Geophysical Research Letters* **30** (15): 1820.

Marland, G., Boden, T. A. and Andres, R. J. (2003). Global regional and national emissions. *Trends: a compendium of data on global change*. Oak Ridge, TN, Carbon Dioxide Information Center, Oak Ridge National Laboratory.

Masiokas, M. and Villalba, R. (2004). Climatic significance of intra-annual bands in the wood of Nothofagus pumilio in southern Patagonia. *Trees-Structure and Function* **18** (6): 696-704.

Mayewski, P. A., Maasch, K. A., White, J. W. C., Steig, E. J., Meyerson, E., Goodwin, I., Morgan, V. I., Van Ommen, T., Curran, M. A. J., Souney, J. and Kreutz, K. (2004). A 700 year record of Southern Hemisphere extratropical climate variability. *Annals of Glaciology* **39**: 127-132.

McGregor, S., Timmermann, A., England, M. H., Elison Timm, O. and Wittenberg, A. T. (2013). Inferred changes in El Niño-Southern Oscillation variance over the past six centuries. *Clim. Past* **9** (5): 2269-2284.

Melvin, T. M. and Briffa, K. R. (2008). A "signal-free" approach to dendroclimatic standardisation. *Dendrochronologia* **26** (2): 71-86.

Melvin, T. M., Briffa, K. R., Nicolussi, K. and Grabner, M. (2007). Time-varying-response smoothing. *Dendrochronologia* **25** (1): 65-69.

- Moberg, A., Sonechkin, D. M., Holmgren, K., Datsenko, N. M. and Karlen, W. (2005). Highly variable Northern Hemisphere temperatures reconstructed from low- and high-resolution proxy data. *Nature* **433** (7026): 613-617.
- Morales, M. S., Villalba, R., Grau, H. R. and Paolini, L. (2004). Rainfall-controlled tree growth in high-elevation subtropical treelines. *Ecology* **85** (11): 3080-3089.
- Morice, C. P., Kennedy, J. J., Rayner, N. A. and Jones, P. D. (2012). Quantifying uncertainties in global and regional temperature change using an ensemble of observational estimates: The HadCRUT4 data set. *J. Geophys. Res.* **117** (D8): D08101.
- Mosley-Thompson, E., Thompson, L. G., Grootes, P. and Gundestrup, N. (1990). Little Ice Age (Neoglacial) paleoenvironmental conditions at Siple Station, Antarctica. *Annals of Glaciology* **14**: 199-204.
- Mulvaney, R., Oerter, H., Peel, D. A., Graf, W., Arrowsmith, C., Pasteur, E. C., Knight, B., Littot, G. C. and Miners, W. D. (2002). 1000 year ice-core records from Berkner Island, Antarctica. *Annals of Glaciology* **35**: 45-51.
- Mundo, I., Roig Juñent, F., Villalba, R., Kitzberger, T. and Barrera, M. (2012). Araucaria araucana tree-ring chronologies in Argentina: spatial growth variations and climate influences. *Trees - Structure and Function* **26** (2): 443-458.
- Nash, D. J. and Endfield, G. H. (2008). 'Splendid rains have fallen': links between El Niño and rainfall variability in the Kalahari, 1840-1900. *Climatic Change* **86** (3-4): 257-290.
- Nash, D. J. and Grab, S. W. (2010). "A sky of brass and burning winds": documentary evidence of rainfall variability in the Kingdom of Lesotho, Southern Africa, 1824–1900. *Climatic Change* **101** (3-4): 617–653.
- Neukom, R. and Gergis, J. (2012). Southern Hemisphere high-resolution palaeoclimate records of the last 2000 years. *The Holocene* **22** (5): 501-524.
- Neukom, R., Luterbacher, J., Villalba, R., Küttel, M., Frank, D., Jones, P. D., Grosjean, M., Esper, J., Lopez, L. and Wanner, H. (2010). Multi-centennial summer and winter precipitation variability in southern South America. *Geophysical Research Letters* **37**: L14708.
- Neukom, R., Luterbacher, J., Villalba, R., Kuttel, M., Frank, D., Jones, P. D., Grosjean, M., Wanner, H., Aravena, J. C., Black, D. E., Christie, D. A., D'Arrigo, R., Lara, A., Morales, M., Soliz-Gamboa, C., Srur, A., Urrutia, R. and von Gunten, L. (2011). Multiproxy summer and winter surface air temperature field reconstructions for southern South America covering the past centuries. *Climate Dynamics* **37** (1-2): 35-51.
- Neukom, R., Nash, D. J., Endfield, G. H., Grab, S. W., Grove, C. A., Kelso, C., Vogel, C. H. and Zinke, J. (2013). Multi-proxy summer and winter precipitation reconstruction for southern Africa over the last 200 years. *Climate Dynamics*: doi: 10.1007/s00382-013-1886-6.
- Neukom, R., Prieto, M. D., Moyano, R., Luterbacher, J., Pfister, C., Villalba, R., Jones, P. D. and Wanner, H. (2009). An extended network of documentary data from South America and its potential for quantitative precipitation reconstructions back to the 16th century. *Geophysical Research Letters* **36**: L12703.

North, G., Bell, T., Cahalan, F. and Moeing, F. (1982). Sampling Errors in the Estimation of Emerical Orthogonal Functions. *American Meteorological Society* **110**: 699-706.

Nurhati, I., Cobb, K. and Di Lorenzo, E. (2011). Decadal-scale SST and Salinity Variations in the Central Tropical Pacific: Signatures of Natural and Anthropogenic Climate Change. *Journal of Climate* **24**: 3294-3308.

PAGES-2k-Consortium (2013). Continental-scale temperature variability during the past two millennia. *Nature Geoscience* **6**: 339-346.

Pfeiffer, M., Timm, O., Dullo, W. C. and Podlech, S. (2004). Oceanic forcing of interannual and multidecadal climate variability in the southwestern Indian Ocean: Evidence from a 160 year coral isotopic record (La Réunion, 55°E, 21°S). *Paleoceanography* **19** (4): PA4006.

Phipps, S. J., McGregor, H. V., Gergis, J., Gallant, A. J. E., Neukom, R., Stevenson, S., Ackerley, D., Brown, J. R., Fischer, M. J. and van Ommen, T. D. (2013). Paleoclimate Data-Model Comparison and the Role of Climate Forcings over the Past 1500 Years. *Journal of Climate* **26** (18): 6915-6936.

Phipps, S. J., Rotstayn, L. D., Gordon, H. B., Roberts, J. L., Hirst, A. C. and Budd, W. (2011). The CSIRO Mk3L climate system model version 1.0 – Part 1: Description and evaluation. *Geoscientific Model Development* **4**: 483-509.

Phipps, S. J., Rotstayn, L. D., Gordon, H. B., Roberts, J. L., Hirst, A. C. and Budd, W. F. (2012). The CSIRO Mk3L climate system model version 1.0 - Part 2: Response to external forcings. *Geoscientific Model Development* **5**: 649-682.

Pongratz, J., Raddatz, T., Reick, C. H., Esch, M. and Claussen, M. (2009). Radiative forcing from anthropogenic land cover change since A.D. 800. *Geophysical Research Letters* **36** (2): L02709.

Pongratz, J., Reick, C., Raddatz, T. and Claussen, M. (2008). A reconstruction of global agricultural areas and land cover for the last millennium. *Global Biogeochem. Cycles* **22** (3): GB3018.

Prieto, M. R. (2007). ENSO signals in South America: rains and floods in the Parana River region during colonial times. *Climatic Change* **83** (1-2): 39-54.

Prieto, M. R. and Herrera, R. (2001). De sequías, hambrunas , plagas y “otras varias y continuas calamidades acaecidas en la Jurisdicción de Córdoba” durante el siglo XVIII. *Serie Economía y Sociedad. Cuadernos de Historia* **4**: 131-158.

Prieto, M. R., Herrera, R. and Dussel, P. (1999). Historical evidences of streamflow fluctuations in the Mendoza River, Argentina, and their relationship with ENSO. *Holocene* **9** (4): 473-481.

Prieto, M. R., Herrera, R. and Dussel, P. (2000). Archival evidence for some aspects of historical climate variability in Argentina and Bolivia during the 17th and 18th centuries. *Southern Hemisphere Paleo and Neo-Climates: Methods and Concepts*. P. P. Smolka and W. Volkheimer. Berlin, Springer: 127-142.

Prieto, M. R., Herrera, R., Dussel, P., Gimeno, L., Ribera, P., Garcia, R. and Hernandez, E. (2001). Interannual oscillations and trend of snow occurrence in the Andes region since 1885. *Australian Meteorological Magazine* **50** (2): 164-168.

Quinn, T. M., Crowley, T. J., Taylor, F. W., Henin, C., Joannot, P. and Join, Y. (1998). A multicentury stable isotope record from a New Caledonia coral: Interannual and decadal sea surface temperature variability in the southwest Pacific since 1657 AD. *Paleoceanography* **13** (4): 412-426.

Quinn, T. M., Taylor, F. W. and Crowley, T. J. (1993). A 173 year stable-isotope record from a tropical South-Pacific coral. *Quaternary Science Reviews* **12** (6): 407-418.

Quinn, T. M., Taylor, F. W. and Crowley, T. J. (2006). Coral-based climate variability in the Western Pacific Warm Pool since 1867. *Journal of Geophysical Research-Oceans* **111** (C11).

Quinn, W. H. and Neal, V. T. (1992). The historical record of El Niño events. *Climate since A.D. 1500*. R. Bradley and P. D. Jones. London, Routledge: 623-648.

Ramirez, E., Hoffmann, G., Taupin, J. D., Francou, B., Ribstein, P., Caillon, N., Ferron, F. A., Landais, A., Petit, J. R., Pouyaud, B., Schotterer, U., Simoes, J. C. and Stievenard, M. (2003). A new Andean deep ice core from Nevado Illimani (6350 m), Bolivia. *Earth and Planetary Science Letters* **212** (3-4): 337-350.

Rasbury, M. and Aharon, P. (2006). ENSO-controlled rainfall variability records archived in tropical stalagmites from the mid-ocean island of Niue, South Pacific. *Geochemistry Geophysics Geosystems* **7**: Q07010.

Rein, B. (2007). How do the 1982/83 and 1997/98 El Niños rank in a geological record from Peru? *Quaternary International* **161** (1): 56-66.

Reuter, J., Stott, L., Khider, D., Sinha, A., Cheng, H. and Edwards, R. L. (2009). A new perspective on the hydroclimate variability in northern South America during the Little Ice Age. *Geophys. Res. Lett.* **36** (21): L21706.

Roig, F. (1991). Dendrocronología y dendroclimatología del bosque de Pilgerodendron uviferum en su área norte de dispersión. *Bul. Soc. Argent. Bot.* **27**: 217-234.

Roig, F. and Boninsegna, J. (1990). Environmental factors affecting growth of Adesmia communities as determined from tree rings. *Dendrochronologia* **8**: 39-65.

Russell, A., McGregor, G. R. and Marshall, G. J. (2006). 340 years of atmospheric circulation characteristics reconstructed from an eastern Antarctic Peninsula ice core. *Geophysical Research Letters* **33** (8): L08702.

Russell, J. M. and Johnson, T. C. (2007). Little Ice Age drought in equatorial Africa: Intertropical Convergence Zone migrations and El Niño-Southern Oscillation variability. *Geology* **35** (1): 21-24.

Schmelter, A. (2000). Climatic response and growth-trends of Nothofagus pumilio along altitudinal gradients from arid to humid sites in northern Patagonia - A progress report. *Dendrochronología en América Latina*. F. Roig. Mendoza, Editorial Nacional de Cuyo: 193-215.

Schmidt, G. A., Jungclaus, J. H., Ammann, C. M., Bard, E., Braconnot, P., Crowley, T. J., Delaygue, G., Joos, F., Krivova, N. A., Muscheler, R., Otto-Bliesner, B. L., Pongratz, J., Shindell, D. T., Solanki, S. K., Steinhilber, F. and Vieira, L. E. A. (2011). Climate forcing reconstructions for use in PMIP simulations of the last millennium (v1.0). *Geoscientific Model Development* **4** (1): 33-45.

Schmidt, G. A., Jungclaus, J. H., Ammann, C. M., Bard, E., Braconnot, P., Crowley, T. J., Delaygue, G., Joos, F., Krivova, N. A., Muscheler, R., Otto-Bliesner, B. L., Pongratz, J., Shindell, D. T., Solanki, S. K., Steinhilber, F. and Vieira, L. E. A. (2012). Climate forcing reconstructions for use in PMIP simulations of the Last Millennium (v1.1). *Geosci. Model Dev.* **5** (1): 185-191.

Schmidt, G. A., Ruedy, R., Hansen, J. E., Aleinov, I., Bell, N., Bauer, M., Bauer, S., Cairns, B., Canuto, V., Cheng, Y., Del Genio, A., Faluvegi, G., Friend, A. D., Hall, T. M., Hu, Y., Kelley, M., Kiang, N. Y., Koch, D., Lacis, A. A., Lerner, J., Lo, K. K., Miller, R. L., Nazarenko, L., Oinas, V., Perlitz, J., Perlitz, J., Rind, D., Romanou, A., Russell, G. L., Sato, M., Shindell, D. T., Stone, P. H., Sun, S., Tausnev, N., Thresher, D. and Yao, M.-S. (2006). Present-Day Atmospheric Simulations Using GISS ModelE: Comparison to In Situ, Satellite, and Reanalysis Data. *Journal of Climate* **19** (2): 153-192.

Schneider, D. P., Steig, E. J. and van Ommen, T. (2005). High-resolution ice-core stable-isotopic records from Antarctica: towards interannual climate reconstruction. *Annals of Glaciology* **41**: 63-70.

Schurer, A., Hegerl, G., Mann, M. E., Tett, S. F. B. and Phipps, S. J. (2013). Separating forced from chaotic climate variability over the past millennium. *Journal of Climate*.

Smerdon, J., Kaplan, A., Chang, D. and Evans, M. (2010). A Pseudoproxy Evaluation of the CCA and RegEM Methods for Reconstructing Climate Fields of the Last Millennium. *Journal of Climate* **23** (18): 4856-4880.

Smith, T., Reynolds, R., Peterson, T. and Lawrimore, J. (2008). Improvements to NOAA's Historical Merged Land–Ocean Surface Temperature Analysis (1880–2006). *Journal of Climate* **21** (10): 2283-2296.

Solíz, C., Villalba, R., Argollo, J., Morales, M. S., Christie, D. A., Moya, J. and Pacajes, J. (2009). Spatio-temporal variations in Polylepis tarapacana radial growth across the Bolivian Altiplano during the 20th century. *Palaeogeography, Palaeoclimatology, Palaeoecology* **281** (3-4): 296-308.

Srur, A. M., Villalba, R., Villagra, P. E. and Hertel, D. (2008). Influences of climatic and CO₂ concentration changes on radial growth of Nothofagus pumilio in Patagonia. *Revista Chilena De Historia Natural* **81** (2): 239-256.

Steig, E., Ding, Q., White, J. W. C., Küttel, M., Rupper, S. B., Neumann, T. A., Neff, P., Gallant, A. J. E., Mayewski, P. A., Taylor, K. C., Hoffmann, G., Dixon, D. A., Schoenemann, S. W., Markle, B., Fudge, T. J., Schneider, D. P., A.J., S., Teel, R. T., Vaughn, B. H., Burgener, L., Williams, J. and Korotkikh, E. (2013). Recent climate and ice sheet changes in West Antarctica compared to the past 2000 years. *Nature Geoscience*: 10.1038/ngeo1778.

Steig, E. J., Mayewski, P. A., Dixon, D. A., Kaspari, S. D., Frey, M. M., Schneider, D. P., Arcane, S. A., Hamilton, G. S., Spikes, V. B., Albert, M., Meese, D., Gow, A. J., Shuman, C.

- A., White, J. W. C., Snead, S., Flaherty, J. and Wumkes, M. (2005). High-resolution ice cores from USITASE (West Antarctica): development and validation of chronologies and determination of precision and accuracy. *Annals of Glaciology*, Vol 41, 2005. **41**: 77-84.
- Steinhilber, F., Beer, J. and Fröhlich, C. (2009). Total solar irradiance during the Holocene. *Geophysical Research Letters* **36** (19): L19704.
- Stenni, B., Proposito, M., Gragnani, R., Flora, O., Jouzel, J., Falourd, S. and Frezzotti, M. (2002). Eight centuries of volcanic signal and climate change at Talos Dome (East Antarctica). *Journal of Geophysical Research-Atmospheres* **107** (D9): 4076.
- Szeicz, J. M., Lara, A., Díaz, S. and Aravena, J. C. (2000). Dendrochronological studies of Pilgerodendron uviferum in southern South America. *Dendrochronología en América Latina*. F. Roig. Mendoza, Editorial Nacional de Cuyo: 245-270.
- Taufetter, F., Oerter, H., Fischer, H., Weller, R. and Miller, H. (2004). Spatio-temporal variability in volcanic sulphate deposition over the past 2 kyr in snow pits and firm cores from Amundsenisen, Antarctica. *Journal of Glaciology* **50**: 137-146.
- Taulis, E. (1934). De la distribution des pluies au Chili. *Materiaux pour l'étude des calamités* **33**: 3-20.
- Taylor, K., Stouffer, R. and Meehl, G. (2012). An overview of CMIP5 and the experiment design. *Bulletin of the American Meteorological Society* **93**: 485-498.
- Therrell, M. D., Stahle, D. W., Ries, L. P. and Shugart, H. H. (2006). Tree-ring reconstructed rainfall variability in Zimbabwe. *Climate Dynamics* **26** (7-8): 677-685.
- Thomas, E. R., Dennis, P. F., Bracegirdle, T. J. and Franzke, C. (2009). Ice core evidence for significant 100-year regional warming on the Antarctic Peninsula. *Geophysical Research Letters* **36** (20): L20704.
- Thomas, E. R., Marshall, G. J. and McConnell, J. R. (2008). A doubling in snow accumulation in the western Antarctic Peninsula since 1850. *Geophysical Research Letters* **35** (1): L01706.
- Thompson, L., Mosley-Thompson, E., Brecher, H., Davis, M., Leo, B., Les , D., Lin, P. N., Mashioita, T. and Mountain, K. (2006). Abrupt tropical climate change: past and present. *Proceedings of the National Academy of Sciences* **103** (28).
- Thompson, L., Mosley-Thompson, E. and Morales Arnao, B. (1984). El Niño-Southern Oscillation events recorded in stratigraphy of the tropical Quelccaya Ice Cap. *Science* **276**: 50-52.
- Thompson, L. G., Peel, D., Mosley-Thompson, E., Mulvaney, R., Dai, J., Lin, P., Davis, M. and Rymond, C. (1994). Climate since AD 1510 on Dyer Plateau, Antarctica Peninsula: evidence for recent climate change. *Annals of Glaciology* **20**: 420–426.
- Trenberth, K. and Hurrell, J. (1994). Decadal atmosphere-ocean variations in the Pacific. *Climate Dynamics* **9**: 303-319.

- Tudhope, A., C., C., Mc Culloch, M., Cook, E., Chappell, J., R., E., Lea, D., Lough, J. and Shimmield, G. (2001). Variability in the El Nino Southern Oscillation through a glacial-interglacial cycle. *Science* **291**: 1511-1517.
- Urban, F., Cole, J. and Overpeck, J. (2000). Influence of mean climate change on climate variability from a 155-year tropical Pacific coral record. *Nature* **407**: 989-993.
- Van Ommen, T. D. and Morgan, V. (2010). Snowfall increase in coastal East Antarctica linked with southwest Western Australian drought. *Nature Geoscience* **3**: 267-272.
- Vieira, L. E. A. and Solanki, S. K. (2010). Evolution of the solar magnetic flux on time scales of years to millennia. *Astron. Astrophys.* **509**.
- Villalba, R. (1990a). Climatic Fluctuations in Northern Patagonia During the Last 1000 Years as Inferred from Tree-Ring Records. *Quaternary Research* **34** (3): 346-360.
- Villalba, R. (1990b). Latitude of the surface high-pressure belt over western South America during the last 500 years as inferred from tree-ring analysis. *Quaternary of South America and Antarctic Peninsula* **7**: 273-303.
- Villalba, R., Boninsegna, J. A., Veblen, T. T., Schmelter, A. and Rubulis, S. (1997a). Recent trends in tree-ring records from high elevation sites in the Andes of northern Patagonia. *Climatic Change* **36** (3-4): 425-454.
- Villalba, R., Cook, E., D' Arrigo, R., Jacoby, G., Jones, P., Salinger, M. and Palmer, J. (1997b). Sea-level pressure variability around Antarctica since A.D. 1750 inferred from sub-Antarctic tree-ring records. *Climate Dynamics* **13**: 375-390.
- Villalba, R., Cook, E. R., Jacoby, G. C., D'Arrigo, R. D., Veblen, T. T. and Jones, P. D. (1998). Tree-ring based reconstructions of northern Patagonia precipitation since AD 1600. *Holocene* **8** (6): 659-674.
- Villalba, R., Holmes, R. L. and Boninsegna, J. A. (1992). Spatial Patterns of Climate and Tree Growth Variations in Subtropical Northwestern Argentina. *Journal of Biogeography* **19** (6): 631-649.
- Villalba, R., Lara, A., Boninsegna, J. A., Masiokas, M., Delgado, S., Aravena, J. C., Roig, F. A., Schmelter, A., Wolodarsky, A. and Ripalta, A. (2003). Large-scale temperature changes across the southern Andes: 20th-century variations in the context of the past 400 years. *Climatic Change* **59** (1-2): 177-232.
- Villalba, R. and Veblen, T. T. (1997). Regional patterns of tree population age structures in northern Patagonia: Climatic and disturbance influences. *Journal of Ecology* **85** (2): 113-124.
- Vogel, C. H. (1989). A documentary-derived climatic chronology for South Africa, 1820–1900. *Climatic Change* **14** (3): 291-307.
- von Gunten, L., Grosjean, M., Rein, B., Urrutia, R. and Appleby, P. (2009). A quantitative high-resolution summer temperature reconstruction based on sedimentary pigments from Laguna Aculeo, Central Chile, back to AD 850. *Holocene* **19** (6): 873-881.

Wahl, E. R. and Smerdon, J. E. (2012). Comparative performance of paleoclimate field and index reconstructions derived from climate proxies and noise-only predictors. *Geophys. Res. Lett.* **39** (6): L06703.

Wang, Y.-M., Lean, J. L. and Sheeley Jr., N. R. (2005). Modeling the Sun's Magnetic Field and Irradiance since 1713. *Astrophysical Journal* **625**: 522-538.

Wolff, C., Haug, G. H., Timmermann, A., Damsté, J. S. S., Brauer, A., Sigman, D. M., Cane, M. A. and Verschuren, D. (2011). Reduced Interannual Rainfall Variability in East Africa During the Last Ice Age. *Science* **333** (6043): 743-747.

Xiao, C., Mayewski, P., Qin, D., Li, Z., Zhang, M. and Yan, Y. (2004). Sea level pressure variability over the southern Indian Ocean inferred from a glaciochemical record in Princess Elizabeth Land, east Antarctica. *J. Geophys. Res.* **109** (D16): D16101.

Xin, X.-G., Wu, T.-W. and Zhang, J. (2013). Introduction of CMIP5 experiments carried out with the climate system models of Beijing Climate Center. *Advances in Climate Change Research* **4** (1): 41-49.

Xiong, L. and Palmer, J. (2000). Reconstruction of New Zealand Temperature Back to AD 1720 Using Libocedrus Bidwillii Tree rings. *Climate Change* **45**: 339-359.

Yongqiang, Y., Rucong, Y., Xuehong, Z. and Hailong, L. (2002). A flexible coupled ocean-atmosphere general circulation model. *Advances in Atmospheric Sciences* **19** (1): 169-190.

Yongqiang, Y., Xuehong, Z. and Yufu, G. (2004). Global coupled ocean-atmosphere general circulation models in LASG/IAP. *Advances in Atmospheric Sciences* **21** (3): 444-455.

Zinke, J., Dullo, W. C., Heiss, G. A. and Eisenhauer, A. (2004). ENSO and Indian Ocean subtropical dipole variability is recorded in a coral record off southwest Madagascar for the period 1659 to 1995. *Earth and Planetary Science Letters* **228** (1-2): 177-194.

Zinke, J., Pfeiffer, M., Timm, O., Dullo, W. and Brummer, G. (2009). Western Indian Ocean marine and terrestrial records of climate variability: a review and new concepts on land-ocean interactions since AD 1660. *International Journal of Earth Sciences* **98**: 115-133.

Inter-hemispheric temperature variability over the past millennium

Raphael Neukom^{1,2*}, Joëlle Gergis³, David J. Karoly^{3,4}, Heinz Wanner¹, Mark Curran^{5,6}, Julie Elbert¹, Fidel González-Rouco⁷, Braddock K. Linsley⁸, Andrew D. Moy^{5,6}, Ignacio Mundo^{9,10}, Christoph C. Raible^{1,11}, Eric J. Steig¹², Tas van Ommen^{5,6}, Tessa Vance⁶, Ricardo Villalba⁹, Jens Zinke^{13,14} and David Frank^{1,2}

¹ Oeschger Centre for Climate Change Research, University of Bern, 3012 Bern, Switzerland

² Swiss Federal Research Institute WSL, Zürcherstrasse 111, CH-8903 Birmensdorf, Switzerland

³ School of Earth Sciences, University of Melbourne, VIC 3010, Australia

⁴ ARC Centre of Excellence for Climate System Science, University of Melbourne, VIC 3010, Australia

⁵ Department of the Environment, Australian Antarctic Division, Kingston, Tasmania 7050, Australia

⁶ Antarctic Climate & Ecosystems Cooperative Research Centre, University of Tasmania, Hobart, Tasmania, 7000, Australia

⁷ Departamento Astrofísica y CC de la Atmósfera, Instituto de Geociencias (CSIC-UCM) Universidad Complutense de Madrid, Madrid, 28040, Spain

⁸ Lamont-Doherty Earth Observatory, Columbia University, Palisades, NY 10964, USA

⁹ Instituto Argentino de Nivología, Glaciología y Ciencias Ambientales (IANIGLA), CCT CONICET-Mendoza, 5500, Argentina

¹⁰ LISEA, Facultad de Ciencias Agrarias y Forestales, Universidad Nacional de La Plata, B1900 La Plata, Argentina

¹¹ Climate and Environmental Physics, University of Bern, 3012 Bern, Switzerland

¹² Quaternary Research Center and Department of Earth and Space Sciences, University of Washington, Seattle, WA 98195, USA

¹³ School of Earth and Environment, University of Western Australia Oceans Institute, 35 Stirling Highway, Crawley WA 6009, Australia

¹⁴ Australian Institute of Marine Science, Nedlands WA 6009, Australia

*Corresponding author

Raphael Neukom

Now at institute of Geography, University of Zurich, Switzerland

Email: neukom@giub.unibe.ch

Contents

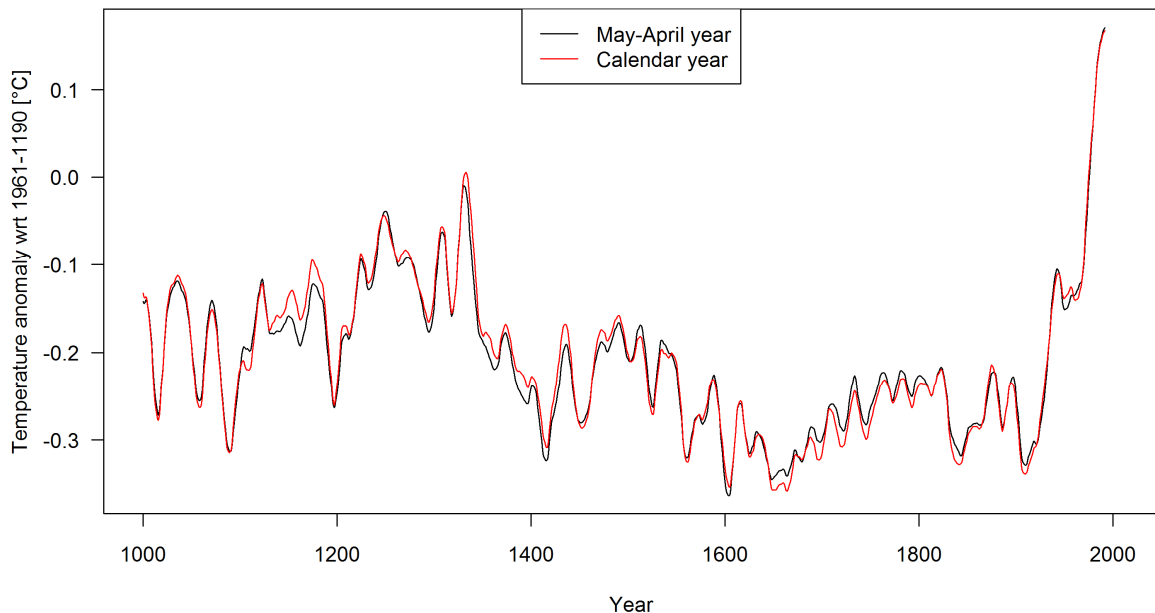
1.	Data processing and predictor selection.....	3
1.1.	Instrumental Data.....	3
1.2.	Proxy database	4
1.2.1.	Tree-ring records.....	5
1.2.2.	Subannually resolved coral records.....	5
1.2.3.	Documentary records	5
1.3.	Predictor selection.....	10
1.4.	Missing values 1911-1990	12
2.	Ensemble reconstruction.....	17
2.1.	Reconstruction methodology	17
2.2.	Ensemble parameters	17
2.3.	Required number of ensemble members	21
2.4.	Reconstruction uncertainties	23
2.5.	Unfiltered SH mean reconstruction.....	24
3.	Reconstruction reliability.....	26
3.1.	Reconstruction skill	26
3.1.1.	Ensemble validation	27
3.1.2.	Ensemble mean early verification	27
3.1.3.	Ensemble mean verification and calibration years	28
3.1.4.	Ensemble mean RMSE.....	28
3.1.5.	Noise predictors.....	28
3.1.6.	Ensemble vs. single reconstruction	30
3.2.	Reconstruction robustness.....	32
3.2.1.	Alternative reconstruction methods: CPS.....	32
3.2.2.	Alternative reconstruction methods: LNA.....	34
3.2.3.	Influence of changes in proxy replication.....	37
3.2.4.	Influence of different proxy screening approaches.....	41
3.2.5.	Influence of different proxy archives	42
3.2.6.	Influence of individual proxy records.....	44
3.2.7.	Ensemble median vs. mean	46
3.3.	Conclusions.....	47
4.	Sensitivity to instrumental target data.....	48
5.	NH reconstruction ensemble.....	49
6.	Simultaneous extreme periods	50
7.	Details on climate model simulations	51
8.	Lag between the hemispheres	54
9.	Alternative reference period and comparison with earlier SH and regional reconstructions.....	55
10.	Alternative illustrations of inter-hemispheric differences	59
10.1.	Inter-model comparisons.....	59
10.2.	Raw vs. detrended data.....	61
10.3.	Bimodal distribution in Figure 4b	62
10.4.	Outlier in the model simulations (Figures 4b and 4c)	63
11.	NH-SH differences in the individual model simulations.....	64
12.	References	88

1. Data processing and predictor selection

1.1. Instrumental Data

We use the Goddard Institute for Space Studies surface temperature analysis (GISTEMP) combined land and ocean temperature grid (Hansen *et al.*, 2010) as target data for our reconstructions. The version allowing for a search radius of 1200 km for the temperature station measurements of each grid cell is used (details see Hansen *et al.*, 2010). We use the latitude weighted spatial average of all grid cells south of the equator as the reconstruction target.

We choose the May to April year as the target seasonal window, because phase changes in ENSO, typically occur in austral autumn (Karoly, 1989; Trenberth and Hurrell, 1994; Karoly *et al.*, 1996; Karoly and Vincent, 1998). Also, calendar years are not an optimal window for Southern Hemisphere (SH) reconstructions because the tree-ring growing season in the SH extends over two calendar years during austral summer. Supplementary Figure 1 compares our final reconstruction using a May-April target seasonal window to a reconstruction using a calendar year mean target. The two reconstructions are very similar, and so the choice of the target seasonal window does not affect our conclusions.



Supplementary Figure 1 | Reconstruction based on different target seasons. Comparison of our reconstruction using May-April averages for the instrumental target data (black) and a calendar year average (red).

1.2. Proxy database

As a basis for our proxy selection we use the SH proxy network presented by Neukom and Gergis (2012). Additionally, new records are added to the network (details and references see Supplementary Tables 1-4): Laguna Pumacocha and Lake Challa Sediments, the high resolution sections (<5 years) of El Junco Lake, Lake Edward and Lake Masoko, a new documentary record from New South Wales and sea salt from an ice core at Law Dome, Antarctica.

Some tree-ring records from South America that were used in Neukom and Gergis (2012) had to be excluded because of lack of permission from the original authors to make the chronologies publicly available (Supplementary Table 1). Correlations of all proxies with the dominant climate modes of the SH in the May to April window are provided by Neukom and Gergis (2012).

The most important details of proxy data preparation are summarized in the following paragraphs. For further details we refer to Neukom & Gergis (2012).

1.2.1. Tree-ring records

Tree-ring records from individual sites are grouped into regional composites where possible. This grouping strengthens the common signal, reduces the number of records from more than 200 to 84 and improves the balance of records from different climate archives. All composite records are listed in Supplementary Table 1, and the individual sub-chronologies that were aggregated into the composites are listed in Table S1 in Neukom & Gergis (2012). All tree-ring chronologies are established using either signal free detrending (Melvin *et al.*, 2007; Melvin and Briffa, 2008) or negative exponential curves. In order to avoid reconstruction biases based on the detrending method, we randomly choose between one of the two methods for each tree-ring record and ensemble member (see below, section 2.2). Years where less than five samples are available or where the expressed population signal (EPS; Briffa and Jones, 1990) is <0.85 are excluded.

1.2.2. Subannually resolved coral records

All coral records with higher than annual resolution are averaged over the May to April window. All coral records are listed in Supplementary Table 2.

1.2.3. Documentary records

Some documentary records did not originally cover the 20th century (Supplementary Table 4). In order to be able to calibrate them, we extend them to present using the “pseudo documentary” approach described by Neukom et al. (2009; 2013). In this approach, the representative instrumental data for each record are degraded with white noise and then classified into the index categories of the documentary record in order to realistically mimic its statistical properties and not overweight the record in the multiproxy calibration process. The amount of noise to be added is determined based on the overlap correlations with the instrumental data. In order to avoid potential biases by using only one iteration of noise-

degrading, we create 1,000 “pseudo documentaries” for each record and randomly sample one realization for each ensemble member (see below, Section 2.2). All documentary records are listed in Supplementary Table 4.

Supplementary Table 1 (next page) | Metadata of the available tree-ring records (before the proxy screening). Site name, longitude ($^{\circ}$ E), latitude ($^{\circ}$ N), altitude (m.a.s.l.), start year (Common Era CE), end year (CE), species code, sample depth, number of sub-sites for composite records, reference(s). Updated from Neukom & Gergis (2012). The red shaded records are excluded from the reconstructions because of lack of permission to publish the final chronology.

SiteName	Lon	Lat	Alt	Start	End	Species	n	Subs	Reference(s)
Africa									
Zimbabwe	27.33	-18.5	1000	1875	1996	PTAN	36		Therrell et al. (2006)
Die Bos, South Africa	19.2	-32.4		1763	1976	WICE	55		Dunwiddie and LaMarche (1980)
Australasia									
Teak Indonesia	111	-7		1780	2005	TEGR	239		D'Arrigo et al. (2006)
Northern Territory Callitris	132	-13		1896	2006	CAIN	54		Baker et al. (2008)
Western Australia Callitris	120.8	-33.03	300	1758	2005	CACO	37		Cullen et al. (2009)
Kauri NZ	174	-36	200	1577	2002	AGAU	527		Cook et al. (2006), Fowler et al. (2008)
Baw Baw Victoria	148.3	-36.42	2000	1818	2002	EUPA	223		Brookhouse et al. (2008)
Urewera NZ	177.2	-38.68	930	1462	1987	LIBI	68		Xiong and Palmer (2000)
North Island LIBI Composite 2	174.1	-39.27	1000	1651	1990	LIBI	129	2	Xiong and Palmer (2000)
Mangawhero NZ	175.5	-39.35	1000	1551	1994	LGCO	56		D'Arrigo et al. (2000)
North Island LIBI Composite 1	175.5	-39.5	1100	1526	1992	LIBI	235	5	Xiong and Palmer (2000)
Takapari NZ	176	-40.07	960	1533	1992	LIBI	63		Xiong and Palmer (2000)
Moa Park NZ	172.9	-40.93	1036	1623	1991	LIBI	49		Xiong and Palmer (2000)
Flanagan's Hut NZ	172.6	-41.27	950	1776	1991	LIBI	33		Xiong and Palmer (2000)
CTP East Tasmania	148	-42	600	1430	1994	PHAS	165	2	Allen et al. (2001)
CTP West Tasmania	146	-42	600	1547	1998	PHAS	301	8	Allen et al. (2001), Allen (2002), LaMarche et al. (1979c)
Mount Read Tasmania	147	-42	600	494	1999	LGFR	317		Cook et al. (2000), Cook et al. (2006)
Pink Pine NZ	172	-42		1457	1999	HABI	356	7	Duncan et al. (2010)
Buckley's Chance Tasmania	145.9	-42.26	900	1463	1991	LGFR	84		Buckley et al. (1997)
Oroko Temperature recon	170.3	-43.23	110	1	2003	LGCO	330		Cook et al. (2006)
Stewart Island NZ	168	-47	450	1758	1993	HABI	106	3	D'Arrigo et al. (1995), D'Arrigo et al. (2000)
South America									
ALT Composite 1	-69	-17.5	4300	1872	2002	POTA	77	3	Soliz et al. (2009)
ALT Composite 2	-69.08	-18.45	4730	1542	2002	POTA	78	2	Soliz et al. (2009), Christie et al. (2009b)
ALT Composite 3	-67.5	-21.5	4500	1630	2003	POTA	214	6	Argollo et al. (2004), Soliz et al. (2009), Morales et al. (2004)
La Meseda	-65.02	-23	1600	1822	1999	CELI	23		unpublished (R. Villalba pers. comm. 2007)
NWA Composite 1	-65	-23	1200	1899	1998	JGAU	35	2	Villalba et al. (1992)
NWA Composite 4	-65	-24	1750	1858	1981	CEAN	50	2	Villalba et al. (1992)
NWA Composite 2	-65	-24	2200	1858	1995	ALAC, CELI, JGAU	126	4	Villalba et al. (1992), Morales et al. (2004)
Rio Sala and Popayan	-64.6	-24.6	700	1879	2002	JGAU	39		Villalba et al. (1992)
NWA Composite 5	-65.5	-25	2000	1874	2001	JGAU	92	3	Villalba et al. (1992)
Dique Escaba	-65.78	-27.7	900	1877	1985	JGAU	24		Villalba et al. (1992)
EI Asiento	-70.82	-32.48	1800	1515	1972	AUCH	65		La Marche et al. (1979b)
Le Quesne precip recon	-70.5	-34	1700	1200	2000	AUCH	525	7	Le Quesne et al. (2006)
CAN Composite 1	-70.5	-34.5	1200	1520	1975	AUCH	165	3	La Marche et al. (1979b)
Vilches	-71.03	-35.6	1530	1873	1996	NOPU	49		Lara et al. (2001)
Christie AUCH Composite	-71.3	-37	1135	1346	2004	AUCH	511	5	Christie et al. (2009a)
Huinganco	-70.6	-37.75	1400	1673	2000	AUCH	101		La Marche et al. (1979a)
CAN Composite 2	-71	-37.83	1530	1714	2006	ARAR	83	3	La Marche et al. (1979a), Mundo et al. (2012)
CAN Composite 3	-71.25	-38	1570	1868	1975	ARAR	41	2	La Marche et al. (1979a)
Volcan Lonquimay	-71.57	-38.38	1510	1700	1975	ARAR	47		La Marche et al. (1979b)
CAN Composite 6	-71.5	-38.5	1400	1435	2006	ARAR	357	8	La Marche et al. (1979a), Villalba (1990a), Mundo et al. (2012)
CAN Composite 5	-71.58	-38.62	1640	1843	1996	NOPU	76	2	Lara et al. (2001)
Pino Hachado	-70.75	-38.63	1400	1767	1974	ARAR	31		La Marche et al. (1979a)
Conguillio (Lenga abajo)	-71.6	-38.63	1490	1788	1996	NOPU	55		Lara et al. (2001)
CAN Composite 4	-71.5	-39	1500	1807	1994	NOPU	120	4	Lara et al. (2001), Schmelter (2000)
CAN Composite 8	-71.17	-39.17	1125	1773	1989	AUCH	69	2	Villalba and Veblen (1997)
CAN Composite 31	-71.3	-39.2	1168	1731	2006	ARAR	83	2	Mundo et al. (2012)
Lago Rucachoroi	-71.17	-39.22	1330	1721	1976	AUCH	26		La Marche et al. (1979a)
CAN Composite 9	-71.25	-39.33	1100	1636	2006	ARAR	283	6	La Marche et al. (1979a), Mundo et al. (2012)
CAN Composite 10	-70.83	-39.5	1320	1784	1989	ARAR, AUCH	44	2	La Marche et al. (1979a), Villalba and Veblen (1997)
CAN Composite 12	-71	-40	800	1645	1992	AUCH	175	5	La Marche et al. (1979b), Villalba and Veblen (1997)
Chapelo	-71.23	-40.33	1700	1814	1985	NOPU	29		ITRDB series arge029
CAN Composite 11	-72.32	-40.62	805	1567	2002	PLUV	146	3	Lara et al. (2008)
Paso Cordova	-71.25	-40.67	1890	1811	1986	NOPU	37		ITRDB series arge050
CAN Composite 13	-71.25	-41	1000	1532	2003	AUCH	360	11	Villalba and Veblen (1997), Lara et al. (2008)
CAN Composite 16	-71.8	-41.13	1500	1857	1991	NOPU	43	2	Villalba et al. (1997b)
CAN Composite 14	-71.8	-41.13	1500	1859	1994	NOPU	79	3	Villalba et al. (1997b), Schmelter (2000)
CAN Composite 17	-71.83	-41.17	1700	1892	1994	NOPU	55	3	Villalba et al. (1997b), Schmelter (2000)
CAN Composite 15	-71.92	-41.17	1300	1582	1991	NOPU	102	4	Villalba et al. (1997b)
CAN Composite 19	-72.27	-41.17	1225	1858	1998	NOPU	130	2	Lara et al. (2005)
CAN Composite 18	-71.5	-41.25	1550	1639	1994	NOPU	113	3	Schmelter (2000)
CAN Composite 20	-71.83	-41.33	900	1117	1995	FICU	184	4	Villalba (1990b), Lara et al. (2000)
CAN Composite 21	-71.5	-41.5	670	1790	1991	AUCH	38	2	Villalba and Veblen (1997)
CAN Composite 22	-71.75	-41.75	1300	1720	1994	NOPU	71	3	Villalba et al. (1998), Schmelter (2000)
CAN Composite 23	-71.83	-42	1220	1204	1993	FICU	60	2	Lara et al. (2000)
CAN Composite 24	-71.33	-42.5	765	1749	2002	AUCH	33	2	La Marche et al. (1979a), Lara et al. (2008)
CAN Composite 26	-73.83	-42.5	750	1794	1987	FICU, PLUV	60	2	Villalba (1990a), Roig (1991)
CAN Composite 25	-71.83	-42.5	550	769	1990	FICU	137	3	Lara et al. (2000)
Santa Lucia	-72.5	-43	540	1680	1986	PLUV	60		Szeicz et al. (2000)
Cisnes	-71.7	-44.65	1100	1834	1997	NOPU	54		Lara et al. (2005)
Puesto Miraflores	-72.15	-48.45	1039	1755	1998	NOPU	23		Unpublished (R. Villalba pers. comm. 2010)
CAN Composite 32	-72.25	-48.45	945	1730	2007	NOPU	88	2	Villalba et al. (2003)
O Higgins	-72.5	-48.5	1200	1886	1999	NOPU	24		Lara et al. (2005)
CAN Composite 27	-72	-49	800	1715	2002	NOPU	199	3	Boninsegna et al. (1989), Sru et al. (2008)
El Chalten bajo	-72.9	-49.37	760	1826	2003	NOPU	100		Sru et al. (2008)
CAN Composite 33	-73.33	-49.45	775	1726	2007	NOPU	125	3	Villalba et al. (2003), unpublished (R. Villalba pers. comm. 2010)
Torre Morena 4	-73.5	-49.5	658	1798	2007	NOPU	42		Unpublished (R. Villalba pers. comm. 2010)
Valle Ameghino	-72.17	-50.42	700	1766	1997	NOPU	41		Masiokas and Villalba (2004)
CAN Composite 34	-73.7	-50.6	461	1795	2007	NOPU	67	2	Unpublished (R. Villalba pers. comm. 2010)
Heim Morena Este	-73.7	-50.6	650	1806	2007	NOPU	33		Unpublished (R. Villalba pers. comm. 2010)
CAN Composite 30	-70	-53	220	1851	1986	NOPU	128	2	Aravena et al. (2002)
SAN Composite 5	-67.67	-54.75	600	1718	1984	NOBE	131	4	Boninsegna et al. (1989)
Puerto Parryn	-64.37	-54.83	20	1893	1986	NOBE	25		Boninsegna et al. (1989)
SAN Composite 6	-64.33	-54.83	40	1781	1986	NOBE	49	2	Boninsegna et al. (1989)

Supplementary Table 2 | Metadata of the available coral records (before the proxy screening). Site name, longitude ($^{\circ}$ E), latitude ($^{\circ}$ N), start year (CE), end year (CE), species, temporal resolution, proxy variable(s), reference(s). Updated from Neukom & Gergis (2012).

SiteName	Longitude	Latitude	Start	End	Species	Resolution	Proxy	Reference(s)
<i>Indian Ocean</i>								
Malindi	40.00	-3.00	1801	1994	Porites lutea	Annual	d18O	Cole et al. (2000)
Mafia, Tanzania	40.00	-8.00	1622	1998	Diplastrea heliopora	Monthly	d18O	Damassa et al. (2006)
Ifaty, Madagascar 1	43.00	-23.00	1882	1994	Porites lutea	Annual	d18O, Sr/Ca	Unpublished (J. Zinke pers. comm.)
Ifaty, Madagascar 4	43.58	-23.15	1858	2007	Porites lutea	Bim., ann.	d18O, Sr/Ca	Zinke et al. (2004), unpublished (J. Zinke pers. comm.)
Mayotte	45.10	-12.65	1865	1993	Porites solida	Bimonthly	d18O	Zinke et al. (2009)
La Reunion	55.25	-21.03	1832	1995	Porites	Bimonthly	d18O	Pfeiffer et al. (2004)
Seychelles	55.80	-4.62	1846	1995	Porites lutea	Monthly	d18O	Charles et al. (1997), Abram et al. (2008)
Rodrigues	63.00	-19.00	1789	2005	Porites	Ann., mon.	d18O, Sr/Ca	Unpublished (J. Zinke pers. comm.)
Mentawai West Sumatra	98.50	-4.00	1858	1997	Porites	Monthly	d18O	Abram et al. (2008)
Abrolhos	113.77	-28.45	1794	1993	Porites lutea	Bimonthly	d18O	Kuhnert et al. (1999)
Ningaloo	113.97	-21.90	1878	1995	Porites lutea	Seasonal	d18O	Kuhnert et al. (2000)
Bali	115.00	-8.00	1783	1990	Porites	Monthly	d18O	Charles et al. (2003)
Bunaken	123.00	2.80	1863	1990	Porites	Monthly	d18O	Charles et al. (2003)
<i>Pacific Ocean</i>								
Laing	144.88	-4.15	1884	1993	Porites	Seasonal	d18O	Tudhope et al. (2001)
Guam	145.00	13.00	1790	2000	Porites lobata	Monthly	d18O	Asami et al. (2005)
Madang Lagoon	145.82	-5.22	1880	1993	Porites	Seasonal	d18O	Tudhope et al. (2001)
Great Barrier Reef precip recon	147.00	-18.00	1630	1981	Porites	Annual	Luminescence	Lough (2011)
Kavieng, Papua New Guinea	150.50	-2.50	1823	1997	Porites	Monthly	Sr/Ca, Ba/Ca	Alibert and Kinsley (2008a,b)
Rabaul	152.00	-4.00	1867	1997	Porites	Monthly	d18O, Sr/Ca	Quinn et al. (2006)
Abraham	153.00	-20.00	1638	1983	Porites	Annual	d18O	Druffel and Griffin (1999)
Nauru	166.00	-0.83	1897	1995	Porites lutea	Seasonal	d18O	Guilderson et al. (1999)
Amedee New Caledonia	166.45	-22.48	1657	1992	Porites lutea	Seasonal	d18O	Quinn et al. (1998)
Vanuatu	167.00	-15.00	1806	1979	Platygya	Annual	d18O	Quinn et al. (1993)
Tarawa	172.00	1.00	1893	1989	Hydropora microconos	Monthly	d18O	Cole et al. (1993)
Maiana	173.00	1.00	1840	1994	Porites spp.	Bimonthly	d18O	Urban et al. (2000)
Fiji 1F	179.23	-16.82	1780	1997	Porites lutea	Monthly	d18O, Sr/Ca	Linsley et al. (2004)
Fiji AB	179.23	-16.82	1617	2001	Porites lutea	8/year	d18O	Linsley et al. (2006)
Savusau, Fiji	179.23	-16.82	1776	2001	Diplastrea heliopora	Annual	d18O	Bagnato et al. (2005)
Tonga TNI2	-174.82	-20.27	1849	2004	Porites lutea	8/year	d18O	unpublished
Tonga TH1	-174.72	-19.93	1794	2004	Porites lutea	Annual	d18O	unpublished
Palmyra Island	-162.13	5.87	1886 ^a	1998	Porites	Monthly	d18O, Sr/Ca	Cobb et al. (2003), Nurhati et al. (2011)
Rarotonga 3R	-159.83	-21.23	1874	2000	Porites	Seasonal	d18O	Linsley et al. (2006), Linsley et al. (2008)
Rarotonga	-159.83	-21.23	1761	1996	Porites	Seas., mon.	d18O, Sr/Ca	Linsley et al. (2006), Linsley et al. (2008)
Moorea	-149.83	-17.50	1852	1990	Porites lutea	Annual	d18O	Boiseau et al. (1999)
Clipperton Atoll	-109.22	10.30	1893	1994	Porites lobata	Monthly	d18O	Linsley et al. (2000a)
Urvina, Galapagos Islands	-91.23	-0.03	1607	1981	Pavona clavus	Annual	d18O	Dunbar et al. (1994)
Secas	-82.05	7.00	1707	1983	Porites	Seasonal	d18O	Linsley et al. (1994)

^a Non-continuous fossil d18O sequences extend back to AD 928

Supplementary Table 3 | Metadata of the available ice records (before the proxy screening). Site name, longitude (°E), latitude (°N), altitude (m.a.s.l.), start year (CE), end year (CE), proxy variable(s), reference(s). Updated from Neukom & Gergis (2012).

SiteName	Longitude	Latitude	Altitude	Start	End	Proxy	Reference(s)
<i>South America</i>							
Quelccaya	-70.83	-13.93	5670	488	2003	d18O, accumulation	Thompson et al. (1984, 2006)
Illimani	-67.78	-16.65	6300	1750	1998	dD, NH ₃	Hoffmann et al.(2003), Ramirez et al. (2003), Kellerhals et al. (2010)
<i>Antarctica</i>							
James Ross Island	-58.13	-64.37	1640	1791	2000	dD	Aristarain et al. (2004)
Law Dome	112.80	-66.77	1370	179 ^a	2005	d18O, accumulation, Na, sss, chem. species. PC1	VanOmmen & Morgan. (2010), Unpublished (M. Curran, T. Vance, A. Moy & T. van Ommen pers. comm.)
Dyer Plateau	-54.50	-70.66	2002	1505	1988	d18O	Thompson et al. (1994)
Princess Elizabeth Land	77.1	-70.85	1850	1745	1996	d18O, accumulation, chem. species. PC1	Xiao et al. (2004)
Dollman	-61.55	-70.97	398	1652	1992	d18O, chem. species. PC1	Russell et al. (2006)
Talos	159.10	-72.80	2316	1217	1996	dD	Stenni et al. (2002)
Gomez	-70.35	-73.60	1400	1854	2006	d18O, accumulation	Thomas et al. (2008, 2009)
Dronning Maud Land	0.00	-75.00	2900	1025	1997	d18O, accumulation, Na	Graf et al. (2002), Taufetter et al. (2004)
Siple Station	-84.15	-75.92	1054	1417	1983	d18O	Moseley-Thompson et al. (1990)
ITASE 2001 5	-89.14	-77.06	1239	1779	2000	d18O	Schneider et al. (2005)
ITASE 2000 5	-124.00	-77.67	1828	1800	1999	d18O	Schneider et al. (2005)
ITASE 2001 2	-102.91	-77.84	1336	1891	2001	d18O	Steig et al. (2005)
ITASE 2000 4	-120.08	-78.08	2595	1794	1999	d18O	Steig et al. (2005)
ITASE 2001 3	-95.65	-78.12	1620	1858	2000	d18O	Steig et al. (2005)
Vostok Pits	106.83	-78.45	3500	1774	1999	d18O, accumulation	Eckaykin et al. (2004)
WDC05A	-112.13	-79.46	1759	1775	2004	Accumulation	Banta et al. (2008)
WDC05Q	-112.09	-79.47	1759	1521	2004	Accumulation	Banta et al. (2008)
Berkner Island	-45.72	-79.61	886	1000	1994	d18O, accumulation	Mulvaney et al. (2002)
ITASE 2000 1	-111.38	-79.63	1791	1800	1999	d18O, accumulation	Schneider et al. (2005), Banta et al. (2008)
ITASE 1999 1	-122.63	-80.62	1350	1723	1999	d18O	Steig et al. (2005)
Siple Dome A	-148.81	-81.65	615	1000	1993	dD	Steig et al. (2013)
Siple Dome B	-148.81	-81.65	615	1654	1994	d18O	Steig et al. (2013)
Siple Dome Na	-148.81	-81.65	615	0	1980	Na	Mayewski et al. (2004)
ITASE 2002 2	-104.99	-83.50	1957	1894	2001	d18O	Jacobel et al. (2005)
ITASE 2002 4	-107.99	-86.50	2586	1593	1997	d18O	Jacobel et al. (2005)

^a Only d18O goes back to AD 179, the other proxies are available back to the 11th or 13th century

Supplementary Table 4 | Metadata of the available documentary, sediment and speleothem records (before the proxy screening). Site name, longitude ($^{\circ}$ E), latitude ($^{\circ}$ N), start year (CE), end year (CE), proxy variable, reference(s). Updated from Neukom & Gergis (2012).

SiteName	Longitude	Latitude	Start	End	Proxy	Reference(s)
<i>Documentary - Africa</i>						
Southem Kalahari precipitaiton ^a	26.00	-25.00	1815	2002	Historical documents	Nash & Endfield (2008), Neukom et al. (2013)
Namaqualand precipitaiton ^a	17.00	-29.00	1817	1997	Historical documents	Kelso & Vogel (2007), Neukom et al. (2013)
Lesotho precipitaiton ^a	27.50	-29.50	1824	1994	Historical documents	Nash & Grab (2010), Neukom et al. (2013)
Eastern Cape South Africa precipitaiton ^a	24.50	-34.00	1821	2007	Historical documents	Vogel (1989), Neukom et al. (2013)
Southem Cape South Africa precipitaiton ^a	20.00	-34.00	1821	1996	Historical documents	Vogel (1989), Neukom et al. (2013)
<i>Documentary - South America</i>						
Peru ENSO index	-79.02	-8.10	1550	1990	Historical documents	Garcia-Herrera et al. (2008), Quinn & Neal (1992)
Potosi precipitation ^a	-65.75	-19.58	1585	2005	Historical documents	Gioda & Prieto (1999)
Rio Sali / Rio Dulce streamflow ^a	-65.00	-27.00	1750	1977	Historical documents	Herrera et al. (2003)
Tucuman precipitaiton ^a	-65.00	-27.03	1548	2005	Historical documents	Prieto et al. (2000)
Santiago del Estero precipitaiton ^a	-64.27	-27.77	1750	2005	Historical documents	Herrera et al. (2003)
Santa Fe and Corrientes precipitation ^a	-60.00	-30.00	1590	2006	Historical documents	Prieto (2007)
Rio Parana streamflow ^a	-60.00	-30.00	1590	1994	Historical documents	Prieto (2007)
Cordoba precipitaiton ^a	-64.00	-31.00	1700	2005	Historical documents	Prieto & Herrera (2001)
Mendoza precipitaiton	-68.00	-32.00	1600	1985	Historical documents	Prieto et al. (2000)
Rio Mendoza streamflow ^a	-68.00	-32.00	1601	2000	Historical documents	Prieto et al. (1999)
Central Andes snow depth	-70.00	-33.00	1760	1996	Historical documents	Neukom et al. (2009)
Central Andes snow occurrence	-70.00	-33.00	1885	1996	Historical documents	Prieto et al. (2001)
Santiago de Chile precipitaiton ^a	-70.78	-33.38	1540	2006	Historical documents	Taulis (1934)
<i>Documentary - Australia</i>						
NSW precipitation	115.20	-33.90	1788	2008	Historical documents	Fenby & Gergis (2013)
<i>Lake Sediment</i>						
Lake Edward	29.75	-0.4	920 ^b	1974	Mg/Ca ratio	Russell & Johnson (2007)
El Junco Lake	-89.5	-0.9	1791 ^b	2004	Diatoms	Conroy et al. (2009)
Lake Challa	37.75	-3.3	-1050	2005	Varve thickness	Wolff et al. (2011)
Lake Masoko	33.75	-9.35	1779 ^b	2002	Magnetic susceptibility	Garcin et al. (2007)
Laguna Pumacocha	-76.1	-10.75	-277	2007	d18O	Bird et al. (2011)
Laguna Aculeo	-70.90	-33.83	856	1997	Pigment reflection	von Gunten et al. (2009)
Lago Puyehue	-72.45	-40.65	1408	1997	Varve thickness	Boes & Fagel (2008)
Lago Plomo	-72.87	-46.98	1530	2000	Mass accumulation rate	Elbert et al. (2011)
<i>Marine Sediment</i>						
106KL off Peruvian Coast	-77.67	-12.05	-13550	2000	Lithics concentration	Rein (2007)
Cariaco Basin	-64.77	10.75	1222	1990	Mg/Ca	Black et al. (2007)
<i>Speleothem</i>						
Avaiki Cave, Niue	-169.83	-19.00	1829	2001	Lamina thickness	Rasbury & Aharon (2006)
Cascayunga Cave, Peru	-77.20	-6.05	1089	2005	d18O	Reuter et al. (2009)

^a The documentary record ends in the 19th or early 20th century and was extended to present using "pseudo documentaries" (see Neukom et al. 2009 and Neukom et al. 2013)

^b Only the high resolution section (<5 years) is used

1.3. Predictor selection

The predictors for the reconstructions are selected based on their local correlations with the target grid. We use the domain covering 55° S- 10° N and all longitudes for the proxy screening. High latitude regions of the grid are excluded from the correlation analysis because south of 55° S, the instrumental data are not reliable at the grid-point level over large parts of the 20th century due to very sparse data coverage (Hansen *et al.*, 2010). We include the regions between 0° N and 10° N because the equatorial regions have a strong influence on SH

temperature variability. Proxy records from these areas with a significant local temperature correlation are expected to be strongly correlated to SH climate. The spatial mean of the domain 55°S-10°N is very similar to the full SH mean, which is used as the reconstruction target (Supplementary Figure 2).

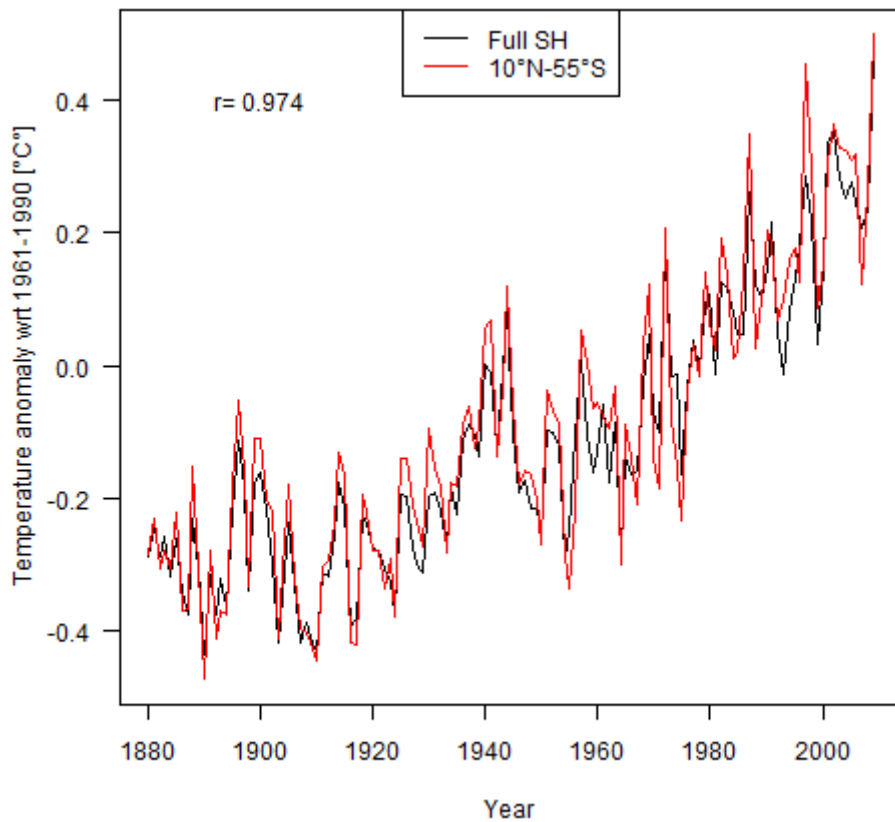
Both the proxy and instrumental data are linearly detrended over the 1911-1990 overlap period prior to the correlation analyses. Correlations of each proxy record with all grid cells are then calculated for the period 1911-1990. The calculations are repeated after lagging the proxy data for one year in both directions. This lagging allows dating uncertainties and the different seasonal windows represented by the proxy data to be accounted for. For example, ice core, documentary and coral records often represent annual averages based on calendar year or rain-year (e.g. July-June) definitions in contrast to our May-April target seasonal window. Significance levels (5% threshold) are calculated taking AR1 autocorrelation into account (Bretherton et al., 1999). We consider the “local” correlation of each record as the highest absolute correlation of a proxy with all grid cells within a radius of 1000 km and for all the three lags (0, 1 or -1 years). A proxy record is included in the predictor set if this local correlation is significant ($p < 0.05$). Reconstruction results using an alternative search radius of 500 km, leading to a smaller predictor set (85 instead of 111 records) are similar (Supplementary Figure 20, see section 3.2.2). Proxies from Antarctica, which are outside the domain used for proxy screening, are included, if they correlate significantly with at least 10% of the grid-area used for screening (latitude weighted). An alternative reconstruction using the full un-screened proxy network yields very similar results (Supplementary Figure 20, see section 3.2.2), demonstrating that the screening procedure has only a limited effect on the reconstruction outcome. The spatial and temporal distribution of the 111 proxy records that passed the screening is shown in Figure 1 in the main text and their properties are listed in Supplementary Table 5. Supplementary Table 6 shows the local correlations of all selected proxies as well as their correlations with the SH mean reconstruction target.

More than 99% of the SH proxies are independent from the records used in the NH reconstruction (see section 5). The one exception in the 111 records is the Quelccaya d₁₈O dataset, which was one out of thirteen proxies in one (Juckes *et al.*, 2007) of the nine reconstructions in the NH ensemble. Juckes *et al.* (2007) furthermore note that this record is only of very minor importance in their NH reconstruction, as it is only weakly correlated with the composite of their remaining proxies ($r=0.15$) and omitting the record does not change the maximum pre-industrial temperature in their NH reconstruction ($\Delta T=0.000K$).

Nine out of the 111 selected records are from sites located slightly north of the equator (Supplementary Table 5). None of these time series has been used in one of the NH reconstructions that we use for comparison. With two exceptions, all of the nine low-latitude NH-proxies in our dataset have stronger correlations with SH spatial mean temperatures than with the NH. The exceptions are Guam, which has very similar correlations with both hemispheres (SH: $r=-0.49$, $p<0.01$ over 1911-1990; NH: $r=-0.51$, $p<0.01$) and Bunaken which shows a strong relation to local temperatures ($r=-0.56$, $P<0.01$) and NINO3.4 ($r=0.52$, $p<0.01$) but non-significant correlations with both hemispheric means (SH: $r=-0.08$, $p=0.56$; NH: $r=-0.18$, $p=0.15$). Eight out of the nine low latitude NH proxies are corals, one is a marine sediment. Supplementary Figure 21 (below, page 43) shows that our reconstruction is robust to the removal of corals and marine sediments indicating that our results are not biased by the NH proxy records.

1.4. Missing values 1911-1990

Missing values in the predictor matrix (1.28%) during the 1911-1990 calibration/verification period are infilled using RegEM (Mann *et al.*, 2008).



Supplementary Figure 2 | Reconstruction vs. screening target. Comparison of the field mean of the GISStemp target grid using the full SH average (black; 90°S-0°S) and the domain 55°S-10°N (red) respectively. The first was used as reconstruction target, the latter for the calculation of the local correlations between proxies and instrumental data. Annual averages are shown for the May-April window.

Supplementary Table 5 | Proxies selected for the SH temperature reconstruction.

Name	Archive	Proxy	Start	End	Lat (°S)	Lon (°E)	Reference
Lake Challa Kenya	Lake Sediments	Varve thickness	-1050	2005	3.32	37.7	Wolff et al. (2011)
Mt. Read Tasmania	Tree Rings	Tree ring width	-494	1999	42	147	Cook et al. (2000), Cook et al. (2006)
Laguna Pumacocha	Lake Sediments	d18O	-277	2007	10.7	-76.07	Bird et al. (2011)
Oroko	Tree Rings	Tree ring width	1	2003	43.23	170.28	Cook et al. (2006)
Law Dome d18O	Ice Cores	d18O	179	2007	66.83	112.83	Unpublished
Quelccaya	Ice Cores	d18O	488	2002	13.93	-70.83	Thompson et al. (1984, 2006)
Laguna Aculeo	Lake Sediments	Pigment reflection	856	1997	33.83	-70.9	von Gunten et al. (2009)
Palmyra Island d18O	Corals	d18O	928	1998	-5.87	-162.13	Cobb et al. (2003)
Law Dome sea salt	Ice Cores	Summer sea salt	1000	2009	13	112.83	Unpublished
Talos	Ice Cores	dD	1217	1996	72.8	159.1	Stenni et al. (2002)
Cariaco Basin	Marine Sediments	Mg/Ca	1222	1990	-10.75	-64.77	Black et al. (2007)
Lago Puyehue	Lake Sediments	Lamina thickness	1408	1997	40.65	-72.45	Boes & Fagel (2008)
Siple Station	Ice Cores	d18O	1417	1983	75.92	-84.15	Graf et al. (2002), Taufetter et al. (2004)
CTP East Tasmania	Tree Rings	Tree ring width	1430	1994	42	148	Allen et al. (2001)
CAN Composite 6	Tree Rings	Tree ring width	1435	2006	38.5	-71.5	La Marche et al. (1979a), Villalba (1990a), Mundo et al. (2012)
Pink Pine NZ	Tree Rings	Tree ring width	1457	1999	42	172	Duncan et al. (2010)
Urewera	Tree Rings	Tree ring width	1462	1987	38.68	177.2	Xiong and Palmer (2000)
Buckles Chance	Tree Rings	Tree ring width	1463	1991	42.27	145.87	Buckley et al. (1997)
WDC05Q Accumulation	Ice Cores	Accumulation	1521	2004	79.45	-112.08	Banta et al. (2008)
NI LIBI Composite 1	Tree Rings	Tree ring width	1526	1992	39.5	175.5	Xiong and Palmer (2000)
Takapari	Tree Rings	Tree ring width	1533	1992	40.07	175.98	Xiong and Palmer (2000)
Santiago de Chile	Documentary	Documentary	1540	2006	33.38	-70.78	Taulis (1934), Neukom et al. (2009)
CTP West Tasmania	Tree Rings	Tree ring width	1547	1998	42	146	Allen et al. (2001), Allen (2002), LaMarche et al. (1979c)
Tucuman	Documentary	Documentary	1548	2005	27.03	-65	Prieto et al. (2000), Neukom et al. (2009)
Peru ENSO index	Documentary	Documentary	1550	1990	8.1	-79.02	Garcia-Herrera et al. (2008), Quinn & Neal (1992)
Mangawhero	Tree Rings	Tree ring width	1551	1994	39.35	175.48	D'Arrigo et al. (2000)
Kauri NZ	Tree Rings	Tree ring width	1577	2002	36	174	Cook et al. (2006), Fowler et al. (2008)
CAN Composite 15	Tree Rings	Tree ring width	1582	1991	41.17	-71.92	Villalba et al. (1997b)
ITASE 2002 4	Ice Cores	d18O	1593	1997	86.5	-108	Jacobel et al. (2005)
Rio Mendoza	Documentary	Documentary	1601	2000	32	-68	Prieto et al. (1999), Neukom et al. (2009)
Urina, Galapagos	Corals	d18O	1607	1981	0.03	-91.23	Dunbar et al. (1994)
Fiji AB	Corals	d18O	1617	2001	16.82	179.23	Linsley et al. (2006)
Mafia, Tanzania	Corals	d18O	1622	1998	8	40	Damassa et al. (2006)
Moa Park	Tree Rings	Tree ring width	1623	1991	40.93	172.93	Xiong and Palmer (2000)
CAN Composite 9	Tree Rings	Tree ring width	1636	2006	39.33	-71.25	La Marche et al. (1979a), Mundo et al. (2012)
Abraham	Corals	d18O	1638	1983	20	153	Druffel and Griffin (1999)
CAN Composite 12	Tree Rings	Tree ring width	1645	1992	40	-71	La Marche et al. (1979b), Villalba and Veblen (1997)
NI LIBI Composite 2	Tree Rings	Tree ring width	1651	1990	39.27	174.1	Xiong and Palmer (2000)
Dolleman	Ice Cores	Chem. species PC1	1652	1991	70.57	-60.93	Russell et al. (2006)
Siple Dome B	Ice Cores	d18O	1654	1994	81.65	-148.8	Steig et al. (2013)
Amedee New Caledonia	Corals	d18O	1657	1992	22.48	166.45	Quinn et al. (1998)
Ifaty 4	Corals	d18O	1660	1994	23	43	Unpublished
Ifaty, Madagascar	Corals	d18O	1660	1995	23.15	43.58	Zinke et al. (2004)
Huinganco	Tree Rings	Tree ring width	1673	2000	37.75	-70.6	La Marche et al. (1979a)
Secas	Corals	d18O	1707	1983	-7	-82.05	Linsley et al. (1994)
CAN Composite 2	Tree Rings	Tree ring width	1714	2006	37.83	-71	La Marche et al. (1979a), Mundo et al. (2012)
CAN Composite 27	Tree Rings	Tree ring width	1715	2002	49	-72	Boninsegna et al. (1989), Srur et al. (2008)
SAN Composite 5	Tree Rings	Tree ring width	1718	1984	54.75	-67.67	Boninsegna et al. (1989)
Princess Elizabeth Land	Ice Cores	Chem. species PC1	1745	1996	70.83	77.07	Xiao et al. (2004)
Santiago del Estero	Documentary	Documentary	1750	2005	27.77	-64.27	Herrera et al. (2003), Neukom et al. (2009)
Stewart Island	Tree Rings	Tree ring width	1758	1993	47	168	D'Arrigo et al. (1995), D'Arrigo et al. (2000)

Supplementary Table 5 (continued)

WA Callitris	Tree Rings	Tree ring width	1758	2005	33.03	120.77	Cullen et al. (2009)
Central Andes snow dept	Documentary	Documentary	1760	1996	33	-70	Neukom et al. (2009)
Rarotonga d18O	Corals	d18O	1761	1996	21.23	-159.83	Linsley et al. (2006), Linsley et al. (2008)
Rarotonga SrCa	Corals	Sr/Ca	1761	1996	21.23	-159.83	Linsley et al. (2006), Linsley et al. (2008)
Valle Ameghino	Tree Rings	Tree ring width	1766	1997	50.42	-72.17	Masiokas and Villalba (2004)
Pino Hachado	Tree Rings	Tree ring width	1767	1974	38.63	-70.75	La Marche et al. (1979a)
CAN Composite 8	Tree Rings	Tree ring width	1773	1989	39.17	-71.17	Villalba and Veblen (1997)
Vostok Pits	Ice Cores	d18O	1774	1999	78.45	106.83	Eckaykin et al. (2004)
Flanagans Hut	Tree Rings	Tree ring width	1776	1991	41.27	172.6	Xiong and Palmer (2000)
Savusavu, Fiji	Corals	d18O	1776	2001	16.82	179.23	Bagnato et al. (2005)
Fiji 1F SrCa	Corals	Sr/Ca	1780	1997	16.82	179.23	Linsley et al. (2004)
Teak Indonesia	Tree Rings	Tree ring width	1780	2005	7	111	D'Arrigo et al. (2006)
Fiji 1F d18O	Corals	d18O	1781	1997	16.82	179.23	Linsley et al. (2004)
GBR precip recon rec4	Corals	Luminescence	1783	1981	18	147	Lough (2011)
Eastern NSW	Documentary	Documentary	1788	2008	33.9	115.2	Fenby & Gergis (2013)
CAN Composite 21	Tree Rings	Tree ring width	1790	1991	41.5	-71.5	Villalba and Veblen (1997)
Guam	Corals	d18O	1790	2000	-13	145	Asami et al. (2005)
James Ross Island	Ice Cores	dD	1791	2000	64.37	-58.13	Aristarain et al. (2004)
Abrolhos	Corals	d18O	1794	1993	28.45	113.77	Kuhnert et al. (1999)
Tonga TH1	Corals	d18O	1794	2004	19.93	-174.72	Unpublished
CAN Composite 34	Tree Rings	Tree ring width	1795	2007	50.6	-73.67	Unpublished
Torre Morena 4	Tree Rings	Tree ring width	1798	2007	49.5	-73.5	Unpublished
Illimani	Ice Cores	NH4	1800	1998	16.65	-67.78	Kellerhals et al. (2010)
ITASE 2000 5	Ice Cores	d18O	1800	1999	77.67	-124	Schneider et al. (2005)
Malindi	Corals	d18O	1801	1994	3	40	Cole et al. (2000)
Paso Cordova	Tree Rings	Tree ring width	1811	1986	40.67	-71.25	ITRDB series arge050
Chapelco	Tree Rings	Tree ring width	1814	1985	40.33	-71.23	ITRDB series arge029
Baw Baw	Tree Rings	Tree ring width	1818	2002	36.42	148.33	Brookhouse et al. (2008)
Eastern Cape	Documentary	Documentary	1821	2007	34	24.5	Vogel (1989), Neukom et al. (in review)
La Meseda	Tree Rings	Tree ring width	1822	1999	23	-65.02	Unpublished
Kavieng	Corals	Sr/Ca	1823	1997	2.5	150.5	Alibert and Kinsley (2008a,b)
El Chalten bajo	Tree Rings	Tree ring width	1826	2003	49.37	-72.9	Srur et al. (2008)
Avaiki	Speleothems	Lamina thickness	1829	2001	19	-169.83	Rasbury & Aharon (2006)
Maiana	Corals	d18O	1840	1994	-1	173	Urban et al. (2000)
Seychelles	Corals	d18O	1846	1995	4.62	55.8	Charles et al. (1997), Abram et al. (2008)
Tonga TNI2	Corals	d18O	1849	2004	20.27	-174.82	unpublished
CAN Composite 16	Tree Rings	Tree ring width	1857	1991	41.13	-71.8	Villalba et al. (1997b)
Gomez	Ice Cores	d18O	1857	2005	73.6	-70.35	Thomas et al. (2008, 2009)
ITASE 2001 3	Ice Cores	d18O	1858	2000	78.12	-95.65	Steig et al. (2005)
Mentawai West Sumatra	Corals	d18O	1858	1997	4	98.5	Abram et al. (2008)
CAN Composite 14	Tree Rings	Tree ring width	1859	1994	41.13	-71.8	Villalba et al. (1997b), Schmelter (2000)
Bunaken	Corals	d18O	1863	1990	-2.8	123	Charles et al. (2003)
Rabaul d18O	Corals	d18O	1867	1997	4	152	Quinn et al. (2006)
Rabaul Sr/Ca	Corals	Sr/Ca	1867	1997	4	152	Quinn et al. (2006)
Rarotonga 3R	Corals	d18O	1874	2000	21.23	-159.83	Linsley et al. (2006), Linsley et al. (2008)
Zimbabwe	Tree Rings	Tree ring width	1875	1996	18.5	27.33	Therrell et al. (2006)
Ningaloo	Corals	d18O	1878	1995	21.9	113.97	Kuhnert et al. (2000)
Madang Lagoon	Corals	d18O	1880	1993	5.22	145.82	Tudhope et al. (2001)
Ifaty 1	Corals	d18O	1882	1994	23	43	Unpublished
Laing	Corals	d18O	1884	1993	4.15	144.88	Tudhope et al. (2001)
Central Andes snow occurrence	Documentary	Documentary	1885	1996	33	-70	Prieto et al. (2001), Neukom et al. (2009)
Palmyra Island SrCa	Corals	Sr/Ca	1886	1998	-5.87	-162.13	Nurhati et al. (2011)
GBR precip recon rec17	Corals	Luminescence	1891	1981	18	147	Lough (2011)
ITASE 2001 2	Ice Cores	d18O	1891	2001	77.83	-102.92	Steig et al. (2005)
CAN Composite 17	Tree Rings	Tree ring width	1892	1994	41.17	-71.83	Villalba et al. (1997b), Schmelter (2000)
Clipperton	Corals	d18O	1893	1994	-10.3	-109.22	Linsley et al. (2000a)
Puerto Parryn	Tree Rings	Tree ring width	1893	1986	54.83	-64.37	Boninsegna et al. (1989)
Tarawa	Corals	d18O	1893	1989	-1	172	Cole et al. (1993)
NT Callitris	Tree Rings	Tree ring width	1896	2006	13	132	Baker et al. (2008)
Nauru	Corals	d18O	1897	1995	0.83	166	Guilderson et al. (1999)

Supplementary Table 6 | Temperature correlations of proxies. Local correlations (r_{local}) and correlations with the SH mean reconstruction target (r_{SH}) for the selected predictors. Proxies from outside the screening area have no local correlation (NA).

Name	r_{local}	r_{SH}	Name	r_{local}	r_{SH}
Lake Challa Kenya	-0.38	-0.17	Pino Hachado	-0.25	0.31
Mt. Read Tasmania	0.43	0.65	CAN Composite 8	0.23	0.35
Laguna Pumacocha	-0.34	0.28	Vostok Pits	NA	0.31
Oroko	0.36	0.22	Flanagans Hut	0.36	0.13
Law Dome d18O	NA	-0.05	Savusavu, Fiji	-0.53	-0.26
Quelccaya	0.32	0.17	Fiji 1F SrCa	-0.49	-0.14
Laguna Aculeo	0.36	0.46	Teak Indonesia	0.29	0.16
Palmyra Island d18O	-0.82	-0.61	Fiji 1F d18O	-0.47	-0.24
Law Dome sea salt	NA	-0.21	GBR precip recon rec4	0.30	-0.04
Talos	NA	-0.12	Eastern NSW	-0.39	-0.03
Cariaco Basin	NA	0.76	CAN Composite 21	-0.31	-0.10
Lago Puyehue	0.34	-0.05	Guam	-0.47	-0.49
Siple Station	NA	0.20	James Ross Island	NA	-0.58
CTP East Tasmania	-0.31	0.37	Abrolhos	-0.53	-0.24
CAN Composite 6	-0.31	0.00	Tonga TH1	-0.37	0.07
Pink Pine NZ	0.49	0.24	CAN Composite 34	0.30	0.31
Urewera	-0.45	-0.11	Torre Morena 4	-0.27	-0.12
Buckleys Chance	0.41	-0.03	Illimani	0.45	0.38
WDC05Q Accumulation	NA	0.09	ITASE 2000 5	NA	0.13
NI LIBI Composite 1	-0.30	0.24	Malindi	-0.46	-0.55
Takapari	-0.33	0.59	Paso Cordova	-0.28	-0.27
Santiago de Chile	0.26	0.17	Chapelco	-0.30	-0.06
CTP West Tasmania	0.29	0.57	Baw Baw	-0.41	0.04
Tucuman	0.43	0.37	Eastern Cape	0.31	-0.07
Peru ENSO index	0.67	0.14	La Meseda	-0.29	-0.02
Mangawhero	0.36	0.51	Kavieng	-0.38	-0.02
Kauri NZ	-0.52	0.36	El Chalten bajo	-0.32	0.13
CAN Composite 15	0.28	0.23	Avaiki	-0.31	-0.06
ITASE 2002 4	NA	0.06	Maiana	-0.70	-0.58
Rio Mendoza	0.39	0.12	Seychelles	-0.42	-0.55
Urvina, Galapagos	-0.49	-0.14	Tonga TNI2	-0.45	0.14
Fiji AB	-0.59	-0.09	Gomez	NA	0.14
Mafia, Tanzania	-0.24	-0.50	CAN Composite 16	0.31	0.01
Moa Park	-0.34	0.08	Mentawai West Sumatra	-0.30	-0.41
CAN Composite 9	-0.30	-0.08	ITASE 2001 3	NA	0.00
Abraham	0.27	-0.16	CAN Composite 14	0.38	0.49
CAN Composite 12	-0.41	-0.17	Bunaken	-0.65	-0.08
NI LIBI Composite 2	-0.29	0.38	Rabaul d18O	-0.41	-0.03
Dolleman	NA	0.11	Rabaul Sr/Ca	-0.46	0.01
Siple Dome B	NA	-0.09	Rarotonga 3R	0.41	-0.33
Amedee New Caledonia	-0.44	-0.37	Zimbabwe	-0.33	-0.01
Ifaty, Madagascar	-0.30	-0.20	Ningaloo	-0.35	-0.58
Ifaty 4	-0.27	-0.21	Madang Lagoon	-0.36	-0.08
Huinganco	-0.33	-0.16	Ifaty 1	-0.32	-0.52
Secas	-0.26	-0.31	Laing	-0.54	-0.36
CAN Composite 2	0.28	-0.36	Central Andes snow occurrence	0.28	0.25
CAN Composite 27	0.34	0.19	Palmyra Island SrCa	-0.59	-0.33
SAN Composite 5	-0.37	0.24	GBR precip recon rec17	0.35	0.02
Princess Elizabeth Land	NA	0.43	ITASE 2001 2	NA	0.07
Santiago del Estero	0.27	0.23	CAN Composite 17	0.57	0.64
Stewart Island	0.40	0.25	Tarawa	-0.62	-0.44
WA Callitris	-0.29	-0.03	Clipperton	-0.49	-0.63
Central Andes snow depth	0.24	0.31	Puerto Parryn	-0.29	-0.52
Rarotonga d18O	0.49	-0.22	NT Callitris	0.24	0.19
Rarotonga SrCa	-0.50	0.02	Nauru	-0.46	-0.70
Valle Ameghino	0.32	0.24			

2. Ensemble reconstruction

2.1. Reconstruction methodology

Temperature reconstructions are based on nested multivariate principal component regression (PCR; Luterbacher *et al.*, 2002; Luterbacher *et al.*, 2004; Neukom *et al.*, 2010; Neukom *et al.*, 2011; Neukom *et al.*, 2013). Detailed description of the PCR method is provided in Luterbacher *et al.*(2002), Luterbacher *et al.* (2004) and Wahl and Smerdon (2012).

2.2. Ensemble parameters

The ensemble approach (see also Frank *et al.*, 2010; Neukom *et al.*, 2010; Neukom *et al.*, 2013) allows for the provision of additional uncertainty estimates, complementing the traditional error estimates which quantify the unexplained variance in the calibration period (cf. Wahl and Smerdon, 2012, for an alternative probabilistic ensemble approach using PCR). The outcome of a climate reconstruction depends on the methodological choices that have to be made during the reconstruction process. For most of these choices, objective “best” solutions are largely missing in literature. The main limitation is that the real-world performance of different approaches and parameters can only be verified over the instrumental period, which is short and contains a strong trend, complicating quality assessments. We assess the influence of these methodological choices by varying methodological parameters in the ensemble and quantifying their effect on the reconstruction results. Obviously, the range within which these parameters are varied in the ensemble is also subjective, but we argue that the ranges chosen herein are within reasonable thresholds, based our own experience and the literature. Given the limited possibilities to identify the “best” ensemble members, we treat all reconstruction results equally and consider the ensemble mean our best estimate. Because our ensemble members can be approximated by a normal

distribution (Supplementary Figure 3, see also Supplementary Figure 26 below), the ensemble mean also represents the most probable value in the ensemble distribution function.

We perform an ensemble of 3,000 reconstructions. For each ensemble member we use different settings by randomly:

1. Selecting 10% of the temperature proxies (i.e. 11 records) that are removed from the proxy matrix. In the early parts of the reconstruction (CE 1000–1222) between nine and eleven proxies are available, the number of predictors used for each ensemble member varies between one and eleven.

Rationale: We introduce this ensemble parameter because the proxy matrix in a multi-proxy reconstruction is always dependent on some pre-reconstruction choices such as proxy screening procedures based on statistical calculations, literature review or the effort invested in the data compilation. This perturbation allows us to assess the robustness of the reconstruction against changes in the predictor network and to assess the potential dominance of individual records (see section 3.2.6). This perturbation contributes to approximately 11% of the total ensemble spread (calculated during the 1911-1990 period; this fraction increases back in time due to the decreasing number of proxies available).

2. Sampling the years for calibration (between 40 and 55 years within the 1911-1990 overlap period). The remaining 25-40 years are used for verification.

Rationale: Given the limited number of years available in the instrumental-proxy overlap period, the outcome of a reconstruction strongly depends on the choice of calibration and verification periods (Frank *et al.*, 2010; Gergis *et al.*, 2011). This perturbation contributes to approximately 43% of the total ensemble spread.

3. Sampling the number of PCs to be used. We use the first n PCs that explain between 50%-90% of the total variance of the predictor matrix.

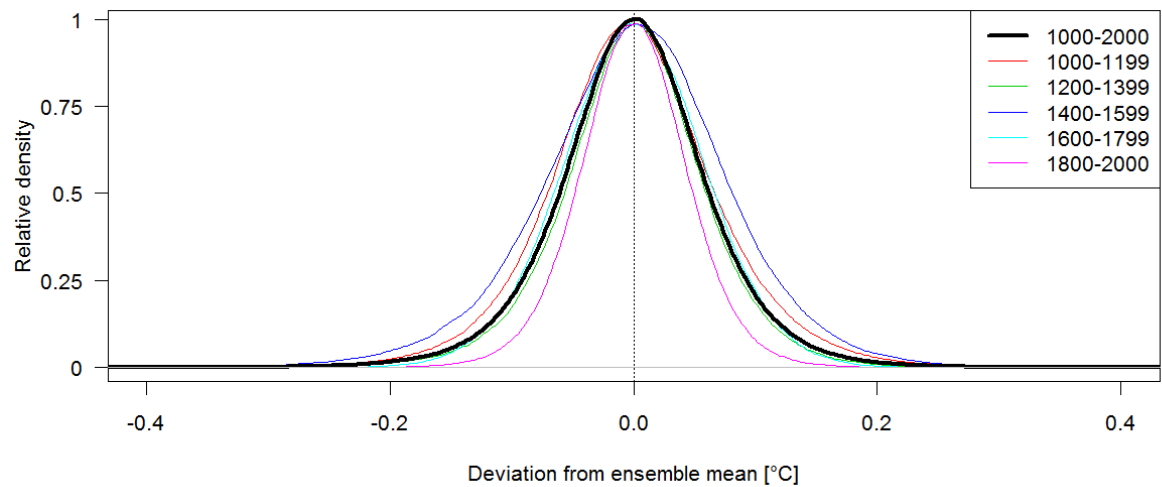
Rationale: There are various approaches described in literature to identify the best PC truncation (North *et al.*, 1982; Smerdon *et al.*, 2010) with currently no widely accepted “best” approach. Furthermore, the eigenvalues of the proxy PCs are strongly depending on the period chosen over which to calculate the PCs. This perturbation contributes to approximately 17% of the total ensemble spread.

4. Sampling the weight that each proxy gets in the PC analysis by increasing its variance by a factor of 0.67-1.5 (after scaling all proxies to mean zero and unit standard deviation over their common period).

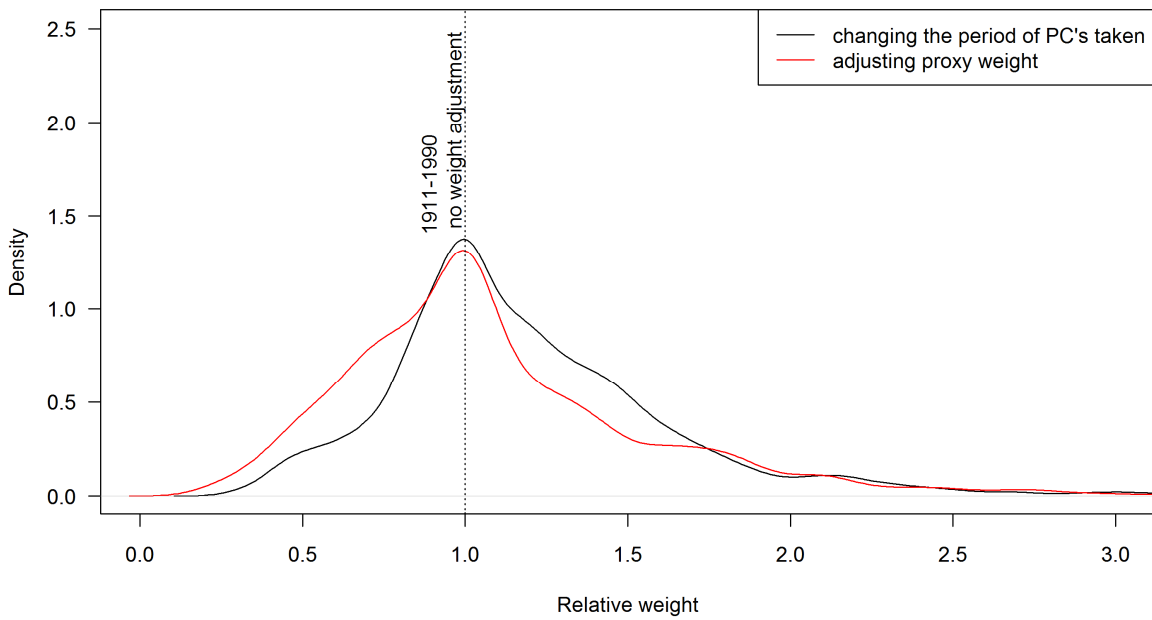
Rationale: The weight that each proxy record gets in the PC analysis is strongly dependent on the time period chosen (Supplementary Figure 4). Given the short period available for calibration, there is a high probability that the resulting proxy weights may not reflect the “true” weight of each proxy in the data matrix. This perturbation contributes to approximately 20% of the total ensemble spread.

5. Selecting one chronology for proxies where multiple time series based on different methods are available (tree-rings and documentaries, sections 1.2.1 and 1.2.3)

Rationale: The pre-processing of some records also involves some subjective choices. To overcome this limitation to a certain extent, we allow multiple versions of the same record to be used in different ensemble members. This perturbation contributes to approximately 8% of the total ensemble spread.



Supplementary Figure 3 | Ensemble distribution. Distribution of the difference between the individual ensemble members and the reconstruction ensemble mean. Distribution over all years within 1000-2000 (bold black) and within 200-year blocks (coloured lines) are shown.

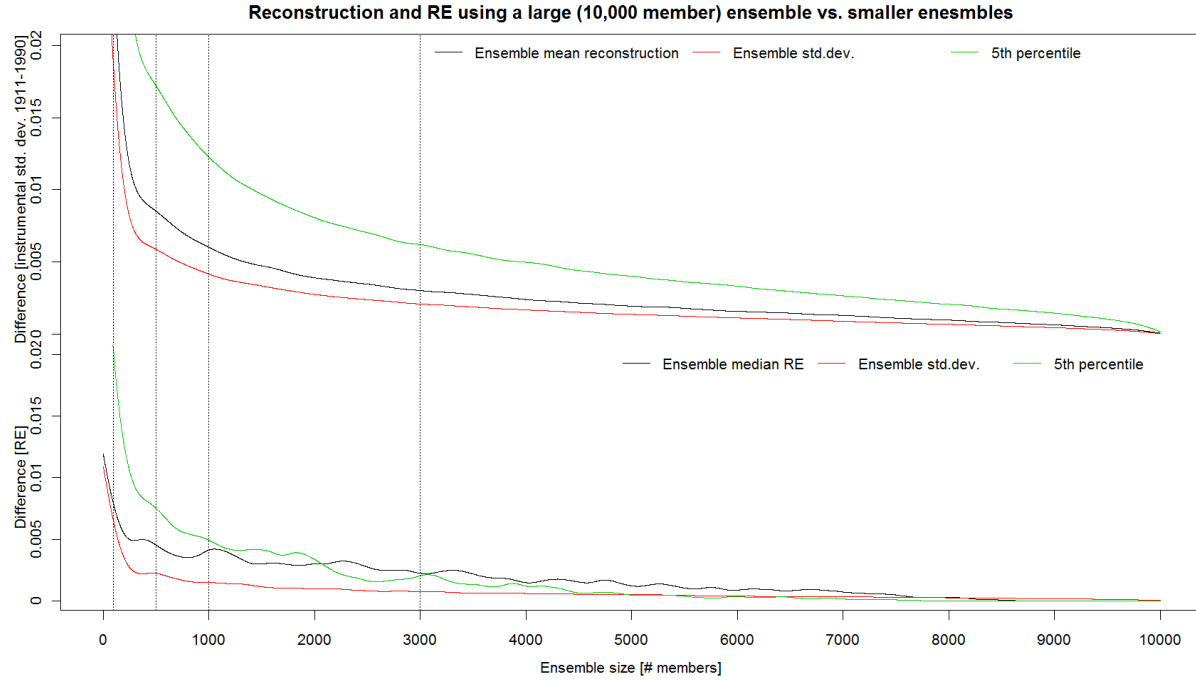


Supplementary Figure 4 | Sensitivity of proxy weight in the PC-routine. PCs of the proxy matrix are calculated over different time windows (black line) and using artificial variance inflation as in the ensemble perturbation #4 (red line). Weights of each proxy record are calculated as the average absolute loading to the first five PCs and expressed relative to the value of the unweighted proxy matrix over 1911–1990. For the temporal dependence (black line) PCs are calculated over 80-year periods starting between 1850 and 1910. Prior to 1850, the number of proxy records available strongly decreases and the change in the composition of the proxy matrix becomes more important, masking the effect of the choice of period. For the red line, variance inflation with random factors between 0.67 and 1.5 was applied to each proxy. The figure illustrates that this variance inflation mimics the temporal sensitivity of the PC calculation.

2.3. Required number of ensemble members

Supplementary Figure 5 shows the variability of different measures as a function of the number of ensemble members. The black line shows the difference between the ensemble mean using n members and the ensemble mean using 10,000 members. For an ensemble of 3,000 members, all measures are sufficiently close to a very large ensemble (e.g. the difference for the ensemble mean reconstruction is less than 0.001°C over the 1911–1990 period) but allow a significant reduction in the computational time and disk space required. For the AR-noise reconstructions (see below section 3.1.5), the use of 1000 member ensembles is sufficient because we only work with the RE skill values of these

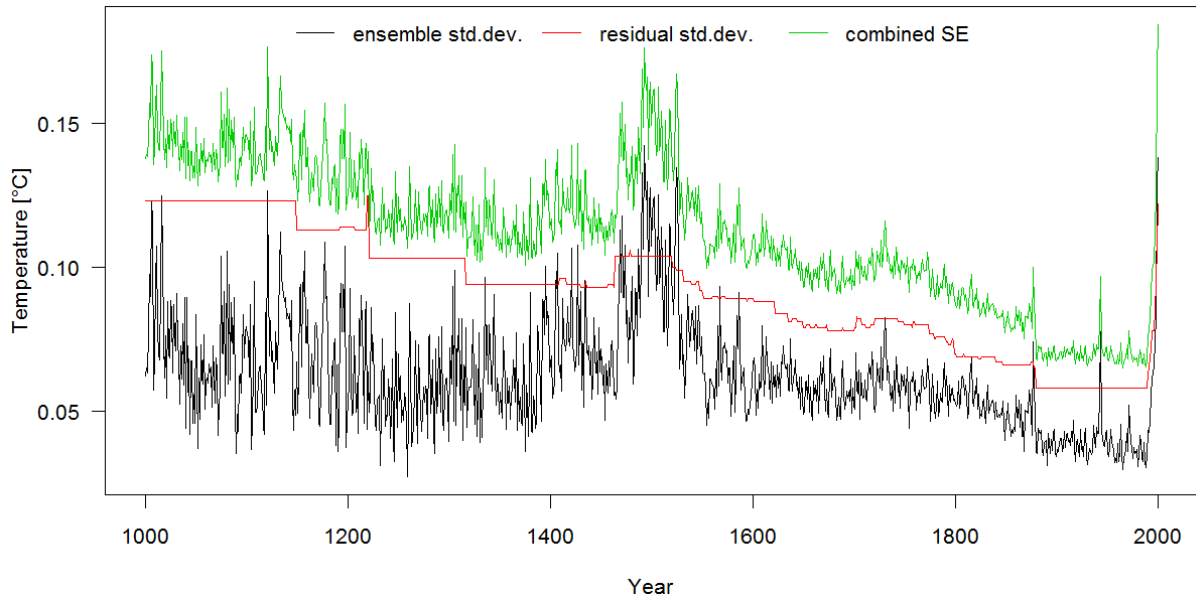
reconstructions, which are still very close to the values of the large 10,000 member ensemble (Supplementary Figure 5, bottom).



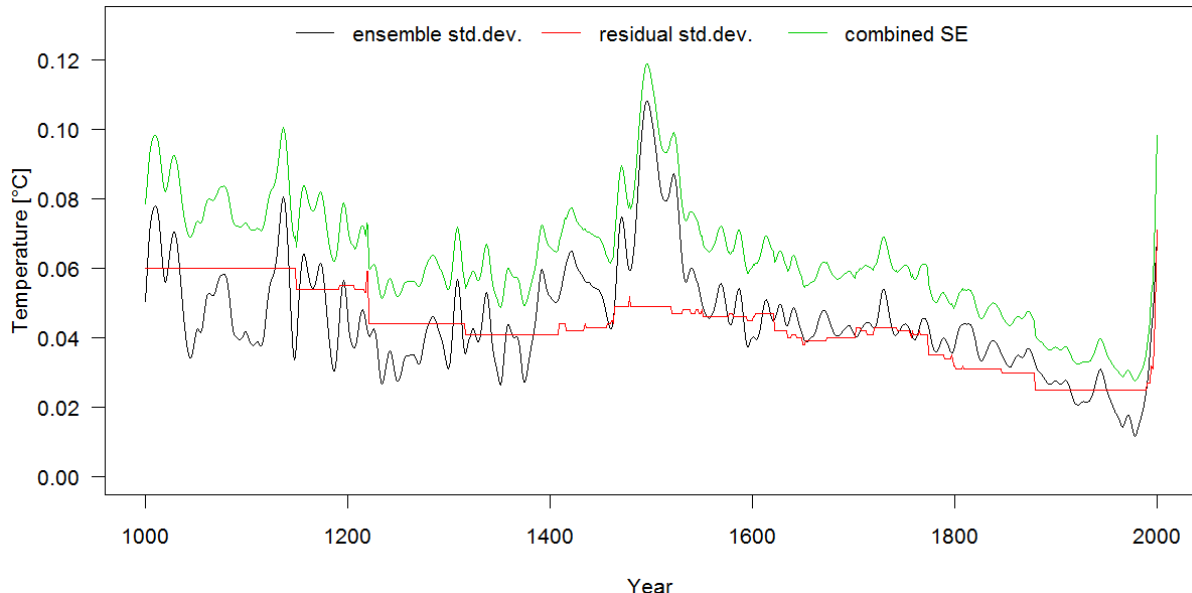
Supplementary Figure 5 | Reconstruction statistics for different ensemble sizes. The absolute differences between an ensemble of n members and an ensemble of 10,000 members is shown. We use the statistics for the period 1911–1990 of the most replicated nest (111 proxies). Top: Ensemble mean reconstruction (black), standard deviation between ensemble members (red) and 5th percentile of ensemble members (green). All values are shown relative to the instrumental standard deviation 1911–1990 (0.15°C). Bottom: Ensemble median RE (black), standard deviation between RE of ensemble members (red) and 5th percentile of RE of ensemble members (green). The dotted vertical lines represent the ensemble sizes used for the SH-mean reconstruction (3,000 members), the AR noise reconstructions (1,000 members, see below) and 500 and 100 members, respectively.

2.4. Reconstruction uncertainties

The combined calibration and ensemble uncertainties (SE) are calculated where $SE = \sqrt{\sigma_{res}^2 + \sigma_{ens}^2}$ with σ_{res} denoting the standard deviation of the regression residuals and σ_{ens} the standard deviation of the ensemble members. σ_{res} remains constant for all years with the same predictor availability, whereas σ_{ens} is different for each year. Blue shaded probabilities in Figure 2 in the main text represent the quantiles of a normal distribution around the ensemble mean with a standard deviation of SE . Temporal evolution of the interannual and 30-year filtered reconstruction uncertainties are shown in Supplementary Figure 6 and Supplementary Figure 7, respectively. The increasing ensemble uncertainties back in time are caused by the decrease of available proxy records further back in time



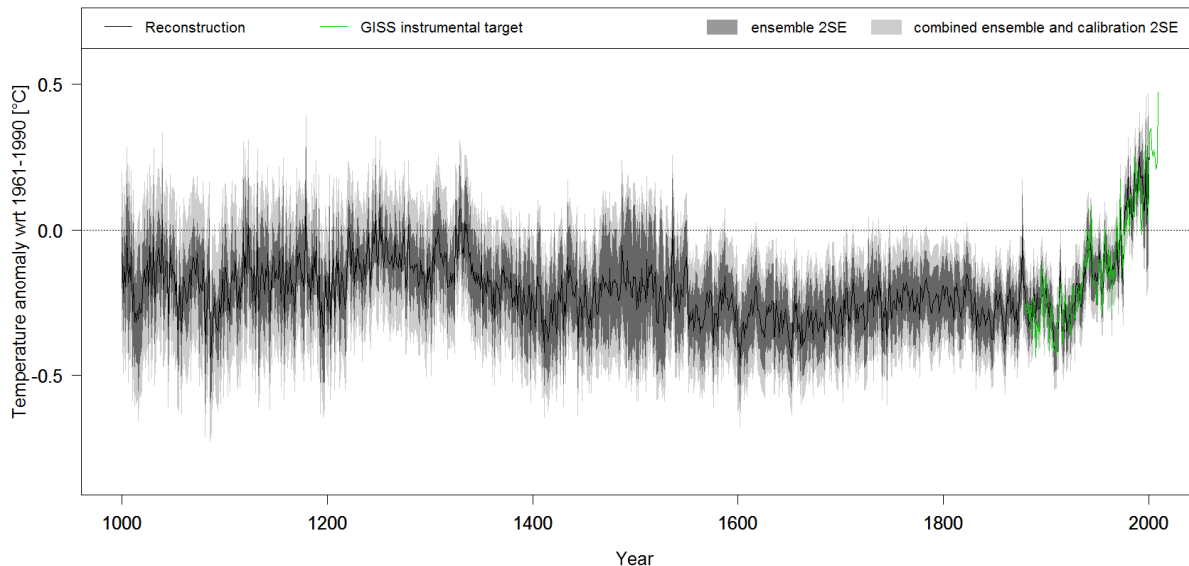
Supplementary Figure 6 | Reconstruction uncertainties. Ensemble standard deviation σ_{ens} (black), residual standard deviation σ_{res} (red) and combined SE uncertainties (green) of the unfiltered reconstruction.



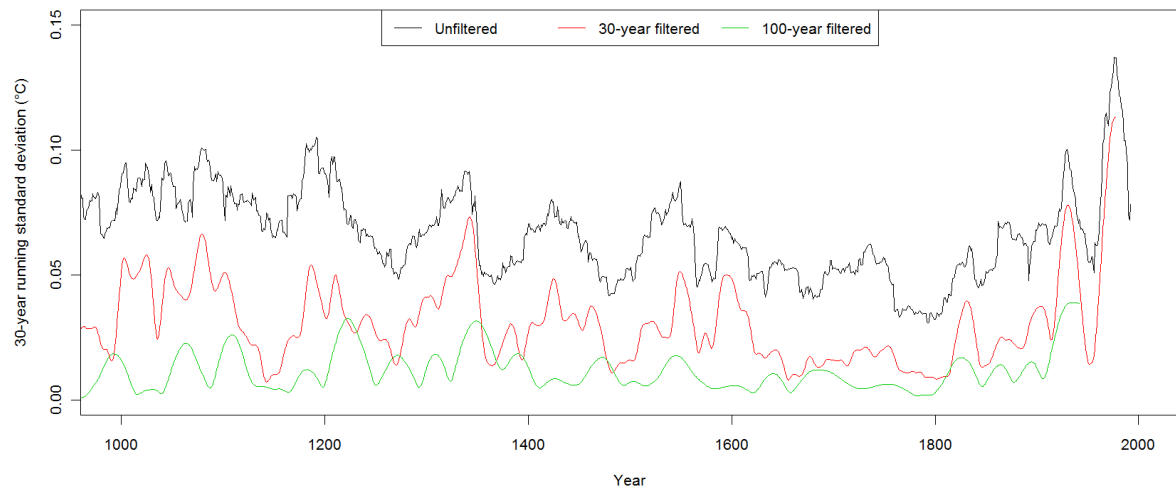
Supplementary Figure 7 | Filtered reconstruction uncertainties. Same as Supplementary Figure 6 but for the 30-year filtered reconstruction.

2.5. Unfiltered SH mean reconstruction

Supplementary Figure 8 shows the unfiltered reconstruction ensemble mean and associated uncertainties. The unfiltered data shows some long-term changes in the variance structure (Supplementary Figure 9) that may be an artifact of changes in proxy replication over time. The long-term changes in variance are not so evident at decadal to centennial time-scales (Supplementary Figure 9). Because our interpretations and conclusions focus on the decadal and lower resolution, these potential variance artifacts do not influence or findings or conclusions. We note that long-term trends in climate variability, e.g., related to ENSO, have been advocated in literature (e.g., McGregor *et al.*, 2013, who also find a reduction of temperature variance in their ENSO record over 1590–1880), so we do not wish to exclude a priori the possibility that long-term changes in climate variability exist, but rather to draw attention to possible uncertainties in the variance structure of our new record.



Supplementary Figure 8 | Unfiltered SH reconstruction. Black: reconstruction ensemble mean; dark grey shading: ensemble 2σ bounds, light grey shading: combined 2SE uncertainties. Green: Instrumental target data.



Supplementary Figure 9 | Running standard deviations. 30-year running standard deviations of the unfiltered SH reconstruction ensemble mean (black) and of the 30-year (red) and 100-year (green) loess filtered ensemble mean.

3. Reconstruction reliability

To assess the ‘reliability’ of the reconstruction we consider a range of reconstruction ‘skill’ and ‘robustness’ measures. Reconstruction skill assesses the ability of our proxies to reconstruct instrumental temperatures over verification periods that are independent from the calibration years. Robustness is assessed by investigating the effect of different reconstruction methods, proxy archives and individual records on the outcome of the reconstruction.

3.1. Reconstruction skill

The aim of reconstruction skill assessments is to verify the ability to capture temperature fluctuations during a verification period, which is independent from the time window used for calibration. Traditionally, a time slice of the overlap-period between proxy and instrumental data is used for this verification exercise. This time slice can be at the beginning, at the end or within the calibration period. The ensemble approach with individual calibration/verification windows for each member allows us to further elaborate this concept to ensemble-based verification metrics. We adapt the traditional RE (reduction of error) and RMSE (root mean square error) statistics (Cook *et al.*, 1994) to quantify the reconstruction skill over the ensemble members as well as for the ensemble mean. The RE measure is defined as

$$RE = 1 - \frac{\sum_{i=1}^n (x_{inst_i} - x_{recon_i})^2}{\sum_{i=1}^n (x_{inst_i} - x_{calib})^2},$$

with x_{inst} denoting instrumental values and x_{recon} the reconstructed values for each year i of the verification period. x_{calib} is the calibration period mean of the instrumental data. The RE tests whether the reconstruction has more predictive skill than the climatology of the calibration period (x_{calib}). RE values between 0 and 1 (a hypothetically perfect reconstruction) indicate a skillful reconstruction, while RE values <0 indicate no predictive skill.

The RMSE is defined as

$$RMSE = \sqrt{\frac{1}{n} \sum_{i=1}^n (x_{inst_i} - x_{recon_i})^2}$$

We calculate the verification values for each existing proxy combination (proxy nest) during the reconstruction period. The value of the calibration/verification exercise using only the proxies available in the year 1000 is assigned to the year 1000 etc. This yields a time series of validation values covering the full reconstruction period (Figure 1b in the main text and Supplementary Figure 10). The ensemble-based validation metrics are described in the following sections.

3.1.1. Ensemble validation

For each reconstruction ensemble member, we calculate the RE statistic from years withheld for verification within the 1911–1990 calibration/verification period. The number of years available for verification varies between 25 and 40 years. The ensemble median RE time series is derived by calculating the median of the RE values of all ensemble members for each year. We use the median here, because the distribution of the RE values is strongly skewed and a small number of very large negative RE values can bias the ensemble distribution and lead to an artificially low ensemble mean RE. The ensemble median RE of our reconstruction is consistently positive over the 1000-2000 period, except for the year 2000 which has a negative value (Supplementary Figure 10).

3.1.2. Ensemble mean early verification

The ensemble mean reconstruction is verified against the instrumental data in the 1880–1910 period, which is independent from the 1911–1990 calibration/verification interval and does not exhibit a significant temperature trend. Note, however, that the quality of the instrumental record is very limited in the SH during this early period. The early verification RE of our reconstruction is positive over the full 1000-2000 period.

3.1.3. Ensemble mean verification and calibration years

For each year over the 1911–1990 calibration/verification period, the ensemble mean reconstruction is calculated for all members where the year was used for verification (and not for calibration). This returns a time series covering 1911–1990 and representing the ensemble mean based only on verification years. This ‘verification ensemble mean’ is then used as x_{recon} and tested against the instrumental target over the full 1911–1990 period. This RE value is slightly different from the traditional RE statistic because the verification years (covered by x_{inst} and x_{recon}) and the calibration years (represented by x_{calib}) are both drawn from the same 1911–1990 period. Similarly we also calculate the calibration years RE using the ensemble mean of all years that are used for calibration as x_{recon} . The calibration and verification years RE are shown in Figure 1b in the main text. They are positive over the full 1000-2000 period.

3.1.4. Ensemble mean RMSE

The RMSE between the ensemble mean reconstruction and the instrumental data is calculated over the 1911-1990 calibration/verification window.

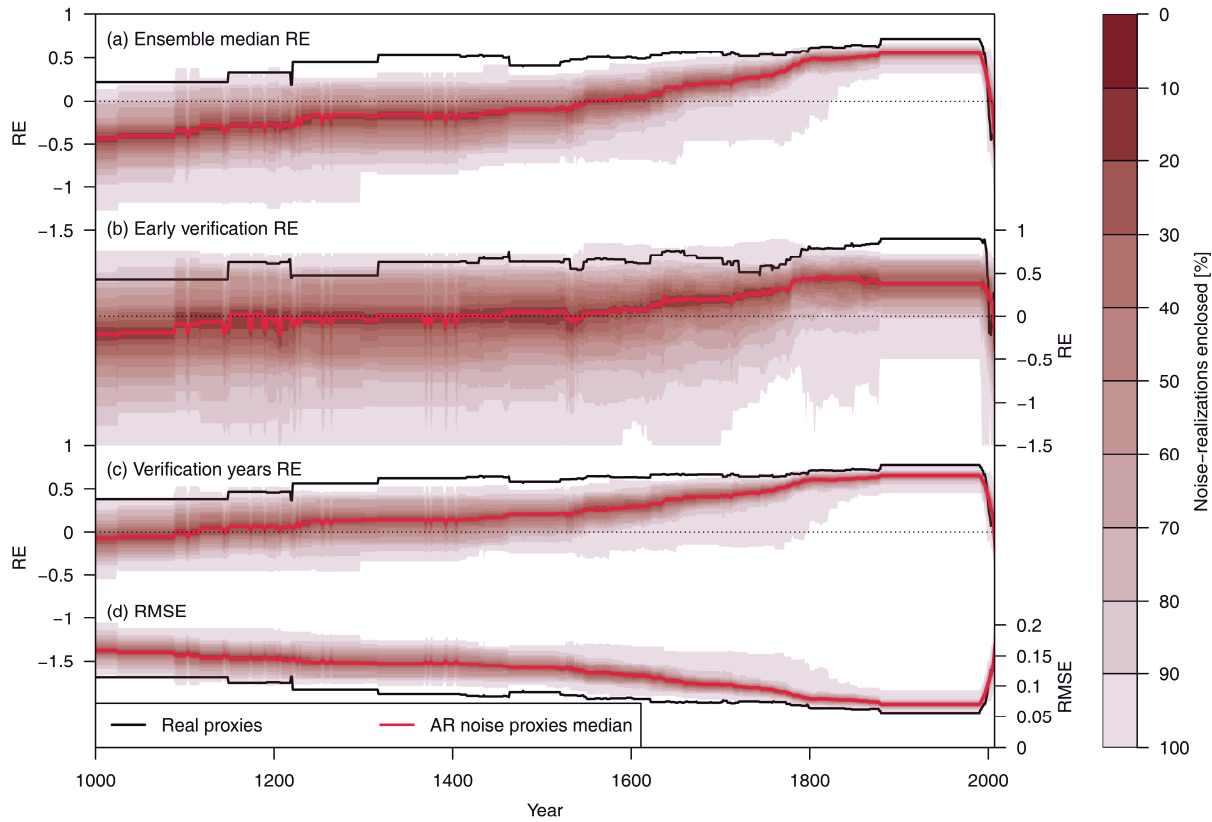
3.1.5. Noise predictors

To test if our reconstruction has more predictive skill than noise predictors, we compare the above RE values against the REs of reconstructions based on AR noise proxies. The ‘AR noise proxies’ are noise time series of the same length and autoregressive properties as our real proxy data (reflecting the full temporal autoregressive structure of the proxies; Wahl and Smerdon, 2012). For this exercise, AR noise proxy generation, screening and reconstructions are repeated 100 times using 1000-member ensembles.

Supplementary Figure 10 shows the temporal evolution of the reconstruction skill measures using real and AR noise proxies. The results demonstrate that RE values using real proxies are consistently positive (except for the negative ensemble median RE in the year 2000) and all

RE and RMSE measures clearly outperform the noise reconstructions, indicating a skillful temperature reconstruction is possible over the full 1000-2000 period. Less than 0.24% of noise reconstructions outperform our real temperature reconstruction over the entire reconstruction period using the ensemble median RE. The corresponding numbers for the early verification RE and verification years RE are 2.88% and 0.50%. Note that the fraction of predictors selected in the proxy-screening procedure (see section 1.3) is much smaller in the case of noise-proxies (74.6 ± 12 out of 191 proxies reflecting a fraction of $39.1\% \pm 6.3\%$) than for the real proxies (111 out of 191 proxies reflecting 58.1%).

Our results demonstrate that even though our conservative approach to derive noise-predictors can yield noise-based reconstructions with positive skill, it is very unlikely that noise predictors can reproduce the levels of predictive skill observed in the real proxy based reconstructions (cf. Wahl and Smerdon, 2012, section 4 and Fig. 2, for a parallel result). As a result, we have increased confidence that the skill we see in the reconstruction is evidence of a realistic estimation of past temperature variations.

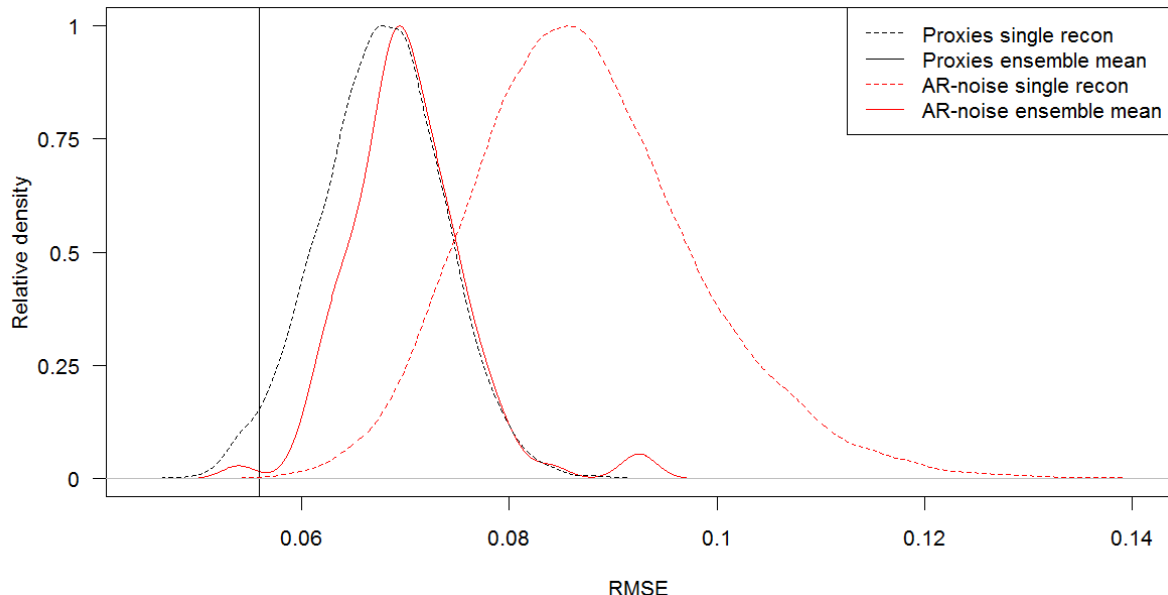


Supplementary Figure 10 | Reconstruction skill: RE and RMSE skill measures of our PCR reconstruction using real proxies (black lines) and median of 100 reconstructions using AR noise proxies (red lines). **a** Ensemble median RE, **b** early verification RE **c** verification years RE and **d** RMSE. The shaded areas represent the relative probability distribution of the results from 100 AR noise proxy reconstructions, expressed as percentiles: the lightest shading encloses the area between the minimum and maximum value, the next darker shading the area between the 5th and 95th percentile and so on. The darkest shading represents the area between the 45th and the 55th percentile. Values below -1.5 are not shown.

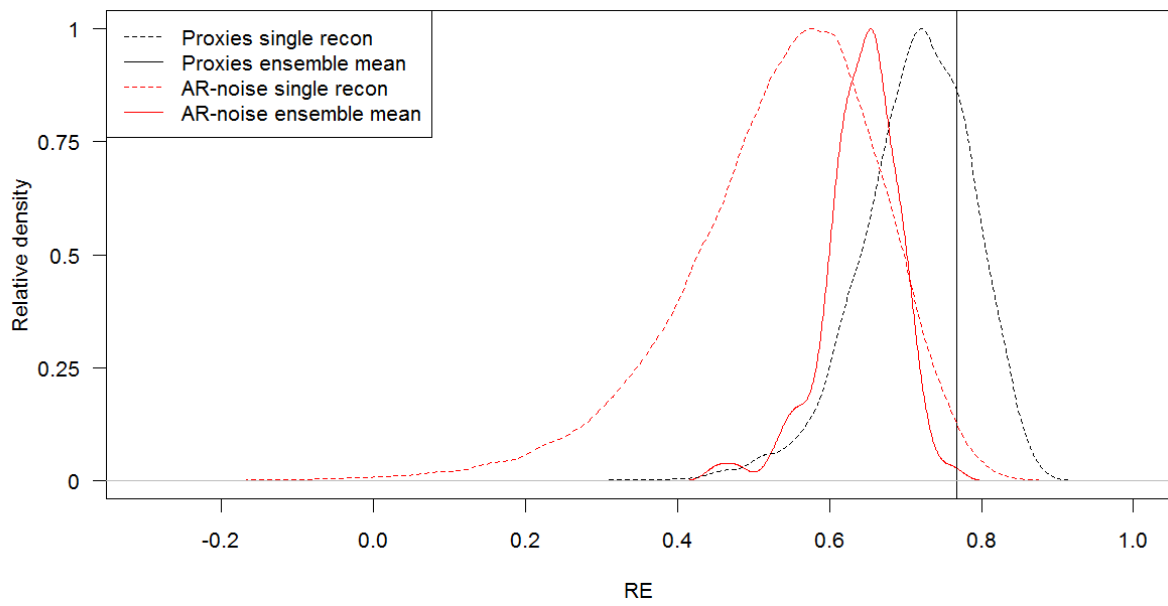
3.1.6. Ensemble vs. single reconstruction

Supplementary Figure 11 and Supplementary Figure 12 illustrate the RMSE and RE values of the individual ensemble members and the ensemble mean, respectively. They show that the skill of the ensemble mean is clearly higher than the average skill of the individual ensemble members, indicating that using ensemble reconstructions not only allows us to better address reconstruction uncertainties but also leads to more accurate results compared to single-member approaches. Supplementary Figure 11 and Supplementary Figure 12 also show that in

the most replicated nest during the 20th century, where AR noise reconstructions also have positive RE values, the real proxies clearly outperform the artificial data.



Supplementary Figure 11 | Ensemble vs. single-reconstruction RMSE: Dashed lines: Ensemble distribution of verification RMSE values of the most replicated proxy nest in the reconstruction using real proxies (black) and AR-noise proxies (red). Solid lines represent the RMSE of the ensemble mean reconstruction using real proxies (black) and distribution of 100 AR-noise based ensemble reconstructions (red).



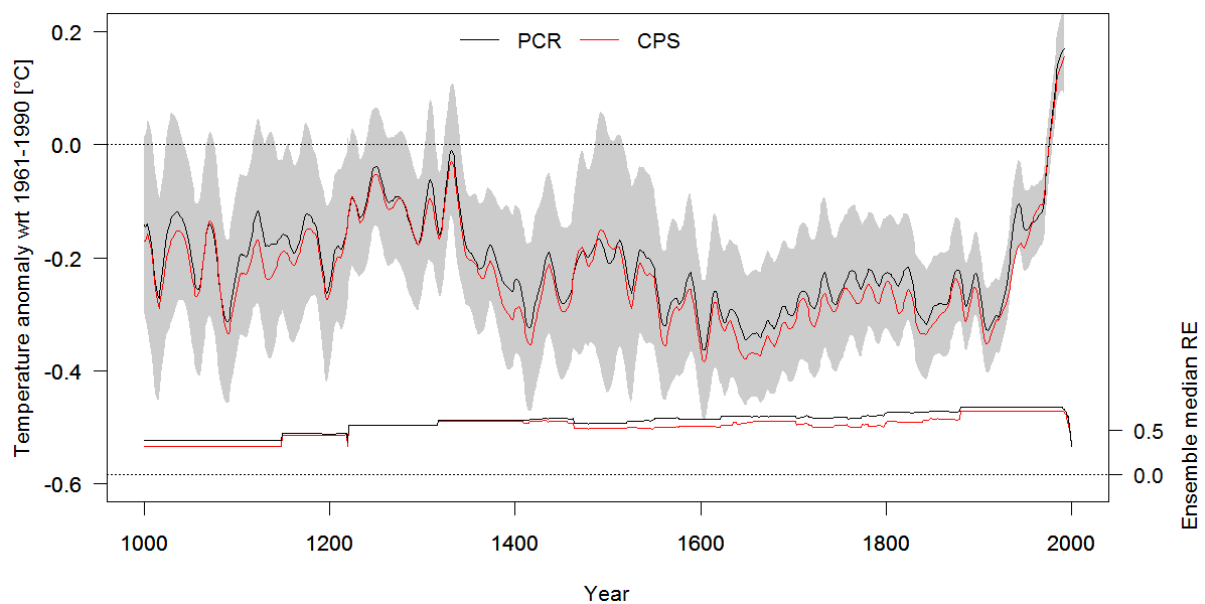
Supplementary Figure 12 | Ensemble vs. single-reconstruction RE. Same as Supplementary Figure 11 but for the RE. Solid lines represent the Verification years RE (see section 3.1.3).

3.2. Reconstruction robustness

Ideally, the reconstructed signal in multi-proxy reconstructions is inherent in multiple predictors and not dominated by a single proxy. Hence, the final reconstruction should not be too sensitive to changes in the proxy network. Similarly, individual archives (such as tree-rings or corals) should not dominate the reconstruction. Also, the choice of the reconstruction method should not influence the conclusions. Our ensemble reconstruction approach allows these questions to be addressed and allows the robustness of our reconstruction to be evaluated.

3.2.1. Alternative reconstruction methods: CPS

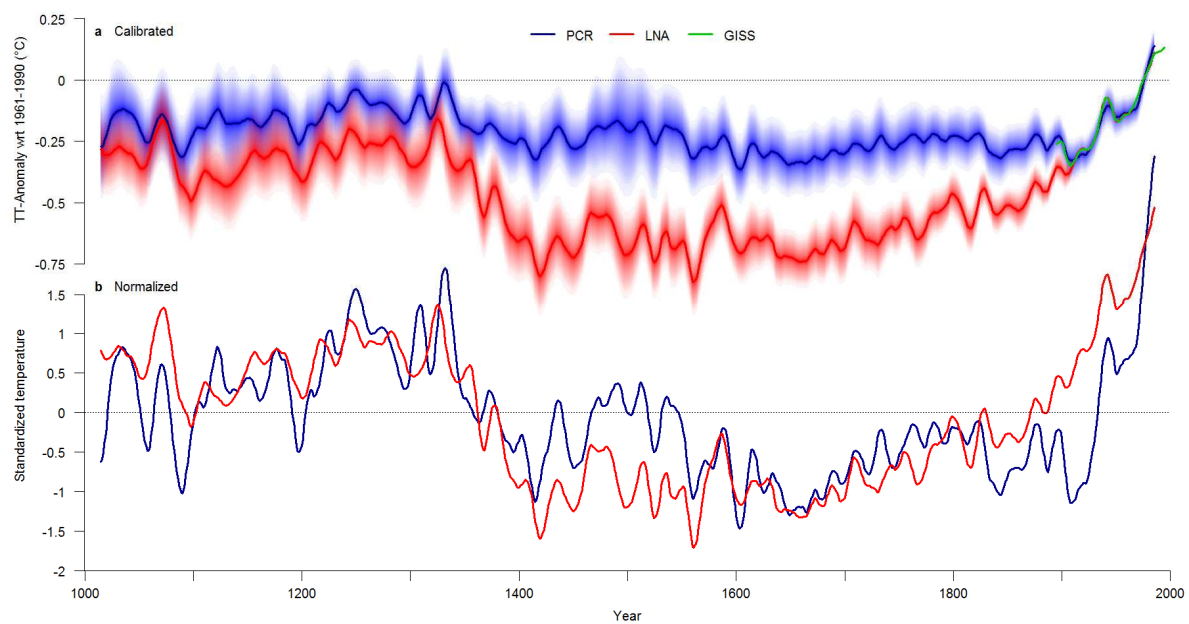
To address the influence of the reconstruction method on our results, we perform an additional 3000-member reconstruction using the Composite Plus Scale method (CPS; Mann *et al.*, 2008; Neukom *et al.*, 2011). We use the CPS approach of Neukom *et al.* (2011), which calculates the predictor composite by weighting each record with its correlation coefficient with the target over the calibration period. Supplementary Figure 13 compares the PCR and CPS reconstructions. They are generally very similar, indicating robustness of the results with regards to the reconstruction methodology. The low frequency amplitude is slightly larger in the CPS reconstruction resulting in colder reconstructed pre-industrial temperatures as compared to PCR. In terms of reconstruction skill, PCR performs slightly better. Therefore PCR is used for the analysis in the main manuscript.



Supplementary Figure 13 | PCR vs. CPS reconstruction. Top: 30-year filtered ensemble mean PCR (black, with grey shaded 2SE uncertainties) and CPS (red) reconstructions. Bottom: Verification years RE values of the PCR (black) and CPS (red) reconstructions.

3.2.2. Alternative reconstruction methods: LNA

We compare our results to an independent reconstruction using Bayesian hierarchical models developed by Li *et al.* (2010) , referred to as “LNA” in Hanhijärvi *et al.* (2013) and PAGES (2013). We used the same parameters as in PAGES (2013). The resulting reconstruction is compared to our PCR reconstruction in Supplementary Figure 14. We use the 2σ ensemble standard deviation of the LNA reconstruction as uncertainties to compare with our combined 2SE (see section 2.4). While the two methods yield a qualitatively similar temperature evolution, the LNA reconstruction shows a much larger amplitude between pre-industrial and present day temperatures. This amplitude is smaller (larger) in the PCR (LNA) reconstruction than in the NH reconstruction and most simulations of both hemispheres. Correlation between the two ensemble mean reconstructions is 0.71 ($p<<0.01$) and 0.74 ($p=0.01$) on interannual and 30-year filtered timescales, respectively. Supplementary Table 7 provides further comparison between the two reconstruction approaches. Notably we find that the early verification statistics of the LNA method are substantially weaker (e.g., RE values of 0.52 versus 0.9 for LNA and PCR, respectively). Yet, interestingly, most of the quantification provided in the main text related to NH-SH coherence and extreme periods (with the exception of the temperature amplitude) is similar for these two reconstruction approaches. The two methods also show very similar results in terms of extreme periods and interhemispheric differences. Given that our conclusions are based on decadal to centennial time-scale analyses, uncertainties in the overall amplitude (e.g., plausibly larger amplitude in the LNA reconstruction despite weaker early verification statistics) do not affect our main findings.



Supplementary Figure 14 | PCR vs. LNA reconstruction. **a** Comparison of 30-year filtered PCR (blue) and LNA (red) reconstruction ensemble means with shaded uncertainties and instrumental data (green). **b** Comparison of 30-year filtered PCR (blue) and LNA (red) reconstruction ensemble means after standardization to a mean of zero and unit standard deviation over the period 1000–2000.

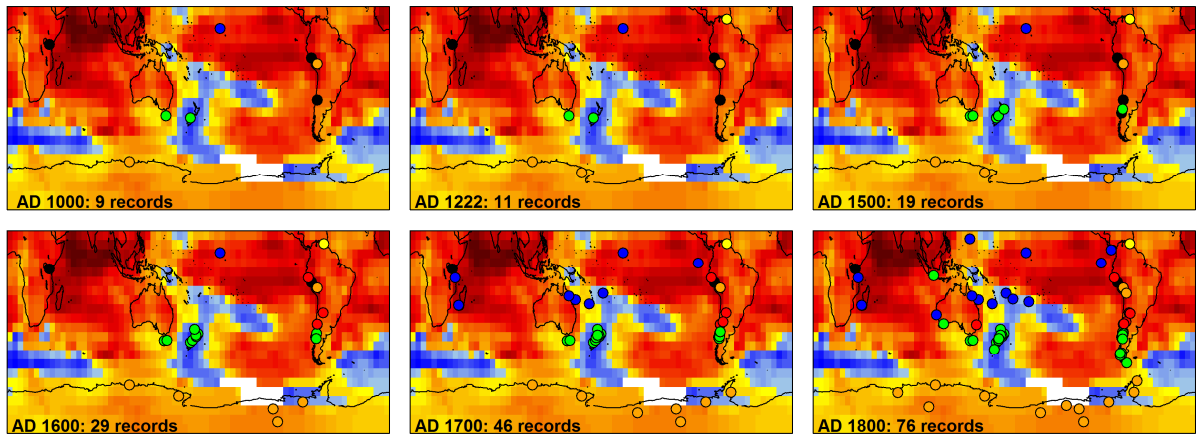
Supplementary Table 7 | Comparison of PCR and LNA reconstructions. Comparison of early verification statistics, uncertainties and the statistics and properties mentioned in the main text.

	PCR	LNA
<i>Early verification statistics (1880-1910; full proxy replication)</i>		
r ²	0.57	0.02
RE	0.9	0.52
Percentage of members with decade of highest temperature after 1970 (main text, line 93)	99.7	98.8
<i>Reconstruction-model correlations (line 114)</i>		
ensemble mean correlations	0.29	0.46
ensemble 2*std. dev.	0.22	0.24
correlation of ensemble means	0.35	0.58
<i>Periods with decades showing a certain fraction of ensemble members with extreme temperatures synchronously in both hemispheres (lines 120ff)</i>		
>= 33% members with cold extremes	within 1594-1677	within 1449-1452 and 1597-1695
>66% members with positive extremes	since 1974	since 1974
>90% members with positive extremes	since 1979	since 1979
Fraction of years (%) with ensemble mean NH-SH difference outside the 10th-90th percentile range of model simulations (line 148)	41.6	43.1
<i>Pre-industrial temperature amplitude (°C; line 155)</i>		
Ensemble mean	0.37	0.75
Ensemble 2*std. dev.	0.11	0.13
<i>Uncertainties (°C; temporal average)</i>		
Interannual data	0.22	0.27
30-year filtered data	0.13	0.11

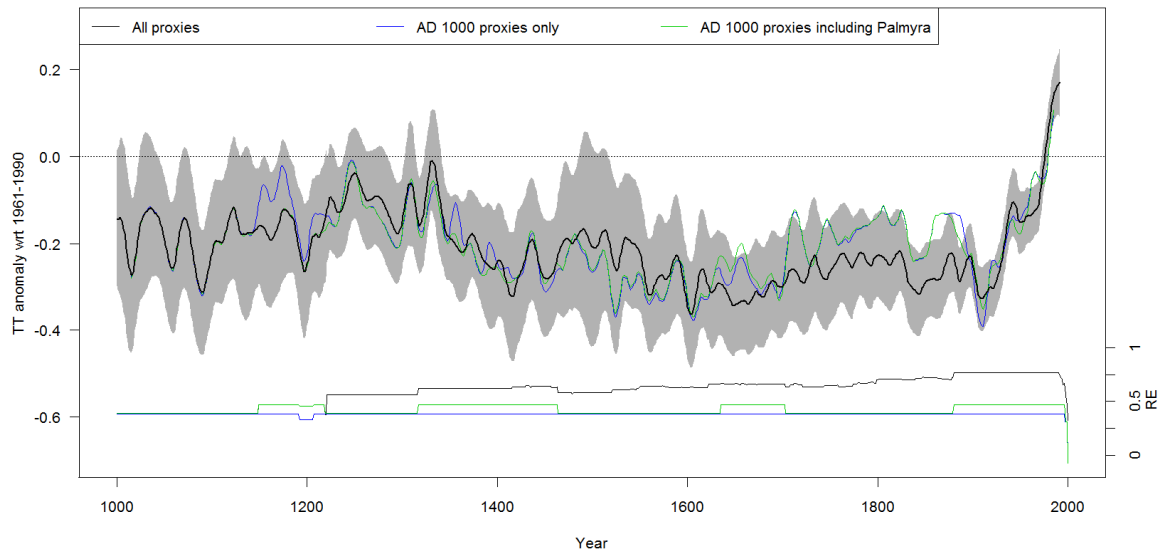
3.2.3. Influence of changes in proxy replication

A potential uncertainty of nested climate reconstructions is that the changes in proxy replication may bias the temporal representativity of the reconstruction. The proxy databases available throughout the reconstruction period may have different properties such as spatial distribution, land/ocean signal, seasonal response and spectral properties. If these differences are substantial, the reconstructions of different proxy combinations (nests) may not be comparable and splicing them together can lead to misinterpretations. To test this, we performed an additional reconstruction using only the records that extend back to the year 1000 or beyond (henceforth R8 reconstruction), resulting in a reconstruction with constant proxy replication over time.

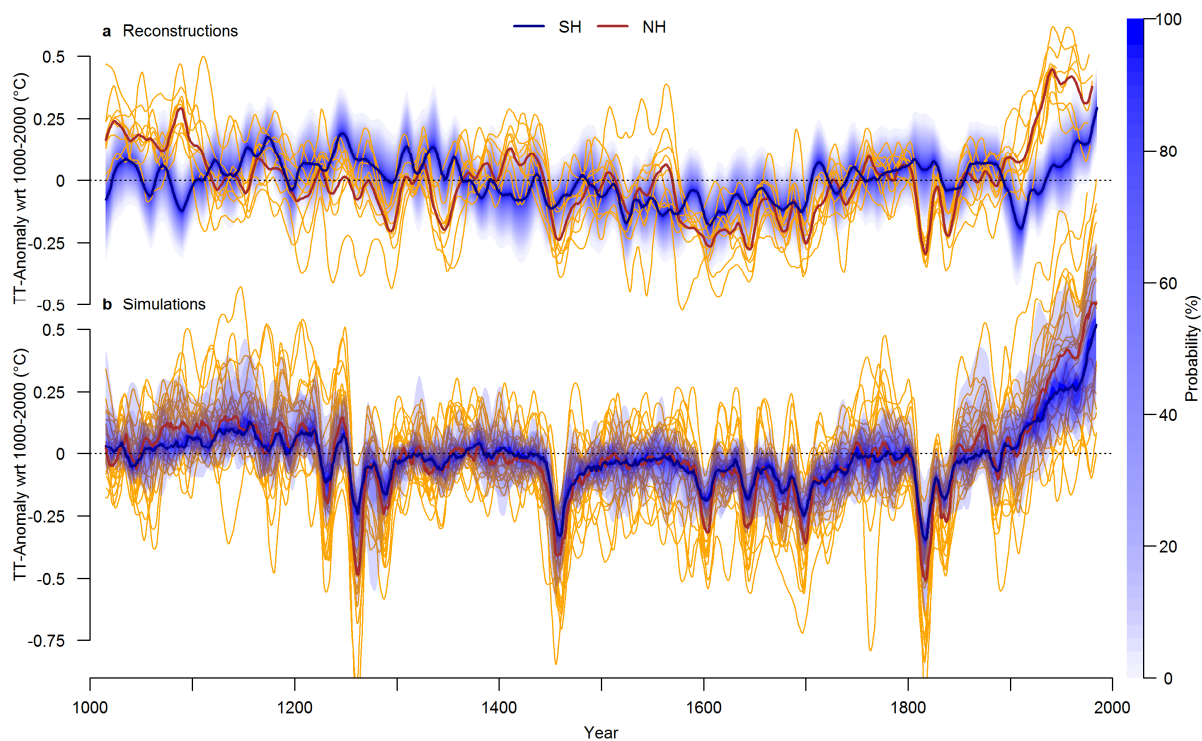
Supplementary Figure 15 shows the spatial distribution of proxy data over time. Supplementary Figure 16 compares the R8 reconstruction to the full spliced reconstruction using all 111 records. The figure shows that the two reconstructions generally have a very similar temperature evolution. The greatest differences occur between 1700 and 1900, where the R8 reconstruction shows warmer temperatures but the fluctuations are mostly in phase with the full reconstruction. Inclusion of the floating Palmyra coral record does not substantially change the R8 reconstruction except that it yields colder conditions in the late 11th century. Supplementary Figure 17-Supplementary Figure 19 show the analogues of Figures 2-4 in the main text for the R8 network. The figures are very similar to the results using the full network, indicating that our conclusions are not affected by the changing proxy replication over time.



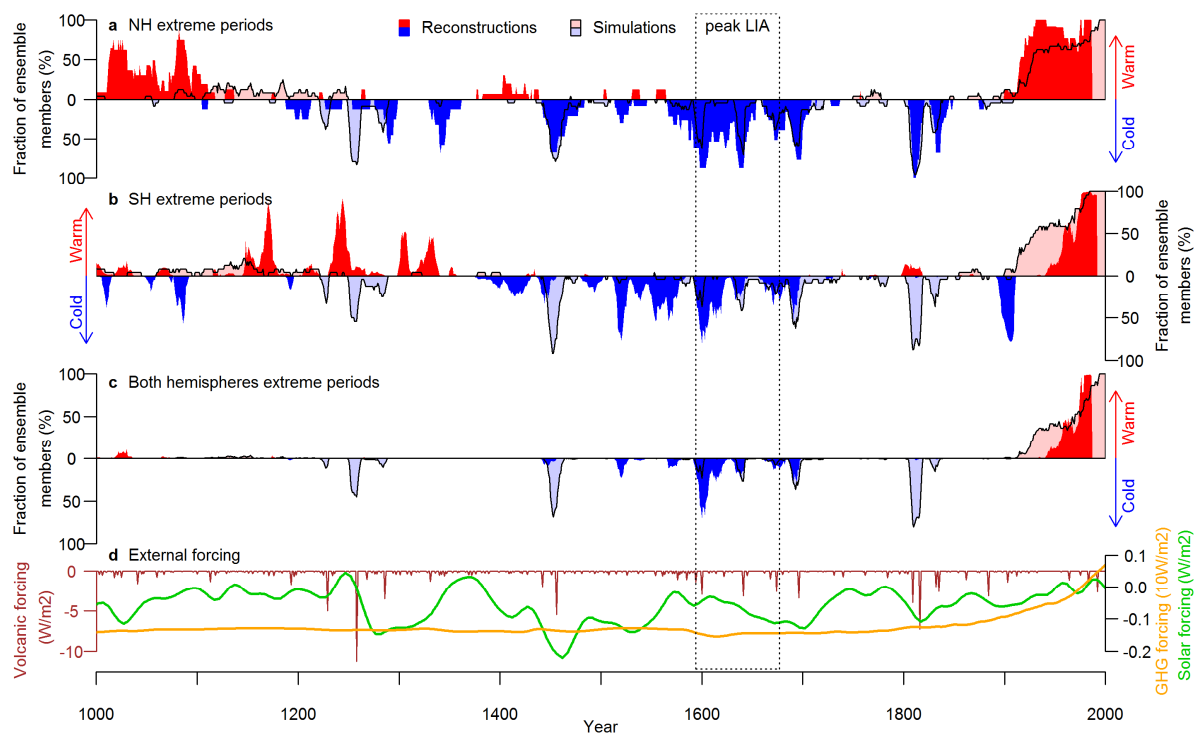
Supplementary Figure 15 | Spatial distribution of proxy data over time. Same as Figure 1a in the main text but showing proxy data availability for different years within the last millennium. The R8 network is shown in the top left panel (where the discontinuous Palmyra coral record is shown additionally as blue circle).



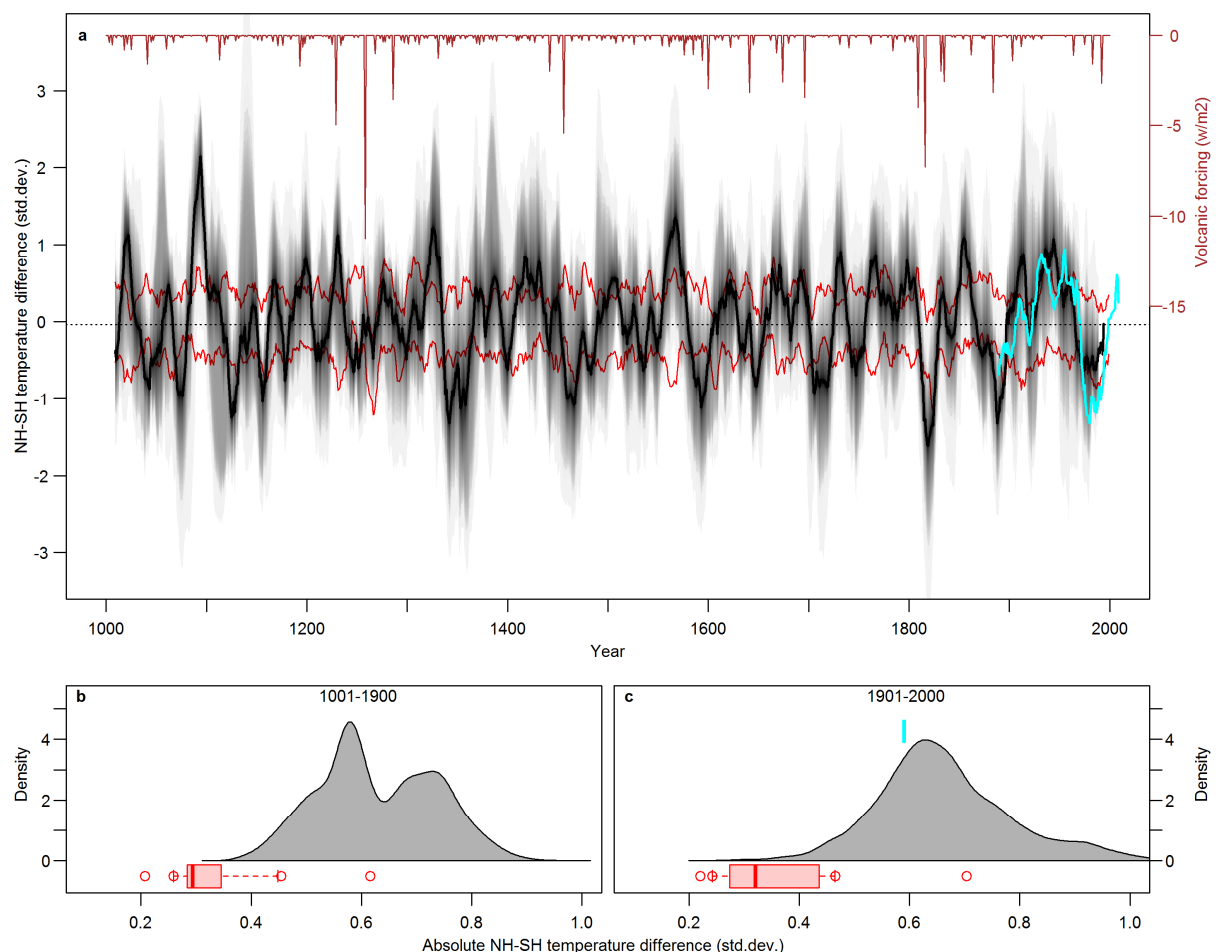
Supplementary Figure 16 | R8 reconstruction. Comparison of our SH reconstruction (black) with alternative reconstructions using only the proxies covering the full AD1000-2000 period (R8, blue) and additionally the floating and interrupted Palmyra coral record (green). Top: 30-year filtered reconstruction ensemble means. Grey shading represents the 2SE uncertainty bounds of the fully replicated reconstruction. Bottom: Corresponding verification years RE values.



Supplementary Figure 17 | Temperature variability over the last millennium using long proxies only. Same as Figure 2 in the main text but using the SH reconstruction that includes only the proxies extending to the year 1000.



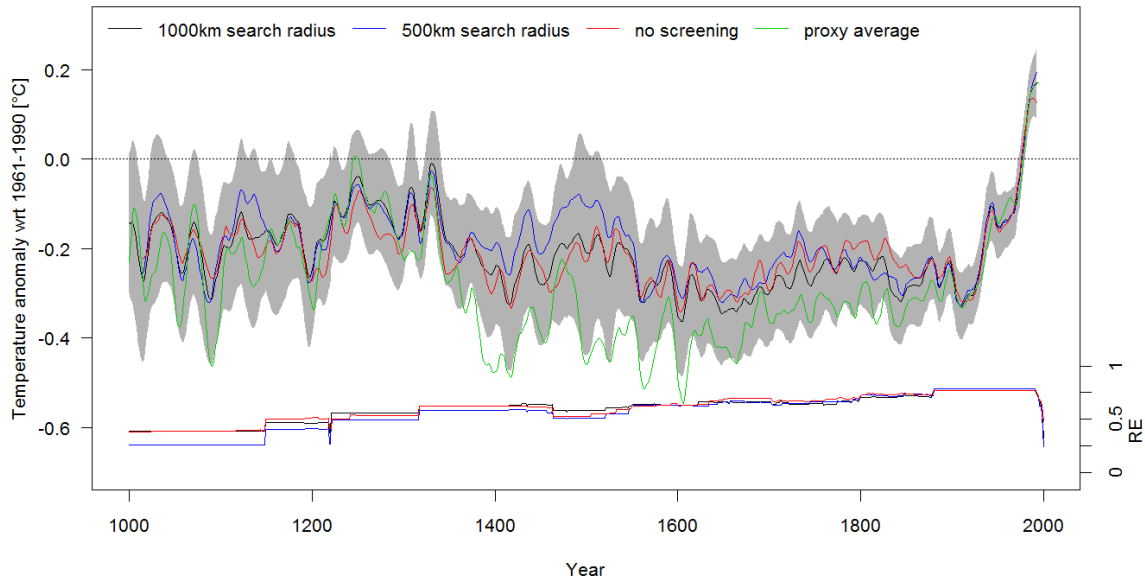
Supplementary Figure 18 | Extreme periods using long proxies only. Same as Figure 3 in the main text but using the SH reconstruction that includes only the proxies extending to the year 1000.



Supplementary Figure 19 | Inter-hemispheric temperature difference using long proxies only. Same as Figure 4 in the main text but using the SH reconstruction that includes only the proxies extending to the year 1000.

3.2.4. Influence of different proxy screening approaches

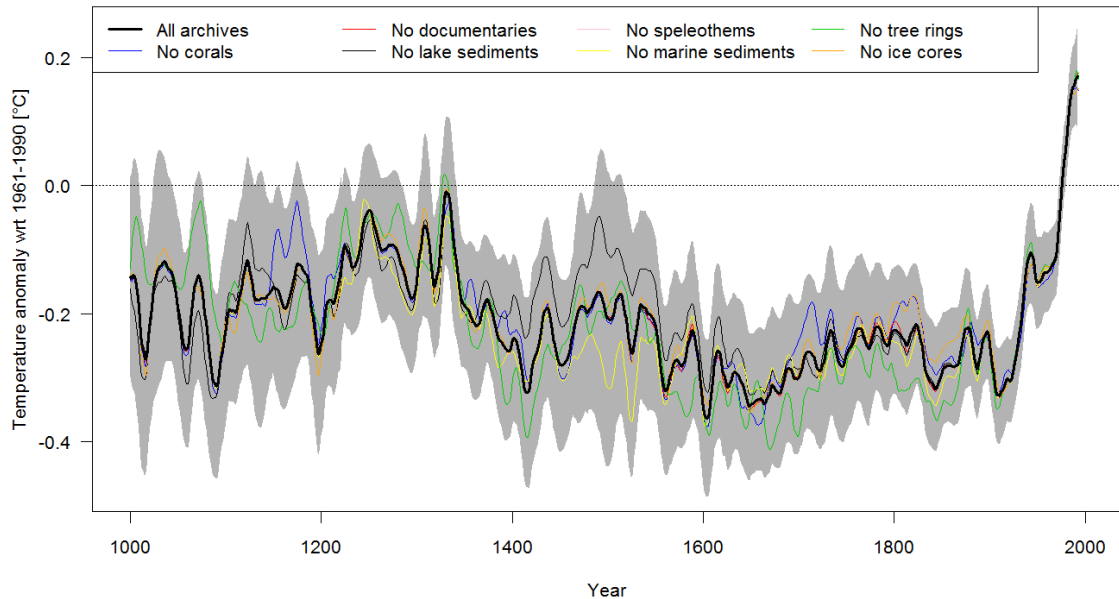
Supplementary Figure 20 compares our 30-year filtered reconstruction with alternative reconstructions using the same method but different proxy matrices: a pre-screened network using a search radius of 500 km (instead of 1000 km) and the full, unscreened network. The resulting reconstructions are very similar to the results presented in the main text and always remain within the 2SE uncertainty bands. Additionally a simple unweighted average of all 111 proxies used in the final reconstruction is shown by the green line in Supplementary Figure 20. This composite shows a similar temperature history, but with stronger cooling during the period 1400-1900. We interpret this difference as meaning that some regions with a high density of proxy data may have experienced colder conditions than the hemispheric average.



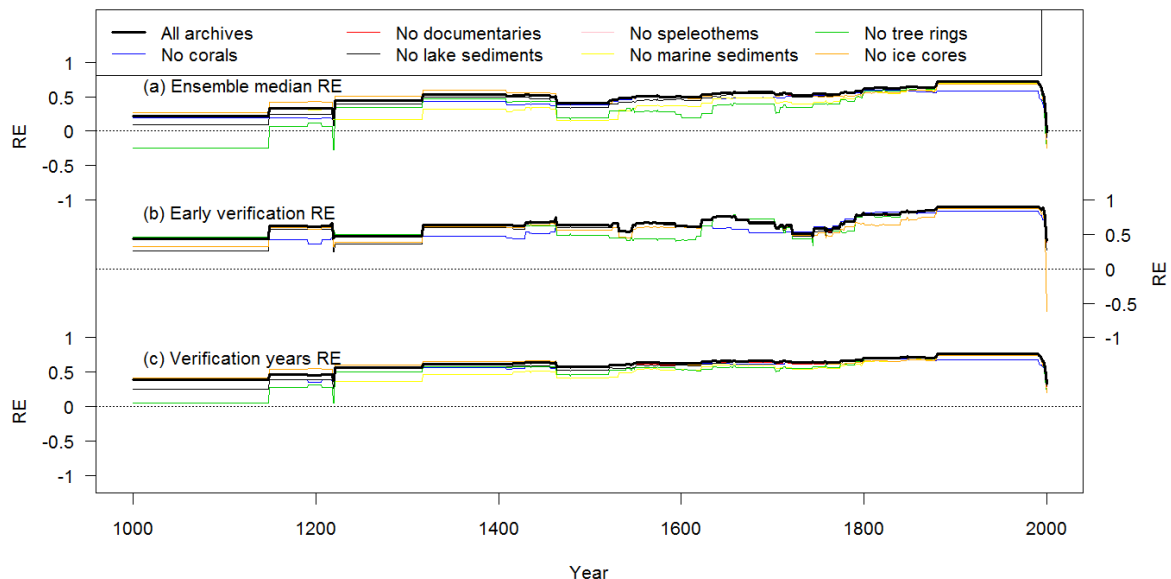
Supplementary Figure 20 | Influence of proxy screening. Comparison of 30-year filtered ensemble mean temperature reconstruction (top) and verification years RE (bottom) based on different predictor sets. Black: final predictor selection based on a search radius of 1,000 km (111 proxies). Blue: Predictor selection based on a search radius of 500 km (85 proxies). Red: No pre-screening of the proxies, all records are used (205 proxies). The green line represents a simple average of the 111 proxies used in the reconstruction (after adjusting them to a mean of zero and unit variance over the 1911-1990 period).

3.2.5. Influence of different proxy archives

Our proxy records are not evenly distributed over the different paleoclimate archives. Figure 1b in the main text shows that tree-rings and corals are the archives with the largest fraction of proxies used. This bias towards tree-rings and corals is very strong in the more recent past, but less distinct in the early period of the reconstruction. In the year 1000, our predictor set consists of three lake sediment and ice core chronologies, two tree-ring and one coral record. To assess whether one archive dominates the reconstruction and biases the results, we recalculated the reconstruction omitting all records from each archive separately. The resulting reconstructions and RE measures are shown in Supplementary Figure 21 and Supplementary Figure 22, respectively. The reconstructions with the individual archives removed always remain within the 2SE uncertainties of the final reconstruction (Supplementary Figure 21). Comparison of the RE values (Supplementary Figure 22) shows that in the first 200 years of the reconstruction, tree-ring data are required to obtain positive ensemble median RE values. For the other archives and skill measures, removing individual archives only marginally changes the reconstruction skill.



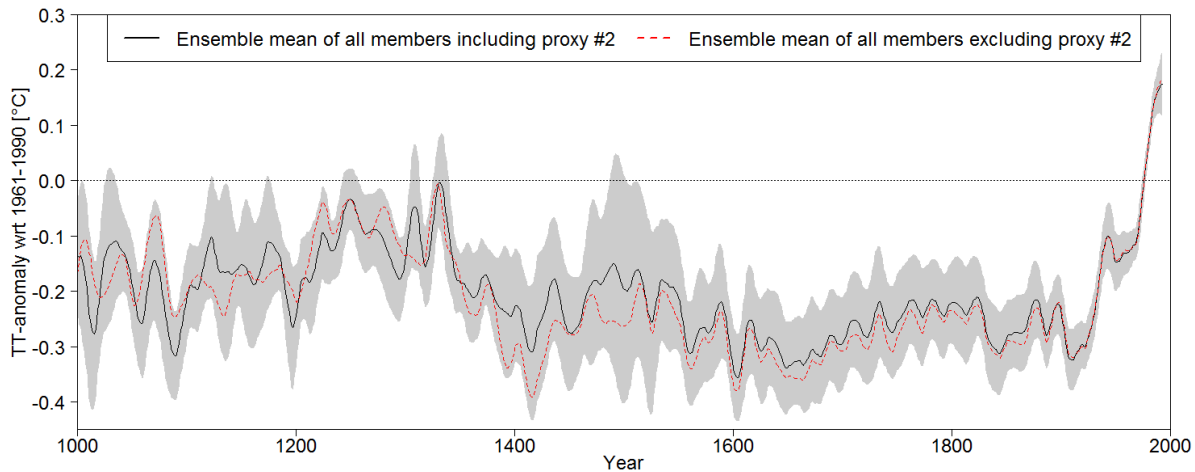
Supplementary Figure 21 | Influence of proxy archives. 30-year filtered ensemble mean reconstructions based on different combinations of proxy archives. Bold black is the final reconstruction using all archives with 2SE uncertainty bands shaded in grey. Blue is the reconstruction after removing all coral records; similarly for documentaries (red), lake sediments (thin black), speleothems (pink), marine sediments (yellow), tree-rings (green) and ice cores (orange).



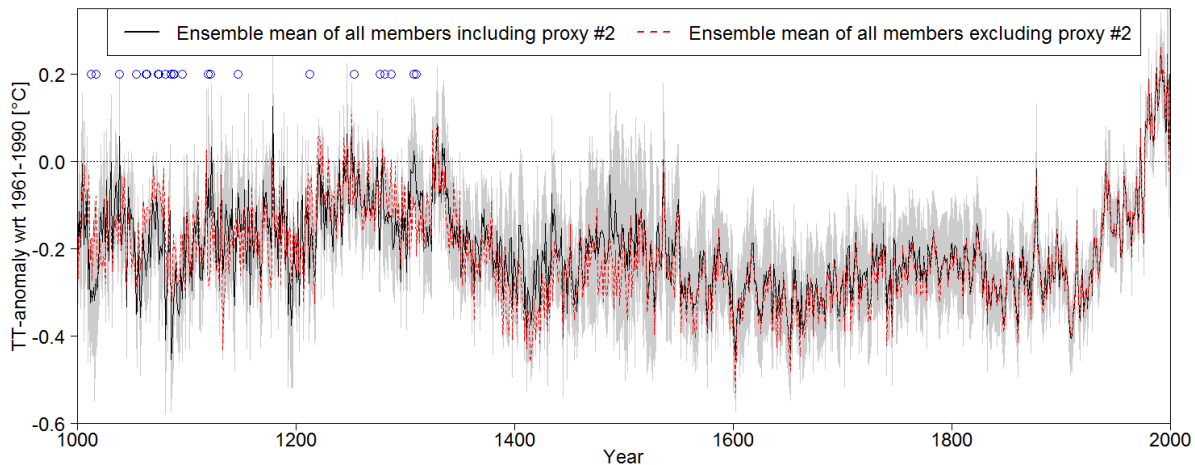
Supplementary Figure 22 | Influence of proxy archives on reconstruction skill. Same as Supplementary Figure 21 but for the RE measures of the reconstructions.

3.2.6. Influence of individual proxy records

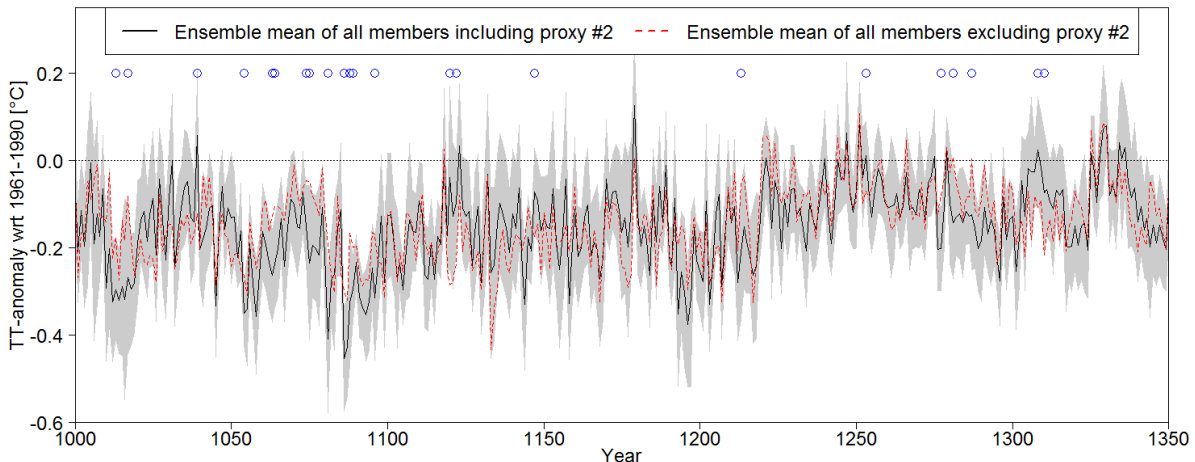
To assess whether our reconstruction is dominated by individual proxy records, we compare the ensemble members where a proxy was included and excluded, respectively. For each proxy we repeat the following calculations. The ensemble mean of all members where the proxy was included in the reconstruction ($mean_{inc}$) and excluded from the reconstruction ($mean_{exc}$) are calculated, respectively. The ensemble standard deviation of all members where the proxy was included (σ_{inc}) was also calculated. If the $mean_{exc}$ fell outside the $mean_{inc} \pm 2\sigma_{inc}$ range in one or more years, these periods are considered less robust. Note that this $\pm 2\sigma_{inc}$ range is different from the total combined uncertainties as it represents only the spread of a sub-sample of the full ensemble and does not include calibration uncertainties. This analysis was repeated using the 30-year filtered data. Supplementary Figure 23 illustrates the results using the example of proxy #2 (Mt. Read Tasmania) and the 30-year filtered data. Supplementary Figure 24 and Supplementary Figure 25 show the results of the interannual analysis for the same proxy. Note that out of all 111 proxies, the effect of removing a record is largest for the proxy #2 shown in these Figures. Over all proxies, this robustness criterion is not fulfilled during 25 (0) years of our unfiltered (30-year filtered) reconstruction. The 25 years where the criterion is not fulfilled on interannual timescales are all between 1000 and 1360. The proxies affected are #2 (Mt. Read; 23 years) and #8 (Palmyra, 2 years). Given this small fraction of years and proxies affected, we conclude that our reconstruction is robust with regard to changes in the predictor network, particularly during the post-1360 period and on decadal timescales.



Supplementary Figure 23 | Example for the influence of single proxies. Effect of removing proxy #2 (Mt. Read) from the predictor set on the 30-year filtered reconstructions. Black: mean of all ensemble members where this proxy was included into the reconstruction ($mean_{inc}$). Grey shading: 2 standard deviation bounds of these ensemble members ($mean_{inc} \pm 2\sigma_{inc}$). Red dashed: mean of all members where this proxy was withheld from the reconstruction ($mean_{exc}$).



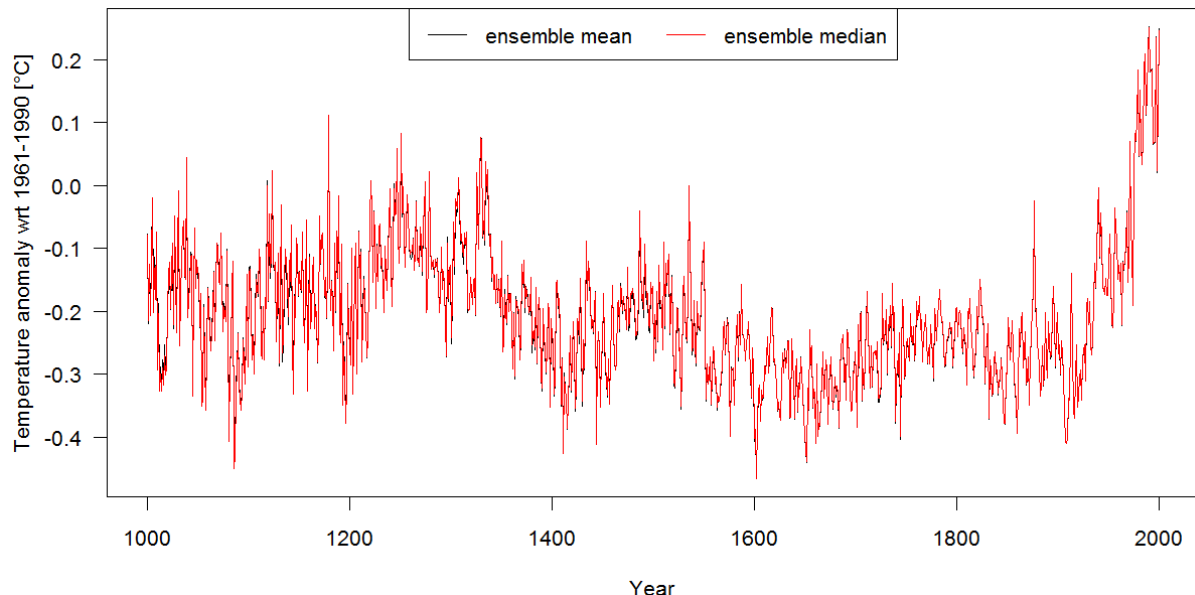
Supplementary Figure 24 | Example for the influence of single proxies on interannual scale. Same as Supplementary Figure 23 but for the unfiltered data. Blue circles indicate less robust years where the red dashed line falls outside the grey 2 standard deviation bounds.



Supplementary Figure 25 | Example for the influence of single proxies on interannual scale between 1000-1350. Same as Supplementary Figure 24 but over the period 1000-1350.

3.2.7. Ensemble median vs. mean

Supplementary Figure 5 shows the reconstruction ensemble median and mean, which are very similar (see also Supplementary Figure 4). The largest (average) absolute difference between the mean and the median over the period 1001-2000 is 0.15 (0.02) standard deviations of instrumental temperatures 1901-1999. For computational reasons we therefore use the ensemble mean to estimate the most probable reconstructed value. However, for the RE measures we use the ensemble median, as the mean is often biased by a small number of ensemble members with extremely large negative REs.



Supplementary Figure 26 | Ensemble mean vs. median. SH mean reconstruction ensemble mean (black) and median (red). See also Supplementary Figure 3

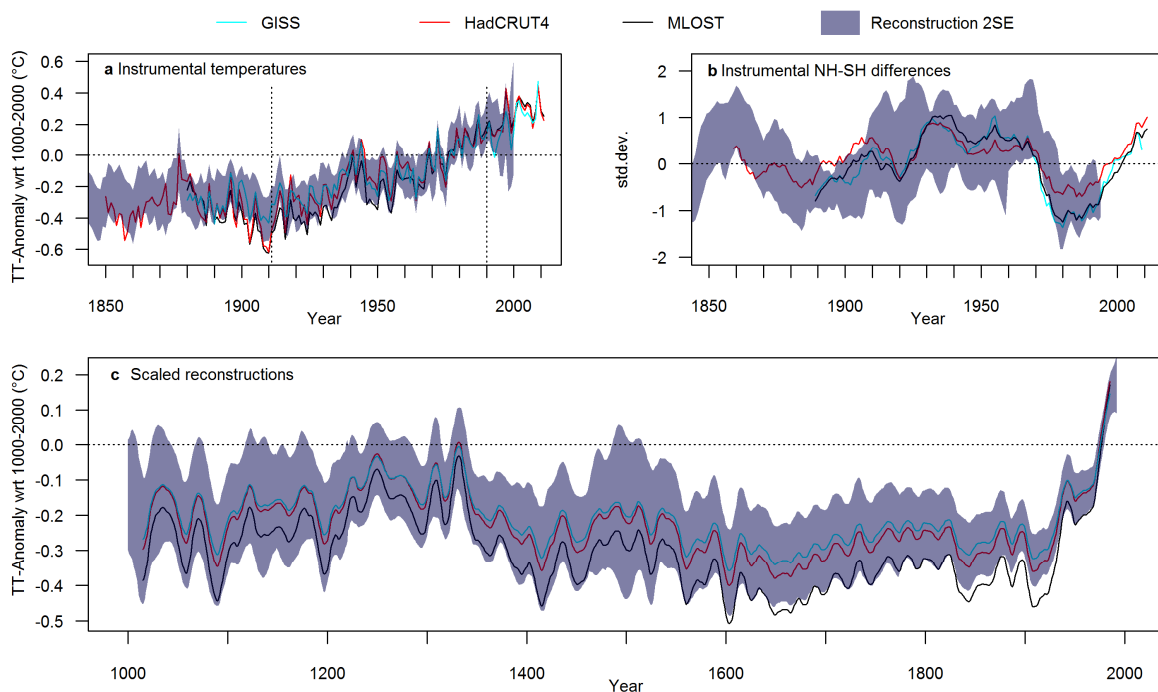
3.3. Conclusions

In summary, our reliability assessments indicate a skilful and robust reconstruction over the last millennium. More high resolution proxy records are required to allow a robust SH temperature reconstruction prior the year 1000.

4. Sensitivity to instrumental target data

Supplementary Figure 27 shows the sensitivity of our reconstruction to the choice of the instrumental dataset used for calibration. While the SH means of the three instrumental grids GISS (Hansen et al., 2010), HadCRUT4 (Morice et al., 2012) and MLOST (Smith et al., 2008) are highly correlated over the 1911-1990 calibration period (all $r>0.94$, $p<<0.01$), they exhibit some differences in amplitude and trend (GISS: $0.50^{\circ}\text{C}/\text{century}$; HadCRUT4: $0.58^{\circ}\text{C}/\text{century}$; MLOST: $0.74^{\circ}\text{C}/\text{century}$). The NH-SH differences, however, are similar and do not affect our conclusions (see also Drost and Karoly, 2012; Drost *et al.*, 2012).

To assess the influence of the instrumental dataset on our reconstruction, we re-scaled our ensemble mean reconstruction to the mean and variance of the three instrumental data (Supplementary Figure 27c). While the results from GISS and HadCRUT4 are very similar, the reconstruction rescaled to MLOST reveals lower pre-industrial temperatures (average offset of 0.1°C between GISS and MLOST over 1000-1850). This suggests that our estimates of the unusual nature of late 20th century temperatures are rather conservative given our choice of the instrumental calibration dataset.



Supplementary Figure 27 | Comparison of different instrumental temperature datasets. Comparison of the GISS dataset (cyan; Hansen et al., 2010) used for our reconstruction with the other gridded instrumental temperature records HadCRUT4 (red; Morice et al., 2012) and NOAA MLOST (black; Smith et al., 2008). Instrumental 2SE envelopes are blue shaded. **a** Instrumental SH mean temperatures (cf. Figure 1c in the main text). Start and end dates of the calibration/verification period of our reconstruction (1911-1990) are indicated by vertical dotted lines. **b** NH-SH differences 1850-2010 (cf. Figure 4a in the main text). **c** 30-year filtered SH reconstruction ensemble means re-scaled to the mean and variance of each instrumental target over the 1911-1990 period.

5. NH reconstruction ensemble

Details concerning the NH reconstructions are provided in Frank *et al.* (2010). The most important difference from our SH reconstruction is that it is not based on a single predictor matrix but uses nine published NH reconstructions, based on different (but not independent) proxy sets and various reconstruction methodologies (Jones *et al.*, 1998; Briffa, 2000; Mann and Jones, 2003; Moberg *et al.*, 2005; D'Arrigo *et al.*, 2006a; Frank *et al.*, 2007; Hegerl *et al.*, 2007; Juckes *et al.*, 2007; Mann *et al.*, 2008). In Frank *et al.* (2010), the individual single-member reconstructions were recalibrated to instrumental temperature data using different calibration periods as ensemble parameters, resulting in a total of 521 ensemble members. Although the approach is different, the NH reconstruction ensemble also represents a combination of calibration, proxy data and methodological perturbations. The latter two are introduced through the nine different original reconstructions in the NH, whereas for the SH they are sampled for each ensemble member. In the NH approach, the variable calibration window resulted in a quantification of amplitude uncertainty only, whereas in our SH approach changing the calibration period also influences the shape of the reconstructed temperature history. The NH ensemble spread is larger than in the SH due to the relatively large differences between some of the original sub-reconstructions and the composite-plus-scaling approach over a range of time-windows in ref. (Frank *et al.*, 2010). Note that the increase in ensemble uncertainties back in time is much larger in the SH (the ratio of uncertainties 11th century/20th century is 2.34 for the SH and 1.2 for the NH). To best illustrate these two approaches, the ensemble means of the nine sub-reconstructions are shown for the NH in Figure 2a. As a consequence of these methodological differences and the larger ensemble spread in the NH, one would expect generally reduced probabilities for extreme periods in the NH. However, Figures 3a-b show similar fractions of periods with high probabilities for extremes, indicating a similar consistency between ensemble members in the timing of extreme periods in both hemispheres. The relatively small ensemble spread in the NH-SH differences (Figure 4a), particularly during extreme phases, where in most cases all ensemble members are of the same sign, also indicates consistency among the NH reconstructions in identifying decadal-scale temperature trends.

6. Simultaneous extreme periods

Supplementary Table 8 | Synchronous extreme periods. Periods where both hemispheres exhibit extreme periods in at least 33% of their reconstruction ensemble members. The years indicated are the start years of 10-year running temperature averages as used to generate Figure 3 in the main text. Extremes are defined as 10-year averages exceeding one standard deviation above or below the 1000-2000 CE baseline. Note that 1986 is the last year of this analysis (representing the average of 1986-1995), because the NH reconstruction ends in 1995.

Negative extremes	1594, 1595, 1596, 1597, 1598, 1599, 1600, 1601, 1602, 1603, 1619, 1620, 1621, 1622, 1623, 1635, 1636, 1639, 1640, 1641, 1642, 1643, 1644, 1645, 1646, 1671, 1672, 1673, 1674, 1675, 1676, 1677
Positive extremes	1030, 1965, 1967, 1968, 1969, 1970, 1971, 1972, 1973, 1974, 1975, 1976, 1977, 1978, 1979, 1980, 1981, 1982, 1983, 1984, 1985, 1986

7. Details on climate model simulations

Supplementary Table 9 provides an overview over the 24 model simulations used in this study. Ten of the simulations belong to the latest coordinated PMIP3-CMIP5 simulation effort (Taylor *et al.*, 2012) using recommendations for forcings from Schmidt et al. (2011; 2012). For further details we refer to the references provided in the table. We use hemispheric averages and May-April years for the SH and calendar years for the NH, as represented by the reconstructions.

Supplementary Table 9 | Details of the model simulations used in this study. Name, time period covered and forcing datasets used. Weak/Strong in the column for solar forcing is a qualitative remark for the strength of solar variability over the last millennium (see e.g. Jungclaus *et al.*, 2010). For further details we refer to the references provided in the table. Note that for some simulations, references for the simulation of the last millennium are not yet available. In these cases, general references to the model are provided. The last column indicates whether the simulation belongs to the latest PMIP3/CMIP5 dataset (Taylor *et al.*, 2012) using recommendations for forcings from Schmidt *et al.* (2011; 2012).

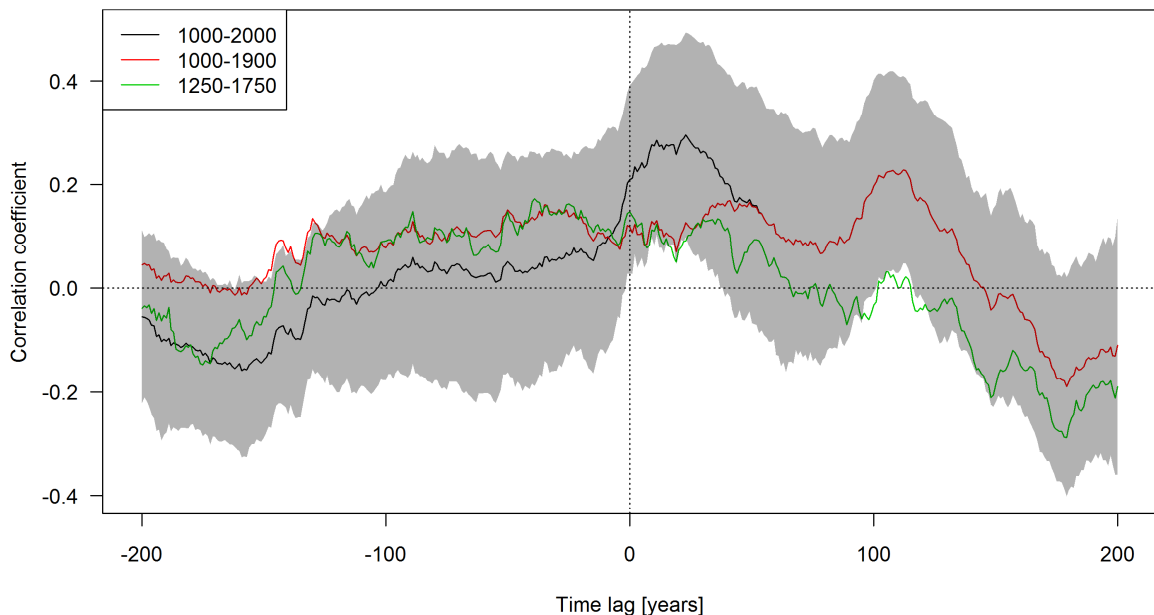
Model	Simulation	Time span	Volcanic forcing	Solar forcing	GHG forcing	Orbital forcing	Land-use-land-cover forcing	Aerosol forcing	Reference(s)	PMIP3/CMIP5
BCC-CSM		0850-2000	(Gao <i>et al.</i> , 2008)	Weak (Vieira and Solanki, 2010) spliced to (Wang <i>et al.</i> , 2005)	(MacFarling-Meure <i>et al.</i> , 2006); (Schmidt <i>et al.</i> , 2011 and references therein)	(Berger, 1978)		(Lamarque <i>et al.</i> , 2010)	(Xin <i>et al.</i> , 2013)	X
CCSM3		1000-2000	(Ammann <i>et al.</i> , 2003)	Strong (Bard <i>et al.</i> , 2000), spliced to (Lean <i>et al.</i> , 1995)	CO ₂ : (Etheridge <i>et al.</i> , 1996), CH ₄ : Blunier <i>et al.</i> (1995), (Blunier <i>et al.</i> , 1995), N ₂ O: (Flückiger <i>et al.</i> , 1999; Flückiger <i>et al.</i> , 2002)				(Hofer <i>et al.</i> , 2011)	
CCSM4		850-2005	(Gao <i>et al.</i> , 2008)	Weak (Vieira and Solanki, 2010) spliced to (Wang <i>et al.</i> , 2005)	(Schmidt <i>et al.</i> , 2011 and references therein)	(Berger, 1978)	(Pongratz <i>et al.</i> , 2009) spliced to (Hurtl <i>et al.</i> , 2006)	(Lamarque <i>et al.</i> , 2010)	(Laundrum <i>et al.</i> , 2013)	X
CSIRO Mk3L-1-2	1-3	1000-2000	(Gao <i>et al.</i> , 2008)	Weak (Steinhilber <i>et al.</i> , 2009) spliced to (Wang <i>et al.</i> , 2005)	(MacFarling-Meure <i>et al.</i> , 2006)	(Berger, 1978)			(Phipps <i>et al.</i> , 2011; Phipps <i>et al.</i> , 2012; Phipps <i>et al.</i> , 2013)	
CSIRO-Mk3L-1-2		0850-2000	(Crowley and Unterman, 2013)	Weak (Steinhilber <i>et al.</i> , 2009) spliced to (Wang <i>et al.</i> , 2005)	(MacFarling-Meure <i>et al.</i> , 2006); (Schmidt <i>et al.</i> , 2011 and references therein)	(Berger, 1978)			(Phipps <i>et al.</i> , 2011; Phipps <i>et al.</i> , 2012)	X
ECHO-G	Erik 1 & 2	1000-1990	(Crowley, 2000)	Strong (Bard <i>et al.</i> , 2000), spliced to (Lean <i>et al.</i> , 1995)	CO ₂ : (Etheridge <i>et al.</i> , 1996), CH ₄ : (Etheridge <i>et al.</i> , 1998), N ₂ O: (Battle <i>et al.</i> , 1996)				(González-Rouco <i>et al.</i> , 2006)	
FGOALS-g1		1000-1999	(Crowley, 2000)	Strong (Bard <i>et al.</i> , 2000), spliced to (Lean <i>et al.</i> , 1995)	CO ₂ : (Etheridge <i>et al.</i> , 1996), CH ₄ : Blunier <i>et al.</i> (1995), (Blunier <i>et al.</i> , 1995), N ₂ O: (Flückiger <i>et al.</i> , 1999; Flückiger <i>et al.</i> , 2002)				(Yongqiang <i>et al.</i> , 2002; Yongqiang <i>et al.</i> , 2004)	X ^a

Model	Simulation	Time span	Volcanic forcing	Solar forcing	GHG forcing	Orbital forcing	Land-use-land-cover forcing	Aerosol forcing	Reference(s)	PMIP3/CMIP5
GISS-E2-R	p121	850-2005	(Crowley and Unterman, 2013)	Weak (Steinhilber et al., 2009) spliced to (Wang et al., 2005)	(MacFarling-Meure et al., 2006); (Schmidt et al., 2011 and references therein)	(Berger, 1978)	(Pongratz et al., 2009) spliced to (Hurtt et al., 2006)	(Lamarque et al., 2010)	(Schmidt et al., 2006)	X
GISS-E2-R	p124	850-2005	(Crowley and Unterman, 2013)	Weak (Vieira and Solanki, 2010) spliced to (Wang et al., 2005)	(MacFarling-Meure et al., 2006); (Schmidt et al., 2011 and references therein)	(Berger, 1978)	(Pongratz et al., 2009) spliced to (Hurtt et al., 2006)	(Lamarque et al., 2010)	(Schmidt et al., 2006)	X
GISS-E2-R	p127	850-2005	(Crowley and Unterman, 2013)	Weak (Vieira and Solanki, 2010) spliced to (Wang et al., 2005)	(MacFarling-Meure et al., 2006); (Schmidt et al., 2011 and references therein)	(Berger, 1978)	(Kaplan et al., 2011)	(Lamarque et al., 2010)	(Schmidt et al., 2006)	X
HadCM3		800-2000	(Crowley and Unterman, 2013)	Weak (Steinhilber et al., 2009) spliced to (Wang et al., 2005)	(MacFarling-Meure et al., 2006); (Schmidt et al., 2011 and references therein)	(Berger, 1978)	(Pongratz et al., 2009) spliced to (Hurtt et al., 2006)	(Johns et al., 2003)	(Schurer et al., 2013)	X
IPSL-CM5A-LR		0850-2005	(Ammann et al., 2007)	Weak (Vieira and Solanki, 2010) spliced to (Wang et al., 2005)	(MacFarling-Meure et al., 2006); (Schmidt et al., 2011 and references therein)	(Berger, 1978)			(Dufresne et al., 2012)	X
MPI-ESM E1	1-5	800-2005	(Crowley and Unterman, 2013)	Weak (Krivova et al., 2007)	CO ₂ : diagnosed (Marland et al., 2003) CH ₄ and N ₂ O: (MacFarling-Meure et al., 2006)	(Bretagnon and Francou, 1988)	(Pongratz et al., 2008)	(Lefohn et al., 1999)	(Jungclaus et al., 2010)	
MPI-ESM E2	1-3	800-2005	(Crowley and Unterman, 2013)	Strong (Bard et al., 2000)	CO ₂ : diagnosed (Marland et al., 2003) CH ₄ and N ₂ O: (MacFarling-Meure et al., 2006)	(Bretagnon and Francou, 1988)	(Pongratz et al., 2008)	(Lefohn et al., 1999)	(Jungclaus et al., 2010)	
MPI-ESM-P		850-2005	(Crowley and Unterman, 2013)	Weak (Vieira and Solanki, 2010) spliced to (Wang et al., 2005)	(MacFarling-Meure et al., 2006); (Schmidt et al., 2011 and references therein)	(Berger, 1978)	(Pongratz et al., 2009) spliced to (Hurtt et al., 2006)	(Lamarque et al., 2010)	(Jungclaus et al., 2012; Jungclaus et al., 2013)	X

^a Does not follow the Schmidt et al. (2011; 2012) guidelines for PMIP3/CMIP5 forcing.

8. Lag between the hemispheres

The statement in the main text that we find no evidence for a consistent lag between NH and SH temperatures is supported by a correlation analysis. We correlate each NH reconstruction ensemble members with a randomly chosen SH reconstruction member which is temporally lagged by -200 to 200 years (Supplementary Figure 28). The maximum correlation ($r=0.30\pm0.19$) is identified at a lag of +23 years, being slightly higher than the correlation at lag 0 ($r=0.21\pm0.18$). However, this peak around lags of 10-30 years is dominated by the industrial period, where the SH temperature rise is ~ 25 years delayed compared to the NH. This peak disappears if the analysis is only calculated over the 1000-1900 period (red line in Supplementary Figure 28). The second peak around a lag of +110 years is not evident if the analysis is reduced to the 1250-1750 period (green line in Supplementary Figure 28), indicating that these peaks are not stable over time but influenced by individual periods.



Supplementary Figure 28 | Lagged inter-hemispheric temperature correlations. Correlation between reconstructed NH and SH temperatures lagging the SH data for -200 to 200 years. Black: Ensemble mean correlations using the full 1000-2000 period. Grey shading represents the 2σ ensemble range. Red (green): Same as black but using only the 1000-1900 (1250-1750) period.

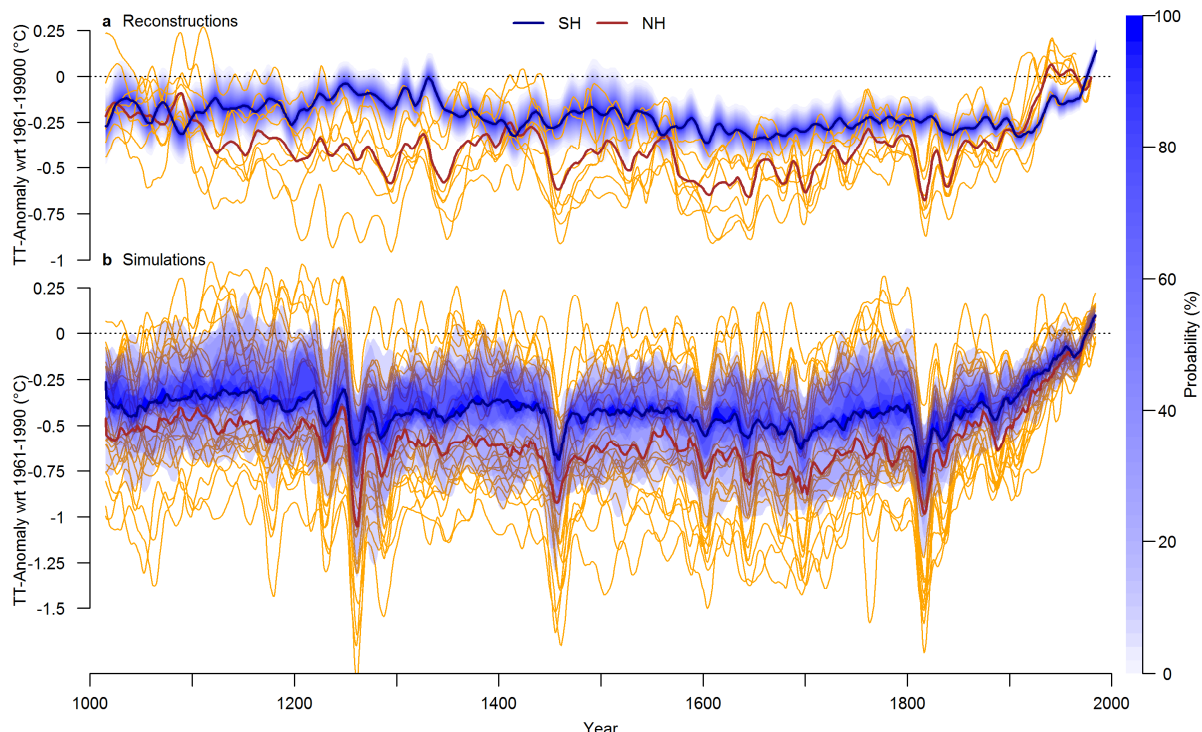
9. Alternative reference period and comparison with earlier SH and regional reconstructions

Supplementary Figure 29 shows an alternative illustration of Figure 2, using 1961-1990 as the reference period. It illustrates the reduced pre-industrial cooling in the SH seen in the reconstructions and simulations (compared to the stronger 20th century warming in the NH, expressed by the 1000-2000 baseline in Figure 2 in the main text).

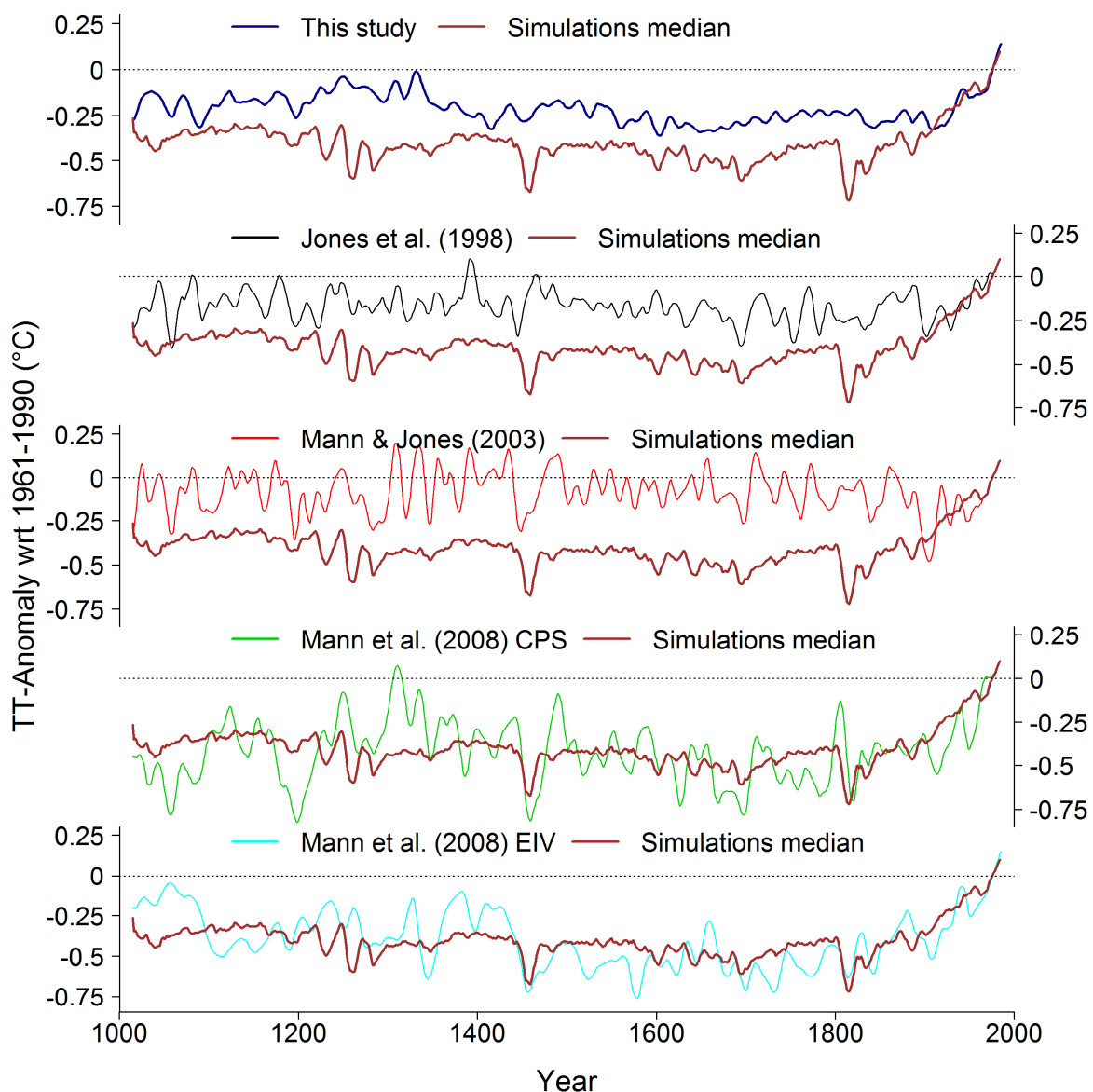
Supplementary Figure 30 compares our SH reconstruction with the model ensemble median and provides comparison with earlier SH temperature reconstructions (Jones *et al.*, 1998; Mann and Jones, 2003; Mann *et al.*, 2008). The number of proxy records available for these earlier reconstructions is seven (Jones *et al.*, 1998), five (Mann and Jones, 2003) and 165 (Mann *et al.*, 2008; 173 records if decadally resolved data are counted as well), respectively, compared to our network of 325 sites (Supplementary Table 1-4; to allow comparison, all tree-ring sites that were aggregated to composites herein need to be counted individually). The overlap of our proxy network with the Mann *et al.* (2008) records is small: Out of the nine long proxies extending to the year 1000, three have also been used by Mann et al. (2008): Mt. Read, Oroko and Quelccaya (Law Dome $\delta^{18}\text{O}$ is in the Mann *et al.* (2008) dataset as well, but they used an older record that covers only the period 1761-1970). For the records extending back to the year 1500 and beyond, 5 out of 18 records overlap (28%) plus one tree-ring composite with partial overlap.

Supplementary Figure 31 compares our SH reconstruction with regional reconstructions from Antarctica, Australasia and South America (PAGES 2013). Note that the regional reconstructions have different targets in terms of seasons and coverage (Antarctica and South America are land only, whereas Australasia is also a combined land-ocean reconstruction). This may explain the large differences in variance among the reconstructions. The SH reconstruction is strongly correlated with the Australasian ($r=0.46$, $p<<0.01$ over 1000-2000) and South American reconstructions ($r=0.33$, $p<<0.01$) and only weakly but significantly with

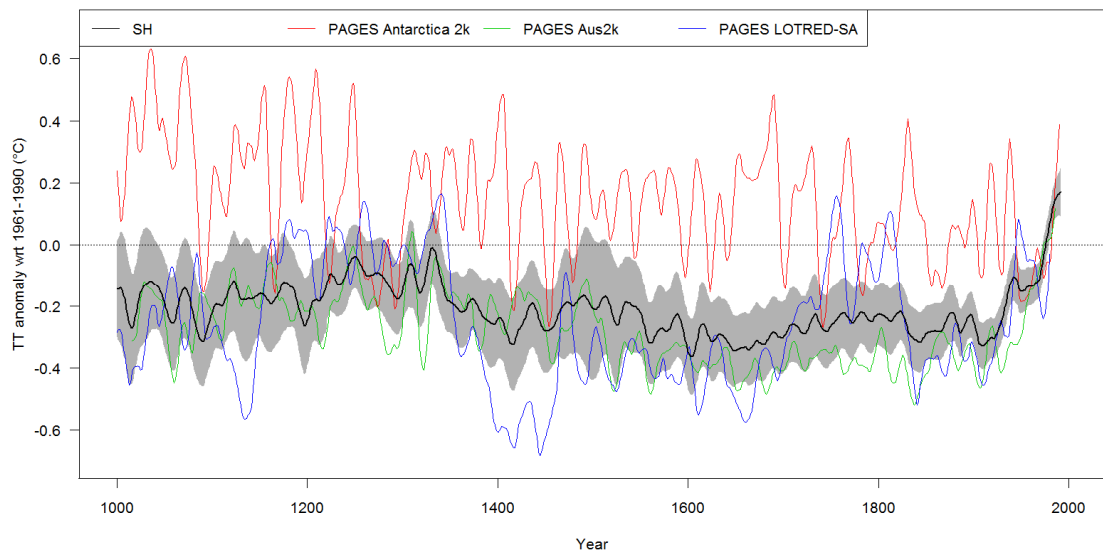
Antarctica ($r=0.15$, $p<<0.01$). These numbers are qualitatively comparable, albeit with lower values, to the corresponding instrumental data (Antarctica: $r=0.33$, $p=0.10$ over 1957-1990; Australasia: $r=0.63$, $p<<0.01$, over 1911-1990; South America: $r=0.42$, $p<0.01$ over 1911-1990). The SH relative warm period between ca. 1250-1350 and the cold periods in the 17th and 19th centuries are also inherent in the Australasian and South American reconstructions. These three datasets also show similar average pre-industrial temperatures relative to the 1961-1990 mean. The 14th-century cooling as well as the relatively warm 18th century are much stronger in the South American data. The Antarctic reconstruction shows a clearly different temperature history with reduced low-frequency variability. Given the small influence of Antarctica on the SH mean temperatures (Supplementary Figure 2), these differences are not surprising. Note that the regional reconstructions are not independent from our SH data due to considerable overlaps in the proxy data.



Supplementary Figure 29 | Temperature variability over the last millennium with alternative reference period. Same as Figure 2 in the main text but using a 1961-1990 reference period.



Supplementary Figure 30 | Direct comparison with simulations and earlier SH reconstructions. Top: Comparison of our SH reconstruction ensemble mean (blue) with the ensemble median of the simulations (brown) relative to the 1961-1990 baseline. Lower panels: Comparisons of earlier SH temperature reconstructions (Jones *et al.*, 1998; Mann and Jones, 2003; Mann *et al.*, 2008) with the model ensemble median.

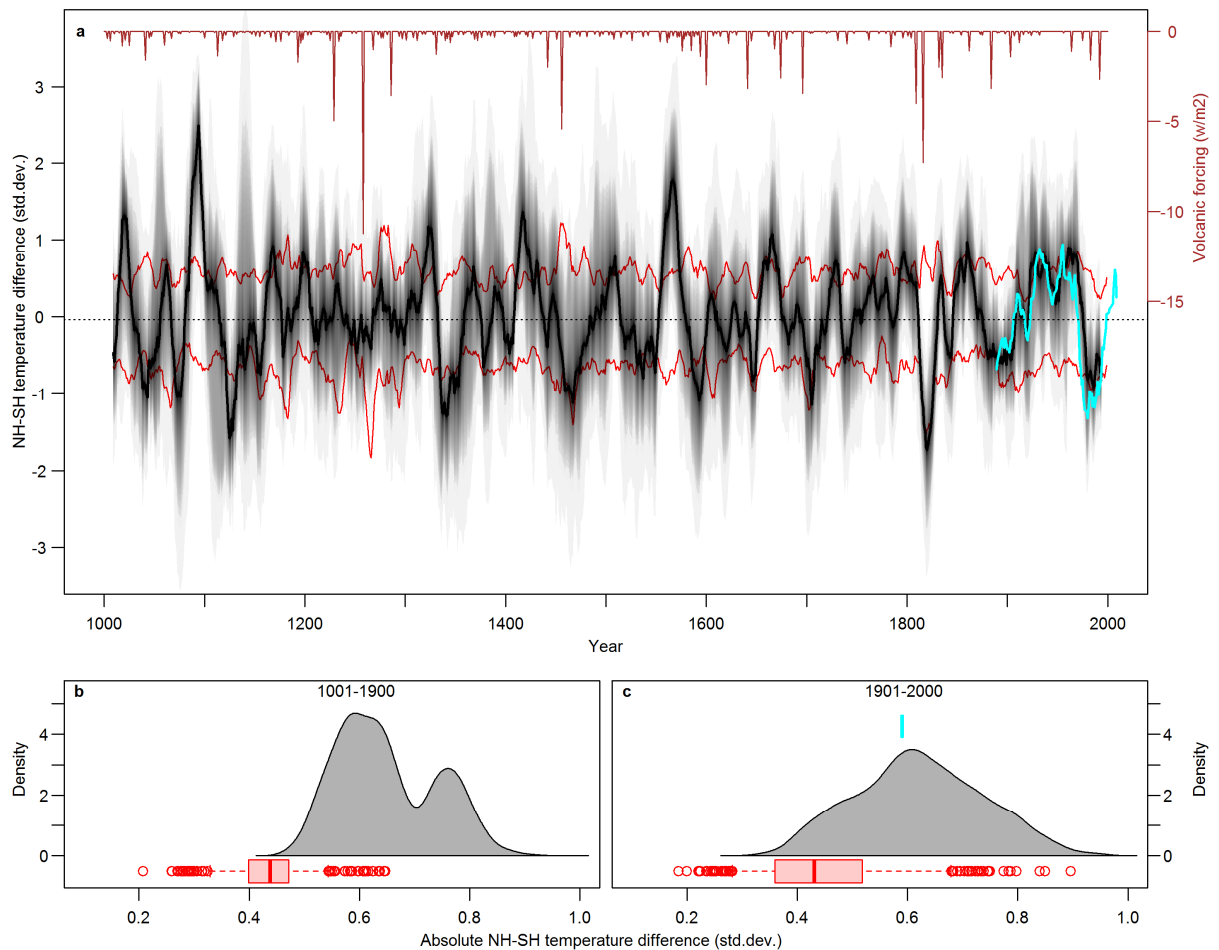


Supplementary Figure 31 | Comparison with regional SH reconstructions. Comparison of our SH reconstruction ensemble mean (black with shaded 2SE bounds), with regional reconstructions from Antarctica (red), Australasia (green) and South America (blue) published in a global synthesis of regional reconstructions (PAGES 2013).

10. Alternative illustrations of inter-hemispheric differences

10.1. Inter-model comparisons

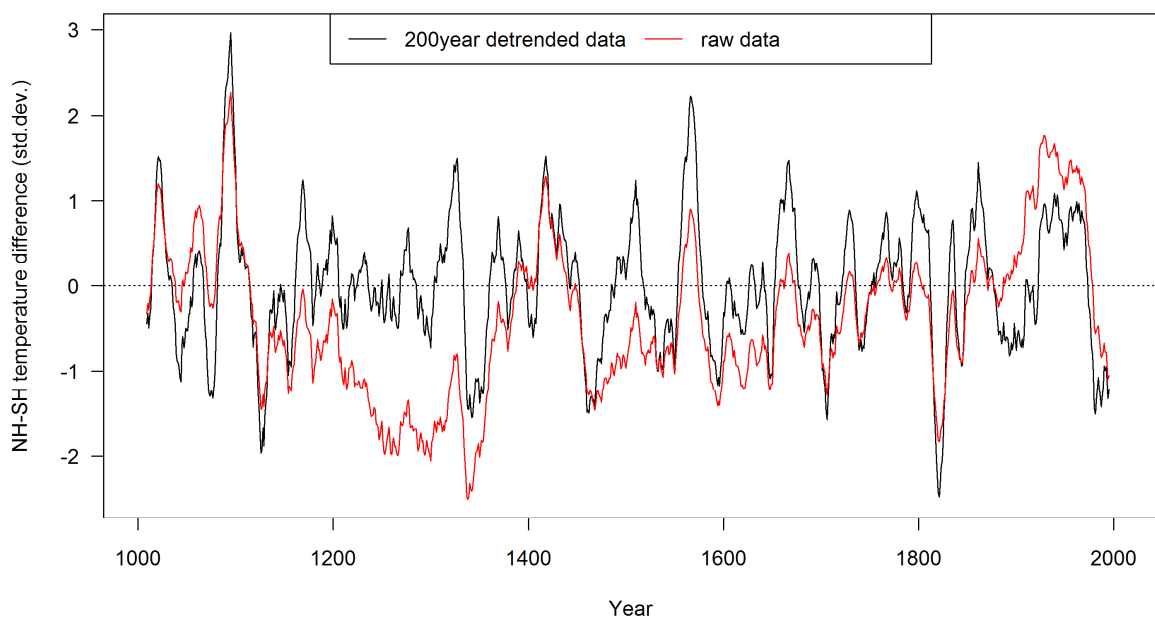
A potential caveat in our data-model comparisons is the fact that the reconstructions are noisy estimates of temperature variability with different and largely independent noise in the reconstructions of the two hemispheres. In contrast, within each model simulation there is no such noise between the hemispheres. Although the simulations do not reflect the true temperature history, the hemispheric extractions reflect a direct picture of temperatures in the model world. Inter-hemispheric differences are potentially inflated in the reconstructions relative to the simulations because of the noisy nature of the reconstructions. This may partially explain the larger values in reconstructed NH-SH differences shown in Figure 4 in the main text. To test this hypothesis, we repeat the analysis calculating the NH-SH differences not only within each simulation but also across the 24 different model simulations, to mimic the noisy behavior of the reconstructions. Results are shown in Supplementary Figure 32. Although the simulated NH-SH differences have increased with the inter-model calculations, they are still clearly smaller than in the reconstructions. We therefore argue that our conclusions are not biased by the different noise structure in reconstructions and simulations but reflect true differences between reconstructed and simulated temperatures.



Supplementary Figure 32 | NH-SH differences using inter-model calculations. Same as Figure 4 in the main text but after calculating the NH-SH differences across all model simulations. Boxes and whiskers of the boxplots in c and d represent the interquartile range and 5th/95th percentiles, respectively; circles represent results outside the 5th and 95th percentiles.

10.2. Raw vs. detrended data

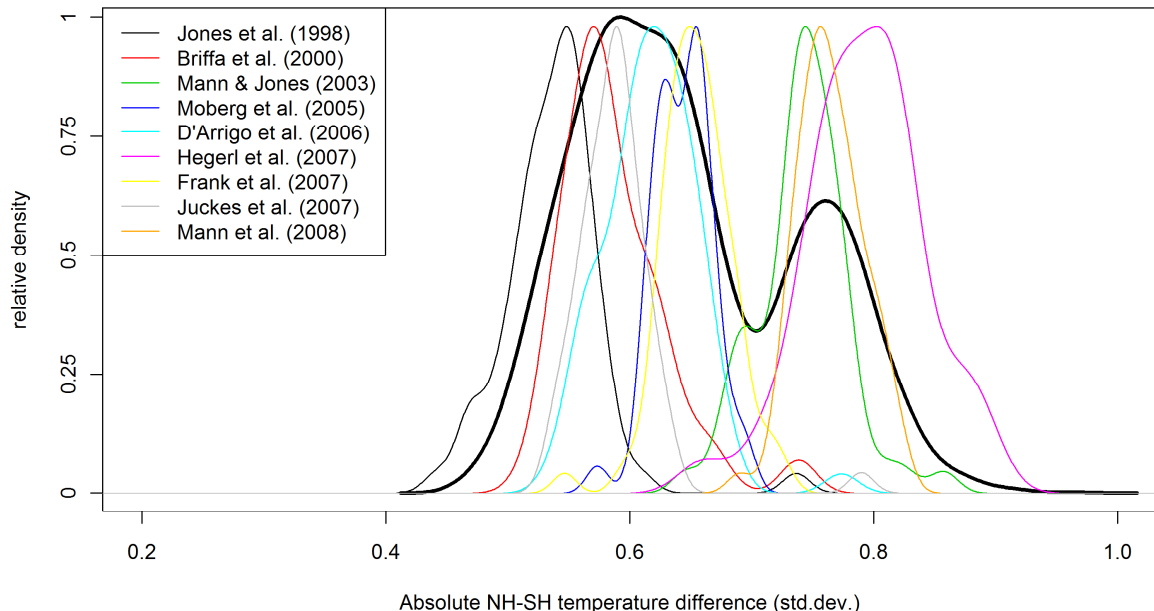
Given that we focus on decadal to multi-decadal timescales in our analyses, we show the NH-SH differences in Figure 4 after detrending reconstructed and simulated temperatures with a 200-year filter. An alternative illustration for the reconstructions using non-detrended data is provided in Supplementary Figure 33. The NH-SH differences based on raw data show larger absolute values before 1400 and in the 20th century (see also Figure 2a), but the general pattern remains similar and the differences do not affect our conclusions. We show the detrended data in the main text, as this illustration is less dependent on the reference period chosen.



Supplementary Figure 33 | Raw vs. detrended NH-SH differences. NH-SH temperature difference using 200-year detrended data (black; as in Figure 4a in the main text) and raw data (red).

10.3. Bimodal distribution in Figure 4b

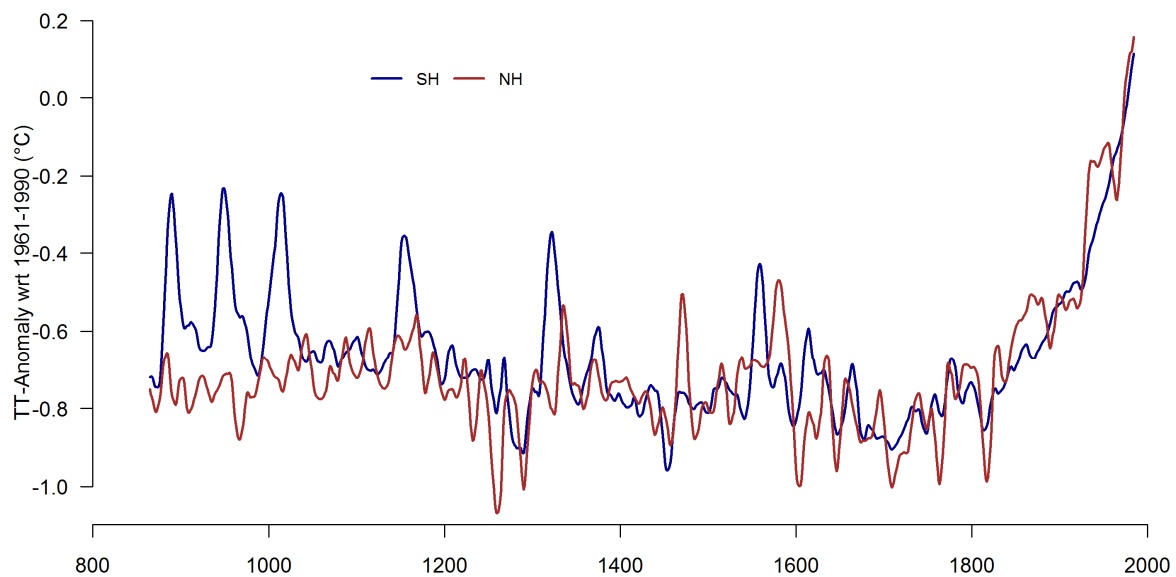
Figure 4b in the main text shows a bimodal distribution for the reconstruction data with two peaks around 0.6 and 0.75. This is caused by the fact that the NH reconstruction ensemble consists of nine sub-ensembles generated from different published reconstructions (see Methods). The distributions for these sub-ensembles are shown in Supplementary Figure 34. Three of these reconstructions (Mann and Jones, 2003; Hegerl et al., 2007; Mann et al., 2008) are only available at decadal resolution, leading to higher values in the NH-SH differences.



Supplementary Figure 34 | NH-SH differences for the NH sub-ensembles. Distribution of absolute NH-SH differences in the reconstructions during the pre-1900 period. Black solid: Full ensemble (as in Figure 4b in the main text); coloured lines: Individual sub-ensembles from the NH reconstruction.

10.4. Outlier in the model simulations (Figures 4b and 4c)

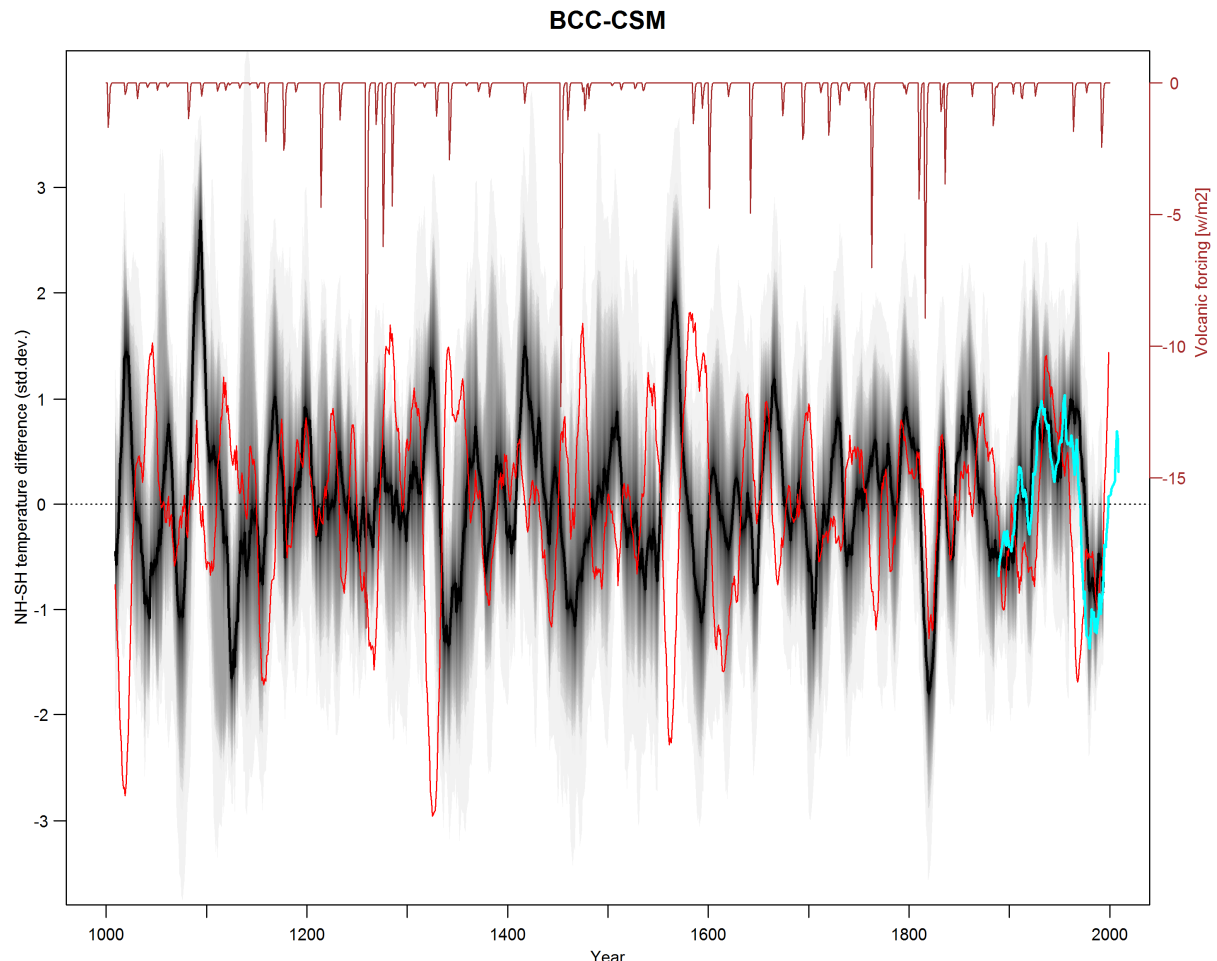
Figure 4b and 4c in the main text show an outlier in the model simulations, which has similar magnitudes in the NH-SH differences as the reconstructions. This outlier represents the model BCC-CSM. The SH temperatures of this model show repeated warming peaks that last about three decades in both the last millennium run (Supplementary Figure 35) as well as the pre-industrial control simulation (not shown). These warm peaks are mostly not reflected in the NH, which leads to very large NH-SH differences during these periods (see Supplementary Figure 36), explaining the larger values compared to the other simulations. The positive excursions in the SH are mostly limited to a very strong warming in the Southern Ocean off Antarctica in the Weddell Sea area (not shown). Given the temporal and spatial nature of these anomalies, we regard these as model-specific features that are unrealistically simulated by the BCC-CSM model.



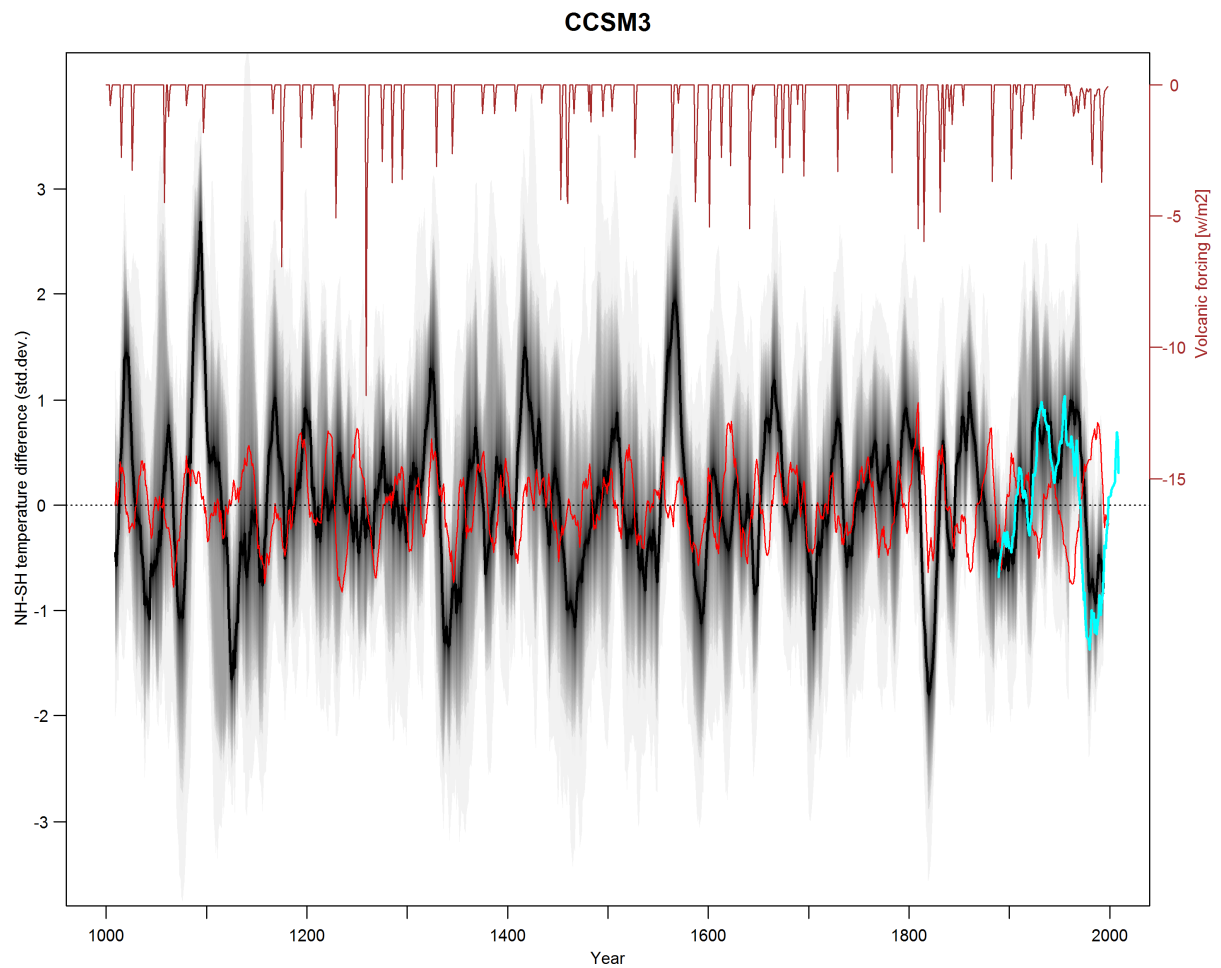
Supplementary Figure 35 | Hemispheric temeperatures in the BCC-CSM model. 30-year filtered SH (blue) and NH (red) temperatures over the period 850-2000 for the BCC-CSM model.

11.NH-SH differences in the individual model simulations

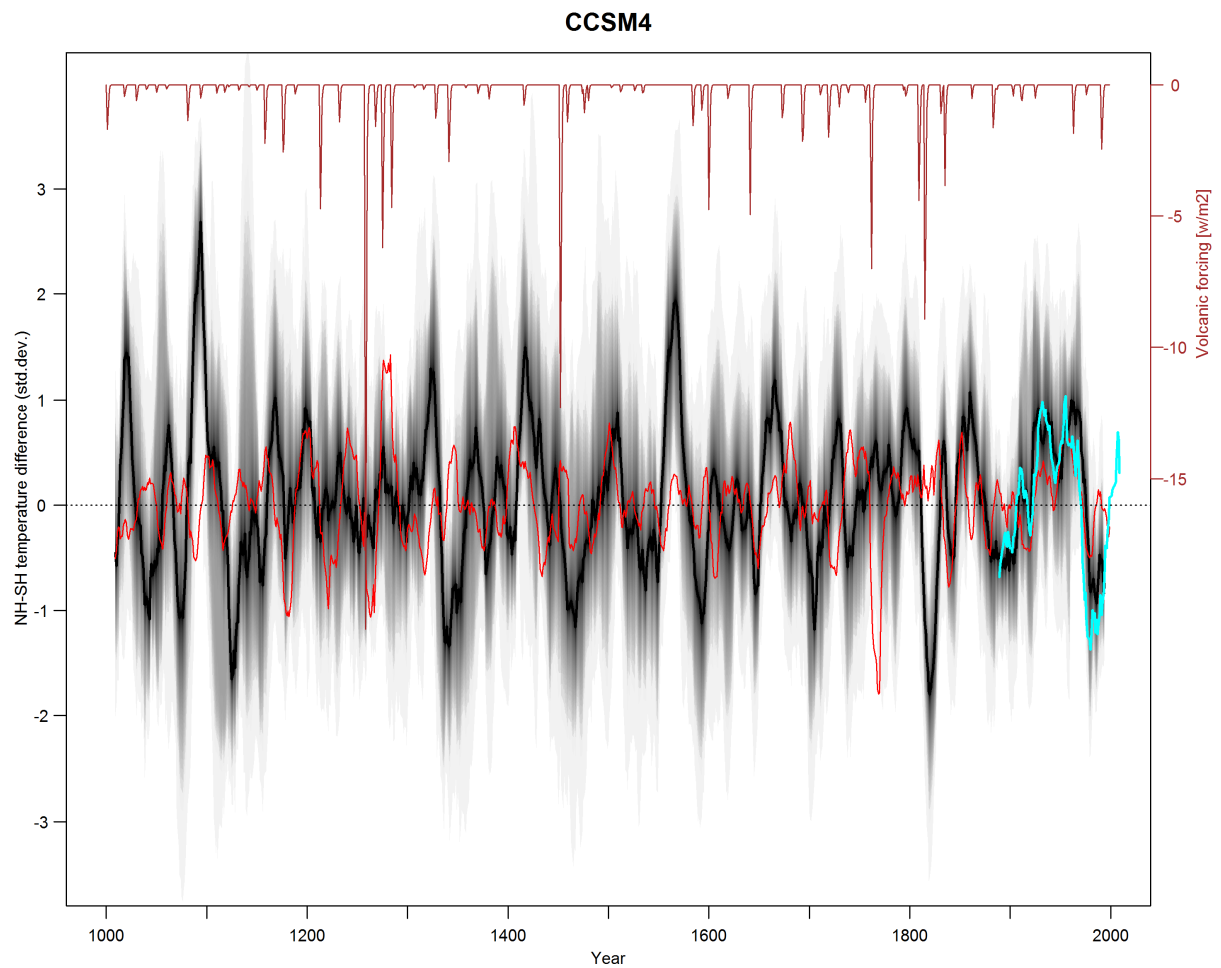
Supplementary Figure 39 - Supplementary Figure 59 show the NH-SH differences over the last millennium for the individual climate model simulations and compare them to the reconstructions (see also Figure 4 in the main text).



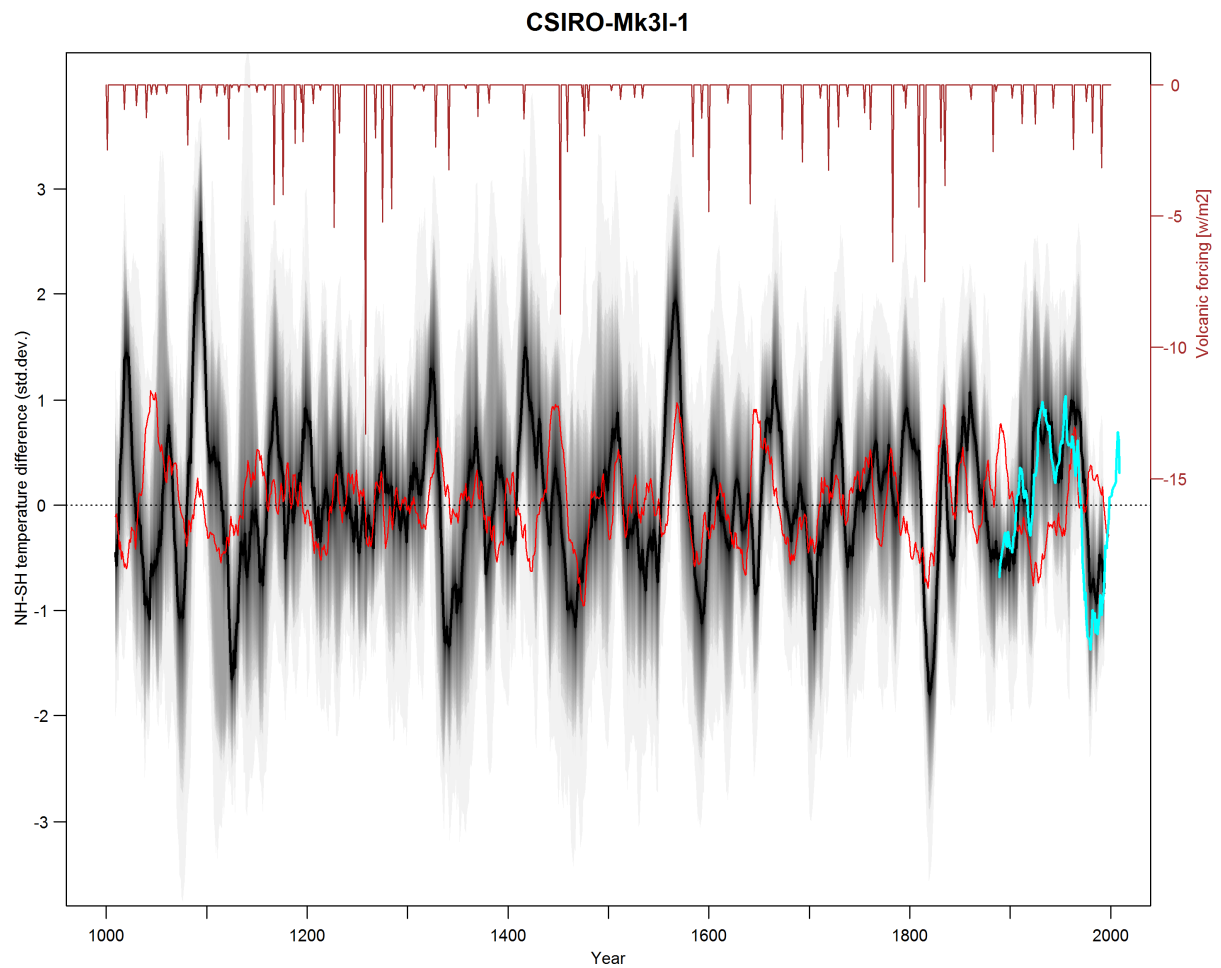
Supplementary Figure 36 | NH-SH differences for individual model simulations: BCC-CSM. Same as Figure 4a in the main text but showing the NH-SH difference for the climate model simulation BCC-CSM in red, instead of the 10th and 90th percentiles of all model simulations. Volcanic dataset (brown) is the forcing time series used for this simulation (Gao *et al.*, 2008). Instrumental data are cyan (Hansen *et al.*, 2010).



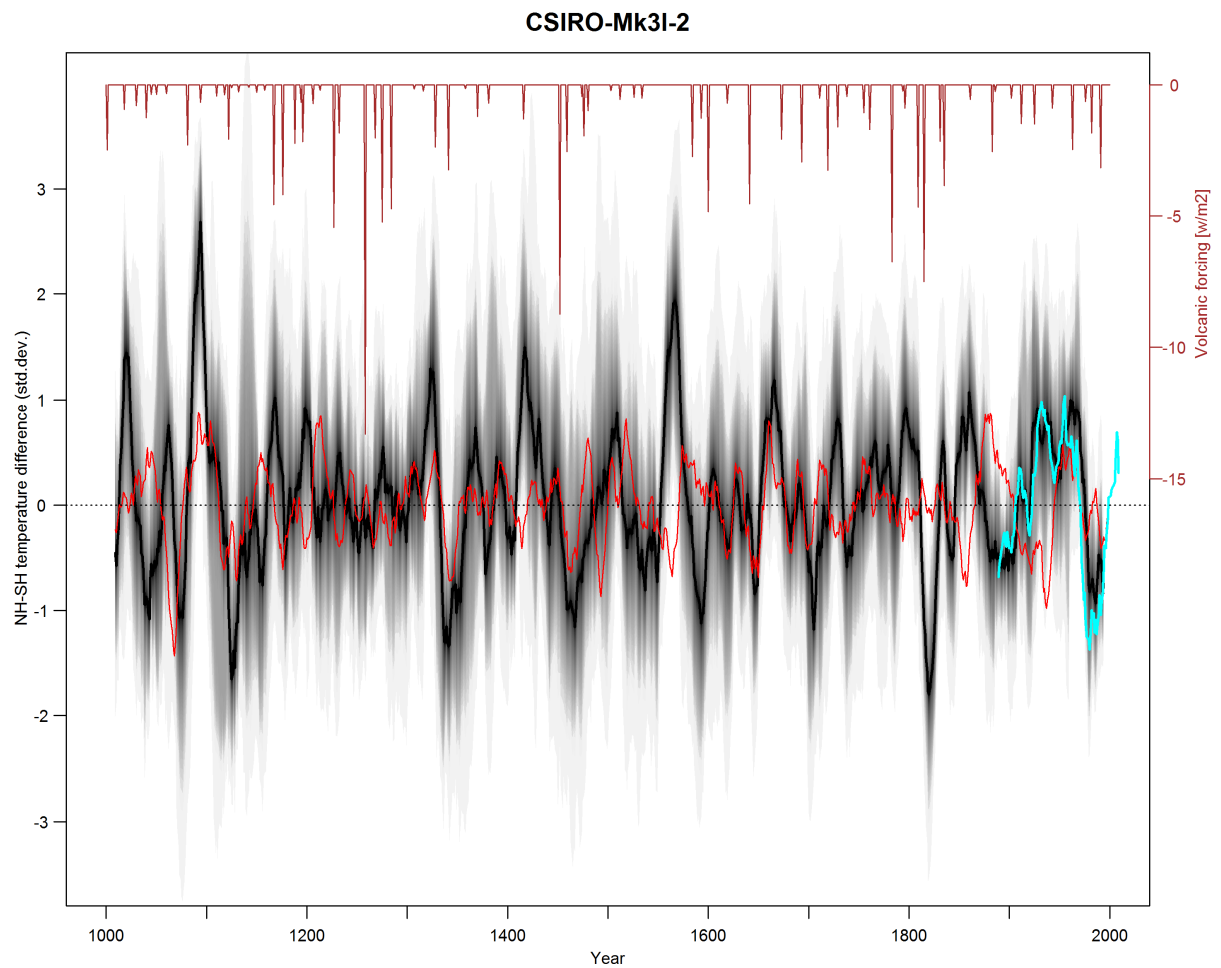
Supplementary Figure 37 | NH-SH differences CCSM3. Same as Supplementary Figure 36 but for the CCSM3 simulation and the corresponding volcanic forcing dataset (Crowley, 2000).



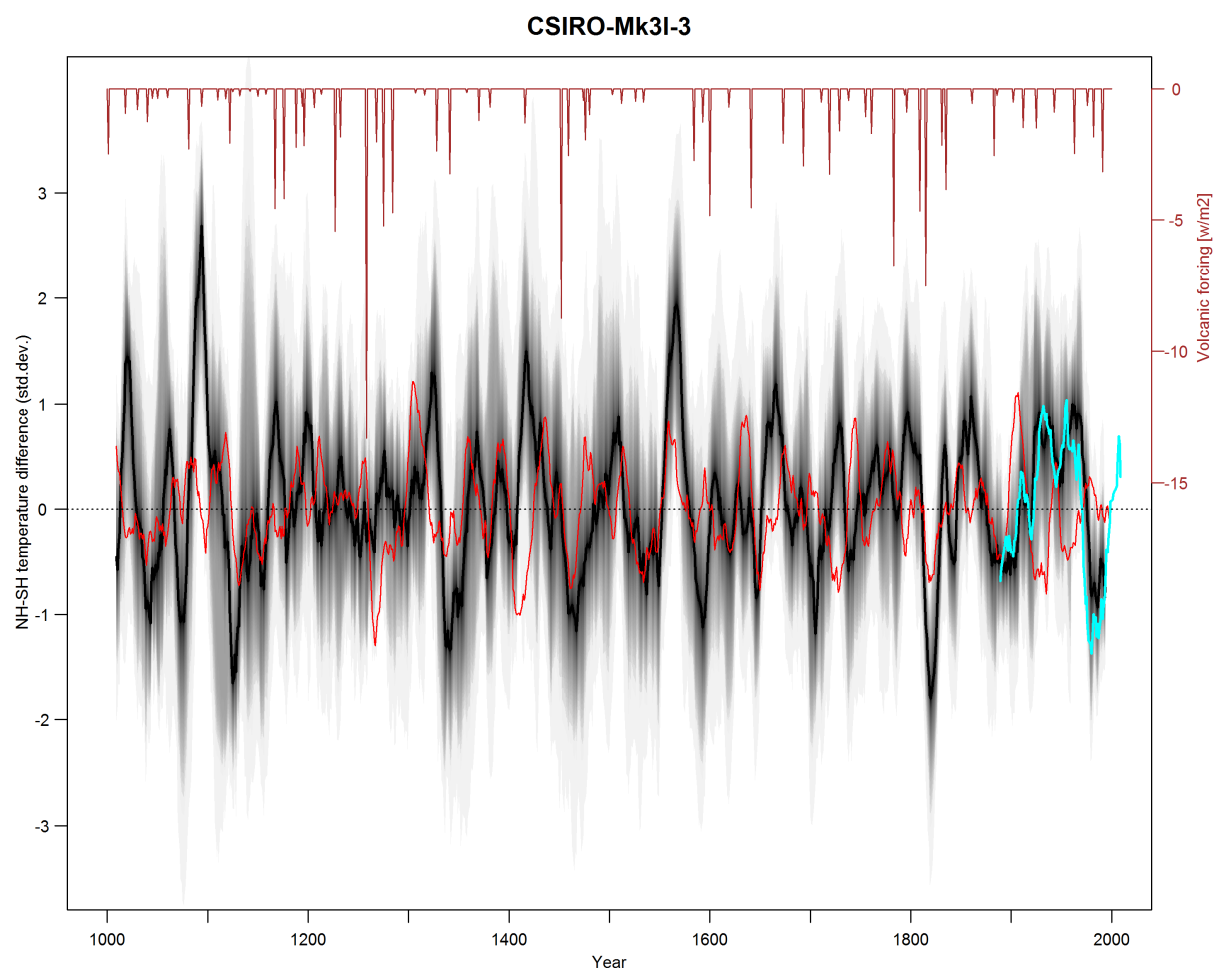
Supplementary Figure 38 | NH-SH differences CCSM4. Same as Supplementary Figure 36 but for the CCSM4 simulation and the corresponding volcanic forcing dataset (Gao *et al.*, 2008).



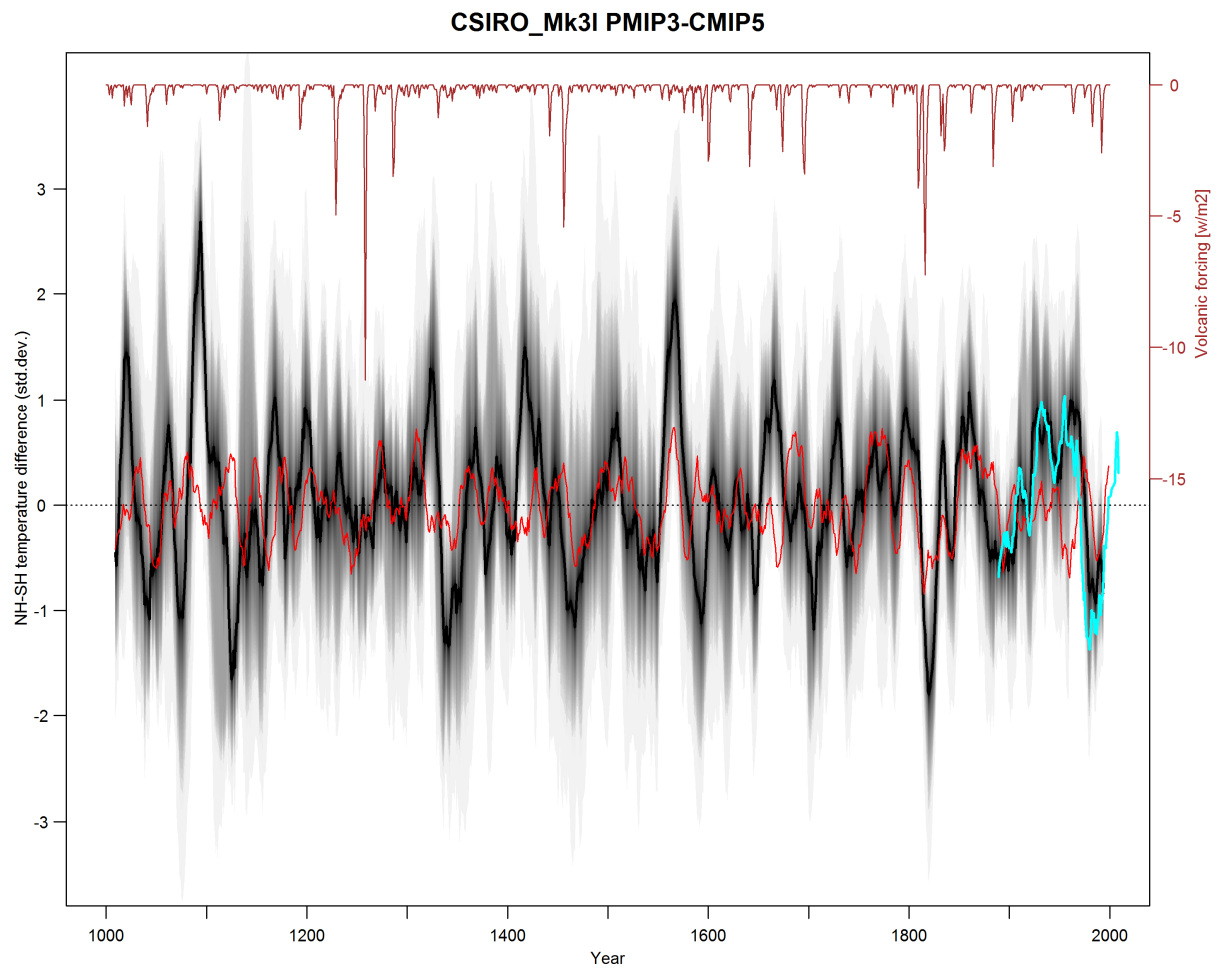
Supplementary Figure 39 | NH-SH differences for individual model simulations: CSIRO Mk3L-1. Same as Supplementary Figure 36 but for the CSIRO Mk3L, ensemble member 1 and the corresponding volcanic forcing dataset (Gao *et al.*, 2008).



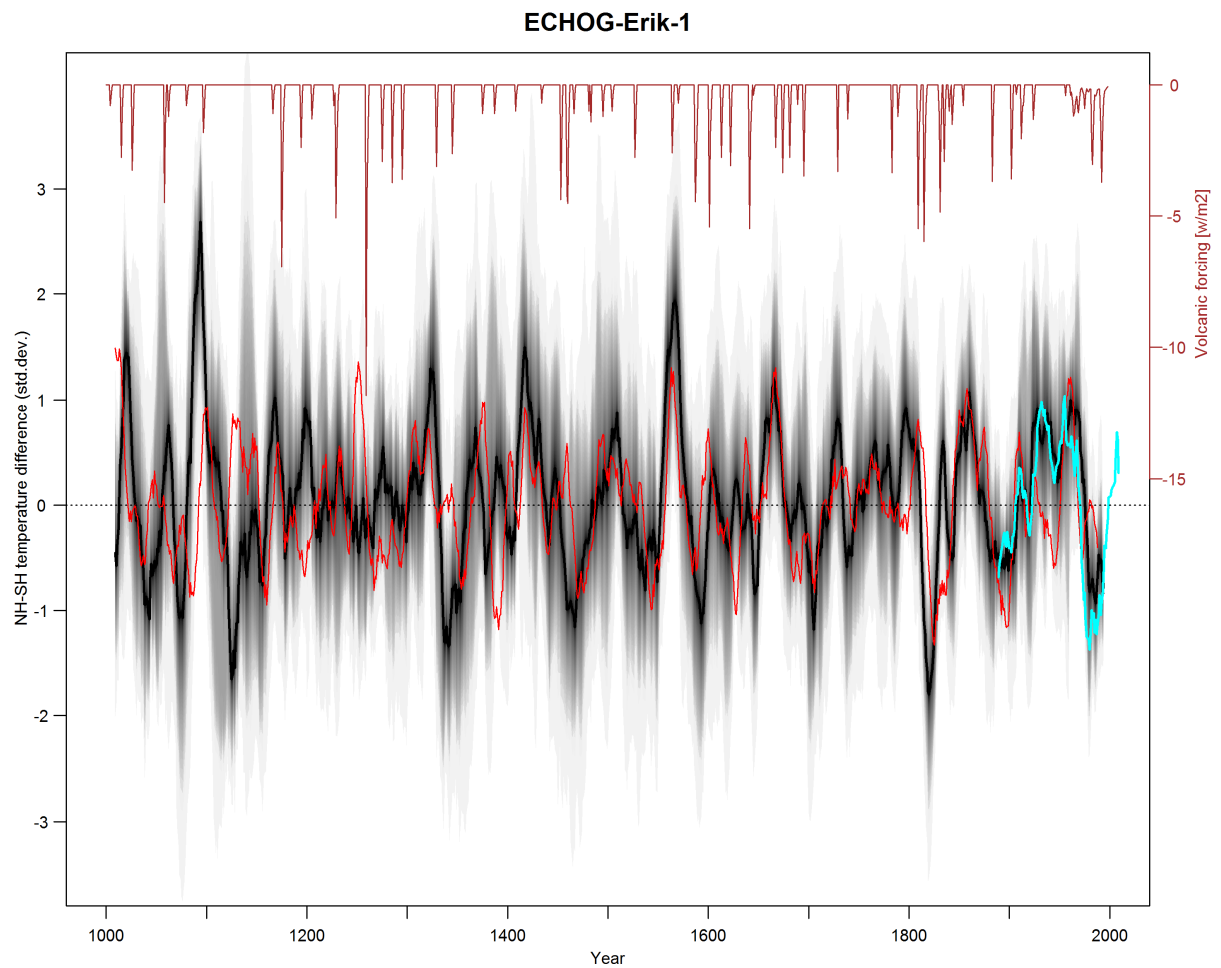
Supplementary Figure 40 | NH-SH differences CSIRO Mk3L-2. Same as Supplementary Figure 36 but for the CSIRO Mk3L simulation, ensemble member 2.



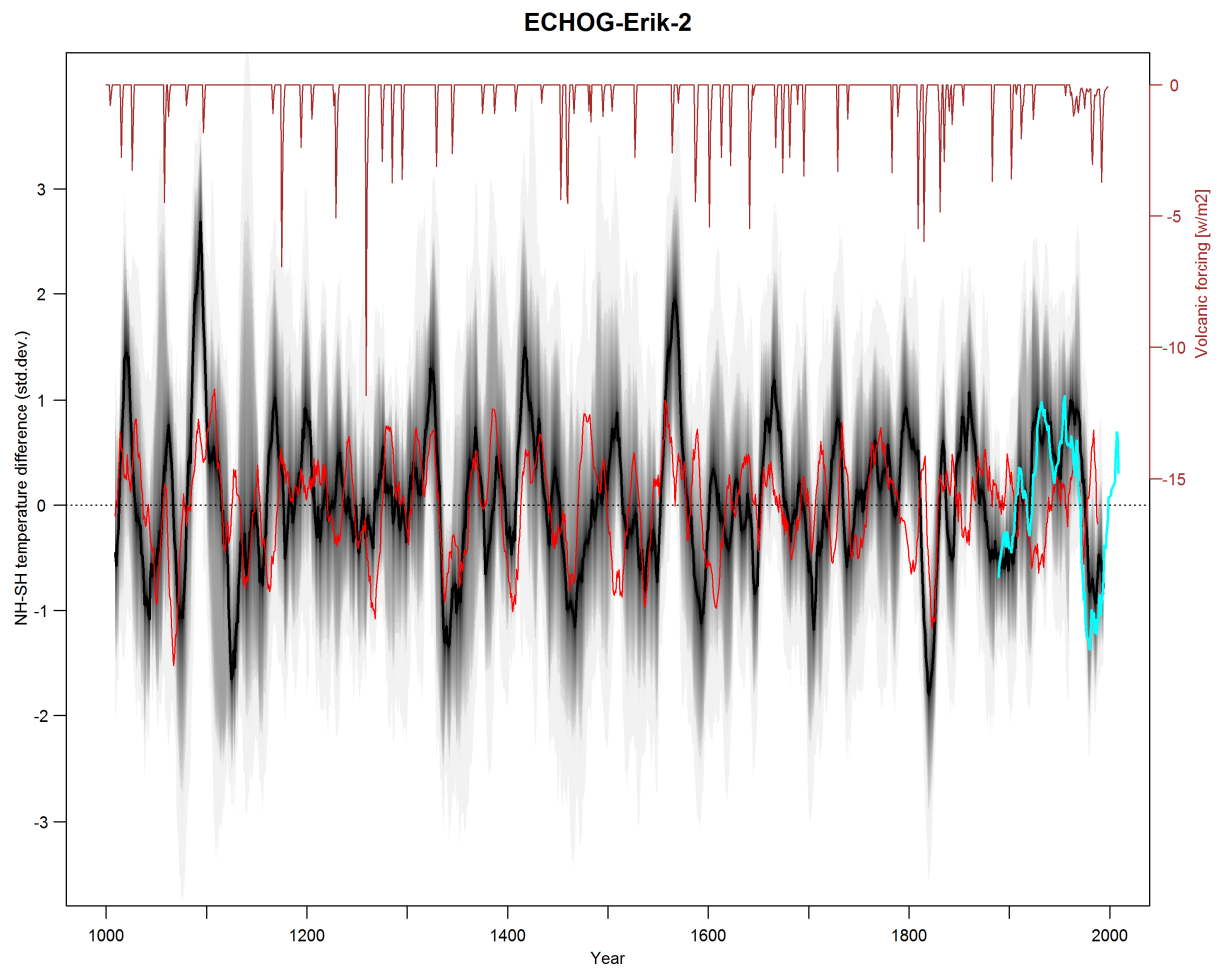
Supplementary Figure 41 | NH-SH differences CSIRO Mk3L-3. Same as Supplementary Figure 36 but for the CSIRO Mk3L simulation, ensemble member 3.



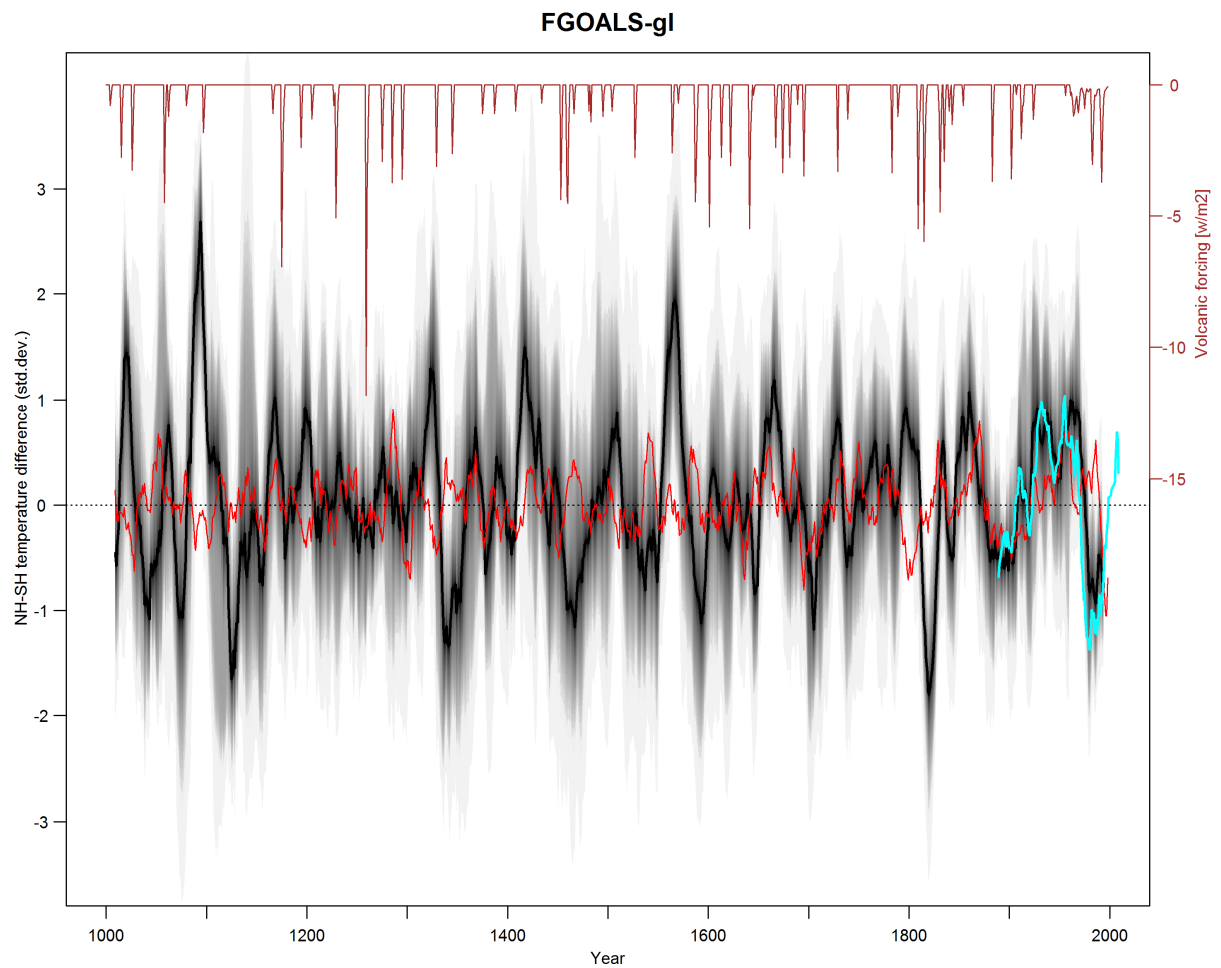
Supplementary Figure 42 | NH-SH differences CSIRO Mk3L PMIP3/CMIP5. Same as Supplementary Figure 36 but for the CSIRO Mk3L PMIP3/CMIP5 simulation and the corresponding volcanic forcing dataset (Crowley and Unterman, 2013).



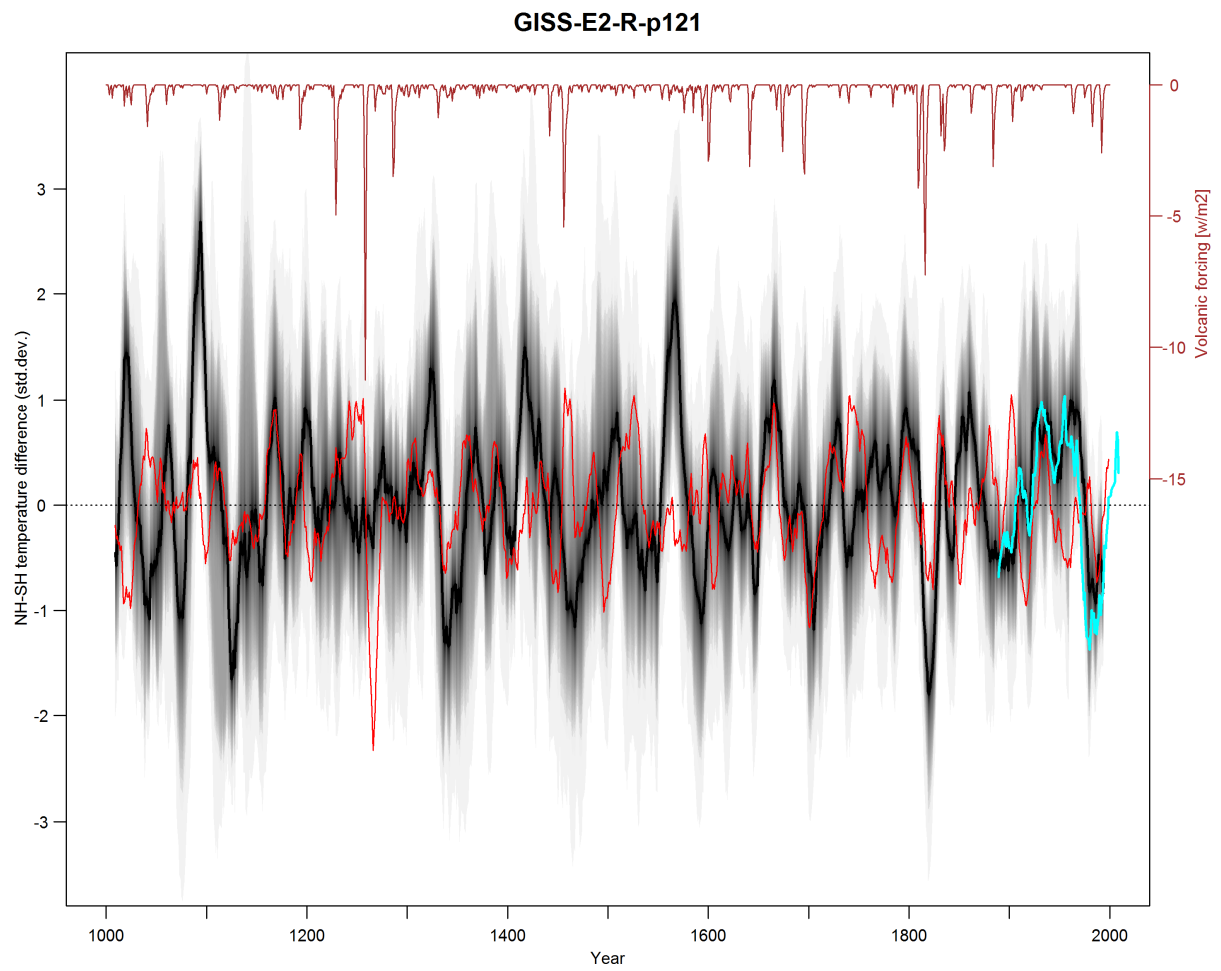
Supplementary Figure 43 | NH-SH differences ECHO-G Erik 1. Same as Supplementary Figure 36 but for the ECHO-G Erik 1 simulation and the corresponding volcanic forcing dataset (Crowley, 2000).



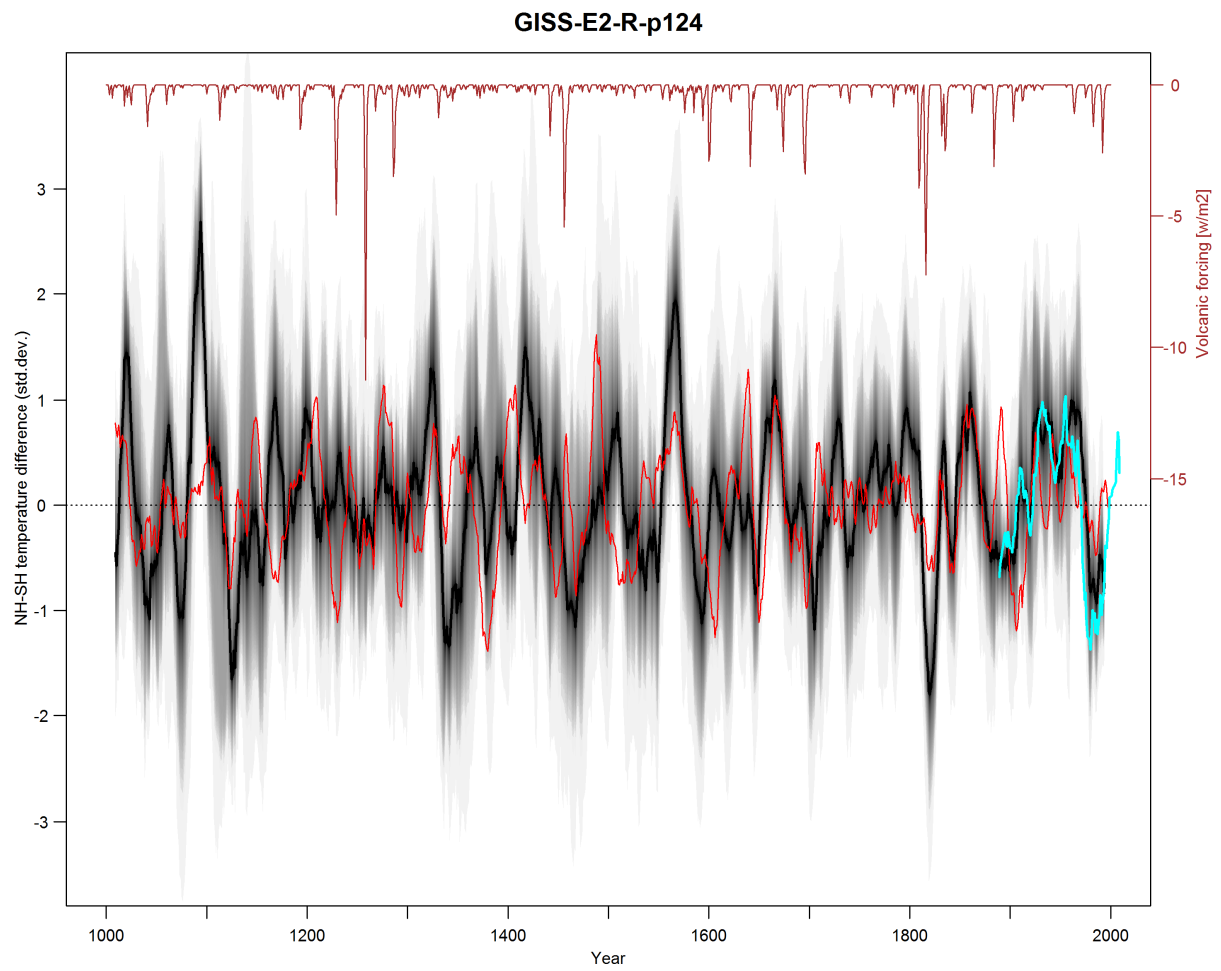
Supplementary Figure 44 | NH-SH differences ECHO-G Erik 2. Same as Supplementary Figure 36 but for the ECHO-G Erik 2 simulation and the corresponding volcanic forcing dataset (Crowley, 2000).



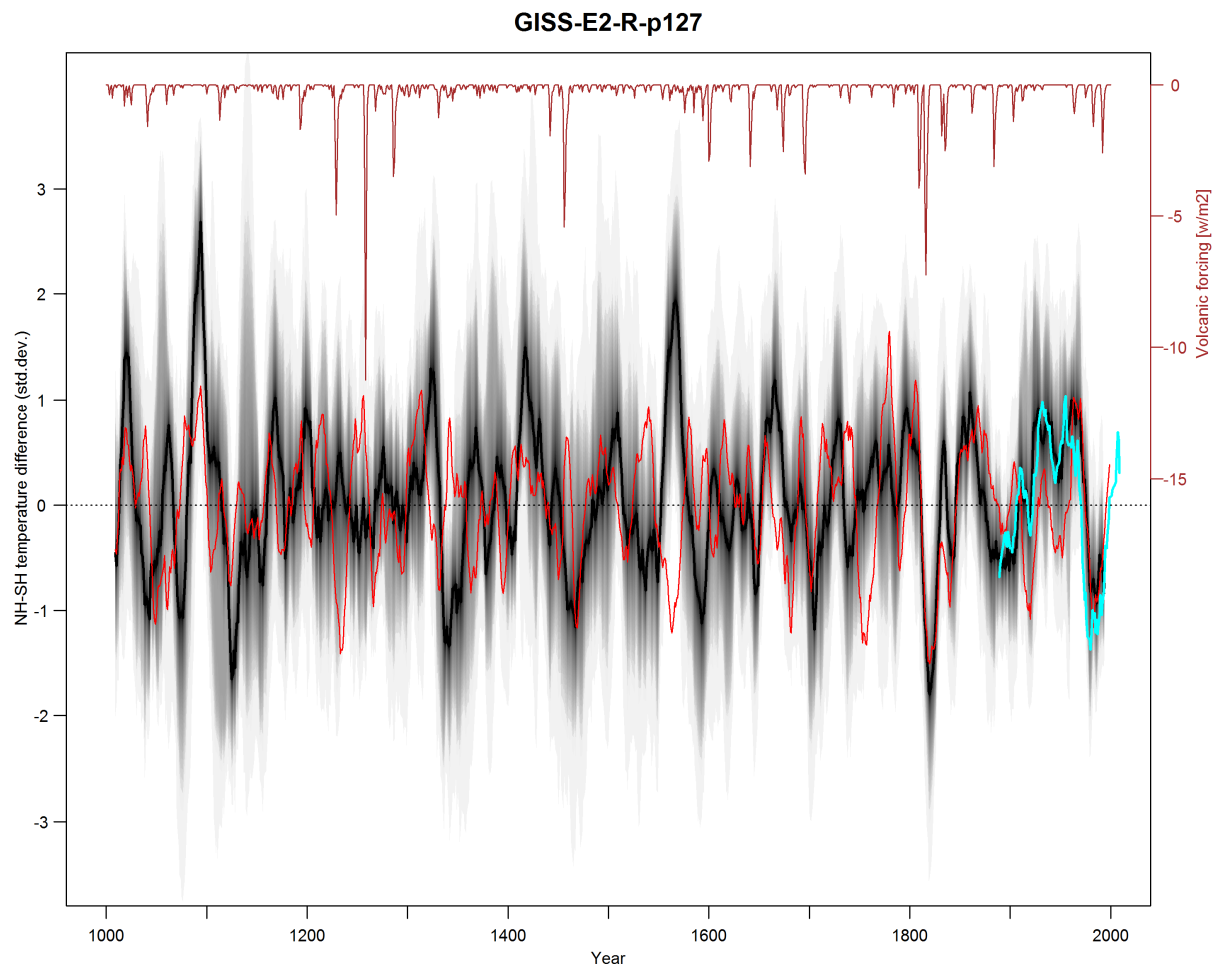
Supplementary Figure 45 | NH-SH differences FGOALS-g1. Same as Supplementary Figure 36 but for the FGOALS-g1 simulation and the corresponding volcanic forcing dataset (Crowley, 2000).



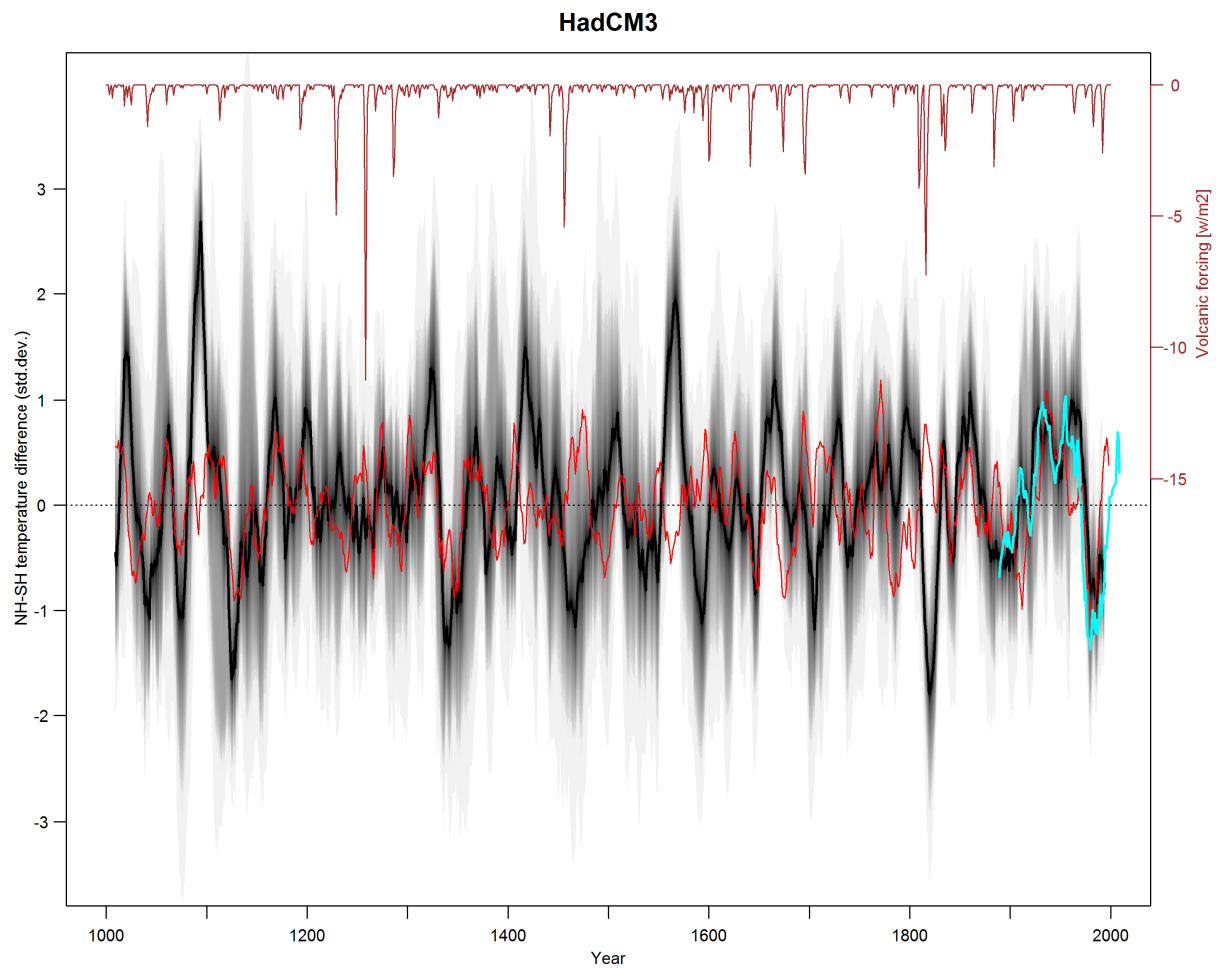
Supplementary Figure 46 | NH-SH differences GISS-E2-R p121. Same as Supplementary Figure 36 but for the GISS-E2-R p121 simulation and the corresponding volcanic forcing dataset (Crowley and Unterman, 2013).



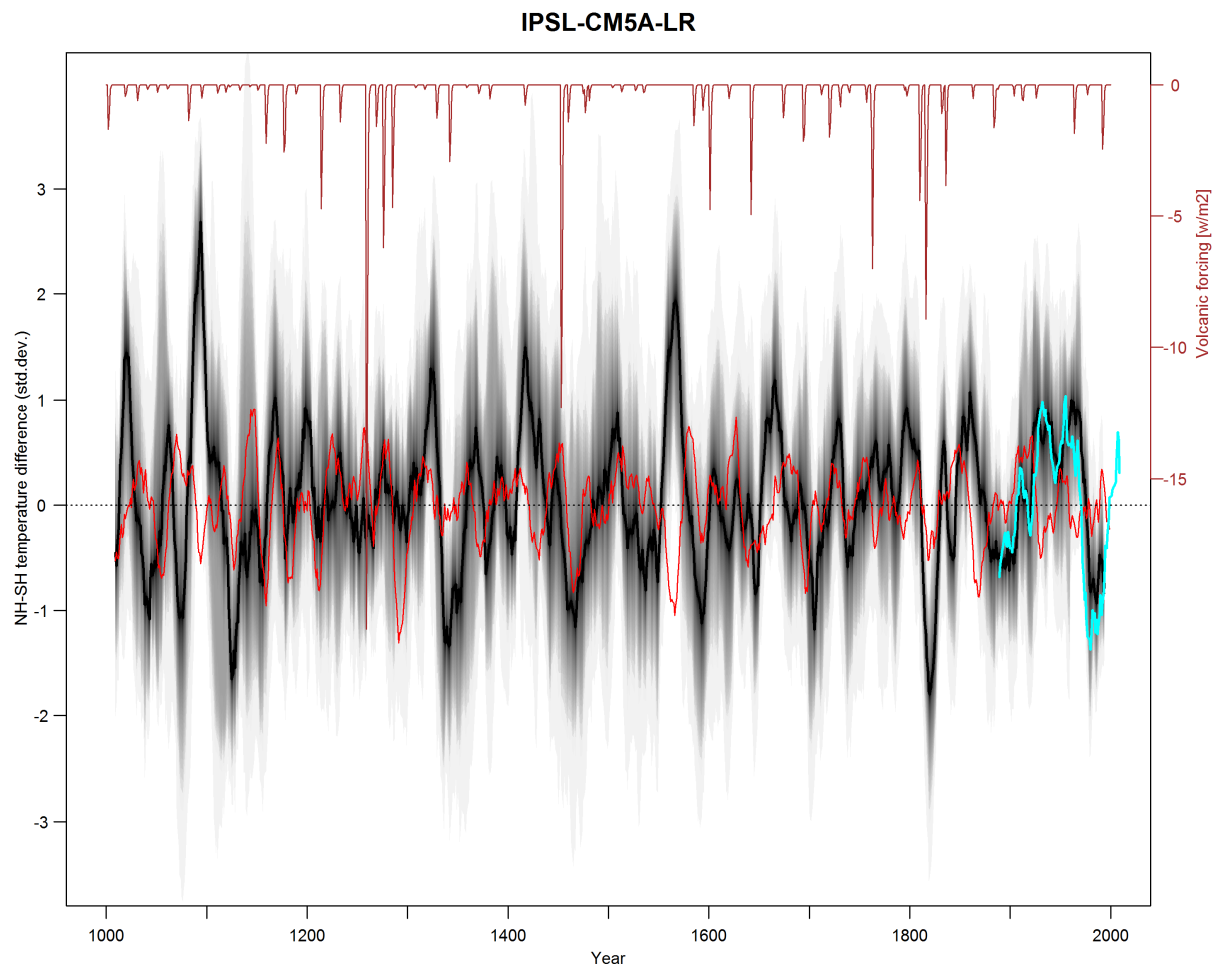
Supplementary Figure 47 | NH-SH differences GISS-E2-R p124. Same Supplementary Figure 36 but for the GISS-E2-R p124 simulation and the corresponding volcanic forcing dataset (Crowley and Unterman, 2013).



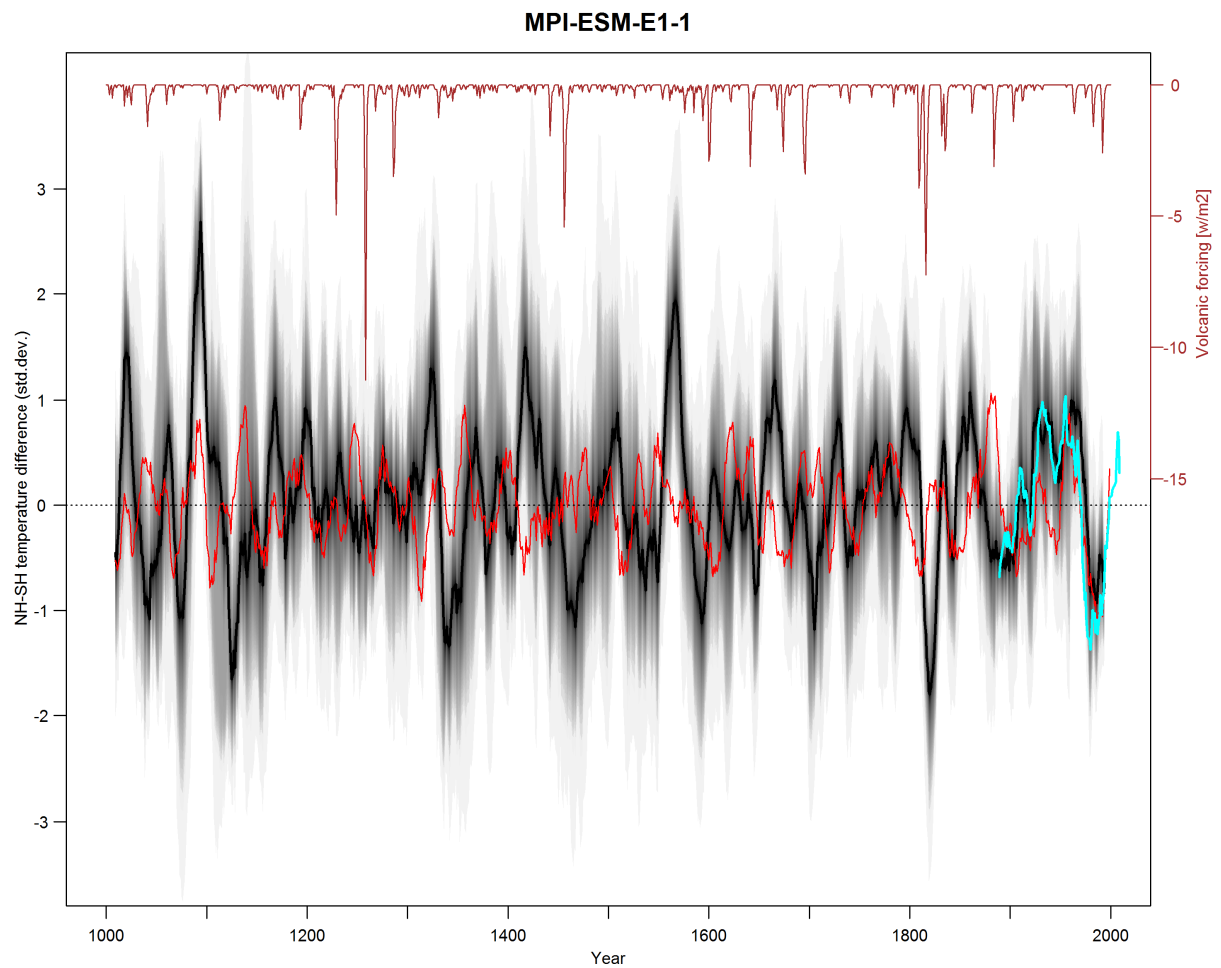
Supplementary Figure 48 | NH-SH differences GISS-E2-R p127. Same as Supplementary Figure 36 but for the GISS-E2-R p127 simulation and the corresponding volcanic forcing dataset (Crowley and Unterman, 2013).



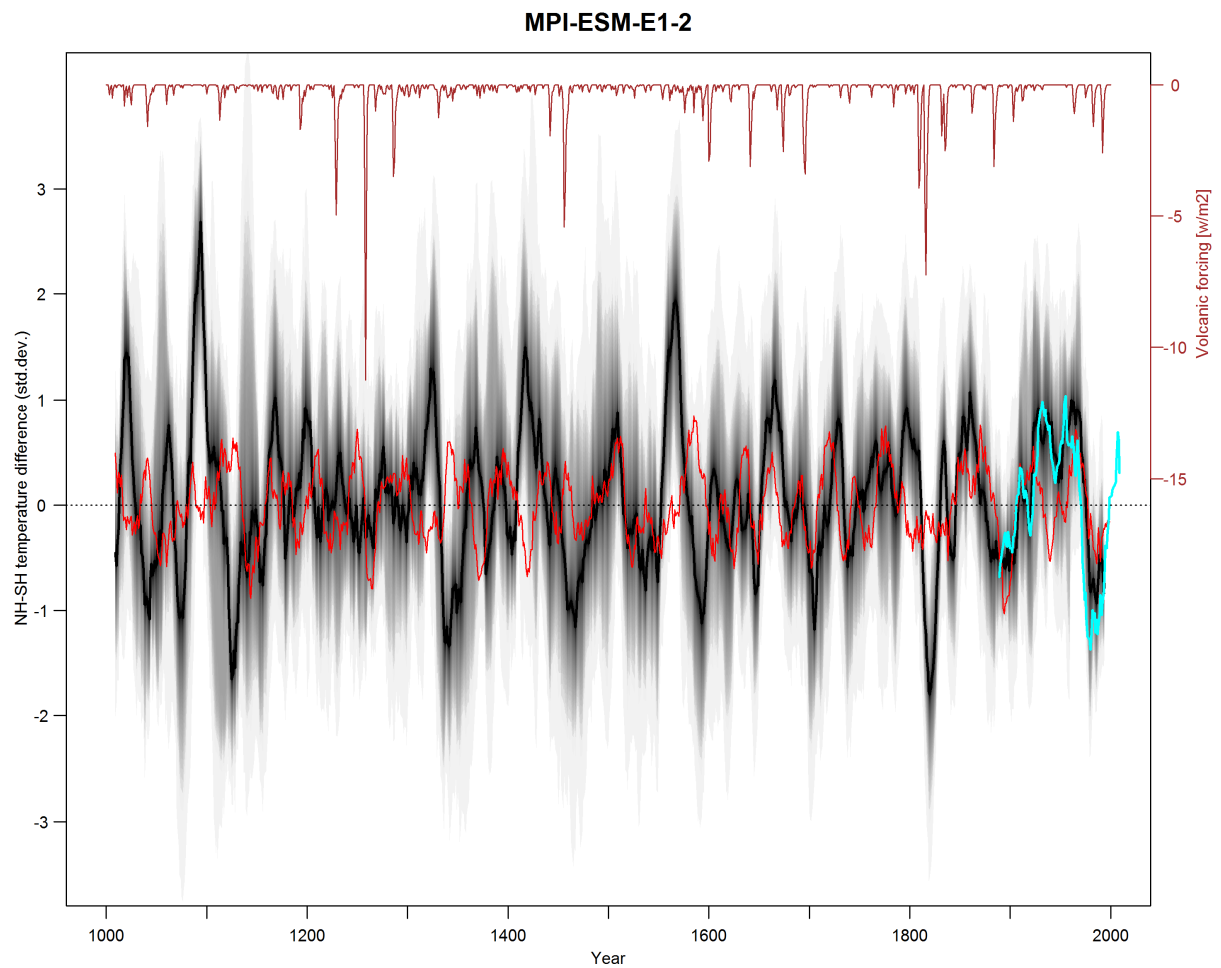
Supplementary Figure 49 | NH-SH differences HadCM3. Same as Supplementary Figure 36 but for HadCM3 simulation and the corresponding volcanic forcing dataset (Crowley and Unterman, 2013).



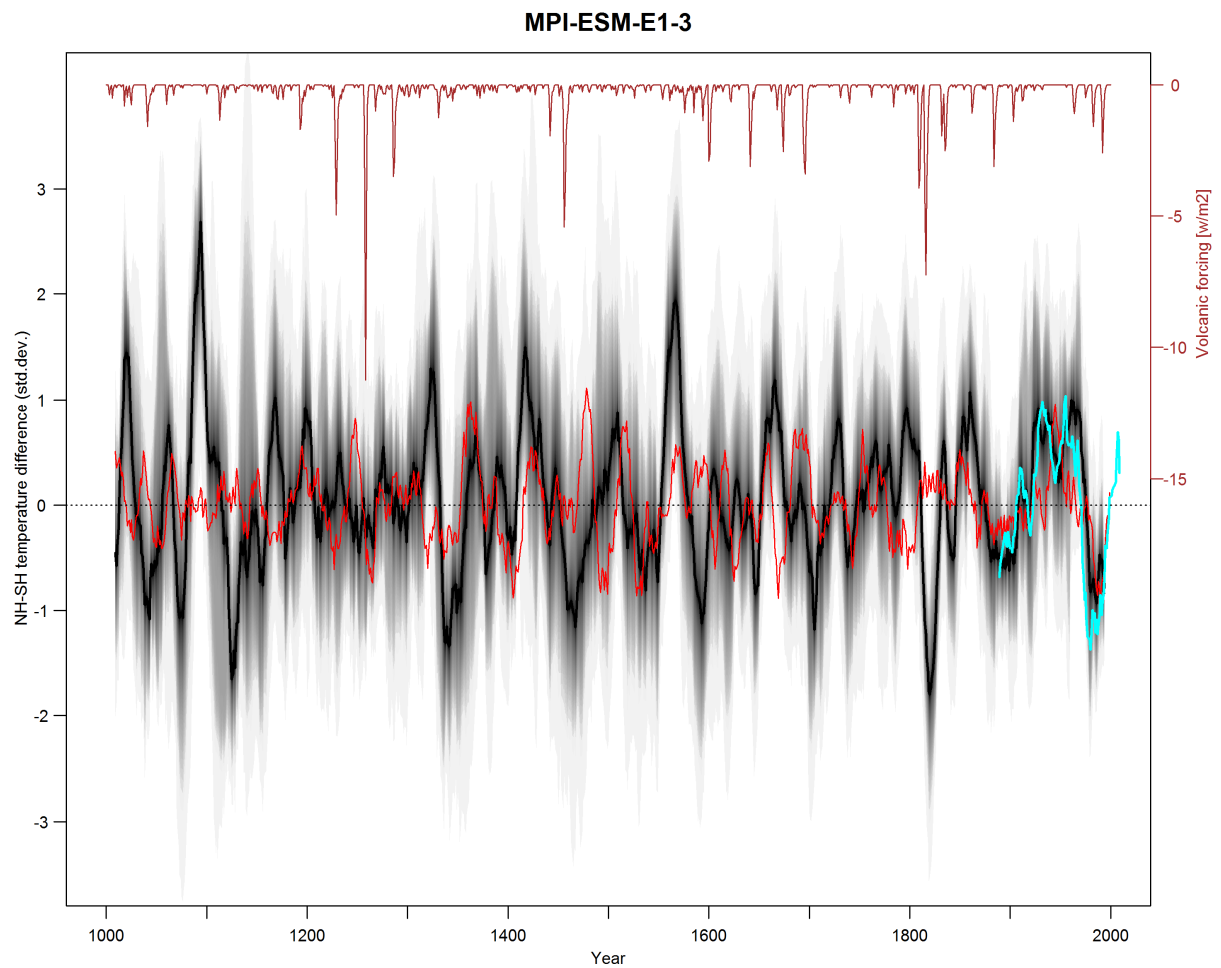
Supplementary Figure 50 | NH-SH differences IPSL-CM5A-LR. Same as Supplementary Figure 36 but for the IPSL-CM5A-LR simulation and the corresponding volcanic forcing dataset (Gao *et al.*, 2008).



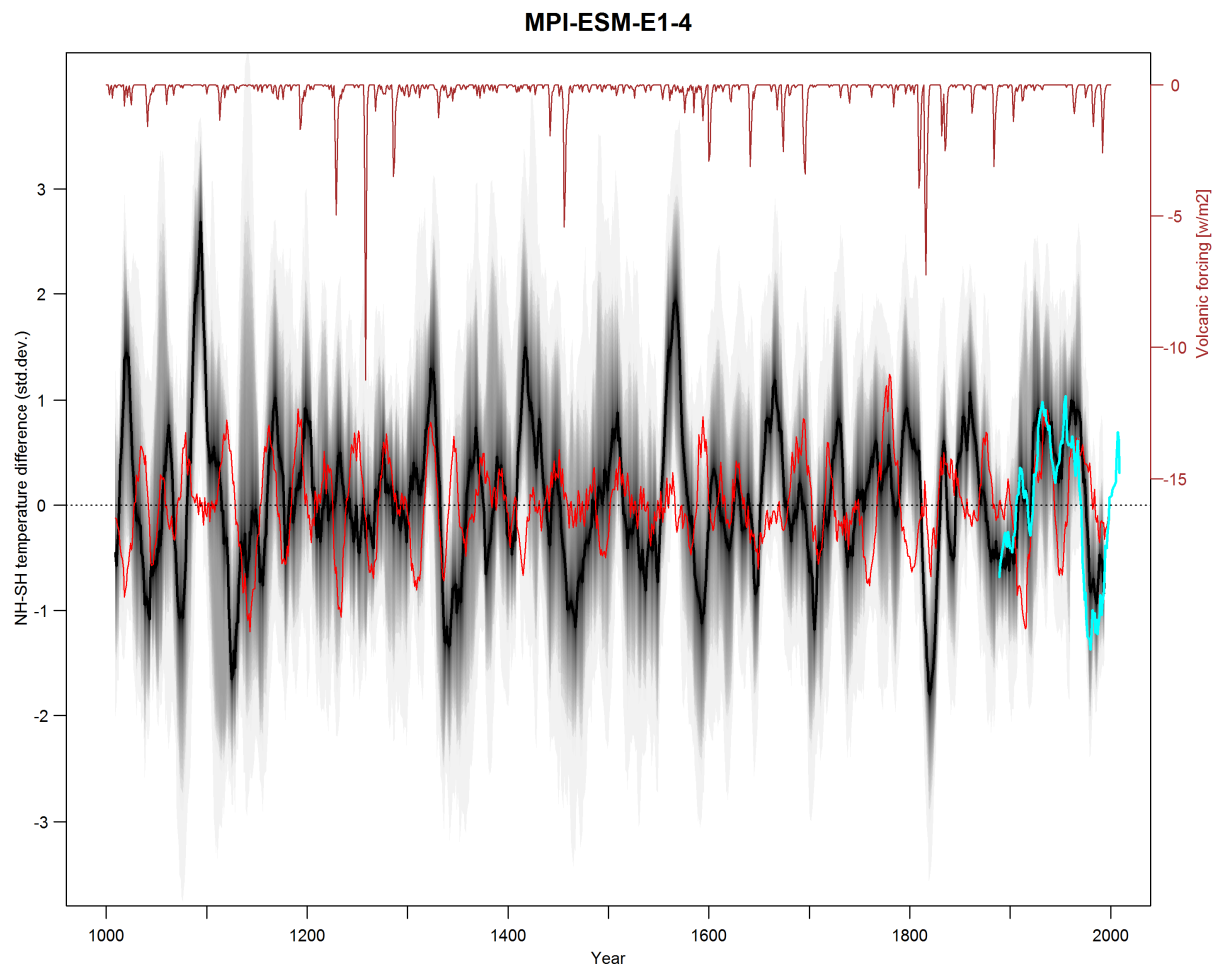
Supplementary Figure 51 | NH-SH differences MPI-ESM E1-1. Same as Supplementary Figure 36 but for the MPI ESM E1 simulation, ensemble member 1 and the corresponding volcanic forcing dataset (Crowley and Unterman, 2013).



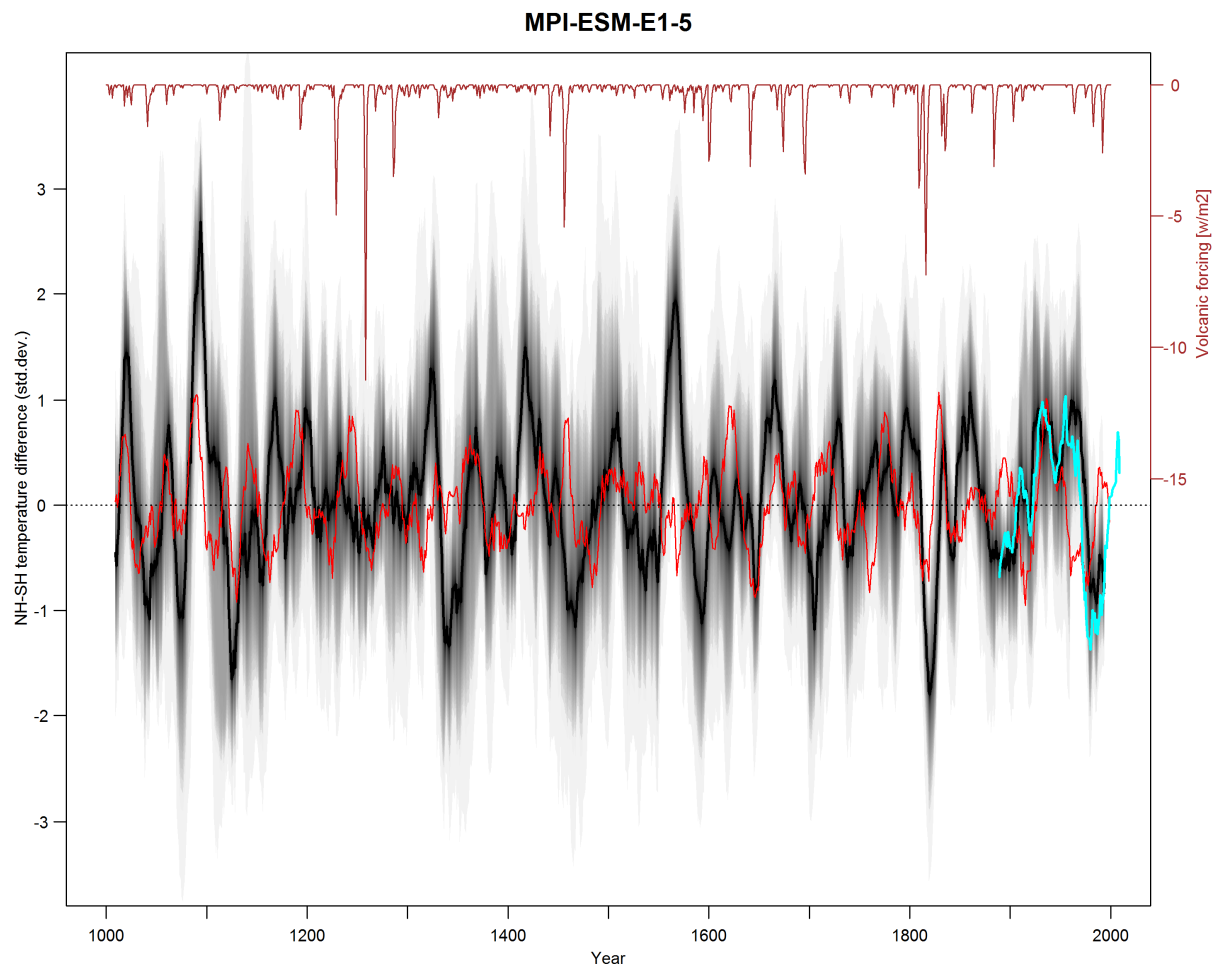
Supplementary Figure 52 | NH-SH differences MPI-ESM E1-2: Same as Supplementary Figure 51 but for the MPI-ESM E1 simulation, ensemble member 2.



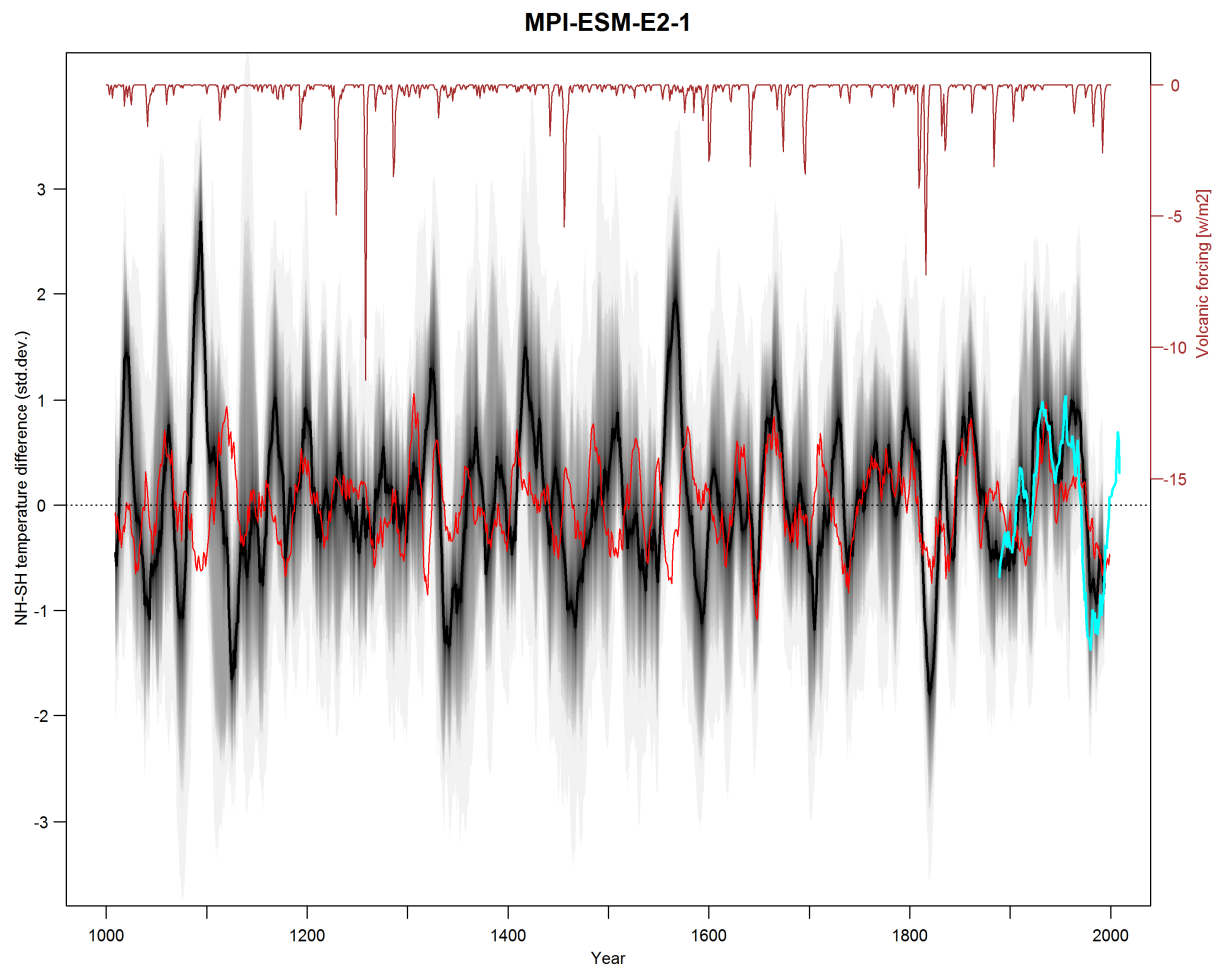
Supplementary Figure 53 | NH-SH differences MPI-ESM E1-3. Same as Supplementary Figure 51 but for the MPI-ESM E1 simulation, ensemble member 3.



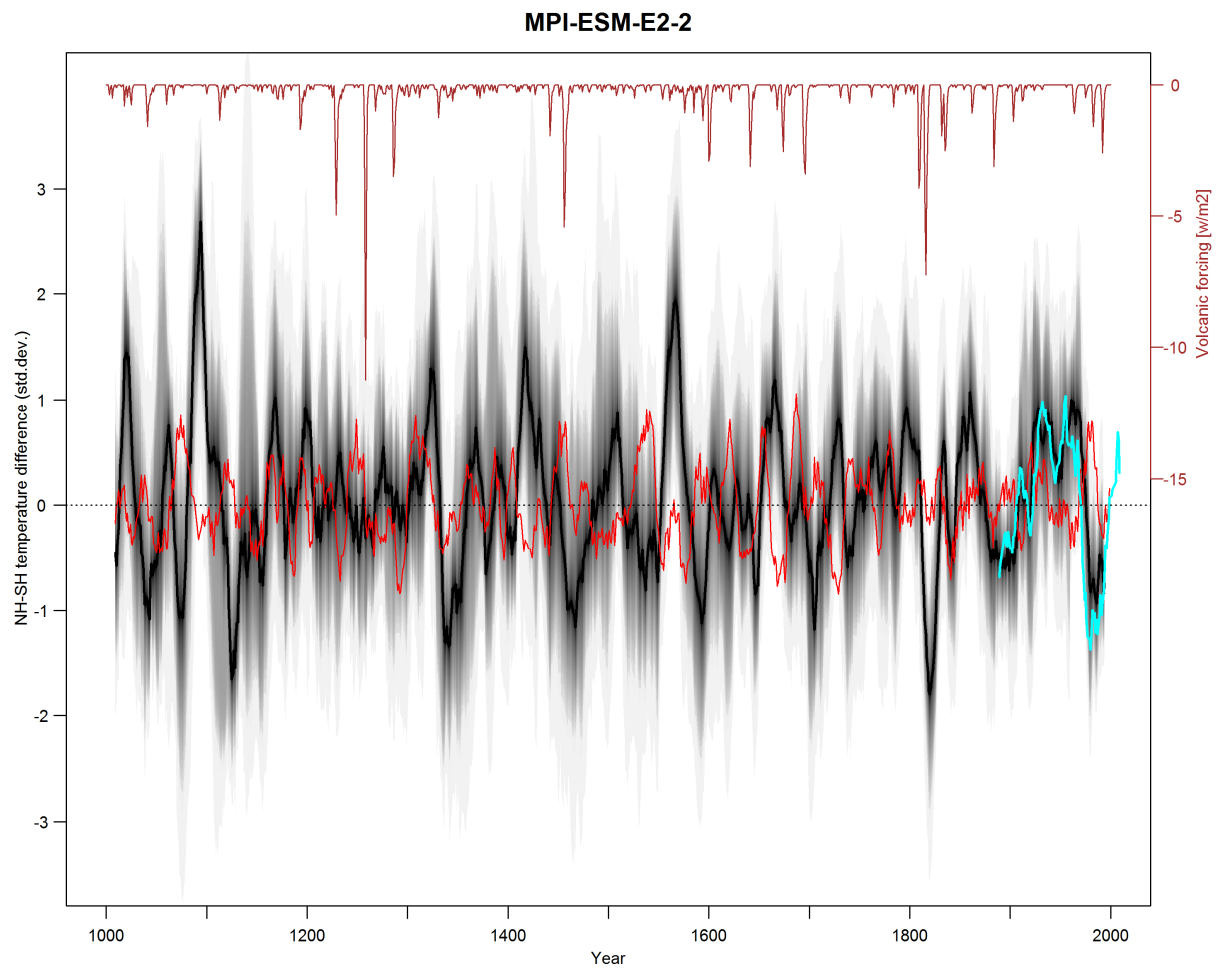
Supplementary Figure 54 | NH-SH differences MPI-ESM E1-4. Same as Supplementary Figure 51 but for the MPI-ESM E1 simulation, ensemble member 4.



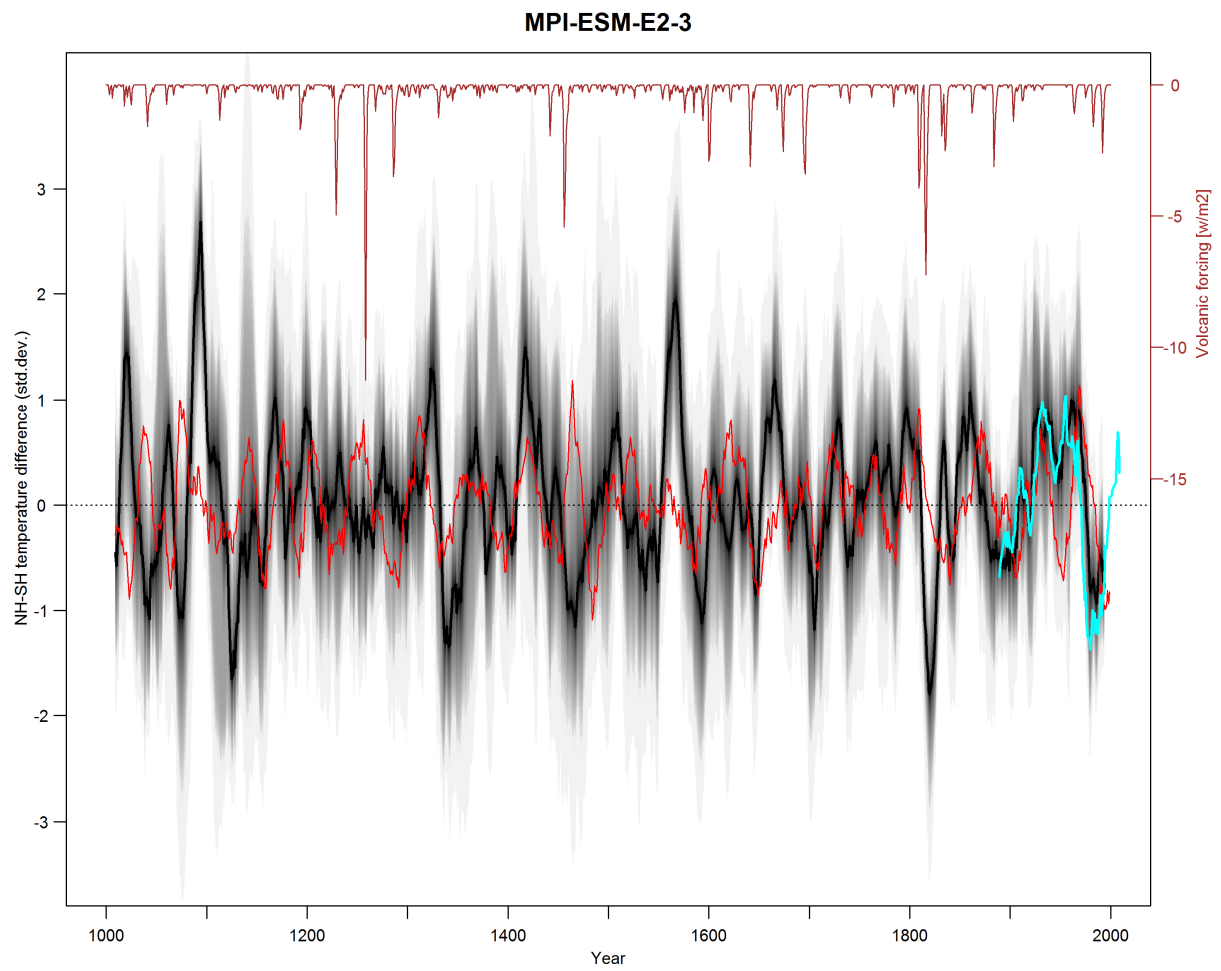
Supplementary Figure 55 | NH-SH differences MPI-ESM E1-5. Same as Supplementary Figure 51 but for the MPI-ESM E1 simulation, ensemble member 5.



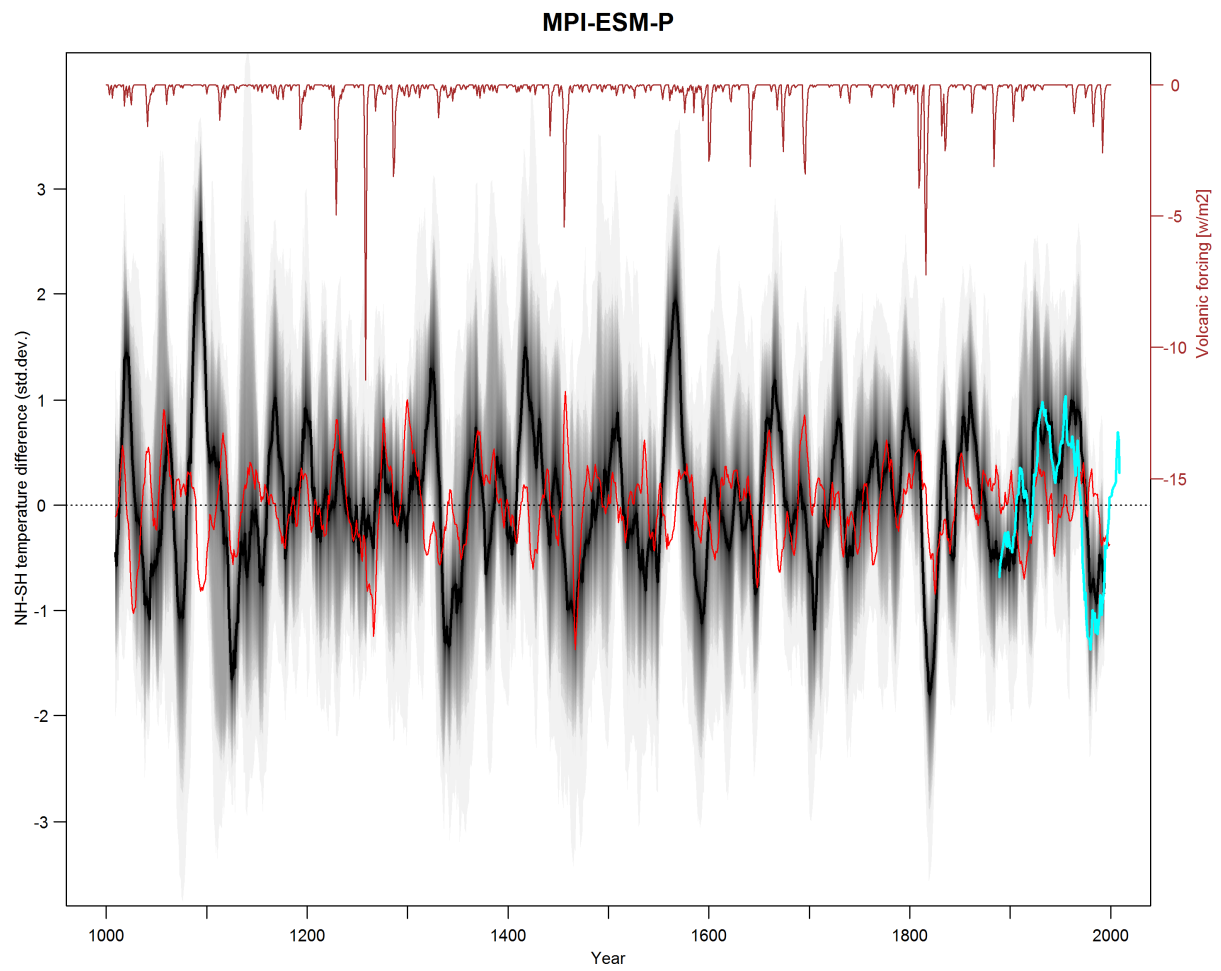
Supplementary Figure 56 | NH-SH differences MPI-ESM E2-1. Same as Supplementary Figure 51 but for the MPI-ESM E2 simulation, ensemble member 1.



Supplementary Figure 57 | NH-SH differences MPI-ESM E2-2. Same as Supplementary Figure 51 but for the MPI-ESM E2 simulation, ensemble member 2.



Supplementary Figure 58 | NH-SH differences MPI-ESM E2-3. Same as Supplementary Figure 51 but for the MPI -ESM E2 simulation, ensemble member 3.



Supplementary Figure 59 | NH-SH differences MPI-ESM-P. Same as Supplementary Figure 36 but for the MPI-ESM-P simulation and the corresponding volcanic forcing dataset (Crowley and Unterman, 2013).

12. References

- Abram, N., Gagan, M., Cole, J., Hantoro, W. and Mudelsee, M. (2008). Recent intensification of tropical climate variability in the Indian Ocean. *Nature Geoscience* **1**: 849-853.
- Alibert, C. and Kinsley, L. (2008a). A 170-year Sr/Ca and Ba/Ca coral record from the western Pacific warm pool: 1. What can we learn from an unusual coral record? *Journal of Geophysical Research* **113** (C4): C04008.
- Alibert, C. and Kinsley, L. (2008b). A 170-year Sr/Ca and Ba/Ca coral record from the western Pacific warm pool: 2. A window into variability of the New Ireland Coastal Undercurrent. *Journal of Geophysical Research* **113** (C6): C06006.
- Allen, K., Cook, E., Francey, R. and Michael, K. (2001). The climatic response of *Phyllocladus aspleniifolius* (Labill.) Hook. f in Tasmania. *Journal of Biogeography* **28**: 305-316.
- Allen, K. J. (2002). The Temperature Response in the Ring Widths of *Phyllocladus Aspleniifolius* (Celery-top Pine) Along an Altitudinal Gradient in the Warra LTER Area, Tasmania. *Australian Geographical Studies* **40** (3): 287-299.
- Ammann, C. M., Joos, F., Schimel, D. S., Otto-Bliesner, B. L. and Tomas, R. A. (2007). Solar influence on climate during the past millennium: results from transient simulations with the NCAR climate system model. *Proceedings of the National Academy of Sciences of the United States of America* **104**: 3713-3718.
- Ammann, C. M., Meehl, G. A., Washington, W. M. and Zender, C. S. (2003). A monthly and latitudinally varying volcanic forcing dataset in simulations of 20th century climate. *Geophysical Research Letters* **30** (12): 1657.
- Aravena, J. C., Lara, A., Wolodarsky-Franke, A., Villalba, R. and Cuq, E. (2002). Tree-ring growth patterns and temperature reconstruction from *Nothofagus pumilio* (Fagaceae) forests at the upper tree line of southern Chilean Patagonia. *Revista Chilena De Historia Natural* **75** (2): 361-376.
- Argollo, J., Soliz, C. and Villalba, R. (2004). Potencialidad dendrocronológica de *Polylepis tarapacana* en los Andes Centrales de Bolivia. *Ecología en Bolivia* **39** (1): 5-24.
- Aristarain, A. J., Delmas, R. J. and Stievenard, M. (2004). Ice-core study of the link between sea-salt aerosol, sea-ice cover and climate in the Antarctic Peninsula area. *Climatic Change* **67** (1): 63-86.
- Asami, R., Yamada, T. and Iryu, Y. (2005). Interannual and decadal variability of the western Pacific sea surface condition for the years 1787–2000: Reconstruction based on stable isotope record from a Guam coral. *Journal of Geophysical Research* **110**: 1-13.
- Bagnato, S., Linsley, B. K., Howe, S. S., Wellington, G. M. and Salinger, J. (2005). Coral oxygen isotope records of interdecadal climate variations in the South Pacific Convergence Zone region. *Geochemistry, Geophysics, Geosystems* **6** (6): Q06001.

- Baker, P., Palmer, J. and D'Arrigo, R. (2008). The dendrochronology of *Callitris intratropica* in Northern Australia: annual ring structure, chronology development and climate correlations. *Australian Journal of Botany* **56**: 311-320.
- Banta, J. R., McConnell, J. R., Frey, M. M., Bales, R. C. and Taylor, K. (2008). Spatial and temporal variability in snow accumulation at the West Antarctic Ice Sheet Divide over recent centuries. *J. Geophys. Res.* **113** (D23): D23102.
- Bard, E., G., R., Yiou, F. and J., J. (2000). Solar irradiance during the last 1200 years based on cosmogenic nuclides *Tellus* **52B**: 985-992.
- Battle, M., Bender, M., Sowers, T., Tans, P. P., Butler, J. H., Elkins, J. W., Ellis, J. T., Conway, T., Zhang, N., Lang, P. and Clarket, A. D. (1996). Atmospheric gas concentrations over the past century measured in air from firn at the South Pole. *Nature* **383**: 231-235.
- Berger, A. L. (1978). Long-Term Variations of Daily Insolation and Quaternary Climatic Changes. *Journal of the Atmospheric Sciences* **35** (12): 2362-2367.
- Bird, B. W., Abbott, M. B., Vuille, M., Rodbell, D. T., Stansell, N. D. and Rosenmeier, M. F. (2011). A 2,300-year-long annually resolved record of the South American summer monsoon from the Peruvian Andes. *Proceedings of the National Academy of Sciences* **108** (21): 8583-8588.
- Black, D. E., Abahazi, M. A., Thunell, R. C., Kaplan, A., Tappa, E. J. and Peterson, L. C. (2007). An 8-century tropical Atlantic SST record from the Cariaco Basin: Baseline variability, twentieth-century warming, and Atlantic hurricane frequency. *Paleoceanography* **22** (4): PA4204.
- Blunier, T., Chappellaz, J., Schwander, J., Stauffer, B. and Raynaud, D. (1995). Variations in atmospheric methane concentration during the Holocene epoch. *Nature* **374**: 46-49.
- Boës, X. and Fagel, N. (2008). Relationships between southern Chilean varved lake sediments, precipitation and ENSO for the last 600 years. *Journal of Paleolimnology* **39** (2): 237-252.
- Boiseau, M., Ghil, M. and Juillet-Leclerc, A. (1999). Climatic trends and interdecadal variability from south-central Pacific coral records. *Geophys. Res. Lett.* **26** (18): 2881-2884.
- Boninsegna, J. A., Keegan, J., Jacoby, G. C., D'Arrigo, R. and Holmes, R. L. (1989). Dendrochronological studies in Tierra del Fuego, Argentina. *Quaternary of South America and Antarctic Peninsula* **7**: 315-326.
- Bretagnon, P. and Francou, G. (1988). Planetary theories in rectangular and spherical variables - VSOP 87 solutions. *Astron. Astrophys.* **202**: 309-315.
- Bretherton, C. S., Widmann, M., Dymnikov, V. P., Wallace, J. M. and Bladé, I. (1999). The Effective Number of Spatial Degrees of Freedom of a Time-Varying Field. *Journal of Climate* **12** (7): 1990-2009.
- Briffa, K. and Jones, P. (1990). Basic chronology statistics and assessment. *Methods of Dendrochronology: applications in the environmental sciences*. E. Cook and L. Kairiukstis. Dordrecht, Kluwer Academic.

- Briffa, K. R. (2000). Annual climate variability in the Holocene: interpreting the message of ancient trees. *Quaternary Science Reviews* **19** (1-5): 87-105.
- Brookhouse, M., Lindesay, J. and Brack, C. (2008). The Potential of Tree Rings in Eucalyptus pauciflora for Climatological and Hydrological Reconstruction. *Geographical Research* **46** (4): 421-434.
- Buckley, B., Cook, E., Peterson, M. and Barbetti, M. (1997). A changing temperature response with elevation for Lagarostrobis franklinii in Tasmania, Australia. *Climatic Change* **36**: 477-498.
- Charles, C., Cobb, K., Moore, M. and Fairbanks, R. (2003). Monsoon–tropical ocean interaction in a network of coral records spanning the 20th century. *Marine Geology* **201** (1-3): 207-222.
- Christie, D. A., Boninsegna, J. A., Cleaveland, M., Lara, A., Le Quesne, C., Morales, M., Mudelsee, M., Stahle, D. and Villalba, R. (2011). Aridity changes in the Temperate-Mediterranean transition of the Andes since AD 1346 reconstructed from tree-rings. *Climate Dynamics* **36**: 1505-1521.
- Christie, D. A., Lara, A., Barichivich, J., Villalba, R., Morales, M. S. and Cuq, E. (2009). El Niño-Southern Oscillation signal in the world's highest-elevation tree-ring chronologies from the Altiplano, Central Andes. *Palaeogeography, Palaeoclimatology, Palaeoecology* **281** (3-4): 309-319.
- Cobb, K., Charles, C., Cheng, H. and Edwards, L. (2003). El Nino/Southern Oscillation and tropical Pacific climate during the last millenium. *Nature* **424**: 271-276.
- Cole, J., Dunbar, R., Mc Clanahan, T. and Muthiga, N. (2000). Tropical Pacific forcing of decadal SST variability in the Western Indian Ocean over the past two centuries. *Science* **287** (5453): 617-619.
- Cole, J., Fairbanks, R. and Shen, G. (1993). Recent variability in the Southern Oscillation; isotopic results from a Tarawa atoll coral. *Science* **260**: 1790-1793.
- Conroy, J. L., Restrepo, A., Overpeck, J. T., Steinitz-Kannan, M., Cole, J. E., Bush, M. B. and Colinvaux, P. A. (2009). Unprecedented recent warming of surface temperatures in the eastern tropical Pacific Ocean. *Nature Geoscience* **2** (1): 46-50.
- Cook, E. R., Briffa, K. R. and Jones, P. D. (1994). Spatial regression methods in dendroclimatology – a review and compariosn of two techniques. *International Journal of Climatology* **14** (4): 379-402.
- Cook, E. R., Buckley, B. M., D'Arrigo, R. D. and Peterson, M. J. (2000). Warm-season temperatures since 1600 BC reconstructed from Tasmanian tree rings and their relationship to large-scale sea surface temperature anomalies. *Climate Dynamics* **16** (2-3): 79-91.
- Cook, E. R., Buckley, B. M., Palmer, J. G., Fenwick, P., Peterson, M. J., Boswijk, G. and Fowler, A. (2006). Millennia-long tree-ring records from Tasmania and New Zealand: a basis for modelling climate variability and forcing, past, present and future. *Journal of Quaternary Science* **21** (7): 689-699.

Cook, E. R., Palmer, J. G., Cook, B. I., Hogg, A. and D'Arrigo, R. D. (2002). A multi-millennial palaeoclimatic resource from Lagarostrobos colensoi tree-rings at Oroko Swamp, New Zealand. *Global and Planetary Change* **33** (3-4): 209-220.

Crowley, T. (2000). Causes of Climate Change over the Past 1,000 years. *Science* **289**: 270-277.

Crowley, T. J. and Unterman, M. B. (2013). Technical details concerning development of a 1200 yr proxy index for global volcanism. *Earth Syst. Sci. Data* **5** (1): 187-197.

Cullen, L. and Grierson, P. (2009). Multi-decadal scale variability in autumn-winter rainfall in south-western Australia since 1655 AD as reconstructed from tree rings of *Callitris columellaris*. *Climate Dynamics* **33** (2-3): 433-444.

D'Arrigo, R., Cook, E., Villalba, R., Buckley, B., Salinger, M., Palmer, J. and Allen, K. (2000). Trans-Tasman Sea Climate Variability Since AD 1740 Inferred From Middle-High Latitude Tree-Ring Data. *Climate Dynamics* **16**: 603-610.

D'Arrigo, R., Wilson, R. and Jacoby, G. (2006a). On the long-term context for late twentieth century warming. *Journal of Geophysical Research-Atmospheres* **111**: D03103.

D'Arrigo, R., Wilson, R., Palmer, J., Krusic, P., Curtis, A., Sakulich, J., Bijaksana, S., Zulaikah, S. and Ngkoimani, L. O. (2006b). Monsoon drought over Java, Indonesia, during the past two centuries. *Geophysical Research Letters* **33** (4): L04709.

D'Arrigo, R. D., Buckley, B. M., Cook, E. R. and Wagner, W. S. (1995). Temperature-sensitive tree-ring width chronologies of pink pine (*Halocarpus biformis*) from Stewart Island, New Zealand. *Palaeogeography Palaeoclimatology Palaeoecology* **119** (3-4): 293-300.

Damassa, T., Cole, J., Barnett, H., Ault, T. and McClanahan (2006). Enhanced multidecadal climate variability in the seventeenth century from coral isotope records in the western Indian Ocean. *Paleoceanography* **21**: PA2016.

Drost, F. and Karoly, D. (2012). Evaluating global climate responses to different forcings using simple indices. *Geophysical Research Letters* **39** (16): L16701.

Drost, F., Karoly, D. and Braganza, K. (2012). Communicating global climate change using simple indices: an update. *Climate Dynamics* **39** (3-4): 989-999.

Druffel, E. R. M. and Griffin, S. (1999). Variability of surface ocean radiocarbon and stable isotopes in the southwestern Pacific. *J. Geophys. Res.* **104** (C10): 23607-23613.

Dufresne, J. L., Foujols, M. A., Denvil, S., Caubel, A., Marti, O., Aumont, O., Balkanski, Y., Bekki, S., Bellenger, H., Benshila, R., Bony, S., Bopp, L., Braconnot, P., Brockmann, P., Cadule, P., Cheruy, F., Codron, F., Cozic, A., Cugnet, D., Noblet, N., Duvel, J. P., Ethé, C., Fairhead, L., Fichefet, T., Flavoni, S., Friedlingstein, P., Grandpeix, J. Y., Guez, L., Guilyardi, E., Hauglustaine, D., Hourdin, F., Idelkadi, A., Ghattas, J., Joussaume, S., Kageyama, M., Krinner, G., Labeyrie, S., Lahellec, A., Lefebvre, M. P., Lefevre, F., Levy, C., Li, Z. X., Lloyd, J., Lott, F., Madec, G., Mancip, M., Marchand, M., Masson, S., Meurdésorff, Y., Mignot, J., Musat, I., Parouty, S., Polcher, J., Rio, C., Schulz, M., Swingedouw, D., Szopa, S., Talandier, C., Terray, P., Viovy, N. and Vuichard, N. (2012).

Climate change projections using the IPSL-CM5 Earth System Model: from CMIP3 to CMIP5. *Climate Dynamics* **40** (9-10): 2123-2165.

Dunbar, R. B., Wellington, G. M., Colgan, M. W. and Glynn, P. W. (1994). Eastern Pacific Sea-Surface Temperature since 1600-AD - the Delta-O-18 Record of Climate Variability in Galapagos Corals. *Paleoceanography* **9** (2): 291-315.

Duncan, R. P., Fenwick, P., Palmer, J. G., McGlone, M. S. and Turney, C. S. M. (2010). Non-uniform interhemispheric temperature trends over the past 550 years. *Climate Dynamics* **35** (7-8): 1429–1438.

Dunwiddie, P. W. and Lamarche, V. C. (1980). A Climatically Responsive Tree-Ring Record from Widdringtonia-Cedarbergensis, Cape-Province, South-Africa. *Nature* **286** (5775): 796-797.

Ekaykin, A. A., Lipenkov, V. Y., Kuzmina, I. N., Petit, J. R., Masson-Delmotte, V. and Johnsen, S. J. (2004). The changes in isotope composition and accumulation of snow at Vostok station, East Antarctica, over the past 200 years. *Annals of Glaciology* **39**: 569-575.

Elbert, J., Grosjean, M., von Gunten, L., Urrutia, R., Fischer, D., Wartenburger, R., Ariztegui, D. and Fujak, M. (2011). Quantitative high-resolution winter (JJA) precipitation reconstruction from varved sediments of Lago Plomo 47°S, Patagonian Andes, AD 1530 - 2001. *The Holocene*.

Etheridge, D., Steele, L., Francey, R. and Langenfelds, R. L. (1998). Atmospheric methane between 1000 A. D. and present: Evidence of anthropogenic emissions and climatic variability. *Journal of Geophysical Research* **103**: 15979-15993.

Etheridge, D. M., Steele, L. P., Langenfelds, R. L., Francey, R. J., Barnola, J. M. and Morgan, V. I. (1996). Natural and anthropogenic changes in atmospheric CO₂ over the last 1000 years from air in Antarctic ice and firn. *Journal of Geophysical Research-Atmospheres* **101**: 4115-4128.

Fenby, C. and Gergis, J. (2013). Rainfall variations in south-eastern Australia part 1: consolidating evidence from pre-instrumental documentary sources, 1788–1860. *International Journal of Climatology*: doi: 10.1002/joc.3640.

Flückiger, J., Dallenbach, A., Blunier, T., Stauffer, B., Stocker, T. F., Raynaud, D. and Barnola, J. M. (1999). Variations in atmospheric N₂O concentration during abrupt climatic changes. *Science* **285**: 227-230.

Flückiger, J., Monnin, E., Stauffer, B., Schwander, J., Stocker, T. F., Chappellaz, J., Raynaud, D. and Barnola, J. M. (2002). High-resolution Holocene N₂O ice core record and its relationship with CH₄ and CO₂. *Global Biogeochemical Cycles* **16**: 1010.

Fowler, A., Boswijk, G., Gergis, J. and Lorrey, A. (2008). ENSO history recorded in *Agathis australis* (Kauri) tree-rings Part A: Kauri's potential as an ENSO proxy. *International Journal of Climatology* **28** (1): 1-20.

Frank, D., Esper, J. and Cook, E. R. (2007). Adjustment for proxy number and coherence in a large-scale temperature reconstruction. *Geophysical Research Letters* **34** (16): L16709.

- Frank, D. C., Esper, J., Raible, C. C., Buntgen, U., Trouet, V., Stocker, B. and Joos, F. (2010). Ensemble reconstruction constraints on the global carbon cycle sensitivity to climate. *Nature* **463** (7280): 527-532.
- Gao, C., Robock, A. and Ammann, C. (2008). Volcanic forcing of climate over the past 1500 years: An improved ice core-based index for climate models. *J. Geophys. Res.* **113** (D23): D23111.
- García-Herrera, R., Diaz, H. F., Garcia, R. R., Prieto, M. R., Barriopedro, D., Moyano, R., Hernández, E. (2008). A Chronology of El Niño Events from Primary Documentary Sources in Northern Peru. *Journal of Climate* **21** (9): 1948-1962.
- Garcin, Y., Williamson, D., Bergonzini, L., Radakovitch, O., Vincens, A., Buchet, G., Guiot, J., Brewer, S., Mathé, P.-E. and Majule, A. (2007). Solar and anthropogenic imprints on Lake Masoko (southern Tanzania) during the last 500 years. *Journal of Paleolimnology* **37** (4): 475-490.
- Gergis, J., Gallant, A., Braganza, K., Karoly, D., Allen, K., Cullen, L., D'Arrigo, R., Goodwin, I., Grierson, P. and McGregor, S. (2011). On the long-term context of the 1997–2009 ‘Big Dry’ in South-Eastern Australia: insights from a 206-year multi-proxy rainfall reconstruction. *Climatic Change*: 1-22.
- Gioda, A. and Prieto, M. R. (1999). Histoire des sécheresses andines. Potosí, El Niño et le Petit Age Glaciaire. *Revue de la Société Météorologique de France. La Météorologie* **27**: 33-42.
- González-Rouco, J. F., Beltrami, H., Zorita, E. and von Storch, H. (2006). Simulation and inversion of borehole temperature profiles in surrogate climates: Spatial distribution and surface coupling. *Geophysical Research Letters* **33**: L01703.
- Graf, W., Oerter, H., Reinwarth, O., Stichler, W., Wilhelms, F., Miller, H. and Mulvaney, R. (2002). Stable-isotope records from Dronning Maud Land, Antarctica. *Annals of Glaciology* **35**: 195-201.
- Guilderson, T. and Schrag, D. (1999). Reliability of coral isotope records from the western Pacific warm pool: A comparison using age-optimized records. *Paleoceanography* **14** (4): 457-464.
- Hanhijärvi, S., Tingley, M. P. and Korhola, A. (2013). Pairwise comparisons to reconstruct mean temperature in the Arctic Atlantic Region over the last 2,000 years. *Climate Dynamics*.
- Hansen, J., Ruedy, R., Sato, M. and Lo, K. (2010). Global surface temperature change. *Reviews of Geophysics* **48** (4): RG4004.
- Hegerl, G., Crowley, T. J., Allen, M., Hyde, W. T., Pollack, H. N., Smerdon, J. and Zorita, E. (2007). Detection of human influence on a new, validated 1500-year temperature reconstruction. *Journal of Climate* **20** (4): 650-666.
- Herrera, R., Prieto, M. R. and García-Herrera, R. (2003). Floods in the semiarid Argentinean Chaco during the 17th to 19th centuries. *Proceedings of Palaeofloods, Historical Data & Climatic Variability: Applications in Flood Risk Assessment*. V. R. Thorndycraft, G. Benito, M. Barriendos and M. Llasat. Madrid, CSIC-Centro de Ciencias Medioambientales: 107-112.

Hofer, D., Raible, C. C. and Stocker, T. F. (2011). Variations of the Atlantic meridional overturning circulation in control and transient simulations of the last millennium. *Climate of the Past* **7** (1): 133-150.

Hoffmann, G., Ramirez, E., Taupin, J. D., Francou, B., Ribstein, P., Delmas, R., Durr, H., Gallaire, R., Simoes, J., Schotterer, U., Stievenard, M. and Werner, M. (2003). Coherent isotope history of Andean ice cores over the last century. *Geophysical Research Letters* **30** (4).

Hurtt, G. C., Frolking, S., Fearon, M. G., Moore, B., Shevliakova, E., Malyshev, S., Pacala, S. W. and Houghton, R. A. (2006). The underpinnings of land-use history: three centuries of global gridded land-use transitions, wood-harvest activity, and resulting secondary lands. *Global Change Biology* **12** (7): 1208-1229.

Jacobel, R. W., Welch, B. C., Steig, E. J. and Schneider, D. P. (2005). Glaciological and climatic significance of Hercules Dome, Antarctica: An optimal site for deep ice core drilling. *Journal of Geophysical Research-Earth Surface* **110** (F1).

Johns, T. C., Gregory, J. M., Ingram, W. J., Johnson, C. E., Jones, A., Lowe, J. A., Mitchell, J. F. B., Roberts, D. L., Sexton, D. M. H., Stevenson, D. S., Tett, S. F. B. and Woodage, M. J. (2003). Anthropogenic climate change for 1860 to 2100 simulated with the HadCM3 model under updated emissions scenarios. *Climate Dynamics* **20** (6): 583-612.

Jones, P. D., Briffa, K. R., Barnett, T. P. and Tett, S. F. B. (1998). High-resolution palaeoclimatic records for the last millennium: interpretation, integration and comparison with General Circulation Model control-run temperatures. *The Holocene* **8** (4): 455-471.

Juckes, M., Allen, M., Briffa, K., Esper, J., Hegerl, G., Moberg, A., Osborn, T. and Weber, S. (2007). Millennial temperature reconstruction intercomparison and evaluation. *Climate of the Past* **3**: 591–609.

Jungclaus, J., Giorgetta, M., Reick, C., Legutke, S., Brovkin, V., Crueger, T., Esch, M., Fieg, K., Fischer, N., Glushak , K., Gayler, V., Haak, H., Hollweg, H.-D., Kinne, S., Kornblueh , L., Matei, D., Mauritzen, T., Mikolajewicz, U., Müller, W., Notz, D., Pohlmann, T., Raddatz, T., Rast, S., Roeckner, E., Salzmann, M., Schmidt, H., Schnur, R., Segschneider, J., Six, K., Stockhouse, M., Wegner, J., Widmann, H., Wieners, K.-H., Claussen, M., Marotzke, J. and Stevens, B. (2012). MIP5 simulations of the Max Planck Institute for Meteorology (MPI-M) based on the MPI-ESM-P model: The past1000 experiment, served by ESGF. World Data Center for Climate doi:10.1594/Wdcc/CMIP5.MXEPpk.

Jungclaus, J. H., Fischer, N., Haak, H., Lohmann, K., Marotzke, J., Matei, D., Mikolajewicz, U., Norz, D. and von Storch, J. S. (2013). Characteristics of the ocean simulations in MPIOM, the ocean component of the MPI-Earth System Model. *Journal of Advances in Modelling Earth Systems*: 10.1002/jame.20023.

Jungclaus, J. H., Lorenz, S. J., Timmreck, C., Reick, C. H., Brovkin, V., Six, K., Segschneider, J., Giorgetta, M. A., Crowley, T. J., Pongratz, J., Krivova, N. A., Vieira, L. E., Solanki, S. K., Klocke, D., Botzet, M., Esch, M., Gayler, V., Haak, H., Raddatz, T. J., Roeckner, E., Schnur, R., Widmann, H., Claussen, M., Stevens, B. and Marotzke, J. (2010). Climate and carbon-cycle variability over the last millennium. *Clim. Past* **6** (5): 723-737.

Kaplan, J. O., Krumhardt, K. M., Ellis, E. C., Ruddiman, W. F., Lemmen, C. and Goldewijk, K. K. (2011). Holocene carbon emissions as a result of anthropogenic land cover change. *The Holocene* **21** (5): 775-791.

Karoly, D. J. (1989). Southern-Hemisphere Circulation Features Associated with El Niño - Southern Oscillation Events. *Journal of Climate* **2** (11): 1239-1252.

Karoly, D. J., Hope, P. and Jones, P. D. (1996). Decadal variations of the Southern Hemisphere circulation. *International Journal of Climatology* **16** (7): 723-738.

Karoly, D. J. and Vincent, D. G. (1998). *Meteorology of the Southern Hemisphere*. Boston, USA, American Meteorological Association.

Kellerhals, T., Brutsch, S., Sigl, M., Knusel, S., Gaggeler, H. W. and Schwikowski, M. (2010). Ammonium concentration in ice cores: A new proxy for regional temperature reconstruction? *Journal of Geophysical Research-Atmospheres* **115**: D16123.

Kelso, C. and Vogel, C. H. (2007). The climate of Namaqualand in the nineteenth century. *Climatic Change* **83** (3): 357-380.

Krivova, N. A., Balmaceda, L. and Solanki, S. K. (2007). Reconstruction of solar total irradiance since 1700 from the surface magnetic flux. *Astronomy and Astrophysics* **467**: 335-346.

Kuhnert, H., Patzold, J., Hatcher, B., Wyrwoll, K. H., Eisenhauer, A., Collins, L. B., Zhu, Z. R. and Wefer, G. (1999). A 200-year coral stable oxygen isotope record from a high-latitude reef off western Australia. *Coral Reefs* **18** (1): 1-12.

Kuhnert, H., Pätzold, J., Wyrwoll, K. and Wefer, G. (2000). Monitoring climate variability over the past 116 years in coral oxygen isotopes from Ningaloo Reef, Western Australia. *International Journal of Earth Sciences* **88**: 725-732.

LaMarche, V. C., Holmes, R. L., Dunwiddie, P. W. and Drew, L. G. (1979a). *Tree-ring chronologies of the southern hemisphere: Vol. 1: Argentina. Chronology Series V*. Tucson, AZ, Laboratory of Tree-Ring Research, University of Arizona.

LaMarche, V. C., Holmes, R. L., Dunwiddie, P. W. and Drew, L. G. (1979b). *Tree-ring chronologies of the southern hemisphere: Vol. 2: Chile. Chronology Series V*. Tucson, AZ, Laboratory of Tree-Ring Research, University of Arizona, Tucson, USA.

LaMarche, V. C., Holmes, R. L., Dunwiddie, P. W. and Drew, L. G. (1979c). *Tree-ring chronologies of the Southern Hemisphere: Vol. 4: Australia.*, Laboratory of Tree-Ring Research, University of Arizona, Tucson, USA.

Lamarque, J. F., Bond, T. C., Eyring, V., Granier, C., Heil, A., Klimont, Z., Lee, D., Liousse, C., Mieville, A., Owen, B., Schultz, M. G., Shindell, D., Smith, S. J., Stehfest, E., Van Aardenne, J., Cooper, O. R., Kainuma, M., Mahowald, N., McConnell, J. R., Naik, V., Riahi, K. and van Vuuren, D. P. (2010). Historical (1850-2000) gridded anthropogenic and biomass burning emissions of reactive gases and aerosols: methodology and application. *Atmos. Chem. Phys.* **10** (15): 7017-7039.

Lara, A., Aravena, J. C., Villalba, R., Wolodarsky-Franke, A., Luckman, B. and Wilson, R. (2001). Dendroclimatology of high-elevation Nothofagus pumilio forests at their northern

distribution limit in the central Andes of Chile. *Canadian Journal of Forest Research-Revue Canadienne De Recherche Forestiere* **31** (6): 925-936.

Lara, A., Villalba, R., Aravena, J. C., Wolodarsky, A. and Neira, A. (2000). Desarollo de una red de cronologías de Fitzroya Cupressoides (Alerce) para Chile y Argentina. *Dendrochronología en América Latina*. F. Roig. Mendoza, Editorial Nacional de Cuyo: 193-215.

Lara, A., Villalba, R. and Urrutia, R. (2008). A 400-year tree-ring record of the Puelo River summer-fall streamflow in the Valdivian Rainforest eco-region, Chile. *Climatic Change* **86** (3-4): 331-356.

Lara, A., Villalba, R., Wolodarsky-Franke, A., Aravena, J. C., Luckman, B. H. and Cuq, E. (2005). Spatial and temporal variation in Nothofagus pumilio growth at tree line along its latitudinal range (35 degrees 40 '-55 degrees S) in the Chilean Andes. *Journal of Biogeography* **32** (5): 879-893.

Laundrum, L., Otto-Bliesner, B., Conley, P., Lawrence, P., Rosenbloom, N. and Teng, H. (2013). Last Millennium Climate and Its Variability in CCSM4. *Journal of Climate* **26** (1085): 1111.

Le Quesne, C., Stahle, D. W., Cleaveland, M. K., Therrell, M. D., Aravena, J. C. and Barichivich, J. (2006). Ancient Austrocedrus Tree-Ring Chronologies Used to Reconstruct Central Chile Precipitation Variability from a.d. 1200 to 2000. *Journal of Climate* **19** (22): 5731-5744.

Lean, J., Beer, J. and Bradley, R. (1995). Reconstruction of solar irradiance since 1610: Implications for climate change. *Geophysical Research Letters* **22** (23): 3195-3198.

Lefohn, A. S., Husar, J. D. and Husar, R. B. (1999). Estimating historical anthropogenic global sulfur emission patterns for the period 1850–1990. *Atmospheric Environment* **33** (21): 3435-3444.

Li, B., Nychka, D. and Ammann, C. (2010). The Value of Multiproxy Reconstruction of Past Climate. *Journal of the American Statistical Association* **105** (491): 883–895.

Linsley, B., Ren, L., Dunbar, R. and Howe, S. (2000a). El Niño Southern Oscillation (ENSO) and decadal-scale climate variability at 10N in the eastern Pacific from 1893 to 1994: A coral-based reconstruction from Clipperton Atoll. *Paleoceanography* **15** (3): 322-335.

Linsley, B., Wellington, G. and Schrag, D. (2000b). Decadal Sea Surface Temperature Variability in the Subtropical South Pacific from 1726 to 1997 AD. *Science* **290**: 1145-1149.

Linsley, B., Wellington, G., Schrag, D., Ren, L., Salinger, J. and Tudhope, A. (2004). Geochemical evidence from corals for changes in the amplitude and spatial pattern of South Pacific interdecadal climate variability over the last 300 years. *Climate Dynamics* **22**: 1-11.

Linsley, B. K., Dunbar, R. B., Wellington, G. M. and Mucciarone, D. A. (1994). A Coral-Based Reconstruction of Intertropical Convergence Zone Variability over Central-America since 1707. *Journal of Geophysical Research-Oceans* **99** (C5): 9977-9994.

Linsley, B. K., Kaplan, A., Gouriou, Y., Salinger, J., Demenocal, P. B., Wellington, G. M. and Howe, S. S. (2006). Tracking the extent of the South Pacific Convergence Zone since the early 1600s. *Geochemistry Geophysics Geosystems* **7**.

Linsley, B. K., Zhang, P. P., Kaplan, A., Howe, S. S. and Wellington, G. M. (2008). Interdecadal-decadal climate variability from multicoral oxygen isotope records in the South Pacific Convergence Zone region since 1650 A.D. *Paleoceanography* **23** (2): PA2219.

Lough, J. M. (2011). Great Barrier Reef coral luminescence reveals rainfall variability over northeastern Australia since the 17th century. *Paleoceanography* **26** (2): PA2201.

Luterbacher, J., Dietrich, D., Xoplaki, E., Grosjean, M. and Wanner, H. (2004). European seasonal and annual temperature variability, trends, and extremes since 1500. *Science* **303** (5663): 1499-1503.

Luterbacher, J., Xoplaki, E., Dietrich, D., Rickli, R., Jacobbeit, J., Beck, C., Gyalistras, D., Schmutz, C. and Wanner, H. (2002). Reconstruction of sea level pressure fields over the Eastern North Atlantic and Europe back to 1500. *Climate Dynamics* **18** (7): 545-561.

MacFarling-Meure, C., Etheridge, D., Trudinger, C., Steele, P., Langenfelds, R., van Ommen, T., Smith, A. and Elkins, J. (2006). Law Dome CO₂, CH₄ and N₂O ice core records extended to 2000 years BP. *Geophysical Research Letters* **33** (14): L14810.

Mann, M., Zhang, Z., Hughes, M., Bradley, R., Miller, S., Rutherford, S. and Ni, F. (2008). Proxy-based reconstructions of hemispheric and global surface temperature variations over the past two millennia. *Proceedings of the National Academy of Sciences* **105** (36): 13252–13257.

Mann, M. E. and Jones, P. D. (2003). Global surface temperatures over the past two millennia. *Geophysical Research Letters* **30** (15): 1820.

Marland, G., Boden, T. A. and Andres, R. J. (2003). Global regional and national emissions. *Trends: a compendium of data on global change*. Oak Ridge, TN, Carbon Dioxide Information Center, Oak Ridge National Laboratory.

Masiokas, M. and Villalba, R. (2004). Climatic significance of intra-annual bands in the wood of Nothofagus pumilio in southern Patagonia. *Trees-Structure and Function* **18** (6): 696-704.

Mayewski, P. A., Maasch, K. A., White, J. W. C., Steig, E. J., Meyerson, E., Goodwin, I., Morgan, V. I., Van Ommen, T., Curran, M. A. J., Souney, J. and Kreutz, K. (2004). A 700 year record of Southern Hemisphere extratropical climate variability. *Annals of Glaciology* **39**: 127-132.

McGregor, S., Timmermann, A., England, M. H., Elison Timm, O. and Wittenberg, A. T. (2013). Inferred changes in El Niño-Southern Oscillation variance over the past six centuries. *Clim. Past* **9** (5): 2269-2284.

Melvin, T. M. and Briffa, K. R. (2008). A "signal-free" approach to dendroclimatic standardisation. *Dendrochronologia* **26** (2): 71-86.

Melvin, T. M., Briffa, K. R., Nicolussi, K. and Grabner, M. (2007). Time-varying-response smoothing. *Dendrochronologia* **25** (1): 65-69.

- Moberg, A., Sonechkin, D. M., Holmgren, K., Datsenko, N. M. and Karlen, W. (2005). Highly variable Northern Hemisphere temperatures reconstructed from low- and high-resolution proxy data. *Nature* **433** (7026): 613-617.
- Morales, M. S., Villalba, R., Grau, H. R. and Paolini, L. (2004). Rainfall-controlled tree growth in high-elevation subtropical treelines. *Ecology* **85** (11): 3080-3089.
- Morice, C. P., Kennedy, J. J., Rayner, N. A. and Jones, P. D. (2012). Quantifying uncertainties in global and regional temperature change using an ensemble of observational estimates: The HadCRUT4 data set. *J. Geophys. Res.* **117** (D8): D08101.
- Mosley-Thompson, E., Thompson, L. G., Grootes, P. and Gundestrup, N. (1990). Little Ice Age (Neoglacial) paleoenvironmental conditions at Siple Station, Antarctica. *Annals of Glaciology* **14**: 199-204.
- Mulvaney, R., Oerter, H., Peel, D. A., Graf, W., Arrowsmith, C., Pasteur, E. C., Knight, B., Littot, G. C. and Miners, W. D. (2002). 1000 year ice-core records from Berkner Island, Antarctica. *Annals of Glaciology* **35**: 45-51.
- Mundo, I., Roig Juñent, F., Villalba, R., Kitzberger, T. and Barrera, M. (2012). Araucaria araucana tree-ring chronologies in Argentina: spatial growth variations and climate influences. *Trees - Structure and Function* **26** (2): 443-458.
- Nash, D. J. and Endfield, G. H. (2008). 'Splendid rains have fallen': links between El Niño and rainfall variability in the Kalahari, 1840-1900. *Climatic Change* **86** (3-4): 257-290.
- Nash, D. J. and Grab, S. W. (2010). "A sky of brass and burning winds": documentary evidence of rainfall variability in the Kingdom of Lesotho, Southern Africa, 1824–1900. *Climatic Change* **101** (3-4): 617–653.
- Neukom, R. and Gergis, J. (2012). Southern Hemisphere high-resolution palaeoclimate records of the last 2000 years. *The Holocene* **22** (5): 501-524.
- Neukom, R., Luterbacher, J., Villalba, R., Küttel, M., Frank, D., Jones, P. D., Grosjean, M., Esper, J., Lopez, L. and Wanner, H. (2010). Multi-centennial summer and winter precipitation variability in southern South America. *Geophysical Research Letters* **37**: L14708.
- Neukom, R., Luterbacher, J., Villalba, R., Kuttel, M., Frank, D., Jones, P. D., Grosjean, M., Wanner, H., Aravena, J. C., Black, D. E., Christie, D. A., D'Arrigo, R., Lara, A., Morales, M., Soliz-Gamboa, C., Srur, A., Urrutia, R. and von Gunten, L. (2011). Multiproxy summer and winter surface air temperature field reconstructions for southern South America covering the past centuries. *Climate Dynamics* **37** (1-2): 35-51.
- Neukom, R., Nash, D. J., Endfield, G. H., Grab, S. W., Grove, C. A., Kelso, C., Vogel, C. H. and Zinke, J. (2013). Multi-proxy summer and winter precipitation reconstruction for southern Africa over the last 200 years. *Climate Dynamics*: doi: 10.1007/s00382-013-1886-6.
- Neukom, R., Prieto, M. D., Moyano, R., Luterbacher, J., Pfister, C., Villalba, R., Jones, P. D. and Wanner, H. (2009). An extended network of documentary data from South America and its potential for quantitative precipitation reconstructions back to the 16th century. *Geophysical Research Letters* **36**: L12703.

North, G., Bell, T., Cahalan, F. and Moeing, F. (1982). Sampling Errors in the Estimation of Emerical Orthogonal Functions. *American Meteorological Society* **110**: 699-706.

Nurhati, I., Cobb, K. and Di Lorenzo, E. (2011). Decadal-scale SST and Salinity Variations in the Central Tropical Pacific: Signatures of Natural and Anthropogenic Climate Change. *Journal of Climate* **24**: 3294-3308.

PAGES-2k-Consortium (2013). Continental-scale temperature variability during the past two millennia. *Nature Geoscience* **6**: 339-346.

Pfeiffer, M., Timm, O., Dullo, W. C. and Podlech, S. (2004). Oceanic forcing of interannual and multidecadal climate variability in the southwestern Indian Ocean: Evidence from a 160 year coral isotopic record (La Réunion, 55°E, 21°S). *Paleoceanography* **19** (4): PA4006.

Phipps, S. J., McGregor, H. V., Gergis, J., Gallant, A. J. E., Neukom, R., Stevenson, S., Ackerley, D., Brown, J. R., Fischer, M. J. and van Ommen, T. D. (2013). Paleoclimate Data-Model Comparison and the Role of Climate Forcings over the Past 1500 Years. *Journal of Climate* **26** (18): 6915-6936.

Phipps, S. J., Rotstayn, L. D., Gordon, H. B., Roberts, J. L., Hirst, A. C. and Budd, W. (2011). The CSIRO Mk3L climate system model version 1.0 – Part 1: Description and evaluation. *Geoscientific Model Development* **4**: 483-509.

Phipps, S. J., Rotstayn, L. D., Gordon, H. B., Roberts, J. L., Hirst, A. C. and Budd, W. F. (2012). The CSIRO Mk3L climate system model version 1.0 - Part 2: Response to external forcings. *Geoscientific Model Development* **5**: 649-682.

Pongratz, J., Raddatz, T., Reick, C. H., Esch, M. and Claussen, M. (2009). Radiative forcing from anthropogenic land cover change since A.D. 800. *Geophysical Research Letters* **36** (2): L02709.

Pongratz, J., Reick, C., Raddatz, T. and Claussen, M. (2008). A reconstruction of global agricultural areas and land cover for the last millennium. *Global Biogeochem. Cycles* **22** (3): GB3018.

Prieto, M. R. (2007). ENSO signals in South America: rains and floods in the Parana River region during colonial times. *Climatic Change* **83** (1-2): 39-54.

Prieto, M. R. and Herrera, R. (2001). De sequías, hambrunas , plagas y “otras varias y continuas calamidades acaecidas en la Jurisdicción de Córdoba” durante el siglo XVIII. *Serie Economía y Sociedad. Cuadernos de Historia* **4**: 131-158.

Prieto, M. R., Herrera, R. and Dussel, P. (1999). Historical evidences of streamflow fluctuations in the Mendoza River, Argentina, and their relationship with ENSO. *Holocene* **9** (4): 473-481.

Prieto, M. R., Herrera, R. and Dussel, P. (2000). Archival evidence for some aspects of historical climate variability in Argentina and Bolivia during the 17th and 18th centuries. *Southern Hemisphere Paleo and Neo-Climates: Methods and Concepts*. P. P. Smolka and W. Volkheimer. Berlin, Springer: 127-142.

Prieto, M. R., Herrera, R., Dussel, P., Gimeno, L., Ribera, P., Garcia, R. and Hernandez, E. (2001). Interannual oscillations and trend of snow occurrence in the Andes region since 1885. *Australian Meteorological Magazine* **50** (2): 164-168.

Quinn, T. M., Crowley, T. J., Taylor, F. W., Henin, C., Joannot, P. and Join, Y. (1998). A multicentury stable isotope record from a New Caledonia coral: Interannual and decadal sea surface temperature variability in the southwest Pacific since 1657 AD. *Paleoceanography* **13** (4): 412-426.

Quinn, T. M., Taylor, F. W. and Crowley, T. J. (1993). A 173 year stable-isotope record from a tropical South-Pacific coral. *Quaternary Science Reviews* **12** (6): 407-418.

Quinn, T. M., Taylor, F. W. and Crowley, T. J. (2006). Coral-based climate variability in the Western Pacific Warm Pool since 1867. *Journal of Geophysical Research-Oceans* **111** (C11).

Quinn, W. H. and Neal, V. T. (1992). The historical record of El Niño events. *Climate since A.D. 1500*. R. Bradley and P. D. Jones. London, Routledge: 623-648.

Ramirez, E., Hoffmann, G., Taupin, J. D., Francou, B., Ribstein, P., Caillon, N., Ferron, F. A., Landais, A., Petit, J. R., Pouyaud, B., Schotterer, U., Simoes, J. C. and Stievenard, M. (2003). A new Andean deep ice core from Nevado Illimani (6350 m), Bolivia. *Earth and Planetary Science Letters* **212** (3-4): 337-350.

Rasbury, M. and Aharon, P. (2006). ENSO-controlled rainfall variability records archived in tropical stalagmites from the mid-ocean island of Niue, South Pacific. *Geochemistry Geophysics Geosystems* **7**: Q07010.

Rein, B. (2007). How do the 1982/83 and 1997/98 El Niños rank in a geological record from Peru? *Quaternary International* **161** (1): 56-66.

Reuter, J., Stott, L., Khider, D., Sinha, A., Cheng, H. and Edwards, R. L. (2009). A new perspective on the hydroclimate variability in northern South America during the Little Ice Age. *Geophys. Res. Lett.* **36** (21): L21706.

Roig, F. (1991). Dendrocronología y dendroclimatología del bosque de Pilgerodendron uviferum en su área norte de dispersión. *Bul. Soc. Argent. Bot.* **27**: 217-234.

Roig, F. and Boninsegna, J. (1990). Environmental factors affecting growth of Adesmia communities as determined from tree rings. *Dendrochronologia* **8**: 39-65.

Russell, A., McGregor, G. R. and Marshall, G. J. (2006). 340 years of atmospheric circulation characteristics reconstructed from an eastern Antarctic Peninsula ice core. *Geophysical Research Letters* **33** (8): L08702.

Russell, J. M. and Johnson, T. C. (2007). Little Ice Age drought in equatorial Africa: Intertropical Convergence Zone migrations and El Niño-Southern Oscillation variability. *Geology* **35** (1): 21-24.

Schmelter, A. (2000). Climatic response and growth-trends of Nothofagus pumilio along altitudinal gradients from arid to humid sites in northern Patagonia - A progress report. *Dendrochronología en América Latina*. F. Roig. Mendoza, Editorial Nacional de Cuyo: 193-215.

Schmidt, G. A., Jungclaus, J. H., Ammann, C. M., Bard, E., Braconnot, P., Crowley, T. J., Delaygue, G., Joos, F., Krivova, N. A., Muscheler, R., Otto-Bliesner, B. L., Pongratz, J., Shindell, D. T., Solanki, S. K., Steinhilber, F. and Vieira, L. E. A. (2011). Climate forcing reconstructions for use in PMIP simulations of the last millennium (v1.0). *Geoscientific Model Development* **4** (1): 33-45.

Schmidt, G. A., Jungclaus, J. H., Ammann, C. M., Bard, E., Braconnot, P., Crowley, T. J., Delaygue, G., Joos, F., Krivova, N. A., Muscheler, R., Otto-Bliesner, B. L., Pongratz, J., Shindell, D. T., Solanki, S. K., Steinhilber, F. and Vieira, L. E. A. (2012). Climate forcing reconstructions for use in PMIP simulations of the Last Millennium (v1.1). *Geosci. Model Dev.* **5** (1): 185-191.

Schmidt, G. A., Ruedy, R., Hansen, J. E., Aleinov, I., Bell, N., Bauer, M., Bauer, S., Cairns, B., Canuto, V., Cheng, Y., Del Genio, A., Faluvegi, G., Friend, A. D., Hall, T. M., Hu, Y., Kelley, M., Kiang, N. Y., Koch, D., Lacis, A. A., Lerner, J., Lo, K. K., Miller, R. L., Nazarenko, L., Oinas, V., Perlitz, J., Perlitz, J., Rind, D., Romanou, A., Russell, G. L., Sato, M., Shindell, D. T., Stone, P. H., Sun, S., Tausnev, N., Thresher, D. and Yao, M.-S. (2006). Present-Day Atmospheric Simulations Using GISS ModelE: Comparison to In Situ, Satellite, and Reanalysis Data. *Journal of Climate* **19** (2): 153-192.

Schneider, D. P., Steig, E. J. and van Ommen, T. (2005). High-resolution ice-core stable-isotopic records from Antarctica: towards interannual climate reconstruction. *Annals of Glaciology* **41**: 63-70.

Schurer, A., Hegerl, G., Mann, M. E., Tett, S. F. B. and Phipps, S. J. (2013). Separating forced from chaotic climate variability over the past millennium. *Journal of Climate*.

Smerdon, J., Kaplan, A., Chang, D. and Evans, M. (2010). A Pseudoproxy Evaluation of the CCA and RegEM Methods for Reconstructing Climate Fields of the Last Millennium. *Journal of Climate* **23** (18): 4856-4880.

Smith, T., Reynolds, R., Peterson, T. and Lawrimore, J. (2008). Improvements to NOAA's Historical Merged Land–Ocean Surface Temperature Analysis (1880–2006). *Journal of Climate* **21** (10): 2283-2296.

Solíz, C., Villalba, R., Argollo, J., Morales, M. S., Christie, D. A., Moya, J. and Pacajes, J. (2009). Spatio-temporal variations in Polylepis tarapacana radial growth across the Bolivian Altiplano during the 20th century. *Palaeogeography, Palaeoclimatology, Palaeoecology* **281** (3-4): 296-308.

Srur, A. M., Villalba, R., Villagra, P. E. and Hertel, D. (2008). Influences of climatic and CO₂ concentration changes on radial growth of Nothofagus pumilio in Patagonia. *Revista Chilena De Historia Natural* **81** (2): 239-256.

Steig, E., Ding, Q., White, J. W. C., Küttel, M., Rupper, S. B., Neumann, T. A., Neff, P., Gallant, A. J. E., Mayewski, P. A., Taylor, K. C., Hoffmann, G., Dixon, D. A., Schoenemann, S. W., Markle, B., Fudge, T. J., Schneider, D. P., A.J., S., Teel, R. T., Vaughn, B. H., Burgener, L., Williams, J. and Korotkikh, E. (2013). Recent climate and ice sheet changes in West Antarctica compared to the past 2000 years. *Nature Geoscience*: 10.1038/ngeo1778.

Steig, E. J., Mayewski, P. A., Dixon, D. A., Kaspari, S. D., Frey, M. M., Schneider, D. P., Arcane, S. A., Hamilton, G. S., Spikes, V. B., Albert, M., Meese, D., Gow, A. J., Shuman, C.

- A., White, J. W. C., Snead, S., Flaherty, J. and Wumkes, M. (2005). High-resolution ice cores from USITASE (West Antarctica): development and validation of chronologies and determination of precision and accuracy. *Annals of Glaciology*, Vol 41, 2005. **41**: 77-84.
- Steinhilber, F., Beer, J. and Fröhlich, C. (2009). Total solar irradiance during the Holocene. *Geophysical Research Letters* **36** (19): L19704.
- Stenni, B., Proposito, M., Gragnani, R., Flora, O., Jouzel, J., Falourd, S. and Frezzotti, M. (2002). Eight centuries of volcanic signal and climate change at Talos Dome (East Antarctica). *Journal of Geophysical Research-Atmospheres* **107** (D9): 4076.
- Szeicz, J. M., Lara, A., Díaz, S. and Aravena, J. C. (2000). Dendrochronological studies of Pilgerodendron uviferum in southern South America. *Dendrochronología en América Latina*. F. Roig. Mendoza, Editorial Nacional de Cuyo: 245-270.
- Taufetter, F., Oerter, H., Fischer, H., Weller, R. and Miller, H. (2004). Spatio-temporal variability in volcanic sulphate deposition over the past 2 kyr in snow pits and firm cores from Amundsenisen, Antarctica. *Journal of Glaciology* **50**: 137-146.
- Taulis, E. (1934). De la distribution des pluies au Chili. *Materiaux pour l'étude des calamités* **33**: 3-20.
- Taylor, K., Stouffer, R. and Meehl, G. (2012). An overview of CMIP5 and the experiment design. *Bulletin of the American Meteorological Society* **93**: 485-498.
- Therrell, M. D., Stahle, D. W., Ries, L. P. and Shugart, H. H. (2006). Tree-ring reconstructed rainfall variability in Zimbabwe. *Climate Dynamics* **26** (7-8): 677-685.
- Thomas, E. R., Dennis, P. F., Bracegirdle, T. J. and Franzke, C. (2009). Ice core evidence for significant 100-year regional warming on the Antarctic Peninsula. *Geophysical Research Letters* **36** (20): L20704.
- Thomas, E. R., Marshall, G. J. and McConnell, J. R. (2008). A doubling in snow accumulation in the western Antarctic Peninsula since 1850. *Geophysical Research Letters* **35** (1): L01706.
- Thompson, L., Mosley-Thompson, E., Brecher, H., Davis, M., Leo, B., Les , D., Lin, P. N., Mashioita, T. and Mountain, K. (2006). Abrupt tropical climate change: past and present. *Proceedings of the National Academy of Sciences* **103** (28).
- Thompson, L., Mosley-Thompson, E. and Morales Arnao, B. (1984). El Niño-Southern Oscillation events recorded in stratigraphy of the tropical Quelccaya Ice Cap. *Science* **276**: 50-52.
- Thompson, L. G., Peel, D., Mosley-Thompson, E., Mulvaney, R., Dai, J., Lin, P., Davis, M. and Rymond, C. (1994). Climate since AD 1510 on Dyer Plateau, Antarctica Peninsula: evidence for recent climate change. *Annals of Glaciology* **20**: 420–426.
- Trenberth, K. and Hurrell, J. (1994). Decadal atmosphere-ocean variations in the Pacific. *Climate Dynamics* **9**: 303-319.

- Tudhope, A., C., C., Mc Culloch, M., Cook, E., Chappell, J., R., E., Lea, D., Lough, J. and Shimmield, G. (2001). Variability in the El Nino Southern Oscillation through a glacial-interglacial cycle. *Science* **291**: 1511-1517.
- Urban, F., Cole, J. and Overpeck, J. (2000). Influence of mean climate change on climate variability from a 155-year tropical Pacific coral record. *Nature* **407**: 989-993.
- Van Ommen, T. D. and Morgan, V. (2010). Snowfall increase in coastal East Antarctica linked with southwest Western Australian drought. *Nature Geoscience* **3**: 267-272.
- Vieira, L. E. A. and Solanki, S. K. (2010). Evolution of the solar magnetic flux on time scales of years to millennia. *Astron. Astrophys.* **509**.
- Villalba, R. (1990a). Climatic Fluctuations in Northern Patagonia During the Last 1000 Years as Inferred from Tree-Ring Records. *Quaternary Research* **34** (3): 346-360.
- Villalba, R. (1990b). Latitude of the surface high-pressure belt over western South America during the last 500 years as inferred from tree-ring analysis. *Quaternary of South America and Antarctic Peninsula* **7**: 273-303.
- Villalba, R., Boninsegna, J. A., Veblen, T. T., Schmelter, A. and Rubulis, S. (1997a). Recent trends in tree-ring records from high elevation sites in the Andes of northern Patagonia. *Climatic Change* **36** (3-4): 425-454.
- Villalba, R., Cook, E., D' Arrigo, R., Jacoby, G., Jones, P., Salinger, M. and Palmer, J. (1997b). Sea-level pressure variability around Antarctica since A.D. 1750 inferred from sub-Antarctic tree-ring records. *Climate Dynamics* **13**: 375-390.
- Villalba, R., Cook, E. R., Jacoby, G. C., D'Arrigo, R. D., Veblen, T. T. and Jones, P. D. (1998). Tree-ring based reconstructions of northern Patagonia precipitation since AD 1600. *Holocene* **8** (6): 659-674.
- Villalba, R., Holmes, R. L. and Boninsegna, J. A. (1992). Spatial Patterns of Climate and Tree Growth Variations in Subtropical Northwestern Argentina. *Journal of Biogeography* **19** (6): 631-649.
- Villalba, R., Lara, A., Boninsegna, J. A., Masiokas, M., Delgado, S., Aravena, J. C., Roig, F. A., Schmelter, A., Wolodarsky, A. and Ripalta, A. (2003). Large-scale temperature changes across the southern Andes: 20th-century variations in the context of the past 400 years. *Climatic Change* **59** (1-2): 177-232.
- Villalba, R. and Veblen, T. T. (1997). Regional patterns of tree population age structures in northern Patagonia: Climatic and disturbance influences. *Journal of Ecology* **85** (2): 113-124.
- Vogel, C. H. (1989). A documentary-derived climatic chronology for South Africa, 1820–1900. *Climatic Change* **14** (3): 291-307.
- von Gunten, L., Grosjean, M., Rein, B., Urrutia, R. and Appleby, P. (2009). A quantitative high-resolution summer temperature reconstruction based on sedimentary pigments from Laguna Aculeo, Central Chile, back to AD 850. *Holocene* **19** (6): 873-881.

Wahl, E. R. and Smerdon, J. E. (2012). Comparative performance of paleoclimate field and index reconstructions derived from climate proxies and noise-only predictors. *Geophys. Res. Lett.* **39** (6): L06703.

Wang, Y.-M., Lean, J. L. and Sheeley Jr., N. R. (2005). Modeling the Sun's Magnetic Field and Irradiance since 1713. *Astrophysical Journal* **625**: 522-538.

Wolff, C., Haug, G. H., Timmermann, A., Damsté, J. S. S., Brauer, A., Sigman, D. M., Cane, M. A. and Verschuren, D. (2011). Reduced Interannual Rainfall Variability in East Africa During the Last Ice Age. *Science* **333** (6043): 743-747.

Xiao, C., Mayewski, P., Qin, D., Li, Z., Zhang, M. and Yan, Y. (2004). Sea level pressure variability over the southern Indian Ocean inferred from a glaciochemical record in Princess Elizabeth Land, east Antarctica. *J. Geophys. Res.* **109** (D16): D16101.

Xin, X.-G., Wu, T.-W. and Zhang, J. (2013). Introduction of CMIP5 experiments carried out with the climate system models of Beijing Climate Center. *Advances in Climate Change Research* **4** (1): 41-49.

Xiong, L. and Palmer, J. (2000). Reconstruction of New Zealand Temperature Back to AD 1720 Using Libocedrus Bidwillii Tree rings. *Climate Change* **45**: 339-359.

Yongqiang, Y., Rucong, Y., Xuehong, Z. and Hailong, L. (2002). A flexible coupled ocean-atmosphere general circulation model. *Advances in Atmospheric Sciences* **19** (1): 169-190.

Yongqiang, Y., Xuehong, Z. and Yufu, G. (2004). Global coupled ocean-atmosphere general circulation models in LASG/IAP. *Advances in Atmospheric Sciences* **21** (3): 444-455.

Zinke, J., Dullo, W. C., Heiss, G. A. and Eisenhauer, A. (2004). ENSO and Indian Ocean subtropical dipole variability is recorded in a coral record off southwest Madagascar for the period 1659 to 1995. *Earth and Planetary Science Letters* **228** (1-2): 177-194.

Zinke, J., Pfeiffer, M., Timm, O., Dullo, W. and Brummer, G. (2009). Western Indian Ocean marine and terrestrial records of climate variability: a review and new concepts on land-ocean interactions since AD 1660. *International Journal of Earth Sciences* **98**: 115-133.